FÁTIMA RAQUEL AZEVEDO MAIA

PhD Thesis

NANOSTRUCTURED 3D MATRICES TO DIRECT MESENCHYMAL STEM CELLS BEHAVIOUR

Dissertação submetida à Faculdade de Engenharia da Universidade do Porto
para obtenção do grau de Doutora em Engenharia Biomédica

Faculdade de Engenharia
Universidade do Porto
2013

This thesis was supervised by:

- Doutora Cristina Maria Santos Alves de Carvalho Barrias (supervisor)

  INEB - Instituto de Engenharia Biomédica, Divisão de Biomateriais, NEWTherapies Group.

- Doutor Pedro Lopes Granja (co-supervisor)

  INEB - Instituto de Engenharia Biomédica, Divisão de Biomateriais, NEWTherapies Group.

  FEUP - Universidade do Porto, Faculdade de Engenharia, Departamento de Engenharia Metalúrgica e de Materiais.

  ICBAS - Instituto de Ciências Biomédicas Abel Salazar, Universidade do Porto.

The research described in this thesis was conducted at:

- NEWTherapies Group, INEB - Instituto de Engenharia Biomédica, Universidade do Porto, Portugal.
- Department of Animal Biotechnology, University of Nevada, USA.
- FCUL – Faculdade de Ciências, Departamento de Biologia Animal, Universidade de Lisboa, Portugal.

The research described in this thesis was financially supported by:

- INL - International Iberian Nanotechnology Laboratory (PhD scholarship).
- FEDER funds through the Programa Operacional Fatores de Competitividade (COMPETE) and by Portuguese funds through FCT (Fundação para a Ciência e a Tecnologia) in the framework of the projects BIOMATRIX PTDC/SAU-BEB/101235/2008 and FCOMP-01-0124-FEDER-010915, and grant SFRH/BD/30057/2006.
- INEB, for Internal INEB project NanoCues.
- FLAD - Fundação Luso-Americana, for Project 004/2010, and for partial funding for the in vivo experiments.

I think to myself, what a wonderful world

Yes, I think to myself, what a wonderful world

(written by Bob Thiele e George David Weiss
and Sung by Louis Armstrong)

Aos que de mais perto me
apoiaram e tiveram que lidar
com as minhas indisposições
(Pai, Mãe, Maninha e Fofi)

AGRADECIMENTOS

Esta tese foi o fruto de um grande esforço, que resultou da colaboração de várias pessoas e instituições a quem eu devo um muito obrigada por tudo.

Em primeiro lugar, obrigada ao Professor Mário Barbosa por me ter aberto as portas do INEB e permitir esta façanha.

Este longo percurso foi acompanhado pela minha orientadora, Cristina Barrias. Sem ela dúvido que tivesse conseguido. Para além da incrível capacidade de trabalho, a sua paciência comigo foi indescrítivel. Ela vai ficar para sempre na minha mente e no meu coração. Obrigada Chefinha.

Claro que não me posso esquecer do meu co-orientador Dr Pedro Granja. Ele foi o terceiro elemento responsável por eu estar aqui e com quem eu tive a minha primeira reunião juntamente com a Cristina. Dessa reunião retive o incentivo e simpatia dele. Obrigada.

No único período em que não estive no INEB a trabalhar, estive a trabalhar com a Dra Graça Almeida Porada. Obrigada por me ter acompanhado durantes os 6 meses que estive em Reno. De Reno trouxe as amizades que lá fiz, a maior parte portuguesas ou brasileiras. Estamos em todo o lado. Ainda bem! Obrigada pelas noitadas e pelo samba no pé.

Não me posso esquecer da Dr. Solveig Thorsteinsdóttir e da Dr. Gabriela Rodrigues do Departamento de Biologia Animal da Faculdade de Ciências da Universidade de Lisboa, por toda a simpatia, disponibilidade e conhecimento transmitido. Permitiram-me aprofundar o meu conhecimento em matriz extracelular o que foi fundamental no meu trabalho. Obrigada.

Mas para além dos chefes, uma das melhores partes foi conhecer os meus colegas Inebianos. Durante estes anos aconteceu de tudo. Alegrias, tristezas, muito trabalho, muito cansaço e muita diversão. Um Obrigada especial do fundo do coração por tudo.

A todos os meus colegas de equipa, um enorme obrigada por toda a ajuda preciosa. Mas um maior ainda a ti Sílvia, companheira das culturas em grande escala. Aprendi muito ao longo destes anos e grande parte devo-te a ti. Obrigada pela paciência e pelo sorriso constante.

E por fim, mas sem dúvida os mais importantes. A minha família! Pai, Mãe, Maninha e Fofi (sim, já não te livras de mim), Obrigada por toda a compreensão nestes últimos tempos. Eu sei que sou uma resingona insuportável quando ando cansada, mas vocês passaram com distinção. Obrigada Pai e Mãe por todo o esforço que fizeram por mim. Tenho muito orgulho em vós! Nunca me faltou nada. Sempre tive o vosso apoio e muito amor acima de tudo. Sem dúvida que sem vocês nada disto era possivel. Espero não ter desiludido e ter estado à altura. Obrigada maninha por me aturares desde que me lembro. Obrigada pelas brincadeiras, pelas lutas, pelas birras e pelo companheirismo.

Por último Obrigada Fofi. Quem diria que virias a ser o meu grande apoio durante esta jornada. Sem ti não sei se tinha conseguido e tu sabes disso. Obrigada por todo o carinho, mimos e amor que me deste quando me fui a baixo e jurava que não ía conseguir. Obrigada por todo o chocolate que me compraste. Obrigada meu amor.

ABSTRACT

Despite substantial advances in orthopaedics, different types of bone lesions still remain clinically difficult to manage. The delivery of adequate cell types, such as mesenchymal stem cells (MSCs), and osteoinductive factors via biomaterial carriers represents a promising strategy to promote local tissue repair. Hydrogels show great potential as cell delivery vehicles, as they provide three-dimensional (3D) microenvironments that partially recapitulate the native extracellular-matrix (ECM). An optimal carrier should increase cell retention, survival and engraftment, provide a template for new tissue formation and, ideally, induce guided-differentiation of transplanted cells.

The main aim of this thesis was to develop injectable vehicles able to direct MSCs differentiation down the osteoblastic lineage, which represent a relevant strategy in the context of bone regeneration. A specific target was to better understand how MSCs behave in 3D and translate that knowledge into the design of improved MSCs carriers.

The modulation of cell behaviour in 3D microenvironments is a challenging task, as it must take into account the influence of multiple parameters, as well as their interplay. These include not only matrix extrinsic factors, such as soluble and direct cell-cell contact signaling, but also several matrix-related factors, which must be carefully controlled as they differentially affect distinct cellular activities. This thesis specifically focused on the behavior of human bone marrow MSCs (hMSCs), which are currently recognized as a powerful cell source for bone tissue regeneration, when cultured under 3D conditions within alginate hydrogels, which are among the most common materials used for cell entrapment and delivery.

The first study addressed the effect of the cell entrapping density on hMSCs response, which represents a critical and frequently overlooked parameter. Different cell densities were tested and in all conditions hMSCs presented steady-state levels of metabolic activity and remained in a nearly non-proliferating state. Yet, cells recovered “normal” activity levels after being retrieved from 3D matrices and re-cultured as 2D monolayers. A high cell density showed to be crucial for promoting the establishment of cell-cell contacts and consequent formation of multicellular clusters rich in endogenous ECM, and stimulated hMSCs osteogenic differentiation. The study clearly highlighted the importance of optimizing the initial cell density when establishing 3D cultures for specific applications.

Envisaging the potential clinical interest of such aggregates, it was then investigated how their formation could be driven by specific matrix cues. The process of cell self-assembly involves mechanosensing mechanisms and depends on a balance between cell-matrix and cell-cell signaling. Because the combined effect of these cues is still not fully clarified, particularly in 3D, the behaviour of hMSCs cultured within hydrogels with tailored stiffness and composition was evaluated. As demonstrated, hMSCs aggregation only occurred in more compliant matrices ($G' \leq 120$ Pa), both in the presence and absence of matrix-bound adhesion ligands ([RGD]: 0, 100 and 200 μM). Fibronectin assembly stabilized cell-cell contacts within aggregates, even in

non-adhesive matrices. However, hMSCs were only able to substantially contract the artificial matrix when RGD was present. Moreover, compliant matrices facilitated cell proliferation and provided a permissive environment for hMSCs osteogenic differentiation, even without RGD. Cell interactions with the original artificial matrix became less important as time progressed, while the *de novo* produced ECM turned into a more critical determinant of cell fate. This study provided further insights into the mechanisms by which hMSCs sense their microenvironment to organize into tissues, and established a biomaterial-based strategy to promote the formation of ECM-MSCs microtissues in 3D.

After demonstrating that both matrix-intrinsic and extrinsic factors affected hMSCs behaviour in 3D, the use of osteoinductive cues as a strategy to specifically guide their differentiation along the osteoblastic lineage was pursued. The idea was to design a multifunctional carrier system to be used for the co-delivery of hMSCs and osteoinductive peptides. The osteogenic growth peptide (OGP) inspired the design of two peptide sequences, where the bioactive fragment of OGP was either flanked by a protease-sensitive linker or by its scrambled sequence, to provide faster and slower release rates, respectively. These peptides were fully characterized and chemically grafted to alginate. The two OGP analogues released bioactive fragments *in vitro*, at different kinetics, which stimulated hMSCs proliferation and osteogenesis. hMSCs-laden OGP-alginate hydrogels were further tested at an ectopic site in a xenograft mouse model. After 4 weeks, OGP-alginate hydrogels were more degraded and colonized by new vascularized tissue than the control (without OGP). hMSCs produced endogenous ECM, migrated outward the hydrogels and proliferated to some extent. OGP groups stimulated hMSCs osteogenic differentiation, as compared with the control, and none of the groups expressed adipogenic genes. Interestingly, the OGP analogue with slower release kinetics also stimulated hMSCs chondrogenic differentiation. Overall, this study demonstrated the ability of the proposed platform to direct the fate of transplanted hMSCs *in loco*, and OGP-releasing hydrogels emerged as a potentially useful system to promote bone regeneration.

In summary, the results presented in this thesis provide new insights to the design of cell-instructive ECM-like artificial 3D matrices, and represent a step forward towards the development of improved carriers for MSCs-based bone regenerative therapies.

RESUMO

Apesar dos avanços substanciais em ortopedia, diferentes tipos de lesões ósseas ainda permanecem clinicamente difíceis de gerir. A distribuição de tipos adequados de células, tais como células estaminais mesenquimais (MSCs), e fatores osteoindutores, através do uso de biomateriais, representa uma estratégia promissora para promover a reparação local de tecido. Os hidrogéis apresentam um grande potencial como veículos de entrega de células, uma vez que proporcionam microambientes tridimensionais (3D) que recapitulam parcialmente a matriz extracelular nativa (ECM). Um veículo ideal deve aumentar a retenção das células no local, a sua sobrevivência e enxerto, e fornecer um modelo para a formação de novo tecido. Idealmente, deverá também induzir a diferenciação guiada das células transplantadas.

O principal objetivo desta tese foi desenvolver veículos injetáveis capazes de direcionar a diferenciação de MSCs ao longo da linhagem osteoblástica, o que representam uma estratégia relevante no contexto da regeneração óssea. Um objectivo específico era entender melhor como se comportam as MSCs em 3D e traduzir esse conhecimento no desenvolvimento de melhores veículos de MSCs.

O controlo do comportamento celular em microambientes 3D é uma tarefa desafiadora pois deve levar em conta a influência de vários parâmetros, bem como a sua interação. Estes incluem não apenas os fatores extrínsecos à matriz, tais como sinalização solúvel e contato direto célula-célula, mas também vários fatores relacionados com a matriz, que devem ser cuidadosamente controlados já que eles afetam, de diferentes formas, atividades celulares distintas. Esta tese centrou-se especificamente no comportamento de MSCs de medula óssea humana (hMSCs), que são atualmente reconhecidas como uma fonte de células promissora para a regeneração de tecido ósseo, quando cultivadas em condições 3D dentro de hidrogéis de alginato, que estão entre os materiais mais frequentemente utilizados para a cultura e entrega de células.

O primeiro estudo abordou o efeito da densidade celular na resposta de hMSCs em 3D, o qual representa um parâmetro crítico e muitas vezes desconsiderado. Diferentes densidades celulares foram testadas e em todas as condições as hMSCs apresentaram níveis estacionários de atividade metabólica e reduzidos de proliferação. No entanto, as células recuperaram os níveis "normais" de atividade após serem recuperadas das matrizes 3D e re-cultivadas em monocamadas em 2D. A mais alta densidade celular mostrou-se crucial para promover o estabelecimento de contatos célula-célula e consequente formação de aglomerados multicelulares ricos em ECM endógena, e estimulou a diferenciação osteogénica de hMSCs. O estudo destacou claramente a importância de otimizar a densidade celular inicial no estabelecimento de culturas em 3D para aplicações específicas.

Vislumbrando o potencial interesse clínico de tais agregados, foi então investigado como a sua formação pode ser orientada por sinais específicos da matriz. O processo de agregação celular envolve mecanismos de resposta a estímulos mecânicos e depende do equilíbrio entre

a célula-matriz e a sinalização célula-célula. Uma vez que o efeito combinado destas pistas não é ainda totalmente esclarecido, particularmente em 3D, foi avaliado o comportamento das hMSCs cultivadas dentro de hidrogéis com rigidez e composição controlada. Como demonstrado, a agregação das hMSCs só ocorreu em matrizes menos rígidas, tanto na presença como na ausência de péptidos de adesão ligados à matriz. A formação de uma rede de fibronectina estabilizou os contatos célula-célula dentro dos agregados, mesmo em matrizes não-adesivas. No entanto, as hMSCs só foram capazes de contrair substancialmente a matriz artificial na presença de RGD. Além disso, as matrizes menos rígidas facilitaram a proliferação celular e proporcionaram um ambiente permissivo para a diferenciação osteogénica das hMSCs, mesmo sem RGD. As interações da célula com a matriz original tornou-se menos importante com a progressão do tempo, enquanto a produção da nova ECM se transformou num fator mais crítico e determinante do destino celular. Este estudo permitiu elucidar alguns mecanismos através dos quais as hMSCs sentem o seu microambiente e o usam para se organizarem em tecidos, e estabeleceu uma estratégia baseada em biomateriais para promover a formação de microtecidos compostos por ECM-MSCs em 3D.

Depois de demonstrar que diversos fatores, tanto intrínsecos como extrínsecos à matriz, afetam o comportamento das hMSCs em 3D, foi idealizado o uso de pistas osteoindutivas como uma estratégia para guiar especificamente a sua diferenciação ao longo da linhagem osteoblástica. A ideia era conceber um sistema multifuncional para ser utilizado na entrega simultânea das hMSCs e péptidos osteoindutores. O péptido de crescimento osteogénico (OGP) inspirou o desenho de duas sequências peptídicas, onde o fragmento bioativo de OGP foi ladeado por uma ligação sensível à ação de proteases, ou pela sua sequência misturada, por forma a resultar numa taxa de libertação mais rápida ou mais lenta, respetivamente. Estes péptidos foram caraterizados e quimicamente ligados ao alginato. Os dois análogos de OGP libertaram fragmentos bioativos *in vitro* com diferentes cinéticas, o que estimulou a proliferação das hMSCs e a osteogénese. Hidrogéis de alginato-OGP contendo hMSCs foram testados de forma ectópica num modelo de xenotransplante em ratinho. Após 4 semanas, os hidrogéis de alginato-OGP degradaram-se mais e foram mais eficientemente colonizados por novo tecido vascularizado do que o controlo (sem OGP). As hMSCs produziram ECM endógena, migraram para fora dos hidrogéis e proliferaram. Os grupos com OGP estimularam a diferenciação osteogénica das hMSCs, em comparação com o controlo, e em nenhum dos grupos foi detetada a expressão de genes adipogénicos. Curiosamente, o análogo de OGP com a cinética de libertação mais lenta também estimulou a diferenciação condrogénica das hMSCs. Em geral, este estudo demonstrou a capacidade da plataforma proposta para direcionar o destino das hMSCs transplantadas *in loco*, e os hidrogéis de libertação de OGP emergiram como um sistema potencialmente útil na promoção da regeneração óssea.

Em resumo, os resultados apresentados nesta tese forneceram novos conhecimentos para o desenho de matrizes 3D artificiais, capazes de direcionar o comportamento das hMSCs, representando um contributo para o desenvolvimento de veículos melhorados para terapias celulares de regeneração óssea.

TABLE OF CONTENTS

SHORT BIOGRAPHY

Fátima Raquel Maia was born in Porto, Portugal, in 1985. She obtained her BSc and MSc degrees in Biology from the Faculty of Sciences of the University of Porto (FCUP) in 2007 and 2008, respectively. Her final project was developed at Instituto de Engenharia Biomédica (INEB) under the supervision of Dr Cristina Barrias. In 2008, Fátima Raquel Maia was awarded a PhD scholarship from the International Iberian Nanotechnology Laboratory (INL), and initiated a PhD at INEB, in the framework of the Doctoral Program in Biomedical Engineering from the Faculty of Engineering of the University of Porto (PRODEB, FEUP), under the supervision of Dr Cristina Barrias and Dr Pedro Granja. In 2009 she was granted with a scholarship from Fundação Luso-Americana para o Desenvolvimento (FLAD) for a 6-month internship at the Department of Animal Biotechnology of the University of Nevada-Reno, USA, where she worked under the supervision of Dr. Graça Almeida-Porada. During the course of her PhD she also visited and performed some experimental work in collaboration with the Development and Evolutionary Morphogenesis Group, lead by Dr Solveig Thorsteinsdóttir at the Faculty of Sciences of the University of Lisbon (FCUL), Portugal. In 2010 she has received a Best Poster Award at the "Trends in Nanotechnology" International Conference 2010. As a result of her research efforts she is currently author of 2 publications, with 3 others submitted. Additionally, she has presented 13 communications (4 oral and 9 posters) in International Conferences on the fields of Biomaterials and Regenerative Medicine.

The research performed during the extent of this PhD resulted in the following publications:

LIST OF PUBLICATIONS:

- Fonseca KB, Maia FR, Cruz FA, Andrade D, Juliano MA, Granja PL, Barrias CC. Enzymatic, physicochemical and biological properties of MMP-sensitive alginate hydrogels. Soft Matter 2013, 9. 3283-3292.
- Maia FR, Bidarra SJ, Granja PL, Barrias CC. Functionalization of biomaterials with small osteoinductive moieties. Acta Biomaterialia. 2013;9:8773-89.
- Maia FR, Fonseca KB, Rodrigues G, Granja PL, Barrias CC. Self-assembly of MSC-ECM microtissues on soft alginate hydrogel matrices. (Submitted, 2013).
- Maia FR, Lourenço AF, Granja PL, Gonçalves RM, Barrias CC. Effect of cell density of mesenchymal stem cells re-organization within hydrogel-based 3D matrices. (Submitted, 2013)
- Maia FR, Barbosa M, Gomes DB, Vale N, Gomes P, Granja PL, Barrias CC. Hydrogel depots for local co-delivery of osteoinductive peptides and mesenchymal stem cells. (Submitted, 2013).

MOTIVATION AND AIMS

The controlled delivery of cells, namely mesenchymal stem cells (MSCs), from biomaterial-based vehicles can improve and accelerate functional bone formation. The carrier materials can transport and deliver cells into target sites, increase their survival and engraftment, provide a supportive ECM-like substrate to assist the 3D assembly of the newly formed tissue and, ideally, guide the differentiation of MSCs along the osteoblastic lineage. Hydrogels are amongst the most widely used carrier materials, as they can entrap and protect cells within a real 3D microenvironment, intrinsically present many ECM-like features, and may exhibit easily tunable biochemical and biophysical properties. *In-situ* forming hydrogels are attractive solutions for some applications, as they present the added benefit of injectability. Although this type of strategy shows great promise, clinical trials have not yet resulted in consistent benefits. This suggests that improved delivery systems and further understanding of MSCs biology and MSCs-ECM interactions is needed for optimal efficacy.

In fact, the development of optimized hydrogel-based cell carriers requires a deep knowledge on how cells behave within artificial 3D matrices, and how they react to a number of extrinsic and matrix-intrinsic factors that differentially regulate the activities of different cell types. So, the aim of the first experimental part of this thesis (chapters III and IV), was to investigate how MSCs, which are currently recognized as a powerful cell source for bone tissue regeneration, react to different cues, when cultured within alginate hydrogels, one of the most common materials used for cell entrapment and delivery. Central questions addressed during this investigation were: (i) how do human MSCs (hMSCs) sense and react to cellular and matrix cues in 3D?; (ii) how can MSCs behaviour be dynamically instructed by the 3D matrix they contact with?; and (iii) how can this knowledge translate into more effective cell-based therapies to promote tissue regeneration?.

For enhanced efficacy, the carrier system can also be specifically designed to co-deliver pro-regenerative bioactive molecules, with adequate release kinetics, in a localized and/or spatiotemporal manner. In the context of bone regeneration, the combination of MSCs with biomaterials functionalized with instructive cues can be used as a strategy to direct specific lineage commitment. Therefore, the aim of the second experimental part of this thesis (chapter V) was to synthesize new injectable alginate hydrogels functionalized with osteoinductive peptides. The co-delivery of such factors along with MSCs is expected to stimulate transplanted cells (and also host cells) activity, and thus present synergistic effects towards bone augmentation.

Overall, the results presented on this thesis are expected to contribute with important clues for the design of optimized cell carrier materials, which might improve the therapeutic efficacy of transplanted cells for bone tissue regeneration.

THESIS OUTLINE

The thesis has been organized into six chapters:

Chapter I provide a brief introduction to some general concepts related with the work developed during this thesis.

Chapter II is a literature review that specifically covers the functionalization of biomaterials with small osteoinductive moieties. It describes different strategies that have been used to promote substrate-mediated guidance of osteogenic differentiation of immature osteoblasts, osteoprogenitors and MSCs, through chemically conjugated small moieties, both in 2D and 3D settings, including hydrogels. In each case, the selected moiety, the coupling strategy and the main findings of the study are highlighted. The latest advances and future perspectives in the field are also discussed.

Subsequently, Chapters III, IV and V describe the performed experimental work:

Chapter III addresses the influence of the initial cell entrapping density on the behaviour of human MSCs (hMSCs) cultured within alginate hydrogels, and highlights the relevance of optimizing this parameter when establishing 3D cultures for specific applications. It demonstrates that high cell densities are important for promoting the establishment of cell-cell contacts and the consequent formation of multicellular clusters rich in endogenous extracellular matrix (ECM) components, which in turn promote the osteogenic differentiation of hMSCs.

Chapter IV provides further insights into the mechanisms by which hMSCs sense their microenvironment to organize into microtissues. To evaluate the effect cell-matrix and cell-cell signaling and especially their interplay, the behaviour of hMSCs cultured within alginate hydrogel matrices with tailored stiffness and density of cell-adhesion ligands was evaluated. The most compliant matrices promoted hMSCs aggregation and ECM production and provided a permissive environment for hMSCs osteogenic differentiation.

Chapter V explores the use of osteoinductive cues as a strategy to specifically guide the differentiation of hMSCs along the osteoblastic lineage. Analogues of the Osteogenic Growth Peptide (OGP) were synthesized and chemically grafted to alginate hydrogels using linkers with different protease sensitivity. After *in vitro* characterization, the performance of functionalized alginate hydrogels as local depots for the co-delivery of hMSCs and OGP was analyzed *in vivo*, using a xenograft mouse model. The study demonstrates that the system can be successfully used to direct the fate of transplanted hMSCs at an ectopic site, suggesting that OGP-releasing hydrogels might be useful to stimulate bone formation by inducing osteogenesis and/or chondrogenesis.

Finally, **Chapter VI** provides some concluding remarks, with an overall analysis of the preceding chapters, along with future perspectives.

CHAPTER I

INTRODUCTION

---

1. INTRODUCTION

1.1. Brief overview of bone repair mechanisms

Unlike soft tissues that predominantly produce fibrous scars upon injury, the adult bone possesses an astounding capacity to regenerate upon damage [1]. This complex process recapitulates the skeleton growth during embryogenesis, and involves different cell types, soluble signals and matrix signals (biochemical and mechanical), acting in concert towards the formation of new functional bone, indistinguishable from adjacent uninjured bone tissue [2].

Bone repair can occur through direct (primary) and indirect (secondary) healing mechanisms [2]. The first process is rarely observed, as it requires a correct anatomical reduction of the fracture ends, without significant gap formation, and a stable fixation without interfragmentary strain [3]. It does not involve callus formation, and represents an attempt to directly re-establish an anatomically and mechanically competent lamellar bone structure. There is almost no periosteal involvement, and the key participating cells are osteoblasts, the bone-forming cells, which differentiate from osteoprogenitor cells mainly supplied by blood vessels [2].

Typically, bone repair occurs through an indirect process characterized by four overlapping stages (Fig. 1) where endochondral and intramembranous ossification are combined [2]. These are: A) hematoma formation and inflammatory response, B) soft (cartilaginous) callus formation C) hard callus (ossified) callus formation (osteogenesis) and D) remodeling [4]. In what concerns the basic events occurring along the 4-stage model, it has been established that each phase involves specific set populations and molecular signaling, but as these events frequently overlap, it is difficult to make a clear delineation of each stage during repair [4].

In general terms, the first phase begins immediately after trauma, with the consequent disruption of blood supply and the formation of a hematoma (Fig. 1A). This initiates an inflammatory response, which is essential for the healing process. The blood clot serves as a template for subsequent callus formation and acts as a source of cytokines and growth factors, modulating the inflammatory process and promoting the recruitment of different pro-regenerative cell types into the damage site [4]. One particularly relevant cell type are MSCs, which may derive from surrounding tissues (soft tissues, cortex, periosteum) and bone marrow, or even be systemically recruited as circulating MSCs from remote hematopoetic sites [3]. Still, their precise sources remain unclear.

Following the formation of the initial hematoma, a fibrin-rich granulation tissue is assembled and progressively substituted by cartilaginous tissue, involving an endochondral process where MSCs differentiate into chondrocytes that proliferate and secrete new matrix (Fig. 1B). This results in the formation of a soft callus that bridges the fracture and restores mechanical stability [1] Gradually, chondrocytes became hypertrophic, their ECM starts to

calcify and they become apoptotic [4]. The soft callus is then progressively resorbed and invaded by new blood vessels. The formation of a hard callus then progresses, and the calcified cartilage is replaced with woven bone, as osteoblasts produce a mineralized matrix (Fig. 1C) [5].

Although the hard callus is more solid and mechanically rigid, it does not fully restore the biomechanical properties of normal bone. As such, the healing cascade initiates another resorptive phase, to remodel the hard callus and reestablish the functionality of the damage bone (Fig. 1D). The process involves a balance of hard callus resorption by osteoclasts, and lamellar bone deposition by osteoblasts, which progresses until a fully regenerated bone structure is achieved.

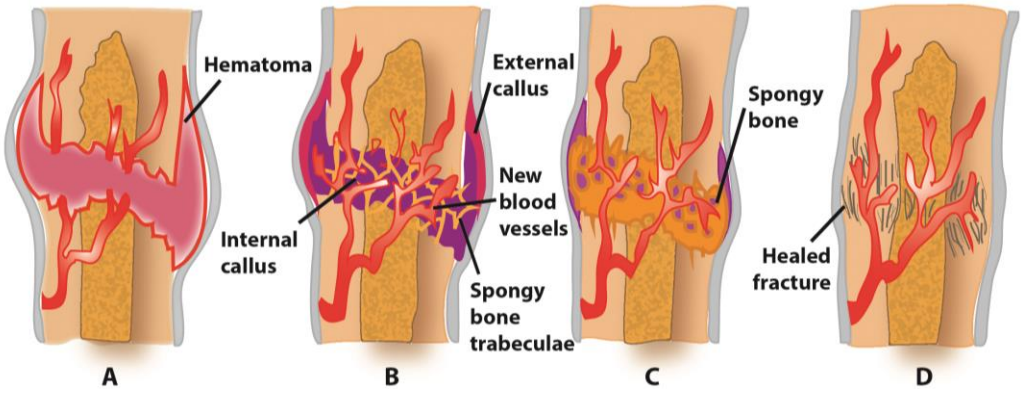

Fig. 1. Schematic representation of the different stages of indirect bone healing. (**A**) hematoma formation and inflammatory response, (**B**) soft callus formation (chondrogenesis), (**C**) hard callus formation (osteogenesis) and (**D**) bone remodeling. Adapted from Pearson Education Inc. publishing as Benjamin Cummings.

When bone lesions occur, the natural ability of bone to repair/regenerate may be compromised by their size, location and type. Despite substantial advances in orthopedic surgery, different bone abnormalities still remain clinically difficult to manage. Common lesions include not only nonunion or delayed consolidation fractures, but also several types of bone defects caused by trauma, infection, prosthesis loosening or tumor resection, among others [6, 7]. In these cases, surgical intervention is needed and there are several bone reconstruction strategies currently available [6].

In alternative to more conventional treatments, which will not be discussed here, there is currently great excitement over the possibility of replacing damaged tissues through the emerging field of regenerative medicine. Potential strategies include cell transplantation, implantation of acellular or cell-laden biomaterial constructs synthesized in the laboratory, and induction of regeneration from the body's own cells by rendering the injury environment and/or host cells regeneration-competent [6, 8-11]. Presently, cell/combination therapies are mainly

indicated for local bone defects, but future targets also include a number of systemic metabolic bone diseases such as osteoporosis.

1.2. Cell-based therapies for bone repair: mesenchymal stem cells as a promising tool

Cell-based regenerative therapies offer an interesting approach to recapitulate the bone healing process. Most cellular therapy strategies for bone regeneration employ adult stem cells, like MSCs, which raise less controversial ethical considerations than embryonic stem cells [12]. MSCs have generated a great deal of excitement, notably for their capacity to self-renew and differentiate into multiple tissues, including bone, cartilage, fat, and others of mesenchymal origin [13]. MSCs have the capacity of homing to injured tissues [14], providing cell populations that regulate local cellular activity for improved repair, either by secreting key trophic factors or by directly participating in the assembly of new tissue [12, 15]. Their high expansion potential and apparent immune modulatory/suppressive effects [16] make them extremely appealing as 'off-the shelf' bioproducts, to be used in both autologous and allogeneic settings.

The presence of MSCs has been detected in different tissues, such as bone marrow [17], fat (adipose) tissue [18], umbilical cord blood [19], peripheral blood [20], synovial membrane [21], deciduous teeth [22], dental pulp [23], amniotic fluid [24], brain, skin, heart, kidneys and liver [25], among others. Despite sharing similar characteristics, MSCs from distinct origins differ in their phenotype and differentiation potential [26]. For regeneration therapies, the selection of the most adequate MSCs source is strongly related with issues of accessibility and/or isolation yield. Bone marrow MSCs, originally isolated by Friedenstein et al. in 1976 [27], are the best characterized and have been considered as the major source of progenitor cells for skeletal tissues repair. More recently, other sources requiring less invasive and easier harvesting procedures have been explored. Adipose tissue-derived MSCs are particularly attractive, and an increasing amount of data is being generated regarding their osteogenic potential [28]. In the case of umbilical cord blood, the isolation process is easy but results in very low yields, requiring extensive amplification [29].

Irrespectively of their source, the high expansion potential of MSCs in culture [30], which has been consistently improved by the use of bioreactors [31], allow to obtain clinically meaningful cell numbers for early stage clinical trials. However, traditional expansion approaches raise some concerns due to the use of animal-derived supplements, mainly related with batch-to-batch variation and safety issues [30]. To address this limitation, several xeno-free cultivation strategies have been recently proposed [29, 32].

The International Society for Cellular Therapy has established minimal criteria to define a cell as a mesenchymal stem cell [33]. These include the property of plastic-adherence; the expression of specific phenotypic markers (presence of typical MSCs markers CD90, CD105, CD73 coupled with the absence of hematopoietic markers such as CD45); and the ability to differentiate into osteoblasts, adipocytes and chondroblasts *in vitro.* Osteogenic differentiation is

traditionally induced in the presence of β-glycerophosphate, ascorbic acid and dexamethasone (Fig. 2) [34]. Other osteoinductive compounds have been tested, as described in more detail in Chapter II. Typically, differentiated cells undergo a morphological change from spindle-shape to polygonal cells, express several well-recognized bone-differentiation markers and mineralize their ECM [34, 35]. *In vivo*, the osteogenic potential of bone marrow MSCs has been clearly demonstrated by subcutaneous implantation within a ceramic carrier in immunocompromised mice, a common assay for evaluating ectopic MSCs differentiation into functional osteoblasts [36].

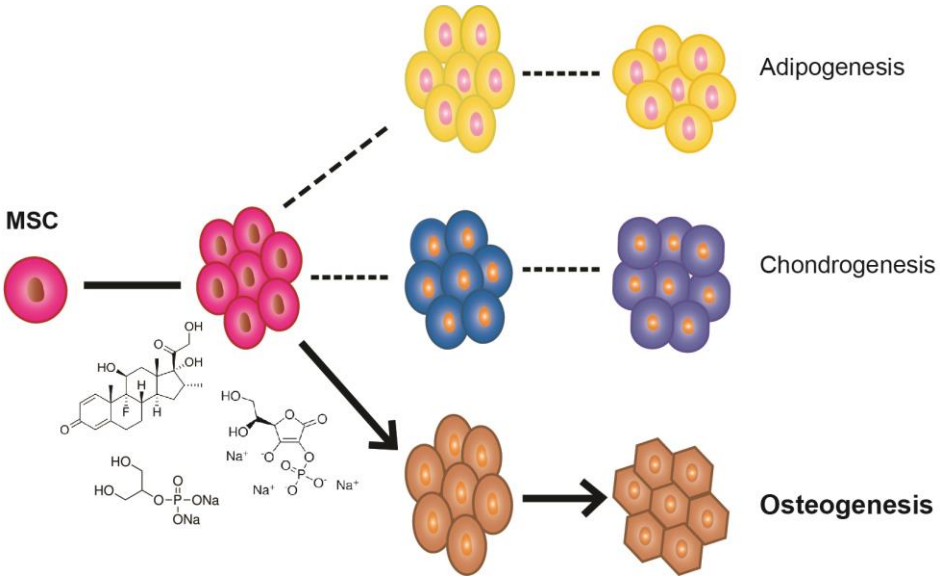

Fig. 2. Induced mesenchymal stem cells differentiation. MSCs have the capacity to differentiate into different lineages *in vitro*, namely adipogenic, chondrogenic and osteogenic. Different types of compounds (β-glycerophosphate, ascorbic acid and dexamethasone are depicted as examples) can be used to specifically induce MSCs to differentiate along the osteoblastic lineage.

In Europe, MSCs are considered “advanced therapy medicinal products” (ATMP), but several scientific, technical, regulatory and safety issues still require a great deal of attention to set up standards for their final quality and efficacy [6]. Also, there are still many open questions regarding the usefulness and limitations associated to the use of MSCs in clinical practice. For example, intravenously administered MSCs have been shown to improve repair of multiple tissues, including bone, as demonstrated in preclinical testing and even in some clinical trials [6, 37].

Yet, the mechanism behind the observed beneficial effects remain largely unexplained [38], and it is not clear how infused MSCs are able to repair distal organs. On the other hand, localized MSCs administration to the defect site is frequently associated with rapid cell disappearance; low survival rates - requiring high amounts of cells to exert a therapeutic effect;

and poor cell engraftment. Some of these obstacles may potentially be overcome through the use of more effective cell delivery approaches [39].

1.3. Biomaterial-based vehicles for cell therapies: hydrogels as ECM mimics

Biomaterial carriers that allow the local delivery of cells at the site of injury can greatly improve the efficacy of cell therapies. These carriers provide the transplanted cells with a protective microenvironment, which enhances their survival, retention and engraftment [39]. Moreover, these materials may act as ECM-mimics for guiding tissue repair, namely by modulating the behaviour and fate of transplanted cells and promoting the infiltration and proliferation of osteoprogenitor cells, and other relevant cell types, for integrative tissue repair [40].

Among the various types of biomaterial carriers, hydrogels are probably the most attractive. Hydrogels are water-swollen polymeric materials with a high water content, which generally possess excellent biocompatibility and high permeability allowing the diffusion of nutrients oxygen and cell metabolites throughout the network [40]. Moreover, their capacity to recreate microenvironments where cells become embedded in real 3D conditions, allows the structural recreation of a natural ECM scenario [41, 42].

Importantly, within such environments, cells become exposed to a range of chemical and mechanical cues that modulate their behavior [9]. As recently recognized, cell-matrix interactions are essential determinants of cellular activity**.** Indeed, it is nowadays clear that, *in vivo,* the native ECM does not serve only as a scaffold to stabilize the structure of tissues, as initially believed, but plays a far more active and complex role in regulating cell behavior [43].

Along with its complex role, the ECM has a correspondingly complex structure and composition incorporating polysaccharide-like hydrogels and numerous structural and functional proteins that directly interact with cells [9, 44, 45]. This is the scenario that a growing tissue expects to find when passing through the difficult process of regenerating, and what artificial scaffolds should ideally mimic. For that reason, the evolution in the design of new biomaterials that mimic the ECM parallels the development of knowledge of the natural matrix [46]. To accomplish these goals, new generations of multifunctional ECM-like biomaterials are being developed [46, 47].

In the past few years increasing efforts have also been devoted to the development of injectable biomaterials as an alternative for bone augmentation or replacement [48, 49]. The main advantage of using injectable materials is the possibility of filling bone-defects of different shapes and sizes using a minimally invasive surgery [50], which provides less discomfort to patients, undergoing a variety of orthopedic procedures, allows a faster recovery and has lower costs.

There are different types of hydrogel-forming polymers, which can be generally classified according to their source, natural or synthetic, each presenting advantages and limitations [51].

For example, protein-based or ECM-derived hydrogels can be used to create “promoting” microenvironments, which intrinsically encourage cell-matrix interaction due to the presence of endogenous bioactive domains on their composition [52]. While this may represent a benefit, it also makes these systems complex and ill defined, making it difficult to determine exactly which signals are promoting specific cellular activities [53]. Also, these materials do not afford enough control over their fine-biochemical and mechanical properties.

Other types of hydrogels, both of natural and synthetic origin, also provide 3D microenvironments that are structurally similar to native ECMs, and are “permissive” in the sense that they generally preserve cell viability, but lack functional sites for cell recognition [54, 55]. This can however be regarded as an advantage, as these materials can be used as ideal “bio-inert” backgrounds, which can be functionalized with bioactive motifs to elicit specific cell responses. Alginate hydrogels, which present these characteristics, were selected for the present investigation and are described in more detail in the following section.

Hydrogels have also been frequently used as drug delivery systems [56]. Specific bioactive agents can be loaded into hydrogels, using different strategies involving physical or chemical interactions. Briefly, physical entrapment can be achieved either through drug absorption by pre-fabricated hydrogels, or drug trapping during hydrogel formation [57, 58]. In this case the main mechanisms of drug release are drug diffusion and/or matrix degradation. The bioactive agents can also be chemically tethered to hydrogels and then be released upon degradation of the matrix and/or labile linkers [59, 60]. This issue will be further discussed for the specific case of alginate hydrogels.

1.4. Alginate hydrogels as vehicles for drug and cell delivery

Alginate is a natural polysaccharide extracted from brown seaweeds and composed of (1-4)-linked β-D-mannuronic acid (M units) and α-L guluronic acid (G units) monomers which vary in number and sequential distribution along the polymer chain [55]. Alginate chains can be composed by homopolymeric M blocks (MMMMMM) or G blocks (GGGGGG), and also composed by heteropolymeric MG blocks (MGMGMGMG) (Fig. 3).

The sequence and composition of the monomers affect the functional properties of alginate. For example, alginate molecules with a high percentage of M block form more flexible gels, whereas alginates with a higher percentage of G blocks form stiffer gels [61]. The relative content of M vs. G blocks is highly dependent on the alginate source.

In what concerns the use of alginate for biomedical applications, many of the disadvantages commonly associated to the use of natural polymers have been overcome. In fact, highly purified and well-characterized alginates developed for use in clinical and pharmaceutical applications are currently commercially available.

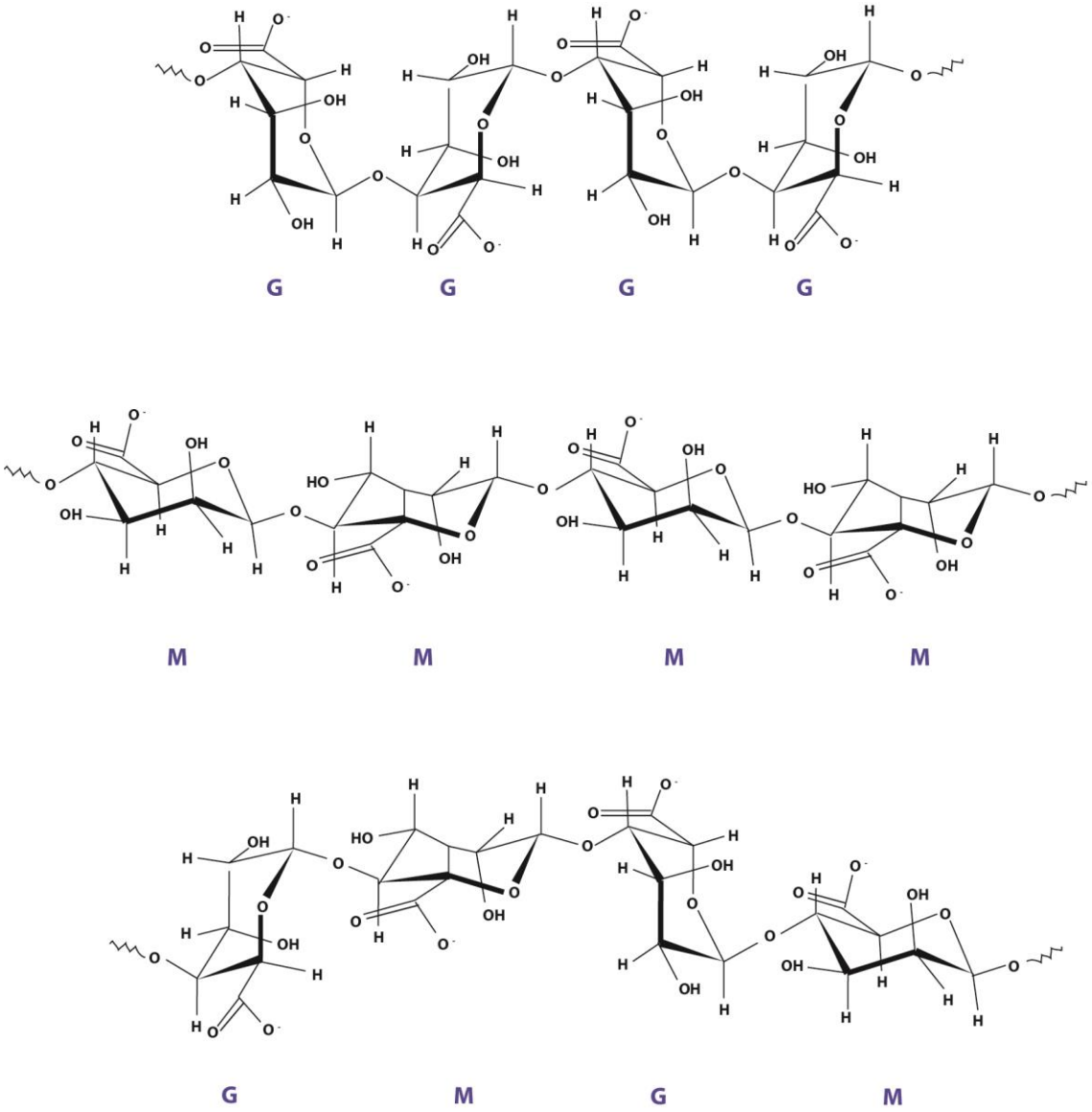

Fig. 3. Schematic illustration of alginate structure. (1-4)-linked β-D-mannuronic acid monomers are indicated by (M) and α-L guluronic acid monomers are indicated by (G). Homopolymeric block are composed of G residues (GGGG) or M residues (MMMM), while heteropolymers are composed of alternating G and M residues (GMGM). Adapted from [62].

To assist customers who are developing medical applications of ultrapure sodium alginates (endotoxin levels lower than 100 EU/g), some manufacturers maintain Drug Master Files with the US Food and Drug Administration (FDA). Within a certain category of products, batch-to-batch variability is negligible, namely in terms of key parameters such alginate molecular weight and G-to-M ratio, which could also be considered a drawback in the use of alginate-based biomaterials at a larger scale, namely for clinical applications.

Alginate solutions can be easily sterilized by filtration, and hydrogels can be obtained by chemical and physical crosslinking methods, being the later the most common ones.

Ionotropic gelation occurs rapidly under physiological conditions when sodium ions from the α-L guluronic acid blocks, exchange with divalent cations (like Ca^{2+}) present in solution, in a highly cooperative manner [63]. The carboxylate functional groups of subsequent G groups have the appropriate structure for cation binding, and this interaction leads to the formation of an egg-box structure (Fig. 4) [63]. The crosslinking process can be carried out under very mild conditions – at low temperature and in the absence of organic solvents, and hydrogels of different shapes can be prepared. *In situ* forming hydrogels can be prepared using internal gelation strategies, which involves the use of calcium salts with low solubility in water at neutral pH, such as $CaCO_3$ and $CaSO_4$ that can be uniformly distributed in the alginate solution without initiating hydrogel gelation. Decreasing the pH, using slowly hydrolyzing acidifying compounds such as glucone-δ-lactone, can then trigger the release of free calcium ions, thereby allowing the gradual crosslinking of the hydrogel network [64, 65]. The gelling time depends on different parameters, such as the concentration of polymer and crosslinking agents, their relative proportion, and the temperature, among others. This way, in a clinical scenario, the injection of fluid gel-precursor solutions that conform to the defect shape and solidify at the target site is possible.

The properties of alginates as delivery systems have been widely investigated. Several proteins, including growth factors [66] and enzymes [67], and also cells, have already been successfully incorporated in alginate gels, retaining a high percentage of biological activity or viability.

Although alginates hydrogels present numerous attractive features, their use as cell scaffolds presents additional requirements. It has been previously reported [55] that attachment-dependent cells are unable to specifically interact with alginate hydrogels, which promote minimal protein adsorption due to their high hydrophilic nature.

A way to circumvent this apparent limitation is the incorporation of the cell-adhesive oligopeptide arginine-glycine-aspartic acids (RGD), as initially proposed by Rowley et al [55]. This motif was identified almost two decades ago by Pierschbacher and Rouslahti as the minimal essential cell-adhesion sequence in fibronectin (Fn) [68]. RGD coupling to alginate was performed through covalent modification utilizing standard aqueous carbodiimide chemistry [55].

Briefly, 1-ethyl-(dimethylaminopropyl) carbodiimide (EDC) was used to form amide linkages between the terminal amine on the peptide and the carboxylate on the alginate as depicted schematically in Fig. 5. The compound *N*-hydroxysulfosuccinimide (sulfo-NHS) was used as a co-reactant to stabilize the reactive EDC-intermediate (O-acylisourea intermediate) against a competing hydrolysis reaction.

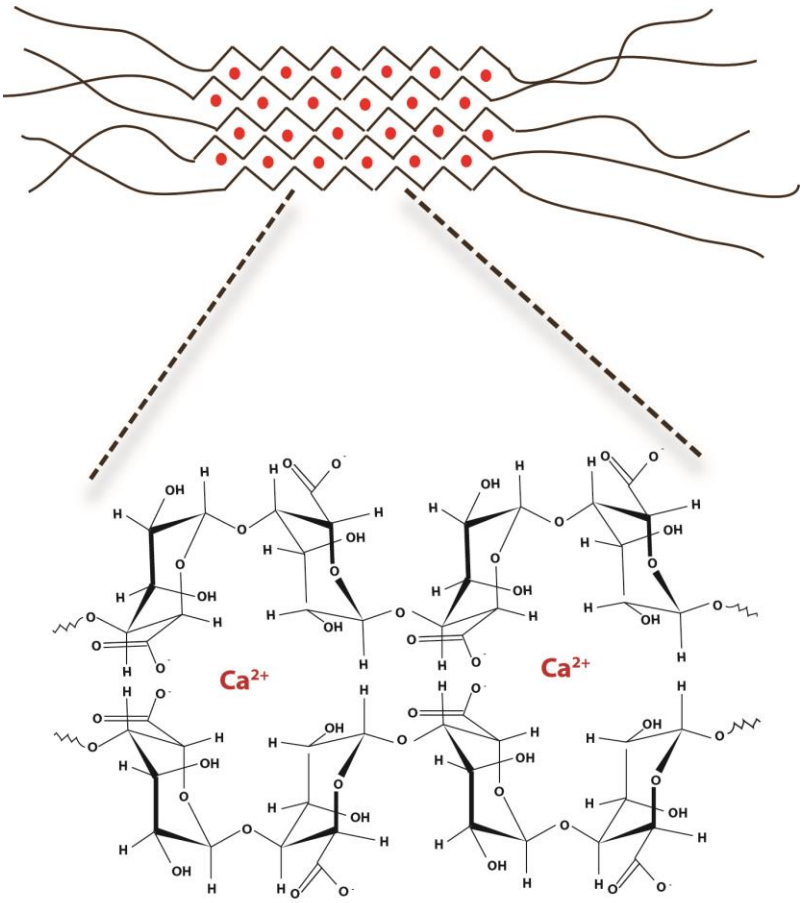

Fig. 4. Model of egg-box structure. Link between paired α-L-guluronic acid sequences of the alginate and divalent ions (Ca^{2+} is depicted as example). Adapted from [61].

Another important modification of alginate hydrogels, which greatly improved their properties as ECM mimics, was the incorporation of enzyme-susceptible groups to render them degradable by cell-secreted proteases [69, 70]. Alginate hydrogels were partially crosslinked with the matrix metalloproteinase (MMP)-cleavable peptide PVGLIG (proline-valine-glycine-leucine-isoleucine-glycine) combined with RGD peptides. The cleavable peptide allowed cells to overcome the biophysical hydrogel resistance while RGD provided for integrin-mediated cell adhesion. This work showed that entrapped MSCs interacted dynamically with the MMP-sensitive hydrogels, being also able to interact with neighboring cells emphasizing the importance of the microenvironment in MSCs' behavior (Fig. 6). The sequence selected for that study, which also explored in the present work (PVG↓LIG - the arrow indicates the cleavage site) is susceptible to cleavage by MMP-2, MMP-9, MMP-13 and MMP-14, as previously demonstrated [70], and was originally deduced from a combinatorial library of MMP-sensitive oligopeptides [71, 72].

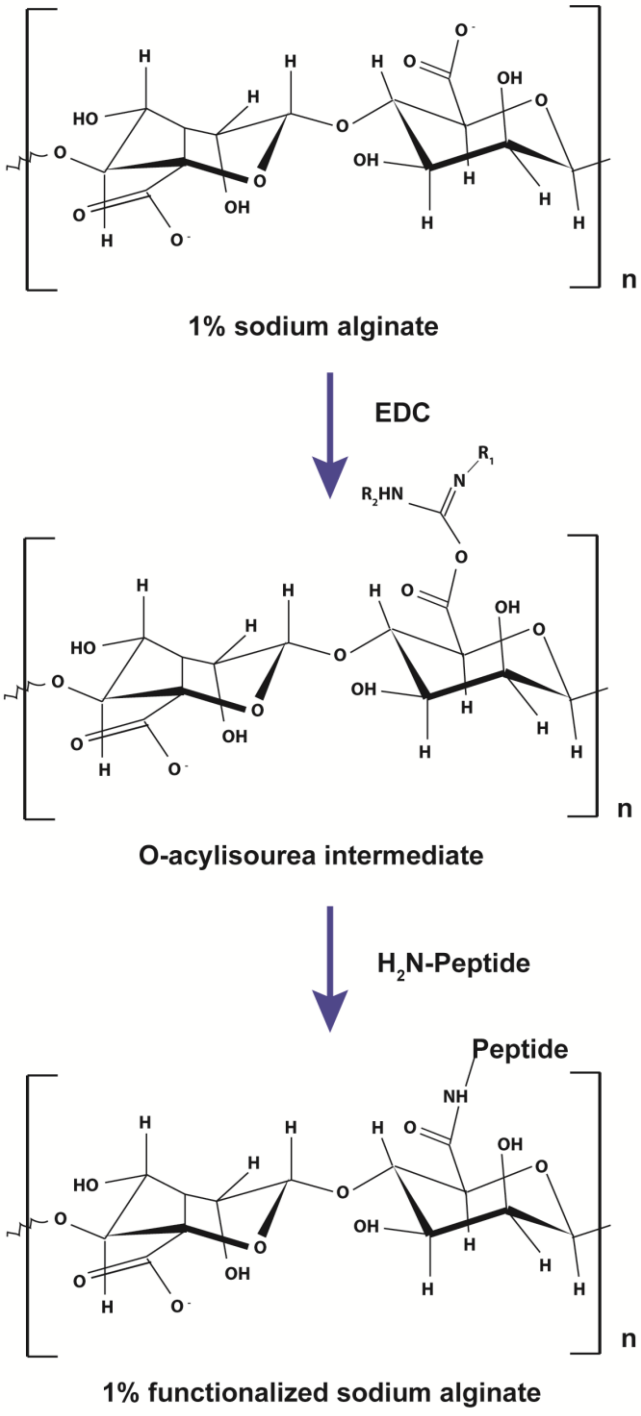

Fig. 5. Reaction scheme of peptide coupling to alginate molecules using carbodiimide chemistry. EDC added to alginate reacts with carboxylic acid groups forming an amide bond where the terminal amine of the peptide link. Adapted from [55].

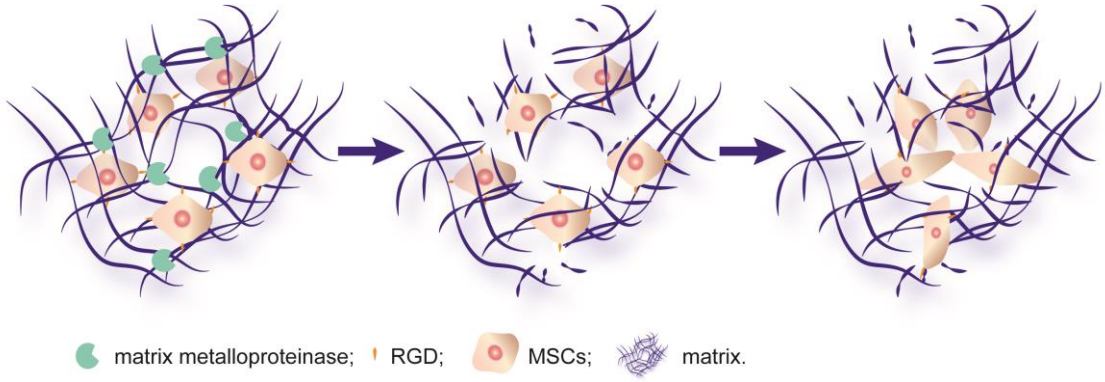

Fig. 6. MMP-degradable alginate hydrogels. Alginate matrices functionalized with crosslinking MMP-sensitive (PVGLIG) and tethered cell-adhesion (RGD) peptides, which not only promote MSCs adhesion, but also enable matrix degradation through cell-driven proteolytic mechanisms [69].

1.4.1. Alginate functionalization with osteoinductive peptides and release mechanisms

In this thesis, the functional modification of alginate with osteoinductive peptides, for subsequent *in vivo* release was investigated. The idea was to develop a system where osteoinductive peptides could be co-delivered with MSCs to induce their differentiation along the osteoblastic lineage, and remain locally available, in close proximity of target cells at the injury site, for prolonged periods of time.

As explained in detail in chapter II, different types of small moieties have been proposed as osteoinductive agents, and some of them have already been conjugated with alginate hydrogels [59, 73]. For this study, the osteogenic growth peptide (OGP) was the one selected, due to a number of reasons, which include its interesting bioactive properties and its small size that facilitates coupling and is less likely to interfere with the hydrogel crosslinking process. OGP is a naturally occurring tetradecapeptide identical to the C-terminal amino acid sequence 89-102 (H-Ala-Leu-Lys-Arg-Gln-Gly-Arg-Thr-Leu-Tyr-Gly-Phe-Gly-Gly-OH) of histone H4 (H4) [74]. It can be found free or combined with OGP binding proteins (OGPBPs), mainly as an inactive complex with α2-macroglobulin (α2M) [75]. Following its dissociation and proteolytic cleavage, it generates the C-terminal pentapeptide H-Tyr-Gly-Phe-Gly-Gly-OH (or OGP_{10-14}) [76], which is the minimal OGP-derived sequence that retains the full mitogenic activity of OGP [77]. OGP_{10-14} interacts with a yet unidentified receptor to activate an intracellular Gi-protein-MAP kinase signaling pathway, a relatively early step in the mitogenic signaling cascade MAP Kinases (Fig. 7) [78].

OGP is a peptide with several functions. *In vivo* it increases bone mass, bone formation and trabecular bone density and hematopoiesis [79, 80]. It has also been demonstrated that OGP_{10-14} induces balanced increase in white blood cell (WBC) count and overall bone marrow cellularity [81], including the engraftment of bone marrow transplants. It also regulates the expression of transforming growth factors, insulin like growth factor, and basic fibroblast growth factor. In cultured osteoblasts, OGP_{10-14} regulates proliferation, alkaline phosphatase activity,

and matrix mineralization [82], via an auto-regulated feedback mechanism. Moreover, OGP_{10-14} stimulates the differentiation of progenitor cells into osteoblasts while concurrently inhibits adipocyte formation [83].

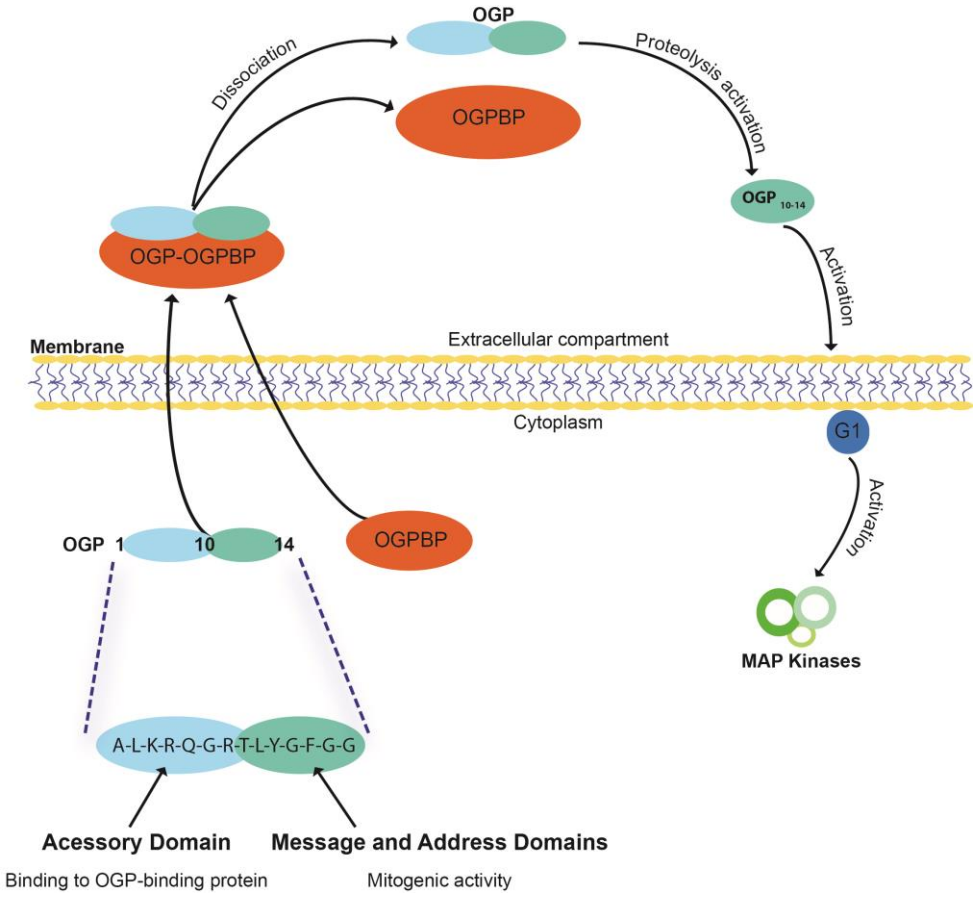

Fig. 7. OGP activation. Model of OGP activation of Gi protein-MAP kinase signaling cascade and functional domains of OGP. Adapted from [84].

When very small molecular-weight drugs, such as peptides, are loaded into alginate hydrogels simply by physical entrapment, the diffusion-controlled release kinetics is generally too fast. If a more sustained release is to be attained, it might be necessary to conjugate both components via stronger interactions such as chemical bounds. So, in this study, OGP was covalently grafted to alginate by carbodiimide chemistry as described previously. Although generally irreversible in nature, the covalent bonding may also be used for delivery purposes, if the carrier is biodegradable or if a labile drug-polymer linker is used. In the specific case of traditional alginates, the first strategy is often inadequate since their degradation in the human body is slow and unpredictable [85]. Moreover, the second approach generally provides a higher degree of versatility and efficacy, as very selective triggering mechanisms can be chosen to enable drug release in response to specific stimuli, under defined locations and/or conditions.

One interesting strategy is the use of metabolically cleavable linkers, often peptides, which are sensitive to the action of specific enzymes, particularly proteases. In this perspective, matrix metalloproteinases (MMPs) are particularly attractive as MMPs actively participate in ECM remodeling and degradation, having a key role in wound healing and tissue regeneration, and some are constitutively expressed by both naïve and differentiated human mesenchymal stem cells [70, 86]. For these reasons, they have been selected as target proteases in the present study, and the previously described PVGLIG sequence inspired the design of proteolytically-degradable linkers, which were used for the preparation of MMP-responsive alginate hydrogels for OGP delivery. In such OGP-functionalized alginate hydrogels, the rate of OGP release will depend on the cleavage kinetics of the peptide linker, the rate of diffusion of the active fragment, and the rate of matrix degradation.

2. REFERENCES

[1] Lieberman J, Friedlaender G. Bone regeneration and repair: biology and clinical applications: Humana Press:Totowa; 2006.

[2] Deschaseaux F, Sensébé L, Heymann D. Mechanisms of bone repair and regeneration. Trends Mol. Med. 2009;15:417-29.

[3] Marsell R, Einhorn TA. The biology of fracture healing. Injury 2011;42:551-5.

[4] Schindeler A, McDonald MM, Bokko P, Little DG. Bone remodeling during fracture repair: The cellular picture. Semin. Cell Dev. Biol. 2008;19:459-66.

[5] Downey PA, Siegel MI. Bone biology and the clinical implications for osteoporosis. Phys. Ther. 2006;86:77-91.

[6] Gómez-Barrena E, Rosset P, Müller I, Giordano R, Bunu C, Layrolle P, et al. Bone regeneration: stem cell therapies and clinical studies in orthopaedics and traumatology. J. Cell. Mol. Med. 2011;15:1266-86.

[7] Feng X, McDonald JM. Disorders of bone remodeling. Annu. Rev. Pathol.: Mech. Dis. 2011;6:121-45.

[8] Du J, Shan Z, Ma P, Wang S, Fan Z. Allogeneic bone marrow mesenchymal stem cell transplantation for periodontal regeneration. J. Dent. Res. 2013;13:13.

[9] Chan G, Mooney DJ. New materials for tissue engineering: towards greater control over the biological response. Trends Biotechnol. 2008;26:382-92.

[10] Reyes R, Pec MK, Sanchez E, del Rosario C, Delgado A, Evora C. Comparative, osteochondral defect repair: stem cells versus chondrocytes versus bone morphogenetic protein-2, solely or in combination. Eur. Cell. Mater. 2013;25:351-65.

[11] Zhang S, Chen L, Jiang Y, Cai Y, Xu G, Tong T, et al. Bi-layer collagen/microporous electrospun nanofiber scaffold improves the osteochondral regeneration. Acta Biomater. 2013;9:7236-47.

[12] Caplan AI. Adult mesenchymal stem cells for tissue engineering versus regenerative medicine. J. Cell. Physiol. 2007;213:341-7.
[13] Blau HM, Brazelton TR, Weimann JM. The evolving concept of a stem cell: entity or function? Cell 2001;105:829-41.
[14] Orlic D, Kajstura J, Chimenti S, Limana F, Jakoniuk I, Quaini F, et al. Mobilized bone marrow cells repair the infarcted heart, improving function and survival. Proc. Natl. Acad. Sci. U. S. A. 2001;98:10344-9.
[15] Park KS, Kim YS, Kim JH, Choi B, Kim SH, Tan AH, et al. Trophic molecules derived from human mesenchymal stem cells enhance survival, function, and angiogenesis of isolated islets after transplantation. Transplant. 2010;89:509-17.
[16] Aggarwal S, Pittenger MF. Human mesenchymal stem cells modulate allogeneic immune cell responses. Blood 2005;105:1815-22.
[17] Bianco P, Riminucci M, Gronthos S, Robey PG. Bone marrow stromal stem cells: nature, biology, and potential applications. Stem Cells 2001;19:180-92.
[18] Zuk PA, Zhu M, Ashjian P, De Ugarte DA, Huang JI, Mizuno H, et al. Human adipose tissue is a source of multipotent stem cells. Mol. Biol. Cell 2002;13:4279-95.
[19] Rosada C, Justesen J, Melsvik D, Ebbesen P, Kassem M. The human umbilical cord blood: a potential source for osteoblast progenitor cells. Calcif. Tissue Int. 2003;72:135-42.
[20] Matsumoto T, Kuroda R, Mifune Y, Kawamoto A, Shoji T, Miwa M, et al. Circulating endothelial/skeletal progenitor cells for bone regeneration and healing. Bone 2008;43:434-9.
[21] De Bari C, Dell'Accio F, Tylzanowski P, Luyten FP. Multipotent mesenchymal stem cells from adult human synovial membrane. Arthritis Rheum. 2001;44:1928-42.
[22] Miura M, Gronthos S, Zhao M, Lu B, Fisher LW, Robey PG, et al. SHED: stem cells from human exfoliated deciduous teeth. Proc. Natl. Acad. Sci. U. S. A. 2003;100:5807-12.
[23] Shi S, Gronthos S. Perivascular niche of postnatal mesenchymal stem cells in human bone marrow and dental pulp. J. Bone Miner. Res. 2003;18:696-704.
[24] In 't Anker PS, Scherjon SA, Kleijburg-van der Keur C, de Groot-Swings GM, Claas FH, Fibbe WE, et al. Isolation of mesenchymal stem cells of fetal or maternal origin from human placenta. Stem Cells 2004;22:1338-45.
[25] Crisan M, Yap S, Casteilla L, Chen CW, Corselli M, Park TS, et al. A perivascular origin for mesenchymal stem cells in multiple human organs. Cell Stem Cell 2008;3:301-13.
[26] Kern S, Eichler H, Stoeve J, Klüter H, Bieback K. Comparative analysis of mesenchymal stem cells from bone marrow, umbilical cord blood, or adipose tissue. Stem Cells 2006;24:1294-301.
[27] Friedenstein AJ, Petrakova KV, Kurolesova AI, Frolova GP. Heterotopic of bone marrow. Analysis of precursor cells for osteogenic and hematopoietic tissues. Transplant. 1968;6:230-47.
[28] Carvalho PP, Leonor IB, Smith BJ, Dias IR, Reis RL, Gimble JM, et al. Undifferentiated human adipose-derived stromal/stem cells loaded onto wet-spun starch-polycaprolactone

scaffolds enhance bone regeneration: nude mice calvarial defect in vivo study. J. Biomed. Mater. Res. A 2013;4:34983.
[29] Simoes IN, Boura JS, dos Santos F, Andrade PZ, Cardoso CM, Gimble JM, et al. Human mesenchymal stem cells from the umbilical cord matrix: successful isolation and ex vivo expansion using serum-/xeno-free culture media. Biotechnol. J. 2013;8:448-58.
[30] Jung S, Panchalingam KM, Rosenberg L, Behie LA. Ex vivo expansion of human mesenchymal stem cells in defined serum-free media. Stem Cells Int. 2012;123030:7.
[31] dos Santos FF, Andrade PZ, da Silva CL, Cabral JM. Bioreactor design for clinical-grade expansion of stem cells. Biotechnol. J. 2013;8:644-54.
[32] Patrikoski M, Juntunen M, Boucher S, Campbell A, Vemuri MC, Mannerstrom B, et al. Development of fully defined xeno-free culture system for the preparation and propagation of cell therapy-compliant human adipose stem cells. Stem Cell Res. Ther. 2013;4:27.
[33] Dominici M, Le Blanc K, Mueller I, Slaper-Cortenbach I, Marini F, Krause D, et al. Minimal criteria for defining multipotent mesenchymal stromal cells. The International Society for Cellular Therapy position statement. Cytotherapy 2006;8:315-7.
[34] Neelam Jaiswal SEH, Arnold I. Caplan, Scott P. Bruder,. Osteogenic differentiation of purified, culture-expanded human mesenchymal stem cells in vitro. J. Cell. Biochem. 1997;64:295-312.
[35] Kotobuki N, Hirose M, Takakura Y, Ohgushi H. Cultured autologous human cells for hard tissue regeneration: preparation and characterization of mesenchymal stem cells from bone marrow. Artif. Organs 2004;28:33-9.
[36] Kuznetsov SA, Krebsbach PH, Satomura K, Kerr J, Riminucci M, Benayahu D, et al. Single-colony derived strains of human marrow stromal fibroblasts form bone after transplantation in vivo. J. Bone Miner. Res. 1997;12:1335-47.
[37] Undale AH, Westendorf JJ, Yaszemski MJ, Khosla S. Mesenchymal stem cells for bone repair and metabolic bone diseases. Mayo Clin. Proc. 2009;84:893-902.
[38] Prockop DJ. Repair of tissues by adult stem/progenitor cells (MSCs): controversies, myths, and changing paradigms. Mol. Ther. 2009;17:939-46.
[39] Vo TN, Kasper FK, Mikos AG. Strategies for controlled delivery of growth factors and cells for bone regeneration. Adv. Drug Delivery Rev. 2012;64:1292-309.
[40] Kopecek Jindrich, Jiyuan Y. Hydrogels as smart biomaterials. Polym. Int. 2007;56:1078-98.
[41] Liu H, Collins SF, Suggs LJ. Three-dimensional culture for expansion and differentiation of mouse embryonic stem cells. Biomaterials 2006;27:6004-14.
[42] James J. Norman, John M. Collins, Sadhana Sharma, Brenda Russell, Desai. TA. Microstructures in 3D biological gels affect cell proliferation. Tissue Eng., Part A 2008;14:379-90.
[43] Engler AJ, Sen S, Sweeney HL, Discher DE. Matrix elasticity directs stem cell lineage specification. Cell 2006;126:677-89.
[44] Rosso F, Giordano A, Barbarisi M, Barbarisi A. From cell-ECM interactions to tissue engineering. J. Cell. Physiol. 2004;199:174-80.

[45] Lukashev ME, Werb Z. ECM signalling: orchestrating cell behaviour and misbehaviour. Trends Cell. Biol. 1998;8:437-41.
[46] MP Lutolf JH. Synthetic biomaterials as instructive extracellular microenvironments for morphogenesis in tissue engineering. Nat. Biotechnol. 2005;23:47-55.
[47] Tibbitt MW, Anseth KS. Hydrogels as extracellular matrix mimics for 3D cell culture. Biotechnol. Bioeng. 2009;103:655-63.
[48] Temenoff JS, Mikos AG. Injectable biodegradable materials for orthopedic tissue engineering. Biomaterials 2000;21:2405-12.
[49] Dreifke MB, Ebraheim NA, Jayasuriya AC. Investigation of potential injectable polymeric biomaterials for bone regeneration. J. Biomed. Mater. Res. A 2013;101:2436-47.
[50] Drury JL, Mooney DJ. Hydrogels for tissue engineering: scaffold design variables and applications. Biomaterials 2003;24:4337-51.
[51] Lee KY, Mooney DJ. Hydrogels for tissue engineering. Chem. Rev. 2001;101:1869-80.
[52] Wolf MT, Daly KA, Brennan-Pierce EP, Johnson SA, Carruthers CA, D'Amore A, et al. A hydrogel derived from decellularized dermal extracellular matrix. Biomaterials 2012;33:7028-38.
[53] Koh CJ, Atala A. Tissue engineering, stem cells, and cloning: opportunities for regenerative medicine. J. Am. Soc. Nephrol. 2004;15:1113-25.
[54] Nilasaroya A, Poole-Warren LA, Whitelock JM, Jo Martens P. Structural and functional characterisation of poly(vinyl alcohol) and heparin hydrogels. Biomaterials 2008;29:4658-64.
[55] Rowley JA, Madlambayan G, Mooney DJ. Alginate hydrogels as synthetic extracellular matrix materials. Biomaterials 1999;20:45-53.
[56] Kim JK, Kim HJ, Chung JY, Lee JH, Young SB, Kim YH. Natural and synthetic biomaterials for controlled drug delivery. Arch. Pharm. Res. 2013;7:7.
[57] Kinard LA, Dahlin RL, Henslee AM, Spicer PP, Chu C-Y, Tabata Y, et al. Tissue response to composite hydrogels for vertical bone augmentation in the rat. J. Biomed. Mater. Res., Part A 2013:n/a-n/a.
[58] Kim MJ, Park JS, Kim S, Moon SH, Yang HN, Park KH, et al. Encapsulation of bone morphogenic protein-2 with Cbfa1-overexpressing osteogenic cells derived from human embryonic stem cells in hydrogel accelerates bone tissue regeneration. Stem Cells Dev. 2011;20:1349-58.
[59] Suzuki Y, Tanihara M, Suzuki K, Saitou A, Sufan W, Nishimura Y. Alginate hydrogel linked with synthetic oligopeptide derived from BMP-2 allows ectopic osteoinduction in vivo. J. Biomed. Mater. Res. 2000;50:405-9.
[60] Arrighi I, Mark S, Alvisi M, von Rechenberg B, Hubbell JA, Schense JC. Bone healing induced by local delivery of an engineered parathyroid hormone prodrug. Biomaterials 2009;30:1763-71.
[61] Jørgensen TE, Sletmoen M, Draget KI, Stokke BT. Influence of oligoguluronates on alginate gelation, kinetics, and polymer organization. Biomacromolecules 2007;8:2388-97.
[62] Gombotz WR, Wee S. Protein release from alginate matrices. Adv. Drug Delivery Rev. 1998;31:267-85.

[63] Grant GT, Morris ER, Rees DA, Smith PJC, Thom D. Biological interactions between polysaccharides and divalent cations_ the egg-box model. FEBS Lett. 1973;32:195-9.
[64] Kuo CK, Ma PX. Ionically crosslinked alginate hydrogels as scaffolds for tissue engineering: Part 1. Structure, gelation rate and mechanical properties. Biomaterials 2001;22:511-21.
[65] Oliveira SM, Barrias CC, Almeida IF, Costa PC, Ferreira MRP, Bahia MF, et al. Injectability of a bone filler system based on hydroxyapatite microspheres and a vehicle with in situ gel-forming ability. J. Biomed. Mater. Res., Part B 2008;87B:49-58.
[66] Evangelista MB, Hsiong SX, Fernandes R, Sampaio P, Kong H-J, Barrias CC, et al. Upregulation of bone cell differentiation through immobilization within a synthetic extracellular matrix. Biomaterials 2007;28:3644-55.
[67] C. C. Barrias ML, P. L. Granja, M. C. Sá Miranda, M. A. Barbosa,. Biological evaluation of calcium alginate microspheres as a vehicle for the localized delivery of a therapeutic enzyme. J. Biomed. Mater. Res., Part A 2005;74A:545-52.
[68] Pierschbacher MD, Ruoslahti E. Cell attachment activity of fibronectin can be duplicated by small synthetic fragments of the molecule. Nature 1984;309:30-3.
[69] Fonseca KB, Bidarra SJ, Oliveira MJ, Granja PL, Barrias CC. Molecularly designed alginate hydrogels susceptible to local proteolysis as three-dimensional cellular microenvironments. Acta Biomater. 2011;7:1674-82.
[70] Fonseca KB, Maia FR, Cruz FA, Andrade D, Juliano MA, Granja PL, et al. Enzymatic, physicochemical and biological properties of MMP-sensitive alginate hydrogels. Soft Matter 2013;9:3283-92.
[71] Chau Y, Tan FE, Langer R. Synthesis and characterization of dextran−peptide−methotrexate conjugates for tumor targeting via mediation by matrix metalloproteinase II and matrix metalloproteinase IX. Bioconjugate Chem. 2004;15:931-41.
[72] Turk BE, Huang LL, Piro ET, LC. C. Determination of protease cleavage site motifs using mixture-based oriented peptide libraries. Nat. Biotechnol. 2001;19:661-7.
[73] Lee J-Y, Choo J-E, Park H-J, Park J-B, Lee S-C, Jo I, et al. Injectable gel with synthetic collagen-binding peptide for enhanced osteogenesis in vitro and in vivo. Biochem. Biophys. Res. Commun. 2007;357:68-74.
[74] Poirier R, Lemaire I, Dumont M, Leduc N, Le H-T, Lemaire S. Correlation between the expression of the histone H4 mRNA variant H4-v.1 and the levels of histone H4-(86-100) and H4-(89-102) (OGP) in various rat tissues and alveolar macrophages. Peptides 2005;26:1503-11.
[75] Greenberg Z, Gavish H, Muhlrad A, Chorev M, Shteyer A, Attar-Namdar M, et al. Isolation of osteogenic growth peptide from osteoblastic MC3T3 E1 cell cultures and demonstration of osteogenic growth peptide binding proteins. J. Cell. Biochem. 1997;65:359-67.
[76] Bab I, Gavish H, Namdar-Attar M, Greenberg Z, Chen Y, Mansur N, et al. Isolation of mitogenically active C-terminal truncated pentapeptide of osteogenic growth peptide from human plasma and culture medium of murine osteoblastic cells. J. Pept. Res. 1999;54:408-14.

[77] Chen, Muhlrad A, Shteyer A, Vidson M, Bab I, Chorev M. Bioactive pseudopeptidic analogues and cyclostereoisomers of osteogenic growth peptide C-terminal pentapeptide, OGP(10-14). J. Med. Chem. 2002;45:1624-32.
[78] Gabarin N, Gavish H, Muhlrad A, Chen Y-C, Namdar-Attar M, Nissenson RA, et al. Mitogenic Gi protein-MAP kinase signaling cascade in MC3T3-E1 osteogenic cells: Activation by C-terminal pentapeptide of osteogenic growth peptide [OGP(10-14)] and attenuation of activation by cAMP. J. Cell. Biochem. 2001;81:594-603.
[79] Hui Z, Yu L, Xiaoli Y, Xiang H, Fan Z, Ningbo H, et al. C-terminal pentapeptide of osteogenic growth peptide regulates hematopoiesis in early stage. J. Cell. Biochem. 2007;101:1423-9.
[80] Mattii L, Battolla B, D'Alessandro D, Trombi L, Pacini S, Cascone MG, et al. Gelatin/PLLA sponge-like scaffolds allow proliferation and osteogenic differentiation of human mesenchymal stromal cells. Macromol. Biosci. 2008;8:819-26.
[81] Fazzi R, Testi R, Trasciatti S, Galimberti S, Rosini S, Piras F, et al. Bone and bone-marrow interactions: haematological activity of osteoblastic growth peptide (OGP)-derived carboxy-terminal pentapeptide. Mobilizing properties on white blood cells and peripheral blood stem cells in mice. Leuk. Res. 2002;26:19-27.
[82] Spreafico A, Frediani B, Capperucci C, Leonini A, Gambera D, Ferrata P, et al. Osteogenic growth peptide effects on primary human osteoblast cultures: potential relevance for the treatment of glucocorticoid-induced osteoporosis. J. Cell. Biochem. 2006;98:1007-20.
[83] Chen Z-x, Chang M, Peng Y-l, Zhao L, Zhan Y-r, Wang L-j, et al. Osteogenic growth peptide C-terminal pentapeptide [OGP(10-14)] acts on rat bone marrow mesenchymal stem cells to promote differentiation to osteoblasts and to inhibit differentiation to adipocytes. Regul. Pept. 2007;142:16-23.
[84] Bab I, Chorev M. Osteogenic growth peptide: From concept to drug design. Pept. Sci. 2002;66:33-48.
[85] Augst AD, Kong HJ, Mooney DJ. Alginate hydrogels as biomaterials. Macromol. Biosci. 2006;6:623-33.
[86] Page-McCaw A, Ewald AJ, Werb Z. Matrix metalloproteinases and the regulation of tissue remodelling. Nat. Rev. Mol. Cell. Biol. 2007;8:221-33.

CHAPTER II

*FUNCTIONALIZATION OF BIOMATERIALS WITH SMALL OSTEOINDUCTIVE MOIETIES**

F. Raquel Maia [a,b], Sílvia J. Bidarra [a], Pedro L. Granja [a,b,c], Cristina C. Barrias [a]

[a] INEB – Instituto de Engenharia Biomédica, Rua do Campo Alegre, No. 823, 4150-180 Porto, Portugal

[b] FEUP – Faculdade de Engenharia da Universidade do Porto, Departamento de Engenharia Metalúrgica e de Materiais, Rua Dr. Roberto Frias, 4200-465 Porto, Portugal

[c] ICBAS – Instituto de Ciências Biomédicas Abel Salazar, Universidade do Porto, Rua de Jorge Viterbo Ferreira, No. 228, 4050-313 Porto, Portugal

* Acta Biomaterialia. 2013;9:8773-89

ABSTRACT

Adult mesenchymal stem cells (MSCs) are currently recognized as a powerful cell source for regenerative medicine, notably for their capacity to differentiate into multiple cell types. The combination of MSCs with biomaterials functionalized with instructive cues can be used as a strategy to direct specific lineage commitment, and can thus improve the therapeutic efficacy of these cells. In terms of biomaterial design, one common approach is the functionalization of materials with ligands capable of directly binding to cell receptors and trigger specific differentiation signaling pathways. Other strategies focus on the use of moieties that have an indirect effect, acting, for example, as sequesters of bioactive ligands present in the extracellular milieu that, in turn, will interact with cells. Compared with complex biomolecules, the use of simple compounds, such as chemical moieties and peptides, and other small molecules can be advantageous by leading to less expensive and easily tunable biomaterial formulations. This review describes different strategies that have been used to promote substrate-mediated guidance of osteogenic differentiation of immature osteoblasts, osteoprogenitors and MSCs, through chemically conjugated small moieties, both in two- and three-dimensional set-ups. In each case, the selected moiety, the coupling strategy and the main findings of the study were highlighted. The latest advances and future perspectives in the field are also discussed.

Keywords: Biomaterials; Bone regeneration; Biofunctionalization; Small moieties; Osteogenesis

1. INTRODUCTION

Stem cells, in particular adult mesenchymal stem cells (MSCs), are currently recognized as a promising cell source for tissue engineering (TE) applications and cell-based therapies, namely for bone repair and regeneration. Under appropriate *in vitro* conditions, in the presence of morphogens and specific chemicals, MSCs can be induced to differentiate along several mesodermal lineages, including osteoblastic [1]. Moreover, *in vivo*, the osteogenic potential of MSCs has been clearly demonstrated by subcutaneous implantation of MSCs within a ceramic or polymer carrier in immunocompromised mice, a common assay for evaluating ectopic MSCs differentiation into functional osteoblasts [2, 3].

In view of the current limitations associated with bone grafting procedures, the combination of MSCs with adequate vehicles or scaffolding materials has been pursued as a therapeutic strategy to promote bone repair in response to injury, which still represents a major challenge and is a global health problem. Over the past years, biomaterials have evolved from essentially ‘‘bioinert’’ materials into sophisticated substrates, with the capability to instruct cells and tune their behavior. In this context, being able to drive MSCs’ fate in a controlled manner, namely by activating their differentiation into osteoblasts, is clearly relevant [4].

The effect of a variety of biochemical and mechanical cues [5], as well as other cues, such as cell shape and size and cell–cell contacts [6–9], on osteogenic differentiation has been extensively investigated. With respect to biochemical cues, which are covered in this review, studies have focused not only on the use of prototypical signaling molecules such as growth factors (GFs), extracellular matrix (ECM) proteins and hormones, but also on a wide variety of small compounds of diverse chemical nature.

In the vast majority of available studies, these cues have been presented to cells and tissues in a soluble form, but their effect in an immobilized form and, in particular, associated with biomaterials has also been extensively investigated. Different immobilization strategies can be used to combine bioactive molecules with a substrate, including covalent bonding, physical adsorption and entrapment (Fig. 1).

This review only covers examples involving the establishment of chemical bonds between the moieties and the material, which generally provides better control over their presentation in terms of density and orientation, and improves stability [10]. Compared with more complex biomolecules, approaches involving the use of smaller and simpler compounds can be advantageous by leading to less expensive and easily tunable biomaterial formulations [11]. These approaches are reviewed herein, and compounds have been organized into three major groups, according to their nature: (i) chemical moieties; (ii) peptides; and (iii) other small molecules.

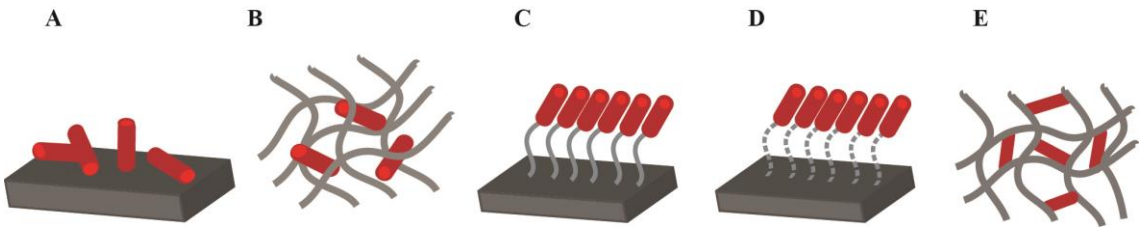

Fig. 1. Different (**A** and **B**) physical- or (**C**–**E**) chemical-based strategies can be used to immobilize a bioactive compound onto a biomaterial, such as: (**A**) adsorption; (**B**) entrapment; (**C** and **D**) covalent binding; and (E) crosslinking. Even when chemical methods are used, the compound can be subsequently released, if desirable, upon degradation of the material and/or the linker (**D**).

The modification of biomaterials with specific functional groups is probably the most straightforward strategy to induce material driven control over cell behavior. In most of the described studies, chemical groups of different character, broadly categorized as hydrophobic, hydrophilic, charged or uncharged, have been selected to convey a wide range of properties to the material surface. In a way, these moieties capture chemical features of the native ECM, as all of them are inherently present in living systems [11, 12].

The selection of the functional properties that are the most akin to specific native microenvironments can be pursued. For example, carboxylic acid groups are a prevalent chemical functionality of cartilaginous matrices, which are rich in glycosaminoglycans; negatively charged phosphate groups are present in the mineral phase of hard tissues, such as bone; and hydrophobic moieties can be associated with adipose tissues, as adipocytes are rich in lipids and secrete them into their extracellular milieu [11, 12].

Mechanistic studies using model surfaces, such as self-assembled monolayers (SAMs), provide a valuable tool for investigating how the presentation of functional groups can be used to control MSCs differentiation. Although SAMs cannot be used as implant materials, the knowledge gathered from such studies can be translated into the surface modification of scaffolds for tissue engineering, leading to more interactive and efficient materials that are able to guide the differentiation pattern of attached stem cells.

As described in Section 2, several *in vitro* studies have demonstrated that surface chemistry can not only modulate short-term cell functions, such as adhesion and morphology (Fig. 2), but also affect long-term cellular functions such as differentiation, which is remarkable, given that most cells rapidly remodel their underlying matrix [13,14].

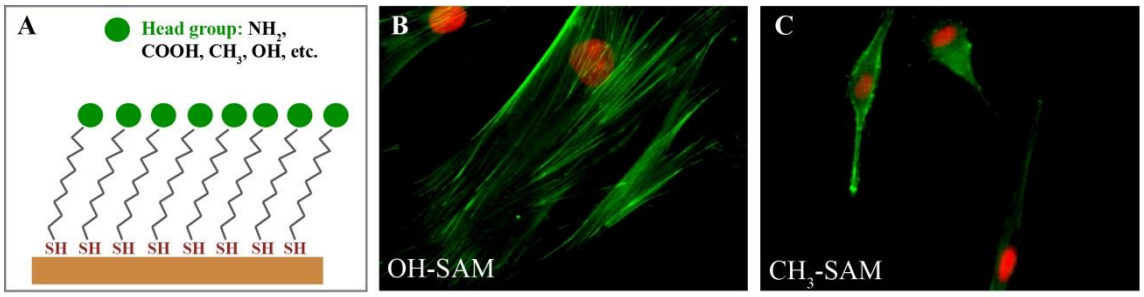

Fig. 2. (**A**) SAMs have been widely used as model surfaces to perform mechanistic studies on cell behavior. These studies clearly demonstrated that the surface chemistry modulates MSCs adhesion and morphology and, ultimately, differentiation. (**B**) In hydrophilic (OH) SAMs, human MSCs exhibit a more spread-out shape and a better organized actin cytoskeleton than in (**C**) hydrophobic (CH_3) SAMs [15].

The molecular design of cell-instructive biomaterials decorated with peptide cues has also been fostered over the last decade or so [16–30]. The rationale for this strategy relies on the inherent bioactivity of such compounds. In fact, molecular recognition is highly dependent on specific amino acid sequences present in peptides and proteins, which regulate key biological and physiological processes, thus modulating cellular function and coordinating intercellular communication. The use of synthetic analogues of peptide sequences from biologically relevant proteins presents obvious advantages over the use of the full-length protein. The latter exhibit intrinsic bioactivity, but may also concomitantly present other binding sites for non-targeted biological ligands that may trigger unwanted, and often interfering, cellular responses. Moreover, whole proteins are much more sensitive and complex to use, are more expensive, and present greater risks of immunogenicity [28]. Peptides are commonly non-toxic, as they are composed of naturally occurring or metabolically acceptable amino acids. However, although generally they do not cause severe immune responses, this possibility must be taken into account, particularly for peptides with longer sequences.

One of the first peptidic sequences to be used for biomaterial functionalization, which is still among the most widely used, is the prototypical cell adhesion sequence Arg-Gly-Asp (RGD). This motif was identified almost two decades ago by Pierschbacher and Rouslahti [31] as the minimal essential cell adhesion sequence in fibronectin (Fn), and shortly after was tested in a covalently immobilized form [32]. Different studies have addressed the effect of RGD surface density and accessibility (frequently controlled with the use of spacers), as these parameters are essential to guarantee that the peptide bioactivity is preserved [33, 34]. Although not discussed in detail herein, the density and distance are clearly important issues when considering covalent bounding of any type of bioactive molecule. For example, the RGD nanospacing has been found to regulate specific cell adhesion [35, 36]. Based upon a unique technical platform to fabricate RGD micropatterns and nanopatterns on PEG hydrogels [37–39] in their group, Wang et al. [40] recently examined MSCs differentiation on RGD nanopatterns with varied nanospacings. Their stimulating finding is that RGD nanospacing regulates stem cell differentiation, including osteogenesis, beyond cell adhesion. In fact, while it has been primarily

used as an adhesive ligand, many studies have demonstrated that RGD is in itself a mild promoter of osteogenic differentiation [25, 41–45].

However, RGD is not selective for a specific integrin, but triggers non-biased cell attachment. Moreover, *in vivo* data on the ability of RGD-modified materials to promote osseointegration and bone formation are contradictory and, in general, rather disappointing [46]. Therefore, for bone-related applications, other cell adhesion peptides have been proposed that selectively target integrin signaling cascades implicated in osteogenesis, which demonstrated improved performance.

The most highly expressed integrins in osteoblastic-like cells belong to the b1 sub-family of integrins [46]. Although data reporting the expression of the specific alpha subunit by osteoblasts has been less consistent, it is well established that the α2β1 integrin is implicated in pro-osteogenic pathways and specifically binds to regions of collagen type I, the most abundant matrix component in bone [46]. Nevertheless, the modification of biomaterials with RGD-like peptides to promote cell adhesion has been often recurrent, as cell anchorage is a prerequisite for the survival of several cell types [47, 48]. Advancements in terms of the grafting strategies and improved ligands have been reported. For example, techniques to covalently bind RGD into both hydrophobic and hydrophilic blocks have been recently set up, and the binding sites have been found to influence the cell adhesion efficacy [49].

A new and very potent peptide ligand combining both cyclic RGD and linear oligolysine has been designed to promote both specific and nonspecific cell adhesion [50]. Notably, many studies have shown that, when RGD and other osteoinductive peptides are co-grafted onto a substrate, they might actually operate synergistically to enhance osteogenic differentiation and mineralization of osteoprogenitor cells [21, 51]. Presumably, as some authors have suggested, the increased adhesion and spreading of cells onto substrate promoted through binding to RGD motifs will in turn favor the interaction of the other peptides with specific cell surface receptors, potentiating their action. Other Fn- derived peptide fragments have shown higher specificities for key integrins, such as α5β1, with important roles in the control of MSCs osteogenic differentiation [46, 52]. In fact, independently of the activation state of α5β1 integrins, RGD alone seems to be insufficient to promote binding, even if it serves to activate and align the α5β1 – Fn interface, and the simultaneous presence of the PHSRN synergy site is required to provide the mechanical strength of the bond [53].

To specifically promote osteoblastic differentiation and matrix mineralization, different peptide sequences derived from the active domains of typical bone ECM proteins, such as collagen type I (COL-I), osteopontin (OPN), osteocalcin (OCN) and bone sialoprotein (BSP), have been suggested. Peptides derived from bone-related GFs (such as bone morphogenetic proteins, BMPs) and peptide/protein hormones with recognized anabolic effects in bone (such as the parathyroid hormone, PTH) have also been suggested. Most of these peptides are expected to directly interact with cell receptors, activating particular signaling pathways similarly to their parental proteins. Alternatively, the immobilized peptides can have an indirect action, by promoting the non-covalent sequestering of key biomolecules present in the extracellular milieu

that, in turn, will exert their bioactivity [54–56]. In a way, these ‘‘indirect’’ strategies set up a new paradigm in biomaterials design, in the sense that these sequestered signaling compounds are not directly presented by the biomaterial. In addition, peptides themselves are paving the way as new biomaterials.

This is the case of a new class of ‘‘smart’’ peptides, which self-assemble into nanofibers and create self-supporting hydrogels that can be used to culture cells under three-dimensional (3-D) conditions. These self-assembling (SA) peptides have been broadly proposed for the therapeutic regeneration of different tissues, including bone [57, 58]. The bioactivity of these peptides can be molecularly tailored by changing their amino acid composition. In a common approach, the original SA sequence is extended, generally at one of its termini, with specific bioactive domains.

Finally, there are a vast number of other classes of small compounds, including dexamethasone and statins, which have also been used as osteoinductive compounds, and these are described briefly here. Collectively, the examples provided in this review are intended to be illustrative rather than inclusive. Importantly, for these compounds to have impact on the field, they must be suitable for use in a wide variety of biomaterials for bone regeneration. As described throughout the text, by selecting appropriate chemical routes, all these small molecules can in theory be used in the functionalization of different classes of materials, including polymers, ceramics, metals and composites, and processed in a variety of ways, such as films, membranes, microparticles, porous TE scaffolds and hydrogel-based cell-encapsulation systems (Fig. 3).

Polymers are the most common material class as they are quite versatile, offering a huge diversity in terms of nature, properties and composition. Additionally, they are generally easy to functionalize, as they intrinsically present adequate reactive groups to directly engage in different chemical modification schemes. Depending on the original material chemistry, pre modification steps to introduce adequate reactive groups might be needed, prior to functionalization with bioactive moieties. On the other hand, the bioactive moieties themselves might be directly reacted to the material or be previously modified. For example, in the case of peptides, the simplest grafting procedures involve a direct coupling via peptide N-terminal and C-terminal groups, or thiol groups present in terminal cystein residues. More complex procedures require the pre-derivatization of peptides with different coupling functionalities, such as azides and acryloyl groups. In special cases, such as SA peptides or recombinant proteins, bioactive amino acid sequences are directly incorporated during biomaterial synthesis.

Table 1 presents some examples of functionalization strategies employed in the covalent modification of different biomaterials with peptides. Throughout this review, the different chemical routes used for the functionalized of biomaterials with different small moieties are described in detail. Within each category of materials, examples describing both surface modifications (when performed after substrate/scaffold formation) and bulk modifications (when performed before scaffold formation) are provided.

Table 1. Examples of functionalization strategies to covalently modify different biomaterials with peptides.

Material	Material reactive group	Reactive group modification	Peptide reactive group	Reactive group modification	Material-peptide coupling reaction	Ref.
Ceramics						
HA/β-TCP	Hydroxyl OH–	Silanization to create NH_2- followed by reaction with PEG disuccinimidyl succinate	NH_2–	–	NHS ester–NH_2 coupling	[59]
HBPs	Hydrazine N_2H_4–	–	OH– (N–terminal Ser)	Oxidation to create CHO–	Hydrazone linkage	[60]
Skelite$_{TM}$	Hydroxyl OH–	Silanization to create NH_2- followed by succinylation to create a NHS ester	NH_2–	–	NHS ester–NH_2 coupling	[61]
Synthetic polymers						
PEG	Hydroxyl OH–	Acrylation to create H_2C=CH–C(=O)–	S– (N–terminal Cys)	–	Thiol-Acrylate coupling	[62]
PET	Carbonyl	Oxidation to create COOH-	NH_2–	–	Carbodiimide chemistry (EDC/NHS)	[63]
pACAA	Carboxyl COOH-	–	NH_2–	–	Carbodiimide chemistry (EDC/NHS)	[64]
PLEOF	Fumarate	Incorporation of propargyl acrylate during hydrogel formation	NH_2–	Derivatization with PEG–N_3 during synthesis	Click chemistry	[21, 65]
	Aldehyde CHO–	–	NH_2–	Derivatization with aminooxy group during synthesis	Oxime ligation	[65]
PLGA-(PEG-ASP)n	Amine NH_2–	–	COOH–	–	Carbodiimide chemistry	[66]
PLGA	Carboxyl COOH–	Derivatized with hydrazide by carbodiimide chemistry	OH– (N–terminal Ser)	Oxidation to create CHO–	Hydrazone linkage	[67]
PEU	–CH_2–		N– and C–termini	Symmetrically functionalized with Lys grafted w/ vinyl groups during synthesis	UV-activated reaction of −CH=CH_2 with –CH_2–	[68]
Natural polymers						
Silk fibroin	Carboxyl COOH–	–	NH_2–	–	Carbodiimide chemistry (EDC/NHS)	[30]
Alginate	Carboxyl COOH–	–	NH_2–	–	Carbodiimide chemistry (EDC/NHS or EDC)	[17, 69] [70]
Agarose	CH–	–	NH_2–	Linked to the NHS-ester of heterobifunctional sulfo-SANPAH	UV-activated reaction of sulfo-SANPAH with CH–	[71]

Cys – cysteine; HA/b-TCP – hydroxyapatite/beta-tricalcium phosphate; HBPs – hydrazine-bisphosphonates; Lys – lysine; OPF – oligo[poly(ethylene glycol) fumarate; pACAA – poly(acrylic acid-co-acrylamide); PCL – polycaprolactone; PEG – polyethylene glycol; PET – polyethylene terephthalate; PEU – polyether urethane; PLEOF – poly(lactide-co-ethylene oxide fumarate); PLG – poly(lactide-co-glycolide); SAMs – self-assembly monolayers; SAP – self-assembling peptide.

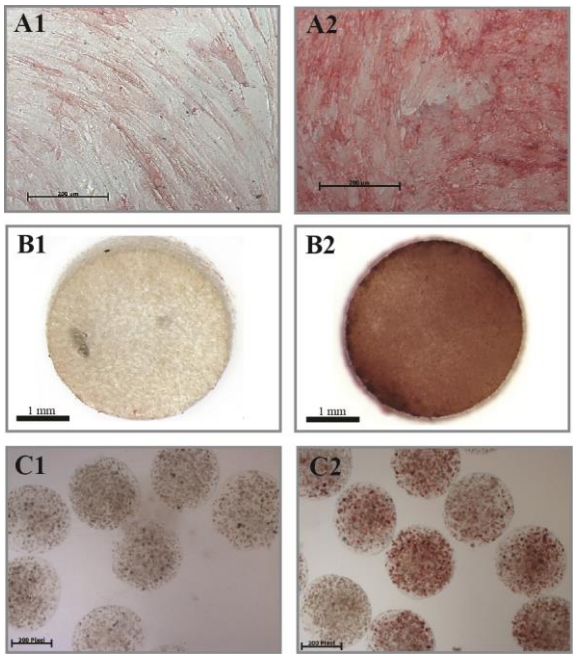

Fig. 3. Osteogenic differentiation of MSCs cultured in different types of materials, namely: (**A**) 2-D surfaces (tissue culture polystyrene); (**B**) 3-D porous scaffolds (chitosan sponge); and (**C**) 3-D hydrogel matrices (alginate microspheres). Upon incubation under standard osteoinductive conditions, differentiated MSCs express high levels of ALP activity (pink staining; A2, B2, C2), a common osteoblastic phenotypic marker.

2. OSTEOINDUCTIVE CHEMICAL GROUPS

2.1. Surface-immobilized chemical groups

SAMs have emerged as an important tool to investigate the effect of specific surface chemistries on stem cell differentiation due to their controllable surface properties [72]. SAMs represent a class of well-ordered organic substrates formed by the adsorption of an active surfactant on a solid surface [73, 74]. SAMs formed via chemisorption of alkanethiolates onto gold-coated substrates are currently considered to be the best available class of model organic surfaces, allowing significant control over chemical properties of the underlying substrate [14, 72, 75, 76]. A key advantage of this system is the simple creation of well-defined and reproducible surfaces presenting a wide range of chemical moieties, which allow the control of protein–surface and cell–surface interactions [14, 77]. Although SAMs can only be used as model surfaces, results from these studies have been laying the groundwork for more complex studies with ‘‘real’’ implant biomaterials towards the identification of surface chemistries that are optimal to achieve the fine control over MSCs differentiation in clinical applications.

Most of the published studies have demonstrated that cell interactions with surfaces are indirectly mediated by the characteristics of a pre-adsorbed protein layer, and the pattern of

protein adsorption has been correlated with the underlying surface chemistry [15, 73, 78–94]. In fact, when a surface comes into contact with a protein-rich physiological medium, it instantaneously becomes coated with layers of adsorbed proteins, which will in turn direct the binding of cell adhesion receptors. The type, amount, conformation and surface distribution of adsorbed proteins modulate focal adhesion formation and intracellular signaling cascades, eventually leading to changes in initial adhesion and the long-term differentiation of cells [15, 85]. Here, a selection of mechanistic studies performed with SAMs and other model surfaces is provided, where it was possible to identify chemical functionalities that were claimed to effectively promote or enhance osteogenic differentiation of MSCs, either in basal or pro-osteogenic conditions. Table 2 summarizes the main findings of the described studies. Phillips and co-authors analyzed [14] SAMs functionalized with four different functional groups, namely methyl ($–CH_3$,), hydroxyl (–OH), carboxyl (–COOH) and amino ($–NH_2$), and were able to demonstrate that the surface chemistry has an effect on the pattern of Fn adsorption, which in turn modulates the osteogenic differentiation of human MSCs (hMSCs). Differences in Fn conformation promoted different integrin–ligand interactions and the consequent activation of different intracellular signaling pathways [85]. In particular, NH_2-SAMs pre-coated with Fn promoted the strongest induction of hMSCs differentiation along the osteoblastic lineage under osteoinductive medium. On this surface, mineralized nodules were primarily observed, alizarin red staining for calcium showed the greatest enhancement, and Runx2, BSP and OCN expression were significantly up-regulated comparing to control surfaces (gold-coated tissue culture polystyrene, TCPS). It is noteworthy that, although the other functionalities also showed some evidence of osteoinductivity, they only affected the global magnitude of one or two phenotypic markers. In fact, only in NH_2-SAMs was it possible to demonstrate how a single surface variable predicts the most profound effect on lineage commitment. Using silane-modified glass surfaces as models, Curran et al. [13] investigated the effect of the same chemical groups and also thiols (–SH) on hMSCs behavior. Again, hMSCs cultured on positively charged NH_2 surfaces were shown to be more likely to differentiate along the osteogenic lineage, rather than maintaining an undifferentiated phenotype or differentiating into other cell types. After 7 days, hMSCs cultured on these surfaces showed higher levels of viable cells adhering and also an increase in mRNA expression of Cbfa-1 (bone transcription factor) compared to day 1, and decreases in COL-I, COL-II, transforming growth factor b (TGF-β) and ornithine decarboxylase (a proliferation marker). Significantly, in this particular study, cells were cultured in basal growth medium, without soluble osteoinductors, allowing a direct correlation between surface chemistry and cell behavior. Although not studied in detail, the pattern of protein adsorption to NH_2 surfaces, and particularly the presence of adsorbed vitronectin, might have contributed to early osteogenic signaling, as suggested by the authors. Unfortunately, the unexpected decrease in COL-I expression were not discussed. The same authors subsequently performed a similar study in which hMSCs behavior was monitored for a longer period of time (28 days) in the presence of basal and osteoinductive media [12]. The results from this study are somewhat confusing, as all the surfaces up-regulated at least one osteogenic gene at

certain time points. In accordance with the previous results, however, NH_2 surfaces were the ones that promoted and maintained cell osteogenic differentiation better overall, both at the gene and protein levels, in the presence and absence of biological stimuli. Interestingly, SH surfaces also had a positive effect on osteogenesis, with the up-regulation of OCN and Cbfa1 compared to control samples being observed at different time points, both in the presence and absence of biological stimuli. This was surprising, since in the previous study [13] –SH surfaces resulted in the decreased expression of proliferation and osteogenic markers after 1 week of culture in basal conditions, though this issue was not discussed.

A number of other chemical functionalities have been investigated with regard to their ability to promote osseointegration. For instance, using the $H_3PO_4/P_2O_5/Et_3PO_4$/hexanol method, Granja et al. [95] grafted phosphate functionalities onto regenerated cellulose surfaces to enhance its bioactivity, inspired by the role of phosphoproteins in biomineralization. They demonstrated *in vitro* that the calcium salt of cellulose phosphate induces the mineralization of the surface, but the highly negatively charged surfaces promoted poor attachment, proliferation and differentiation of human bone marrow stromal cells [96].

This influence of chemical functionality and surface charge seems to be in agreement with the previously discussed effect of positively charged SAM surfaces. *In vivo*, phosphorylated surfaces promoted slightly better osseointegration than non-modified surfaces [96].

2.2. Bulk-immobilized chemical groups

Murphy *et al.* [97] proposed a chemical method for the preparation of silk fibroin derivatives with tailored structure and hydrophilicity, carrying different chemical groups, both hydrophilic (carboxyl, amino and sulfonic acid) and hydrophobic (ketone and heptyloxy). The diazonium coupling chemistry was chosen to target the tyrosine residues, as these are homogeneously distributed along the protein molecules and are present in sufficient amounts [97]. hMSCs were cultured at the surface of modified-silk (azo-silk) films and, after 1 week of culture under osteoinductive conditions, higher expression of alkaline phosphatase (ALP) and COL-I was observed in all silk derivatives compared to non-stimulated cultures. Surprisingly, the variation in the functional groups attached to the silk did not differentially affect the pattern of hMSCs differentiation. The authors did not provide an explanation for this, but proposed future studies to investigate whether azo-silk derivatives with higher surface charge (carboxylic and sulfonic acid) could enhance mineralization.

The effect of phosphoesters on hMSCs differentiation was evaluated in a poly(ethylene glycol) (PEG) dimethacrylate-based cell encapsulation system [98]. Phosphate-containing hydrogels were obtained via photopolymerization of the macromer precursor PEG-di-[ethylphosphatidyl (ethylene glycol) methacrylate], which incorporates PO_4-containing degradable polyester linkages [98, 99]. Co-gels were prepared by combining PhosPEG with PEG. Compared to PEG gels, and in the absence of growth factors or other inducers,

PhosPEG–PEG co-gels increased the gene expression of bone-specific markers (COL-I, ALP and osteonectin (ON)), secretion of bone-related matrix (ON and OCN) and mineralization (both in a cellular and cellularized gels). In this case, the phosphate moieties in the hydrogel backbone played multiple key roles, as they not only acted as osteoinductive moieties, but also provided a site for ALP-responsive scaffold degradation, which, in turn, produced functional groups that promoted autocalcification.

Benoit et al. [11] tested the effect of amino, t-butyl, phosphate (PO_4), fluoro and carboxylic acid groups on hMSCs differentiation, also with the aim of developing PEG-based cell-encapsulating hydrogel systems. In a first stage, hMSCs were cultured on arrays of functionalized-PEG spots, as a 2-D screening platform. Some selected groups, and in particular PO_4 groups, shown to induce osteogenesis, were then tethered to 3-D PEG hydrogels, and their effect on the differentiation of encapsulated hMSCs was evaluated. These, PO_4-PEG hydrogels were prepared by photopolymerization of PEG monomers with ethylene glycol methacrylate phosphate [11,100,101]. Importantly, hydrogels were designed to have different chemistries, and hence different charges and hydrophilicities, but comparable matrix properties, such as stiffness and swelling [11]. In addition, 3-D cultured cells were trapped in a rounded morphology, irrespectively of the material chemistry, in an attempt to eliminate confounding factors and show how a synthetic matrix could modulate hMSCs commitment solely through interactions with small chemical groups. As predicted from the 2-D studies, 3-D encapsulation of hMSCs in PO_4-PEG hydrogels led to osteogenic differentiation in the absence of inducers, as suggested by the up-regulation of Cbfa1 expression and the secretion of a COL-I and OPN-rich ECM [11].

In a previous work, the same group had demonstrated improved viability of hMSCs encapsulated in PO_4-PEG, as compared to unmodified PEG, as the former promoted the formation of an apatite-like mineral phase that sequesters OPN, which in turn mediates cell–gel interactions [100,101].

Recently, the authors tried to uncover the mechanisms that underlie the effect of PO_4-PEG on osteogenesis [102]. hMSCs were shown to attach and spread at the surface of PO_4-PEG hydrogels only in the presence of serum proteins, and cell attachment to adsorbed matrix components (Fn and COL-I) was partially mediated by integrins β1 and β3. Inhibition of focal adhesion kinase (FAK) phosphorylation resulted in down-regulation of the expression of osteogenic markers, suggesting the involvement of an outside-in signaling pathway.

Collectively, these examples clearly demonstrate that the presence of small molecules, in this case negatively charged phosphate groups, promoted a specific pattern of ECM protein adsorption, which in turn directed hMSCs differentiation down the osteogenic lineage without using induction medium.

Table 2. Effect of different chemical groups on hMSCs osteogenic differentiation *in vitro*.

Chemical group	Surface properties	Substrate	Main observed effects	Ref.
– CH_3	Hydrophobic	SA of alkanethiols on gold (pre-coated with Fn)	Supported hMSCs differentiation in OM (similar to control)	[14]
		SA of alkoxysilanes on Glass	Supported hMSCs differentiation in OM (similar to control) *	[12, 13]
		Silk fibroin	Supported hMSCs differentiation in OM (similar to control)	[97]
– OH	Hydrophilic Neutral	SA of alkanethiols on gold (pre-coated with Fn)	↑of Runx2 mRNA in OM	[14]
		SA of alkoxysilanes on Glass	↓of COL-I mRNA in BM	[13]
			Did not support hMSCs differentiation in BM and OM (< control) *	[12, 13]
– COOH (– COO^-)	Hydrophilic Negative	SA of alkanethiols on gold (pre-coated with Fn)	↑of Runx2 mRNA in OM ↑ mineralization	[14]
		SA of alkoxysilanes on Glass	↑of COL-I mRNA in BM	[13]
			Did not support hMSCs differentiation in BM and OM (< control) *	[12, 13]
		Silk fibroin	Supported hMSCs differentiation in OM (similar to control)	[97]
– NH_2 (– NH_3^+)	Hydrophilic Positive	SA of alkanethiols on gold (pre-coated with Fn)	↑Runx2, OCN mRNA in OM, ↑ mineralization	[14]
		SA of alkoxysilanes on Glass	↑of Cbfa and ↓COL-I in BM	[13]
			Promoted hMSCs differentiation in BM and OM (> control) *	[12, 13]
		Silk fibroin	Supported hMSCs differentiation in OM (similar to control)	[97]
– SH	Hydrophilic Neutral	SA of alkoxysilanes on Glass	↓of COL-I and Cbfa1 mRNA in BM	[13]
			Promoted hMSCs differentiation in BM and OM (> control) *	[12, 13]
– SO_3H (– SO_3^-)	Hydrophilic Negative	Silk fibroin	Supported hMSCs differentiation in OM (similar to control)	[97]
– C=O	Hydrophobic	Silk fibroin	Supported hMSCs differentiation in OM (similar to control)	[97]
– PO_3 (– PO_4^-)	Hydrophilic Negative	PEG	↑of several osteogenic markers at gene and protein levels in BM	[11, 100-102]

ALP – alkaline phosphatase; BM – Basal medium; Col-I – collagen type I; hMSCs – human mesenchymal stem cells; OM– osteoinductive medium; PEG – poly (ethylene glycol); SA – self-assembly; ↓ – decreased; ↑ – increased.
* According to the expression of osteogenic markers (OCN; Cbfa1) at the protein level as analysed by immunocytochemistry. RT-PCR results were not included due to their complexity.

3. OSTEOINDUCTIVE PEPTIDES

The general use of osteoinductive peptides in bone regeneration has been recently reviewed by Jabbari [103]. The use of ECM-derived and GF-derived peptides for implant functionalization to promote osseointegration and enhance bone healing within large defects has also been reviewed by Shekaran and García [46]. Although several recent reports exist uncovering the potentialities of new osteoinductive peptides, including collagen-binding peptides from BSP [104], peptides based on the prodomain region of BMP-7 [105], neuropeptides [106,107] and amelogenin-derived peptide sequences present in enamel matrix proteins [108], no studies using such peptides in a covalently immobilized form have been found. Here, an overview of studies exploring the effect of scaffold-grafted peptides on osteogenic differentiation

and bone healing is provided. All peptide sequences are written, according to the usual standards, from the N-terminus to the C-terminus. A compilation of covalently immobilized peptide sequences tested as osteoinductors is presented in Table 3.

3.1. BMP-derived peptides

BMPs are a group of 18 proteins belonging to the TGF-β family. Among them, BMP-2, -7 and -9 are the ones involved in the development of the skeleton and bone formation and remodeling [109–111]. They interact with the BMPR-type I and BMPR-type II cell receptors, which activate different signaling pathways. One of them involves the activation of LIM kinase-1 and has implications on cytoskeleton dynamics [112]; the other involves activation of Smad1/5/8 and its translocation into the nucleus, where it regulates the expression of some osteogenic genes [113–116]. In the case of BMP-2, the majority of its peptide derivatives was obtained from the ‘‘wrist’’ and ‘‘knuckle’’ epitopes of the parental protein, and preferentially interact with type I and type II cell surface receptors, respectively [110,117–119]. BMPs are potent osteoinductive agents, but their clinical use is often limited by their short biological half-life, rapid local clearance, propensity for side effects and high cost [120]. Some of these limitations can be partially overcome by the use of BMP-derived peptides, particularly when used in association with biomaterials.

3.1.1. Surface immobilization of BMP-derived peptides

Using SAMs, Moore and colleagues [51] investigated the synergistic and concentration-dependent effects of the peptides RGD and KIPKASSVPTELSAISTLYL (73–92 residues of the knuckle epitope of BMP-2) [19] on bone marrow stromal cells (BMSCs). Both peptides were derivatized with azide (N_3-GRGDS and N_3-KIPKASSVPTELSAISTLYL) and grafted onto alkyne-SAMs by click chemistry, alone or combined at a 1:1 M ratio, in gradients of 0–140 pmol cm^{-2}. Human BMSCs were seeded onto peptide-modified surfaces and cultured in the absence of osteoinductive supplements for 21 days. Runx2 expression increased in the presence of the BMP-2 peptide, when grafted at 80–120 pmol cm^{-2}, but not in the presence of RGD alone. When both peptides were present (1:1, total of 130 pmol cm^{-2}) there was a synergistic enhancement of BSP expression and some signs of mineralization. This study reinforced the idea that, by providing cell-attachment sites, RGD peptides improve the interaction of BMP-2 peptide with its receptors. Unexpectedly, cell proliferation and BSP expression also increased in the presence of COOH groups alone (200 pmol cm^{-2}), which seems to contradict previous reports [11]. It was hypothesized that COOH groups might interact electrostatically with exogenously expressed proteins, including BMP-2, and increase their accessibility.

Zouani and colleagues [63] tested a very similar BMP-2 derived sequence (RKIPKASSVPTELSAISMLYL) and also two other sequences, derived from BMP-7

(RTVPKPSSAPTOLNAISTLYF, residues 89–117) and BMP-9 (RKVGKASSVPTKLSPISILYK, residues 68–87). RGD peptides were also used to promote cell adhesion. Peptides were grafted through their terminal amines to the COOH groups of oxidized poly (ethylene terephthalate) (PET) by carbodiimide chemistry at the same initial concentration (10^{-3} M). Murine pre-osteoblastic MC3T3-E1 cells were cultured on PET surfaces in osteoinductive medium. Throughout the first 12 h, however, cells were maintained without serum to avoid its proteins from interfering in the initial BMP peptide–cell interaction, which is something that cannot be replicated in an *in vivo* environment. After 24 h, several osteogenic markers were shown to be up-regulated in all BMP–RGD–PET surfaces, namely Runx-2, BSP, OPN and ALP, as compared to oxidized PET and RGD–PET, suggesting that BMP peptides effectively interacted with cell membrane receptors. Unsurprisingly, BMP-2 presenting surfaces were the more osteoinductive ones, which was further confirmed by an increased production of endogenous ECM. These differences were correlated with cell morphology. Moreover, BMP-presenting surfaces, and especially those with BMP-2, increased the mRNA expression of different GFs (BMP-2, TGF-β1 and VEGF), BMP receptors and OCN during 72 h of culture, as well as the extent of mineralization after only 5 days of culture. Overall, these results confirm the possible advantages that BMP-2 peptides may present over other peptides.

More recently, the interplay between biochemical (BMP-2 peptides) and mechanical cues on hMSCs differentiation was addressed by the same group [64]. RGD and RKIPKASSVPTELSAISMLYL were grafted onto poly (acrylamide-co-acrylic acid) (pACAA) surfaces of different stiffnesses through carbodiimide chemistry. hMSCs sensed the different mechanical environments, committing into muscle-like and osteoblast-like cells on RGD–pACAA surfaces with 15 and 48 kPa stiffnesses, respectively, after 96 h of culture. The authors were able to show that the effect of biochemical stimuli may overlap those of mechanical ones (whenever stiffness >13 kPa), as hMSCs only differentiated along the osteogenic lineage when BMP-2 peptides were present. However, osteogenic differentiation was inhibited on the softer BMP-2 surfaces (0.76–3.21 kPa), which presumably did not promote a favorable F-actin cytoskeleton reorganization, which is essential for BMP-induced Smad1/5/8 phosphorylation and nuclear translocation, as the authors also demonstrated. The results from this study contribute to uncovering the key role of matrix mechanical properties during osteogenesis and, importantly, their coordination with the biochemical environment.

He and colleagues [21] tested the same BMP-2 sequence, KIPKASSVPTELSAISTLYL, in the form of an azide-functionalized PEGylated peptide (Az-mPEG–BMP), which was grafted onto RGD-modified or unmodified hydrogels of poly(lactide-co-ethylene oxide fumarate) (PLEOF) by click chemistry. The final peptide concentrations used on cell studies were 1.6 pmol cm^{-2} for RGD and 5.2 pmol cm^{-2} for BMP-2, respectively. Under osteoinductive conditions, ALP activity and mineralization of rat BMSCs were similar in BMP2–PLEOF and RGD–PLEOF hydrogels, but when both peptides were present they acted synergistically to enhance cell differentiation. In a more recent study [65], the OPN-derived sequence SVVYGLR (OPD peptide), which corresponds to residues 162–168 of OPN and is known to influence

vasculogenesis [121], was used as a third peptide. For orthogonal grafting, the RGD–PLEOF hydrogel was first conjugated with propargyl acrylate to create alkyne moieties and with 4-pentenal to create aldehyde moieties, then reacted with Az-mPEG–BMP and aminooxy-mPEG–OPD peptides by click reaction and oxime ligation, respectively. The final peptide concentrations used on cell studies were 13.8 pmol cm^{-2} for OPD and 5.4 pmol cm^{-2} for BMP-2. Rat BMSCs were seeded on top of hydrogel disks and cultured in osteoinductive medium supplemented with vasculogenic factors for 28 days. The tested groups included hydrogels with RGD, RGD + BMP2, RGD + BMP2 + mOPD (a mutated OPD) and RGD + BMP2 + OPD peptides. The RGD hydrogels co-functionalized with OPD and BMP-2 yielded the best results in terms of ALP activity, mRNA expression of OPN and OC, and extent of mineralization. Moreover, both peptides were essential for the expression of vascular markers such as PECAM-1, α-SMA and VE-cadherin. In summary, the three peptides (RGD + BMP2 + OPD) acted cooperatively to provide a favorable microenvironment for concomitant BMSCs osteogenesis and vasculogenesis.

Lin et al. [66] changed the terminal residues (underlined) of the previously described BMP-2 peptide, and showed that the sequence $S^{[PO4]}$ KIPKASSVPTELSAISTLYLDDD (designated by P24) was able to induce bone formation. P24 has a high content of D and (phosphorylated) S that might promote apatite nucleation and enhance mineralization. The peptide was coupled by carbodiimide chemistry through its terminal COOH groups to the amine groups of a biodegradable copolymer of poly(lactic-co-glycolic acid) (PLGA) with segments of PEG and aspartic acid units (PLGA–(PEG–Asp)n) [66,122]. The incorporated PEG and Asp increased the polymer hydrophilicity and provided anionic functional groups that acted as peptide-binding sites. The aim was to use the P24-modified scaffolds as a delivery system for the sustained release of P24. *In vitro*, in osteoinductive medium, the ALP activity and mineralization pattern of rat BMSCs cultured on P24-modified scaffolds were increased compared to on unmodified membranes. Moreover, these scaffolds promoted ectopic bone formation upon subcutaneous implantation in rats. Their performance was significantly better than that of the other groups (unmodified scaffolds or gelatin sponges), as demonstrated by radiographic and histological examination, Western blotting and reverse transcriptase-polymerase chain reaction (COL-I and OPN).

3.1.2. Bulk immobilization of BMP-derived peptides

One successful demonstration of ectopic bone formation using a covalently immobilized BMP-2-derived peptide was provided by Suzuki and colleagues in 2000 [17]. The authors prepared covalently crosslinked alginate hydrogel scaffolds by reacting 1-ethyl-(dimethylaminopropyl)-carbodiimide (EDC) and sodium alginate in aqueous solution, followed by freeze-drying. The peptide, with the sequence NSVNSKIPKACCVPTELSAI, was grafted onto alginate COOH groups by carbodiimide chemistry. A control material was prepared by mixing

the same amount of peptide with alginate but without the coupling agent, resulting in simple entrapment (10 mg of alginate with 180 μg of peptide). Both materials were implanted for 3 and 8 weeks in the calf muscle of Wistar rats. The formation of new bone tissue and vascular channels was only observed in the group with the covalently grafted peptide, highlighting the advantages of this type of immobilization. Surprisingly, given that alginate is non-cell adhesive, good results were obtained even in the absence of RGD peptides. The authors highlighted the importance of further characterizing the time course and dose–response dependence of the observed effects, but no subsequent studies using this exact peptide sequence have been found.

In a subsequent study, Saito and co-workers [70] tested the slightly different sequence KIPKASSVPTELSAISTLYL (already described above). In its soluble form, this peptide was shown to increase ALP activity in the murine multipotent stromal cell line C3H10T1/2, and interact with both types of BMP receptor [19]. Peptide–alginate hydrogel scaffolds were prepared using the methodology described above, and implanted in the same animal model (3 mg of alginate with 75 μg of peptide) [70]. Collagen gels impregnated with recombinant BMP-2 (3 mg of collagen with 3 μg of protein) were used as a control. While the peptide–alginate gel showed prolonged formation of a calcified bone-like tissue for up to 7 weeks, with large numbers of osteoblasts, the control exhibited maximal calcification after 3 weeks, which progressively disappeared, probably being absorbed by osteoclasts, which were present in large amounts. Apparently, in contrast to the impregnated protein, the grafted peptide remained active at the implant site, exerting a continuous local effect. The differences between the materials (alginate vs. collagen) and the quite different molar amounts of peptide vs. protein implanted were not, however, taken into account when the results were discussed.

Using a different rationale, Lee and co-workers [58] tested the osteoinductive effect of several domains from human BMP-2, corresponding to residues 1–25, 26–50, 51–75 and 76–110. The segment 26–50, which provided the best results in terms of cell adhesion, was further segmented into short 4–5 amino acid sequences (VGWN, DWIVA, PPGYH, AFYCHG, and ECPFP), and out of these the sequence DWIVA was the one that presented the highest binding activity to BMP receptors type IA and II. A hydrophobic aliphatic tail (C16) tail was attached to DWIVA, via an amide bond, to create a self-assembling peptide (SAP). In the presence of calcium, this amphiphile self-assembles into a nanofibrous hydrogel with surface-exposed DWIVA (or DFMLG, a control non-bioactive sequence). hMSCs were entrapped within this hydrogel and cultured under osteoinductive medium. Higher levels of phosphorylated Smad, ALP activity and mineralization were found in cells cultured within the DWIVA-SAP hydrogels, as compared to the control. Similar results were obtained when cells were treated with even higher concentrations of free peptide (1.67 vs. 0.7 mM), indicating that the bioactivity of DWIVA is retained upon immobilization.

3.2. Collagen type I-derived peptides

The most highly expressed integrins in osteoprogenitors and osteoblasts belong to the β1 sub-family, being predominant mediators of cell adhesion in these cells [46]. The α2β1 integrin is highly expressed on osteoblasts, being one of the major adhesion receptors for COL-I [123]. The interactions between this integrin and its ligand activate focal adhesion kinases, and initiate key pathways for the induction of osteoblastic differentiation and matrix mineralization [28,124]. Based on this, COL-I-derived peptides have been used as cell adhesion mediators to ultimately induce osteogenic differentiation, as previously pointed out.

3.2.1. Surface immobilization of COL I-derived peptides

Wang and co-workers [61] selected the bone and cartilage synthetic peptide ($BCSP_{TM}$-1), derived from human COL-I, with the sequence NGLPGPIGP. $BCSP_{TM}$-1 was chemically bound to a commercial ceramic surface ($Skelite_{TM}$) in three steps. First, amine moieties were created at the ceramic surface by grafting (3-amino-propyl) triethoxysilane (APTES) to free hydroxyl groups through silanization. Then, through succinylation, amine functionalities were converted into esters, to which peptides where grafted via their terminal amines. Rat calvaria cells were first cultured for 3 days with 0.28 mM of ascorbic acid and then seeded on peptide-bound ceramic surfaces with different peptide densities for 10 days. The specific ALP activity on these surfaces was nearly three-fold higher than in control non-modified ceramics, being the maximum activity achieved at a peptide density of 0.87 nmol cm^{-2}.

3.2.2. Bulk immobilization of COL I-derived peptides

A more complex triple helical sequence with the COL-I-derived motif GFOGER has also been proposed. GFOGER corresponds to residues 502–507 of the α1 chain of COL-I and selectively binds to α2β1 integrin [125]. Promising results were obtained when this peptide was used to non-covalently coat titanium surfaces. Compared to untreated Ti, GFOGER-Ti triggered osteoblastic differentiation and mineral deposition *in vitro*, and enhanced osseointegration *in vivo* [28]. Good osseointegration was also observed when the same peptide was adsorbed at the surface of polycaprolactone scaffolds [126]. However, the effect of GFOGER has not been compared with other peptides, such as RGD, in any of the studies mentioned. In a subsequent work, GFOGER was covalently coupled to agarose hydrogels to evaluate its effect on the regulation of 3-D chondrogenesis [71]. The prototypical RDG sequence and the Fn-derived sequence FnIII7-10, which binds to a5b1 integrin, were also tested [71]. Peptides were grafted onto agarose hydrogels in a two-step reaction. First, their primary amines were reacted with NHS-ester groups of the crosslinker sulfo-SANPAH. The crosslinker was then mixed with agarose, and its photoreactive groups were activated by ultraviolet radiation for conjugation to

agarose CH groups. BMSCs were cultured within peptide–agarose hydrogels (with 1 μM FnIII7-10, 15 μM GFOGER or 100 μM RGD) for 1 week. BMSCs osteogenic differentiation was assessed under basal conditions by looking to the mRNA expression of COL-I and OCN. It was demonstrated that RGD peptides, but not GFOGER or FnIII7-10, increased COL-I. Moreover, the GFOGER and RGD peptides enhanced OCN at similar levels, whereas FnIII7-10 inhibited its expression. In general, the overall effect of GFOGER was not superior to that of RGD. However, the differential effects of the various ligands in osteogenesis were not studied in detail, as that was beyond the scope of the study.

3.3. Small integrin-binding ligand N-linked glycoproteins (SIBLING)-derived peptides

The ECM of bone and dentine is rich not only in collagenous but also in non-collagenous proteins, including those belonging to the SIBLING family [127]. This family of proteins is involved in the process of bone mineralization, and includes matrix extracellular phosphoglycoprotein (MEPE), OPN, BSP, dentin matrix protein 1 and dentin sialophosphoprotein [128]. Although these phosphoproteins are distinct in their structures, they also share some similarities, such as presenting RGD-like motifs, glutamic acid-rich sites known to induce hydroxyapatite nucleation, and collagen-binding domains [127,129].

3.3.1. BSP-derived peptides

BSP is the major non-collagenous protein in bone, and it shows a high degree of specificity in osteoblastic-like cell attachment [130,131]. It is considered as a major nucleator of hydroxyapatite crystal formation, and its expression correlates with the onset of matrix mineralization [132]. BSP is present in the bone matrix at late stages of osteoblast development, being primarily localized around mature osteoblasts and osteoblasts trapped in newly formed matrix [133].

3.3.1.1. Surface immobilization of BSP-derived peptides.

Rezania and colleagues [29,134] tested the effect of the BSP-derived peptide CGGNGEPRGDTYRAY (pRGD) on rat calvaria cells. Peptides were grafted onto maleimide-functionalized quartz surfaces through thiol groups present in terminal C residues. Different peptide densities, ranging from 0.01 to 3.6 pmol cm^{-2}, were tested. After 3 weeks of culture in mineralization medium (basal medium supplemented with ascorbic acid and β-glycerophosphate), enhanced mineralization was observed in cells exposed to ligand concentrations of 0.62 pmol cm^{-2} or higher, as compared with lower concentrations or control surfaces (with RGE in place of RGD). However, the mechanisms by which the initial engagement of adhesive ligands mediated the long-term effect were not elucidated. These

mechanisms were more recently investigated by Drevelle and colleagues [135] using the same peptide, but this time immobilized on polycaprolactone (PCL). The peptides, pRGD or control pRGE, were linked through their C-termini to PCL films previously functionalized with ethaneamine hydrochloride. In serum-free medium, MC3T3-E1 osteoblasts were only able to spread on pRGD–PCL. Additionally, only on those surfaces cells presented an organized cytoskeleton, activated intracellular FAK signaling and responded to BMP-2 by activating their canonical Smad pathway. More recently, the same group tried to elucidate how MC3T3-E1 cells cultured in the presence of these peptides respond to BMPs, in terms of signal transduction and differentiation. Cells were cultured on PCL substrates in serum-free medium, and were treated with 0.38 nM of BMP-2 and/or BMP-9 [136]. Treatment with both BMPs similarly affected the kinetics of MAPK activation, but their effects on Smad activation and b-catenin stabilization were different. In terms of cells osteogenic differentiation, both BMPs increased Dlx5, osterix and OCN transcripts, and also ALP activity, compared to unstimulated samples. This study shed some light on the mechanisms that underlie the effect of biomimetic materials on cells response to GFs.

3.3.2. MEPE-derived peptides

Similarly to other proteins from the SIBLING family, MEPEs also play a key role in phosphate regulation, bone mineralization and osteogenesis. MEPEs contain not only RGD-like motifs, but also the amino acid sequence SGDG known to promote glycosaminoglycan (GAG) attachment [137]. MEPE expression has been predominantly found in osteoblasts. Most of the studies to date have used this peptide in a soluble form [137–139].

3.3.2.1. Surface immobilization of MEPE-derived peptides.

Only recently, Acharya and co-workers [59] immobilized a MEPE-derived peptide, with the sequence TDLQERGDNDISPFSGDGQP, at the surface of hydroxyapatite/β-tricalcium phosphate (HA/β-TCP) particles to induce bone regeneration in local defects. The immobilization strategy comprised two steps. First, OH groups on the ceramic surface were silanized to create amine moieties, which were PEGylated with PEG disuccinimidyl succinate. Peptides were then coupled through the N-terminal to the PEG linker. It is noteworthy that, although the peptide immobilization was demonstrated, the effectively grafted amount was not quantified. Peptide-functionalized ceramic particles were combined with a fibrin vehicle and implanted into calvarial defects created in mice. Eight weeks later, the composite was recovered and increased new bone formation was observed in peptide-modified HA/β-TCP particles compared to unmodified ones, as indicated by microcomputerized tomography and hematoxilin & eosin staining. The newly formed bone was actively remodeled by osteoclasts. Overall, this multifunctional peptide combining RGD with a motif that promotes GAG attachment showed

great potential for *in vivo* bone regeneration strategies. Nevertheless, future studies to elucidate the underlying mechanisms and its effect on MSCs differentiation should be addressed.

3.3.3. OPN-derived peptides

OPN is a glycosylated phosphoprotein expressed by different cell types, but prominently localized in the ECM of mineralized tissues, such as bone, being involved in the regulation of their formation and remodeling [140,141]. OPN is able to bind not only to cells via a RGD sequence that recognizes the α4β1 integrin, but also to other ECM components via less characterized peptide sequences [142]. As previously pointed out, similarly to other phosphoproteins, OPN has the capacity to complex to collagen fibrils and induce bone mineralization. This interaction involves a specific region, called collagen-binding motif [143].

3.3.3.1. Surface immobilization of OPN-derived peptides.

Shin et al. [18, 20,144] have been studying the effect of OPN-derived peptides on MSCs behavior using oligo (poly (ethylene glycol) fumarate) (OPF) macromers with alternating PEG chains and fumarate groups. Two cell adhesion peptides have been covalently grafted onto OPF, namely RGD and the DVDVPDGRGDSLAYG (ODP) sequence derived from rat OPN. To prepare peptide-modified hydrogels, each peptide was acrylated and reacted with acryloyl-PEG–NHS at different concentrations (0.1, 1.0 or 2.0 μmol g^{-1} of hydrogel). In an initial study, osteoblasts were shown to be able to attach and proliferate on ODP-modified and RGD-modified hydrogels at similar rates [20]. For differentiation studies, rat MSCs were seeded on top of both peptide-modified hydrogels and cultured under osteoinductive conditions [144].When compared to unmodified hydrogels and TCPS surfaces, ODP hydrogels enhanced the differentiation and mineralization of MSCs, as verified by higher ALP activity, OPN secretion and calcium deposition, in a concentration-dependent manner. However, the effect ODP in enhancing osteogenic differentiation was not different from the effect of RGD. Lee et al. [69] tested different fragments from human OPN, and identified the sequence GLRSKSRRFRRFDIQYFDATDEDITSHM (CBM, residues 150–177) as the region presenting the highest binding affinity to collagen. Within this sequence, the amino acids D and E are the ones responsible for calcium binding, which in turn promotes mineralization [130]. CBM was grafted onto alginate by carbodiimide chemistry (0.007–35 mg of CBM per g of alginate) and the collagen-binding ability of CBM was apparently maintained in peptide–alginate hydrogels. hMSCs were cultured on top of CBM-modified hydrogels, control peptide-modified hydrogels (residues 53–80, with the lowest collagen affinity) and non-modified gels for 28 days, and the cell response was analyzed. Cells adhesion, spreading and proliferation were improved on CBM–alginate. Differentiation assays were performed using hydrogels with 700 μg of peptide per mg of gel, under standard induction medium, for 28 days. The best results were obtained with CBM–alginate, as shown by the enhancement of ALP activity compared with control

peptide-modified hydrogels, and by the expression of activated Smad. Importantly, when implanted in rabbit calvarial defects for 4 weeks, the CBM–alginate hydrogel induced significantly more new bone formation than unmodified alginate. Although the role and biologic activity of the OPN collagen-binding motif have not yet been well established, this study suggests its applicability as an active component for clinical bone regeneration procedures.

3.4. PTH-derived peptides

PTH is an 84-amino-acid hormone that acts as a regulator of calcium homeostasis and plays important roles in bone remodeling. $PTH_{1–34}$ is a truncated peptide with 34 amino acids derived from the N-terminus of PTH that retains most of its bioactivity. Currently, $PTH_{1–34}$ (commonly referred to as teriparatide) is used as an anabolic agent in the systemic treatment of osteoporosis. However, depending on the dose and administration regimen, it can also have catabolic effects. Moreover, multiple mechanisms of action and target cell types are involved in $PTH_{1–34}$-stimulated bone repair, as recently reviewed by Takahata et al. [145]. A few studies have addressed the effect of immobilized $PTH_{1–34}$ in local therapies and bone TE strategies.

3.4.1. Surface immobilization of PTH-derived peptides

In one of the first available studies, $PTH_{1–34}$ was covalently coupled to silk films [30] by carbodiimide chemistry, at an estimated final density of 20 pmol cm^{-2}. However, no positive effects in terms of differentiation of osteoblast-like cells (Saos-2) were demonstrated when compared to RGD-modified silk. Sharon and Puleo [67] reported a strategy for the controlled immobilization of bioactive $PTH_{1–34}$ through attachment to a biodegradable polymer (PLGA) via its N-terminus. The N-terminal serine residue of the peptide was first oxidized to yield a single aldehyde moiety, which was then specifically bound to hydrazide–PLGA, forming a hydrazone bond. Dihydrazide spacers with different lengths were tested, and the accessibility of the tethered peptide was shown to increase with spacer length, as probed with antibodies directed to both the N- and C-terminus of the peptide. The longest spacers also increased the bioactivity of immobilized $PTH_{1–34}$, compared to randomly bound or adsorbed peptide, showing a higher stimulation of intracellular synthesis of cAMP by pre-osteoblastic MC3T3-E1 cells. In a more recent study by Yewle et al. [60], oxidized $PTH_{1–34}$ was conjugated via the N-terminal aldehyde to single molecules of hydrazine bisphosphonates (HBPs), which present a high bone-binding affinity. The PTH–HBP conjugates were immobilized on bone wafers, to simulate the bone surface, and the bioactivity of $PTH_{1–34}$ was demonstrated as described in the previous study. The selective conjugation of $PTH_{1–34}$ with HBPs increased its affinity to bone and improved its interaction with cells once delivered. Although these results are quite interesting, the effects of conjugated $PTH_{1–34}$ are yet to be investigated further in more specific *in vitro* osteogenesis assays, or in terms of *in vivo* bone formation.

3.4.2. Bulk immobilization of PTH-derived peptides

The beneficial effects of PTH locally delivered into bone defects were recently demonstrated in an elegant work by Arrighi et al. [146]. The strategy consisted on derivatizing fibrin matrices with an engineered active fragment of $PTH_{1–34}$, using a plasmin-sensitive substrate sequence as a linker (pl). Once *in vivo*, the enzymatic cleavage of the linker by endogenous plasmin results in cell-driven release of $PTH_{1–34}$ in situ. The fusion peptide ($TGplPTH_{1–34}$) was obtained by linking the N-terminus of the PTH_{1-34} to the coagulation transglutaminase (TG) factor XIIIa, which covalently crosslinks the peptide into the fibrin network during polymerization. The $TGplPTH_{1–34}$ pro-drug is inactive, preventing the eventual activation of osteoclasts at the time of injection when the local concentration of $PTH_{1–34}$ is high [147], but it converts into fully functional $PTH_{1–34}$ upon plasmin-induced proteolytic cleavage. *In vivo* studies were performed using epiphyseal drill defects created in sheep, which were filled with $TGplPTH_{1–34}$-derivatized (50–1000 μg ml^{-1}) or non-derivatized fibrin gels. Bone formation was observed in the presence of PTH in a dose-dependent fashion, demonstrating a strong healing potential, with evidence of both osteoconductive and osteoinductive mechanisms. The same group started clinical trials in humans to investigate the therapeutic efficacy of this PTH-fibrin matrix in bone healing. In another study, Jung et al. [62] used an RGD-modified PEG-based matrix containing covalently bound $PTH_{1–34}$ peptides. To prepare functionalized PEG hydrogels, cys-$PTH_{1–34}$ and cys-RGD were both added to a four-arm PEG-acrylate solution, and cysteine thiol groups were allowed to react with the PEG-acrylate. Afterwards, this solution was combined with another solution of linear PEG-dithiol and the gelling mixture was loaded into a syringe for surgical application. The final concentrations of each peptide in the PEG hydrogels were 20 μg ml^{-1} ($PTH_{1–34}$) and 350 μg ml^{-1} (RGD). The RGD–$PTH_{1–34}$–PEG matrix and different controls were implanted in canine alveolar bone defects. Histomorphometric analysis after 4 and 12 weeks revealed that the $PTH_{1–34}$ group presented enhanced bone formation when compared with PEG alone or empty defects, with similar results being obtained with autogenous bone. However, the effect of RGD–PEG without $PTH_{1–34}$, which would be an important control, was not evaluated.

3.5. Osteogenic growth peptide (OGP) and OGP-derived peptides

OGP is a naturally occurring tetradecapeptide identical to the C-terminal amino acid sequence (residues 89–102, ALKRQGRTLYGFGG) of histone H4 (H4), which is naturally present in human plasma at micromolar concentrations [148–151]. Chen and co-workers [152–154] demonstrated that the C-terminal sequence of OGP (residues 10–14, YGFGG, hereafter designated as $OGP_{10–14}$) corresponds to the bioactive portion of OGP that directly interacts with the cell surface. Upon intravenous administration in animals, both peptides were shown to promote increased bone mass and promote fracture healing [148,150,151]. *In vitro*, soluble OGP peptides were shown to increase osteoblasts and MSCs proliferation and to promote

osteogenic differentiation in a biphasic concentration-dependent manner [155]. The use of physically [156,157] and chemically immobilized OGP has been explored in a few works.

3.5.1. Surface immobilization of OGP and OGP-derived peptides

To clarify the effect of concentration and bioavailability of surface-immobilized OGP, Moore and colleagues [158] performed a systematic study using SAMs. OGP and $OGP_{10–14}$ derivatized with azide at the N-terminal were grafted by click chemistry onto SAMs functionalized with alkyne gradients [158]. Along the gradients, the density of grafted peptides ranged from 0 to 140 pmol cm^{-2}. MC3T3-E1 cells were cultured on these substrates for up to 7 days in serum-free medium. From day 0 to day 3, immobilized OGP increased cells proliferation independently of concentration. It is possible that OGP activity was dependent on the cleavage of the bioactive (10–14) sequence that, once free, subjected all cells to similar $OGP_{10–14}$ concentrations. Also, there was probably a concomitant effect of cell-secreted OGP. A positive effect of $OGP_{10–14}$ was only observed at a lower density (40 pmol cm^{-2}). Globally, the outcome of immobilized OGP was considered to be small compared to other immobilized GFs described in the literature. In another study, the effect of OGP on gene expression of osteogenic markers was only investigated in cells treated with soluble peptides (at 10^{-7} M). From day 3 to day 7, both peptides increased the expression of COL-I while decreasing the expression of Runx2, apparently indicating a transition of MC3T3-E1 cells from a proliferative to a maturation phase [159].

3.5.2. Bulk immobilization of OGP and OGP-derived peptides

OGP was also used to functionalize the SAP AcN-RADARADARA-DARADA-$CONH_2$ (RADA16), through direct solid-phase synthesis extension at the C-termini (Ac (RADA)4GGALKRQGRTLYGF-$CONH_2$) [22]. Its effect was compared to that of unmodified RADA16, and of RADA16 functionalized with either an OPN-derived motif (Ac(RADA) 4GGDGRGDSVAYG-$CONH_2$) or a double RGD-containing sequence (Ac(RADA)4GPRGDSGYRGDS-$CONH_2$). Gel-precursor solutions were prepared (1 wt.%) by mixing unmodified with modified RADA16 at a ratio of 1:1, and MC3TE-E1 cells were cultured on top of the hydrogels in OM. After 2 weeks, the cell proliferation rate in all modified peptides was higher than that of pure RADA16. ALP activity and OCN expression were also increased, especially when PRG was used. Although this study demonstrated the effectiveness of immobilized OGP in enhancing cellular proliferation and differentiation, the bio-functional region of the peptide was apparently used in a truncated form (YGF) that, according to previous studies, is not fully active [154]. In a recent study, $OGP_{10–14}$ was used as a crosslinker in amino acid-based poly (ester urea) (PEU) scaffolds [68]. $OGP_{10–14}$ was symmetrically functionalized with K residues at both termini (KYGFGGK), with reactive vinyl groups grafted onto K side

chains. It was then used (at 0.5% and 1%) to photochemically crosslink phenylalanine or leucine-based PEU scaffolds, enhancing their mechanical properties in a concentration-dependent manner. The proliferation of MC3T3-E1 cells cultured on PEU scaffolds was slightly increased in the presence of $OGP_{10–14}$ at both concentrations. As the peptide was immobilized through both ends, the release of bioactive $OGP_{10–14}$ into the medium upon enzymatic cleavage is improbable, suggesting that it retains bioactivity even in an immobilized form. Upon subcutaneous implantation in rats (12 weeks), all scaffolds degraded to some extent, but no signs of mineralization were observed in any of the samples. This was attributed to a number of factors, including the implantation site, the absence of porosity and transplanted stem cells, and the time frame of the study. Overall, a positive bioactive effect of $OGP_{10–14}$ has not been clearly demonstrated.

3.6. Heparin-binding peptides

GAG chains of heparin and heparan sulphate (HS), which occur in the form of proteoglycans (PGs), are important components of the ECM, with the ability to bind to and release GFs, protecting them from degradation, increasing their local concentration and regulating their availability [68]. Several types of cells secrete PGs, including hMSCs. Interestingly, when hMSCs are cultured under basal conditions, PGs are primarily located intracellularly, being secreted into the extracellular milieu when cells are cultured in osteoinductive medium [160]. At the cell surface, HS-PGs, along with other PGs, regulate GF activity and morphogenic gradients, being implicated in multiple biological processes. In particular, they have been shown to be involved in fibroblast growth factor type 2-mediated [161] and BMP-mediated [160] differentiation of MSCs along the osteoblastic lineage. Based on their pivotal biological role, a number of methods to incorporate GAGs and PGs into synthetic biomaterials have been proposed [54]. One such example is the functionalization of biomaterials with HBPs, which are able to sequester cell-secreted PGs. These non-covalently immobilized PGs can then modulate cell behavior, similarly to what happens within the natural ECM. Cell surface HS–PG receptors also interact with heparin-binding domains present in adhesion proteins, acting cooperatively with RGD domains in mediating adhesion, and assisting the assembly of focal adhesions and actin fibers [133].

3.6.1. Surface immobilization of heparin-binding peptides

Rezania and Healy [133] produced model surfaces with different ratios of the consensus heparin-binding domain FHRRIKA and an RGD-like sequence, both present in BSP, using a heterobifunctional crosslinker to couple the peptides to amine-functionalized quartz substrates. The behavior of rat calvaria osteoblast-like cells when cultured on these peptide-modified surfaces was examined, namely in terms of matrix mineralization by Von Kossa staining. The

presence of the HBP enhanced mineralization compared to RGD alone, although the effect of grafted RGD proved to be dominant over that of FHRRIKA.

Hudalla and co-authors showed that SAMs modified with the bioinspired heparin-binding sequence GGGKRTGQYKL were able to sequester serum-borne heparin [55], and designed a SAM-based cell culture platform to study the influence of endogenous heparin and GFs on hMSCs behavior [56]. Mixed SAMs with the ability to specifically sequester heparin and resist non-specific adsorption were formed using tri (ethylene glycol) (HS-EG3) and carboxyl-terminated hexa (ethylene glycol) (HS-EG6-COOH) alkanethiolates. HBP or scrambled peptides (SP) and RGD were immobilized onto SAMs by carbodiimide reaction with COOH groups [56]. Using HBP–RGD-SAMs, the authors provided some preliminary evidence that hMSCs osteogenic differentiation was enhanced by sequestered heparin, in a BMP-dependent manner. In fact, under osteoinductive medium, the expression of ALP activity significantly increased in HBP–RGD-SAMs compared to control SP–RGD-SAMs, but this effect was suppressed upon BMP receptor inhibition. The expression of OPN mRNA was higher in heparin-binding RGD-SAMs than in polystyrene surfaces, but it was not significantly different from control RGD-SAMs, and was not affected by BMP signaling, probably being up-regulated on SAMs as a consequence of hMSCs–RGD interactions. In summary, this strategy demonstrated that biomaterials can be designed to indirectly modulate cell behavior by: (i) non-covalently sequestering specific biomolecules from the medium, in this case heparin and heparin-binding GFs such as BMPs; (ii) presenting those GFs at the cell-material interface at a high local concentration; and (iii) amplifying key signaling pathways involved in proliferation and differentiation.

3.6.2. Bulk immobilization of heparin-binding peptides

No studies using bulk-immobilized HBP for promoting osteogenesis were found, even if heparin-functionalized PEG hydrogels have been shown to induce the osteogenic differentiation of 3-D-cultured hMSCs [162]. Alginate scaffolds have been functionalized with HBP and RGD, but have only been tested for cardiac applications, showing good potential to improve cardiac muscle tissue formation *in vitro* [163]. In another, very recent, example, HBP have been used to modify a hydrogel obtained by the copolymerization of N-vinyl pyrolidone, diethylene glycol bis allyl carbonate and acrylic acid. In this case, the HBP consisted on positively charged trilysine (KKK) or triarginine (RRR) sequences, but the objective was the development of a pro-angiogenic biomaterial [164].

3.7. Calcium-binding peptides

Phosphorylated amino acid (serine) residues have a high capacity for binding calcium ions. For this reason, they play a key role in the regulation of the early stages of mineralization

in vivo, being involved in the process of crystal formation. For this reason, these amino acids have been exploited as functionalization molecules to improve the osseointegration of implant materials [165,166].

Recently, peptide amphiphile (PA) materials capable of self-assembling into well-defined nanofibrous hydrogels were designed using peptide sequences that contained phosphoserine residues (S- PA) and RGDS motifs (RGD-PA). The combination of these two modifications, when implanted in a critical-size rat femoral defect, showed greater bone formation compared with serine and RGD alone [57]. The authors hypothesized that the observed effect was related to the capacity of these nanofibers to stimulate hydroxyapatite (HA) nucleation and enhance mineral deposition.

Later, an *in vitro* study, in which calcium-supplemented medium was used, demonstrated that these PA nanofibers containing serine and phosphoserine were effectively able to nucleate spheroidal aggregates of carbonated hydroxyapatite [167].

A number of strategies have been proposed to localize GF activity to mineralized ECMs and mineral-based biomaterials [54].

With this aim, a class of modular peptides conjugating BMP-2-derived peptides with a natural HA binding unit present in OCN (γEPRRγEVCγEL, γ-carboxylated glutamic acid) has been proposed by Lee et al. [168–170]. The Gla residues coordinate with calcium ions in the HA crystal lattice to promote high levels of binding. The modular peptide KIPKASSVPTELSAISTLYL-AAAA-γEPRRγEVAγEL, where the (Ala)4 sequence acts as a spacer, has been prepared by solid-phase peptide synthesis. In a first set of studies, the sequence that more effectively binds to a HA-coated poly (lactide-co-glycolide) surface was identified, and then its biological activity on hMSCs osteogenic differentiation was evaluated. ALP activity, BMP-2 secretion and OCN, OPN and Cbfa1 production were enhanced when cells were cultured in HA surfaces modified with the modular peptide under induction standard medium, as compared with cells treated with the soluble modular peptide.

Recently, another interesting type of material with HA-binding ability has been proposed, consisting on recombinamers (recombinant protein materials obtained from a synthetic gene) containing peptide motifs derived from elastin, a structural protein, and statherin, a salivary protein that has a high affinity for calcium phosphate [171]. Multifunctional elastin-like recombinamers containing the SNA15 domain of statherin (an analogue of the amino-terminal 15-residue fragment) were prepared, and their potential as mineralization templates were tested by incubation in simulated body fluid at 37 ºC. In materials with a triblock structure, it was possible to observe calcium phosphate deposition after 1 week. However, there have been no studies exploiting the effect of such materials on MSCs differentiation *in vitro* nor on bone formation *in vivo*.

Table 3. Examples of covalently immobilized peptide sequences tested as osteoinductors.

Parental molecule	Peptide sequence	Material	Cells	Principal effects	Ref.
BMP-2	KIPKASSVPTELSAISTLYL	SAMs	hBMSCs	↑ of osteogenic markers in OM improved by the synergistic effect of coupled RGD and BMP-2 peptide	[51]
		pACAA	hBMSCs	↑ of osteogenic markers in BM, in stiffer matrices and in the presence of BMP-2 peptide	[64]
		PET	MC3T3-E1	↑ of osteogenic markers in OM (> BMP-7 and BMP-9)	[63]
		PLEOF	Rat BMSCs	Mineralization extent and ALP expression improved by the synergistic effect of coupled RGD and BMP-2 peptide in OM	[21]
		PLEOF	Rat BMSCs	↑ of osteogenic and vasculogenic markers in OM improved by the synergistic effect of coupled RGD, BMP-2 and OPD peptides	[65]
		PLGA	Rat BMSCs	↑ of ALP expression in OM and promotion of ectopic bone formation *in vivo*	[66]
	DWIVA	SAPs	hMSCs	↑ of osteogenic markers in OM through the activation of Smad signal transduction.	[58]
BMP-7	RTVPKPSSAPTOLNAISTLYF	PET	MC3T3-E1	↑ of osteogenic markers in OM (< BMP-2 and > BMP-9)	[63]
BMP-9	RKVGKASSVPTKLSPISILYK			↑ of osteogenic markers in OM (< BMP-2 and < BMP-7)	
COL-I	NGLPGPIGP	Skelite™	Rat calvaria cells	↑ of ALP expression in BM	[61]
	GFOGER	Titanium	Rat BMSCs	↑ of osteogenic markers via α2β1 integrin–ligand interaction in OM, and enhanced osseointegration *in vivo*	[28]
		Agarose	Calf BMSCs	↑ of osteogenic markers and ↓ of chondrogenic markers in CM (similar to RGD)	[71]
BSP	CGGNGEPRGDTYRAY	Quartz	Rat calvaria cells	↑ of mineralization in OM for peptide densities >0.6 pmol/cm^2	[29, 134]
		PCL	MC3T3-E1	Spread on pRGD-PCL and responded to rhBMP-2 by activating their canonical Smad pathway in BM	[135]
OPN	DVDVPDGRGDSLAYG	OPF	Rat MSCs	↑ of osteogenic markers, cell attachment and proliferation in OM in a concentration-dependent manner (similar to RGD)	[20, 144]
	GLRSKSRRFRRFDIQYFDATDEDITSHM	Alginate	hMSCs	↑ of osteogenic markers in OM and new bone formation *in vitro*	[69]
OCN	γEPRRγEVCγEL	HA-PLG	hMSCs	↑ of osteogenic markers in OM	[169]
PTH	SVSEIQLMHNLGKHLNSMERVEWLRKKLQDVHNF	Silk	Saos-2	↑ of osteogenic markers in BM (< than RGD)	[30]
		HBPs	MC3T3-E1	↑ HBPs affinity to bone and improved HBPs interaction with osteoblastic cells in BM	[60]
OGP	YGFGG	SAMs	MC3T3-E1	Higher osteoblastic cells proliferation in BM	[158]
		PEU	MC3T3-E1	↑ cell proliferation in BM and ↑ levels of degradation accompanied by higher number of blood vessels but no mineralization was observed *in vivo*	[68]
	ALKRQGRTLYGF	SAPs	MC3T3-E1	↑ of osteogenic markers in OM (< than PRG)	[22]
Heparin binding peptide	FHRRIKA	Quartz	Rat calvaria cells	↑ of mineralization in OM (< than RGD)	[133]
	GGGKRTGQYKL	SAMs	hMSCs	↑ of osteogenic markers in OM enhanced by the sequester of heparin and improved by the synergistic effect with coupled RGD	[56]

ALP – alkaline phosphatase; BM – Basal medium; BMP-2 – bone morphogenetic protein-2; BMP-7 – bone morphogenetic protein-7; BMP-9 – bone morphogenetic protein-9; BSP – bone sialoprotein; calf BMSCs – calf bone marrow stem cells; CM – chondroinductive medium; Col-I – collagen type I; HA-PLG – hydroxyapatite-poly(lactide-coglycolide); HBPs – hydrazine-bisphosphonates; hBMSCs – human mesenchymal stem cells; OCN – osteocalcin; OGP – osteogenic growth peptide; OM – osteoinductive medium; OPF – oligo[poly(ethylene glycol) fumarate; OPN – osteopontin; pACAA – poly(acrylic acid-co-acrylamide); PCL – polycaprolactone; PET – polyethylene terephthalate; PLEOF – poly(lactide-co-ethylene oxide fumarate); PEU – polyether urethane; PLGA – poly(lactic-co-glycolic acid); PTH – parathyroid hormone; rat BMSCs – rat bone marrow stem cells; rat MSCs – rat mesenchymal stem cells; SAMs – self-assembly monolayers; SAPs – self-assembling peptides; ↓ – decreased; ↑ – increased.

4. OTHER OSTEOINDUCTIVE SMALL MOLECULES

There are several other classes of small compounds, with different mechanisms of action that have also been covalently coupled to biomaterials and used as osteoinductors. In many cases, the beneficial effect of those compounds in a soluble form had been previously demonstrated, providing the rationale for investigating their use as bioactive molecules in drug-releasing scaffolds, to be released in situ upon material and/or linker degradation. For example, Nuttelman et al. [101] covalently grafted dexamethasone, typically used as supplement in osteoinductive medium, to PEG through a degradable lactide acid link using diisopropyl carbodiimide chemistry. Dexamethasone was released from this system upon degradation of the lactic acid bonds, and proved to be biologically active as it enhanced the osteogenic differentiation of encapsulated hMSCs *in vitro*, as suggested by a significant increase in Cbfa1 gene expression. A similar strategy has been followed using statins as bioactive molecules [172]. These small naturally occurring compounds are composed of a dihydroxyheptanoic acid unit and a ring system with different substituents. Structural/compositional variations give rise to different types of statins with distinct pharmacological properties [173]. Statins are widely recognized for their effect in lowering blood cholesterol levels, as inhibitors of the 3-hydroxy-3-methylglutaryl coenzyme A (HMG CoA) reductase. However, back in 1999 [174,175], statins were included in a study in which more than 30,000 compounds were screened for their ability to stimulate the BMP-2 promoter, and hence bone formation. Surprisingly, lovastatin and simvastatin were the only two compounds that showed a positive result [175]. Later, this effect was corroborated in an *in vivo* study, where statins were shown to stimulate bone formation when administered to rats, either systemically or locally in bone. In more recent studies, these compounds were combined with biomaterials for bone regeneration therapies. Benoit et al. [172] synthesized a fluvastatin-releasing monomer that was covalently incorporated into PEG through a lactide acid link. In the absence of other osteoinductive factor, the released fluvastatin not only promoted hMSCs osteogenic differentiation, as suggested by the increase in Cbfa1, ALP and COL-I gene expression, but also stimulated BMP-2 production. Whang et al. [176] grafted simvastatin to hydrolytically degradable poly (lactide-co-glycolide) before scaffold formation, and tested its effect on rat BMCs *in vitro*. The immobilized simvastatin was able to significantly enhance ALP activity and mineralization. Some of these novel molecules have been shown to act cooperatively with BMPs [177], but in many cases the molecular basis for their activity has not yet been identified. Most of these compounds were not included in this review because no studies were found describing their use in an immobilized form. Nevertheless, by way of example, some recently described compounds are listed in Table 4. With the advent of high-throughput screening (HTS), many other small molecules with osteogenesis-inducing activity have been identified recently [177–180]. In fact, HTS not only allows for the rapid checking of thousands of molecules involved in a specific biological process, but may also lead to the discovery of unpredicted signaling pathways and molecular mechanisms. For example, Alves and co-workers [179] recently identified some promising

compounds from a library of 1280 pharmacologically active small molecules using an in-house developed HTS assay, even without the need of expensive robotic techniques. From a tissue engineering perspective, these small molecule discoveries could be valuable for the design of novel biofunctional materials.

Table 4. Examples of small molecules recently shown to have osteogenic-inducing activity.[a]

Molecule	Cell type	Machanism/target(s)	Ref.
cAMP	hMSCs	Activation of PKA pathway	[181]
Forskolin	hMSCs	Activation of PKA pathway	[182]
Flavonoids	hMSCs	BMP and Wnt/beta-catenin signaling pathways	[183]
Purmorphamine	Mouse embryonic mesoderm fibroblasts C3H10T1/2	Unknown	[178]
Phenamil	M2-10B4 (M2) mouse marrow stromal cells, Mouse ES cells, C3H10T1/2 MSCs line, Mouse calvarial organ culture	Trb3-dependent promotion of BMP action	[177]
Resveratrol	Human ES-derived MSCs, canine AD-MSCs, mouse MSCs, mouse MC3T3-E1	Upregulation of RUNX2 gene expression via the SIRT1/FOXO3A axis	[184, 185]

[a] Examples depicted in this table are illustrative rather than inclusive. BMP – bone morphogenetic proteins; cAMP – cyclic adenosine monophosphate; canine AD-MSCs –canine adipose mesenchymal stem cells; C3H10T1/2 MSCs – C3H10T1/2 mesenchymal stem cells; ES cells – mouse embryonic stem; hMSCs – human mesenchymal stromal cells; Human ES-derived MSCs – human embryonic stem cell-derived mesenchymal progenitors; mouse MSCs – mouse mesenchymal stem cells; PKA – protein kinase A; Trb3 – tribbles homolog 3.

Finally, there are additional types of small molecules that target other regulatory processes, namely by modulating the expression of specific genes, which also hold great potential in directing stem cell fate. This is the case, for example, of small interfering RNA [186], and other forms of gene delivery [187–191], which are not covered in the present review.

5. CONCLUSIONS AND FUTURE PERSPECTIVES

It has become clear that biomimetic approaches to modulate cell-material interactions are vital not only to implement advanced TE strategies involving stem cells transplantation, but also to improve osseointegration of current orthopedic biomaterials. In fact, by inducing peri-implant bone formation, these modifications might contribute to decreasing the failure rate of implant devices, which still represents a large socioeconomic burden [192]. As reviewed herein, several small compounds with different mechanisms of action have been described to enhance osteogenesis and bone formation. On the one hand, small molecules are advantageous comparing to more complex ones. On the other hand, immobilized molecules can be more effective than their soluble counterparts. In some cases, as with peptides, the combined use of different bioactive motifs also seems to be an attractive strategy, as they can act synergistically

and potentiate each other's effects. However, while many of these compounds have shown promise as osteoinductors *in vitro*, more studies need to be done to demonstrate their bioactivity *in vivo* as well. Moreover, the beneficial effects of many of them are still limited or controversial, making the search for novel molecules and immobilization strategies essential.

As pointed out, this challenging task is being facilitated by the emergence of new technologies and methodologies for HTS. Yet, while HTS methods will indeed deliver many new molecules, these can only make an impact when they can be applied to a large range of 3-D materials for bone regeneration. HTS approaches have already been applied to the study of cell-material interactions by using miniaturized material-based array platforms obtained by various microfabrication technologies, such as micropatterning, bioprinting and microfluidics [193]. Anderson et al. [194] performed one of the first studies demonstrating the usefulness of material-based HTS systems. This work examined the effects of different biomaterial compositions in human embryonic stem cell attachment, growth and differentiation using an array of synthetic polymers, where 1700 different conditions were screened to evaluate cell-material interactions. Since then, many different other cell-material HTS platforms have been developed, both in two dimensions, e.g., microarrays of SAMs [195], ECM proteins [196] and biomaterials [197], and in three, such as spots of cell-laden hydrogels [198].

Although young, this field has been progressing rapidly and more complex HTS platforms are being produced. Greater investment in existing and new HTS techniques will certainly contribute to our understanding of the role of several cues in MSCs osteogenic differentiation, and help to more rapidly identify novel and unique biomaterial–molecule combinations with a view to optimizing therapeutic approaches. In a certain way, materials become ''cell-instructive'', a property that was previously reserved for GFs and other signaling molecules [199]. This paves the way to the improvement of the biomaterials' biological performance for clinical applications, in a more cost-effective way.

Acknowledgements

This work was financed by FEDER funds through the Programa Operacional Factores de Competitividade (COMPETE) and by Portuguese funds through Fundação para a Ciência e a Tecnologia (FCT), in the framework of the projects Pest-C/SAU/LA0002/2011 and BIOMATRIX (PTDC/SAU-BEB/101235/2008 and FCOMP-01-0124-FEDER-010915). F.R.M. acknowledges INL-International Iberian Nanotechnology Laboratory for her PhD scholarship. S.B. is the recipient of a post-doctoral fellowship from FCT-POPH (SFRH/BPD/80571/2011). C.B. has a research position funded by FCT-POPH-FSE (Ciência 2008). The authors are grateful to Graciosa Teixeira (INEB) for providing the images of MSCs osteogenic differentiation in chitosan scaffolds (Fig. 3).

6. REFERENCES

[1] Pittenger MF, Mackay AM, Beck SC, Jaiswal RK, Douglas R, Mosca JD, et al. Multilineage potential of adult human mesenchymal stem cells. Science 1999;284:143-7.

[2] Kuznetsov SA, Krebsbach PH, Satomura K, Kerr J, Riminucci M, Benayahu D, et al. Single-colony derived strains of human marrow stromal fibroblasts form bone after transplantation *In Vivo*. J. Bone Miner. Res. 1997;12:1335-47.

[3] Wang DX, He Y, Bi L, Qu ZH, Zou JW, Pan Z, et al. Enhancing the bioactivity of poly(lactic-co-glycolic acid) scaffold with a nano-hydroxyapatite coating for the treatment of segmental bone defect in a rabbit model. Int. J. Nanomedicine 2013;8:1855-65.

[4] Firestone AJ, Chen JK. Controlling destiny through chemistry: small-molecule regulators of cell Fate. ACS Chem. Biol. 2009;5:15-34.

[5] Engler AJ, Sen S, Sweeney HL, Discher DE. Matrix elasticity directs stem cell lineage specification. Cell 2006;126:677-89.

[6] Tang J, Peng R, Ding J. The regulation of stem cell differentiation by cell-cell contact on micropatterned material surfaces. Biomaterials 2010;31:2470-6.

[7] Peng R, Yao X, Ding J. Effect of cell anisotropy on differentiation of stem cells on micropatterned surfaces through the controlled single cell adhesion. Biomaterials 2011;32:8048-57.

[8] Peng R, Yao X, Cao B, Tang J, Ding J. The effect of culture conditions on the adipogenic and osteogenic inductions of mesenchymal stem cells on micropatterned surfaces. Biomaterials 2012;33:6008-19.

[9] Yao X, Peng R, Ding J. Effects of aspect ratios of stem cells on lineage commitments with and without induction media. Biomaterials 2013;34:930-9.

[10] Ito Y. Covalently immobilized biosignal molecule materials for tissue engineering. Soft Matter 2008;4:46-56.

[11] Benoit DSW, Schwartz MP, Durney AR, Anseth KS. Small functional groups for controlled differentiation of hydrogel-encapsulated human mesenchymal stem cells. Nat. Mater. 2008;7:816-23.

[12] Curran JM, Chen R, Hunt JA. The guidance of mesenchymal stem cell differentiation *in vitro* by controlled modifications to the cell substrate. Biomaterials 2006;27:4783-93.

[13] Curran JM, Chen R, Hunt JA. Controlling the phenotype and function of mesenchymal stem cells *in vitro* by adhesion to silane-modified clean glass surfaces. Biomaterials 2005;26:7057-67.

[14] Phillips JE, Petrie TA, Creighton FP, Garcia AJ. Human mesenchymal stem cell differentiation on self-assembled monolayers presenting different surface chemistries. Acta Biomater. 2010;6:12-20.

[15] Barrias CC, Martins MCL, Almeida-Porada G, Barbosa MA, Granja PL. The correlation between the adsorption of adhesive proteins and cell behaviour on hydroxyl-methyl mixed self-assembled monolayers. Biomaterials 2009;30:307-16.

[16] Lutolf MP, Hubbell JA. Synthetic biomaterials as instructive extracellular microenvironments for morphogenesis in tissue engineering. Nat. Biotechnol. 2005;23:47-55.
[17] Suzuki Y, Tanihara M, Suzuki K, Saitou A, Sufan W, Nishimura Y. Alginate hydrogel linked with synthetic oligopeptide derived from BMP-2 allows ectopic osteoinduction *in vivo*. J. Biomed. Mater. Res. 2000;50:405-9.
[18] Shin H, Jo S, Mikos AG. Modulation of marrow stromal osteoblast adhesion on biomimetic oligo[poly(ethylene glycol) fumarate] hydrogels modified with Arg-Gly-Asp peptides and a poly(ethylene glycol) spacer. J. Biomed. Mater. Res. 2002;61:169-79.
[19] Saito A, Suzuki Y, Ogata S, Ohtsuki C, Tanihara M. Activation of osteo-progenitor cells by a novel synthetic peptide derived from the bone morphogenetic protein-2 knuckle epitope. BBA-Proteins Proteom 2003;1651:60-7.
[20] Shin H, Zygourakis K, Farach-Carson MC, Yaszemski MJ, Mikos AG. Attachment, proliferation, and migration of marrow stromal osteoblasts cultured on biomimetic hydrogels modified with an osteopontin-derived peptide. Biomaterials 2004;25:895-906.
[21] He X, Ma J, Jabbari E. Effect of Grafting RGD and BMP-2 protein-derived peptides to a hydrogel substrate on osteogenic differentiation of marrow stromal cells. Langmuir 2008;24:12508-16.
[22] Horii A, Wang X, Gelain F, Zhang S. Biological designer self-assembling peptide nanofiber scaffolds significantly enhance osteoblast proliferation, differentiation and 3-D migration. PLoS ONE 2007;2:e190.
[23] Fonseca KB, Bidarra SJ, Oliveira MJ, Granja PL, Barrias CC. Molecularly designed alginate hydrogels susceptible to local proteolysis as three-dimensional cellular microenvironments. Acta Biomater. 2011;7:1674-82.
[24] Bidarra SJ, Barrias CC, Barbosa MA, Soares R, Granja PL. Immobilization of human mesenchymal stem cells within RGD-grafted alginate microspheres and assessment of their angiogenic potential. Biomacromolecules 2010;11:1956-64.
[25] Evangelista MB, Hsiong SX, Fernandes R, Sampaio P, Kong H-J, Barrias CC, et al. Upregulation of bone cell differentiation through immobilization within a synthetic extracellular matrix. Biomaterials 2007;28:3644-55.
[26] Silva GA, Czeisler C, Niece KL, Beniash E, Harrington DA, Kessler JA, et al. Selective differentiation of neural progenitor cells by high-epitope density nanofibers. Science 2004;303:1352-5.
[27] Niu X, Feng Q, Wang M, Guo X, Zheng Q. Porous nano-HA/collagen/PLLA scaffold containing chitosan microspheres for controlled delivery of synthetic peptide derived from BMP-2. J. Contr. Rel. 2009;134:111-7.
[28] Reyes CD, Petrie TA, Burns KL, Schwartz Z, García AJ. Biomolecular surface coating to enhance orthopaedic tissue healing and integration. Biomaterials 2007;28:3228-35.
[29] Rezania A, Thomas CH, Branger AB, Waters CM, Healy KE. The detachment strength and morphology of bone cells contacting materials modified with a peptide sequence found within bone sialoprotein. J. Biomed. Mater. Res. 1997;37:9-19.

[30] Sofia S, McCarthy MB, Gronowicz G, Kaplan DL. Functionalized silk-based biomaterials for bone formation. J. Biomed. Mater. Res. 2001;54:139-48.
[31] Pierschbacher MD, Ruoslahti E. Cell attachment activity of fibronectin can be duplicated by small synthetic fragments of the molecule. Nature 1984;309:30-3.
[32] Brandley BK, Schnaar RL. Covalent attachment of an Arg-Gly-Asp sequence peptide to derivatizable polyacrylamide surfaces: Support of fibroblast adhesion and long-term growth. Anal Biochem. 1988;172:270-8.
[33] Rowley JA, Mooney DJ. Alginate type and RGD density control myoblast phenotype. J. Biomed. Mater. Res. 2002;60:217-23.
[34] Harbers GM, Healy KE. The effect of ligand type and density on osteoblast adhesion, proliferation, and matrix mineralization. J. Biomed. Mater. Res. A 2005;75A:855-69.
[35] Huang J, Gräter SV, Corbellini F, Rinck S, Bock E, Kemkemer R, et al. Impact of order and disorder in RGD nanopatterns on cell adhesion. Nano Lett. 2009;9:1111-6.
[36] Huang J, Ding J. Nanostructured interfaces with RGD arrays to control cell-matrix interaction. Soft Matter 2010;6:3395-401.
[37] Sun J, Graeter SV, Yu L, Duan S, Spatz JP, Ding J. Technique of surface modification of a cell-adhesion-resistant hydrogel by a cell-adhesion-available inorganic microarray. Biomacromolecules 2008;9:2569-72.
[38] Sun J, Tang J, Ding J. Cell orientation on a stripe-micropatterned surface. Chin. Sci. Bull. 2009;54:3154-9.
[39] Liu P, Sun J, Huang J, Peng R, Tang J, Ding J. Fabrication of micropatterns of nanoarrays on a polymeric gel surface. Nanoscale 2010;2:122-7.
[40] Wang X, Yan C, Ye K, He Y, Li Z, Ding J. Effect of RGD nanospacing on differentiation of stem cells. Biomaterials 2013;34:2865-74.
[41] Hsiong SX, Boontheekul T, Huebsch N, Mooney DJ. Cyclic arginine-glycine-aspartate peptides enhance three-dimensional stem cell osteogenic differentiation. Tissue Eng. Part. A 2009;15:263-72.
[42] Fonseca KB, Maia FR, Cruz FA, Andrade D, Juliano MA, Granja PL, et al. Enzymatic, physicochemical and biological properties of MMP-sensitive alginate hydrogels. Soft Matter 2013;9:3283-92.
[43] Munarin F, Petrini P, Tanzi MC, Barbosa MA, Granja PL. Biofunctional chemically modified pectin for cell delivery. Soft Matter 2012;8:4731-9.
[44] Munarin F, Guerreiro SG, Grellier MA, Tanzi MC, Barbosa MA, Petrini P, et al. Pectin-Based Injectable Biomaterials for Bone Tissue Engineering. Biomacromolecules 2011;12:568-77.
[45] Grellier M, Granja PL, Fricain J-C, Bidarra SJ, Renard M, Bareille R, et al. The effect of the co-immobilization of human osteoprogenitors and endothelial cells within alginate microspheres on mineralization in a bone defect. Biomaterials 2009;30:3271-8.
[46] Shekaran A, García AJ. Extracellular matrix-mimetic adhesive biomaterials for bone repair. J. Biomed. Mater. Res. A 2011;96 A:261-72.

[47] Rowley JA, Madlambayan G, Mooney DJ. Alginate hydrogels as synthetic extracellular matrix materials. Biomaterials 1999;20:45-53.
[48] Bidarra SJ, Barrias CC, Fonseca KB, Barbosa MA, Soares RA, Granja PL. Injectable in situ crosslinkable RGD-modified alginate matrix for endothelial cells delivery. Biomaterials 2011;32:7897-904.
[49] Zhang Z, Lai Y, Yu L, Ding J. Effects of immobilizing sites of RGD peptides in amphiphilic block copolymers on efficacy of cell adhesion. Biomaterials 2010;31:7873-82.
[50] Lai Y, Xie C, Zhang Z, Lu W, Ding J. Design and synthesis of a potent peptide containing both specific and non-specific cell-adhesion motifs. Biomaterials 2010;31:4809-17.
[51] Moore NM, Lin NJ, Gallant ND, Becker ML. Synergistic enhancement of human bone marrow stromal cell proliferation and osteogenic differentiation on BMP-2-derived and RGD peptide concentration gradients. Acta Biomater. 2011;7:2091-100.
[52] Martino MM, Mochizuki M, Rothenfluh DA, Rempel SA, Hubbell JA, Barker TH. Controlling integrin specificity and stem cell differentiation in 2D and 3D environments through regulation of fibronectin domain stability. Biomaterials 2009;30:1089-97.
[53] García AJ, Schwarzbauer JE, Boettiger D. Distinct activation states of α5β1 integrin show differential binding to RGD and synergy domains of fibronectin. Biochemistry 2002;41:9063-9.
[54] Hudalla GA, Murphy WL. Biomaterials that regulate growth factor activity via bioinspired interactions. Adv. Funct. Mater. 2011;21:1754-68.
[55] Hudalla GA, Koepsel JT, Murphy WL. Surfaces that sequester serum-borne heparin amplify growth factor activity. Adv. Mater. 2011;23:5415-8.
[56] Hudalla GA, Kouris NA, Koepsel JT, Ogle BM, Murphy WL. Harnessing endogenous growth factor activity modulates stem cell behavior. Integr. Biol. 2011;3:832-42.
[57] Mata A, Geng Y, Henrikson KJ, Aparicio C, Stock SR, Satcher RL, et al. Bone regeneration mediated by biomimetic mineralization of a nanofiber matrix. Biomaterials 2010;31:6004-12.
[58] Lee J-Y, Choo J-E, Choi Y-S, Suh J-S, Lee S-J, Chung C-P, et al. Osteoblastic differentiation of human bone marrow stromal cells in self-assembled BMP-2 receptor-binding peptide-amphiphiles. Biomaterials 2009;30:3532-41.
[59] Acharya B, Chun S-Y, Kim S-Y, Moon C, Shin H-I, Park EK. Surface immobilization of MEPE peptide onto HA/β-TCP ceramic particles enhances bone regeneration and remodeling. J. Biomed. Mater. Biomed. Res. B. 2012;100B:841-9.
[60] Yewle JN, Puleo DA, Bachas LG. Bifunctional bisphosphonates for delivering PTH (1-34) to bone mineral with enhanced bioactivity. Biomaterials 2013;34:3141-9.
[61] Wang V, Misra G, Amsden B. Immobilization of a bone and cartilage stimulating peptide to a synthetic bone graft. J. Mater. Sci. Mater. M. 2008;19:2145-55.
[62] Jung RE, Cochran DL, Domken O, Seibl R, Jones AA, Buser D, et al. The effect of matrix bound parathyroid hormone on bone regeneration. Clin. Oral Implan. Res. 2007;18:319-25.
[63] Zouani OF, Chollet C, Guillotin B, Durrieu M-C. Differentiation of pre-osteoblast cells on poly(ethylene terephthalate) grafted with RGD and/or BMPs mimetic peptides. Biomaterials 2010;31:8245-53.

[64] Zouani OF, Kalisky J, Ibarboure E, Durrieu M-C. Effect of BMP-2 from matrices of different stiffnesses for the modulation of stem cell fate. Biomaterials 2013;34:2157-66.
[65] He X, Yang X, Jabbari E. Combined effect of osteopontin and BMP-2 derived peptides grafted to an adhesive hydrogel on osteogenic and vasculogenic differentiation of marrow stromal cells. Langmuir 2012;28:5387-97.
[66] Lin Z-Y, Duan Z-X, Guo X-D, Li J-F, Lu H-W, Zheng Q-X, et al. Bone induction by biomimetic PLGA-(PEG-ASP)n copolymer loaded with a novel synthetic BMP-2-related peptide *in vitro* and *in vivo*. J. Control. Release 2010;144:190-5.
[67] Sharon JL, Puleo DA. The use of N-terminal immobilization of PTH(1–34) on PLGA to enhance bioactivity. Biomaterials 2008;29:3137-42.
[68] Stakleff KS, Lin F, Smith Callahan LA, Wade MB, Esterle A, Miller J, et al. Resorbable, amino acid-based poly(ester urea)s crosslinked with osteogenic growth peptide with enhanced mechanical properties and bioactivity. Acta Biomater. 2013;9:5132-42.
[69] Lee J-Y, Choo J-E, Park H-J, Park J-B, Lee S-C, Jo I, et al. Injectable gel with synthetic collagen-binding peptide for enhanced osteogenesis *in vitro* and *in vivo*. Biochem. Bioph. Res. Co. 2007;357:68-74.
[70] Saito A, Suzuki Y, Ogata S-I, Ohtsuki C, Tanihara M. Prolonged ectopic calcification induced by BMP-2–derived synthetic peptide. J. Biomed. Mater. Res. A 2004;70A:115-21.
[71] Connelly JT, Petrie TA, García AJ, Levenston ME. Fibronectin- and collagen-mimetic ligands regulate bone marrow stromal cell chondrogenesis in three-dimensional hydrogels. Eur. cells mater. 2011;22:168-76; discussion 76-77.
[72] Hudalla GA, Murphy WL. Using “click” chemistry to prepare SAM substrates to study stem cell adhesion. Langmuir 2009;25:5737-46.
[73] Mrksish M, Whitesides GM. Using self-assembled monolayers to understand the interactions of man made surfaces with proteins and cells. Annu. Rev. Bioph. Biomol. 1996;25:55-78.
[74] Ulman A. Formation and structure of self-assembled monolayers. Chem. Rev. 1996;96:1533-54.
[75] Mrksich M. Using self-assembled monolayers to model the extracellular matrix. Acta Biomater. 2009;5:832-41.
[76] Yan C, Sun J, Ding J. Critical areas of cell adhesion on micropatterned surfaces. Biomaterials 2011;32:3931-8.
[77] Koepsel JT, Loveland SG, Schwartz MP, Zorn S, Belair DG, Le NN, et al. A chemically-defined screening platform reveals behavioral similarities between primary human mesenchymal stem cells and endothelial cells. Integr. Biol. 2012;4:1508-21.
[78] Mrksich M. Tailored substrates for studies of attached cell culture. Cell. Mol. Life Sci. 1998;54:653-62.
[79] Maciel J, Oliveira MI, Gonçalves RM, Barbosa MA. The effect of adsorbed fibronectin and osteopontin on macrophage adhesion and morphology on hydrophilic and hydrophobic model surfaces. Acta Biomater. 2012;8:3669-77.

[80] Coelho NM, González-García C, Salmerón-Sánchez M, Altankov G. Arrangement of type IV collagen on NH2 and COOH functionalized surfaces. Biotechnol. Bioeng. 2011;108:3009-18.
[81] Arima Y, Iwata H. Effect of wettability and surface functional groups on protein adsorption and cell adhesion using well-defined mixed self-assembled monolayers. Biomaterials 2007;28:3074-82.
[82] Elliott JT, Woodward JT, Umarji A, Mei Y, Tona A. The effect of surface chemistry on the formation of thin films of native fibrillar collagen. Biomaterials 2007;28:576-85.
[83] Wang H, He Y, Ratner BD, Jiang S. Modulating cell adhesion and spreading by control of FnIII7–10 orientation on charged self-assembled monolayers (SAMs) of alkanethiolates. J. Biomed. Mater. Res. A 2006;77A:672-8.
[84] Liu L, Chen S, Giachelli CM, Ratner BD, Jiang S. Controlling osteopontin orientation on surfaces to modulate endothelial cell adhesion. J. Biomed. Mater. Res. A 2005;74A:23-31.
[85] Keselowsky BG, Collard DM, García AJ. Integrin binding specificity regulates biomaterial surface chemistry effects on cell differentiation. Proc. Natl. Acad. Sci. 2005;102:5953-7.
[86] Lan MA, Gersbach CA, Michael KE, Keselowsky BG, García AJ. Myoblast proliferation and differentiation on fibronectin-coated self assembled monolayers presenting different surface chemistries. Biomaterials 2005;26:4523-31.
[87] Lee MH, Brass DA, Morris R, Composto RJ, Ducheyne P. The effect of non-specific interactions on cellular adhesion using model surfaces. Biomaterials 2005;26:1721-30.
[88] Faucheux N, Schweiss R, Lützow K, Werner C, Groth T. Self-assembled monolayers with different terminating groups as model substrates for cell adhesion studies. Biomaterials 2004;25:2721-30.
[89] Keselowsky BG, Collard DM, García AJ. Surface chemistry modulates focal adhesion composition and signaling through changes in integrin binding. Biomaterials 2004;25:5947-54.
[90] Keselowsky BG, Collard DM, García AJ. Surface chemistry modulates fibronectin conformation and directs integrin binding and specificity to control cell adhesion. J. Biomed. Mater. Res. A 2003;66A:247-59.
[91] Scotchford CA, Gilmore CP, Cooper E, Leggett GJ, Downes S. Protein adsorption and human osteoblast-like cell attachment and growth on alkylthiol on gold self-assembled monolayers. J. Biomed. Mater. Res. 2002;59:84-99.
[92] McClary KB, Ugarova T, Grainger DW. Modulating fibroblast adhesion, spreading, and proliferation using self-assembled monolayer films of alkylthiolates on gold. J. Biomed. Mater. Res. 2000;50:428-39.
[93] Tegoulia VA, Cooper SL. Leukocyte adhesion on model surfaces under flow: Effects of surface chemistry, protein adsorption, and shear rate. J. Biomed. Mater. Res. 2000;50:291-301.
[94] Margel S, Vogler EA, Firment L, Watt T, Haynie S, Sogah DY. Peptide, protein, and cellular interactions with self-assembled monolayer model surfaces. J. Biomed. Mater. Res. 1993;27:1463-76.

[95] Granja PL, Barbosa MA, Pouységu L, De Jéso B, Rouais F, Baquey C. Cellulose phosphates as biomaterials. Mineralization of chemically modified regenerated cellulose hydrogels. J. Mater. Sci. 2001;36:2163-72.
[96] Granja PL, Jéso BD, Bareille R, Rouais F, Baquey C, Barbosa MA. Cellulose phosphates as biomaterials. *In vitro* biocompatibility studies. React. Funct. Polym. 2006;66:728-39.
[97] Murphy AR, John PS, Kaplan DL. Modification of silk fibroin using diazonium coupling chemistry and the effects on hMSC proliferation and differentiation. Biomaterials 2008;29:2829-38.
[98] Wang DA, Williams CG, Yang F, Cher N, Lee H, Elisseeff JH. Bioresponsive phosphoester hydrogels for bone tissue engineering. Tissue Eng. 2005;11:201-13.
[99] Wang D-a, Williams CG, Li Q, Sharma B, Elisseeff JH. Synthesis and characterization of a novel degradable phosphate-containing hydrogel. Biomaterials 2003;24:3969-80.
[100] Nuttelman CR, Tripodi MC, Anseth KS. Synthetic hydrogel niches that promote hMSC viability. Matrix Biol. 2005;24:208-18.
[101] Nuttelman CR, Benoit DSW, Tripodi MC, Anseth KS. The effect of ethylene glycol methacrylate phosphate in PEG hydrogels on mineralization and viability of encapsulated hMSCs. Biomaterials 2006;27:1377-86.
[102] Gandavarapu NR, Mariner PD, Schwartz MP, Anseth KS. Extracellular matrix protein adsorption to phosphate-functionalized gels from serum promotes osteogenic differentiation of human mesenchymal stem cells. Acta Biomater. 2013;9:4525-34.
[103] Jabbari E. Osteogenic Peptides in Bone Regeneration. Curr. Pharm. Des. 2013.
[104] Choi YJ, Lee JY, Chung C-P, Park YJ. Enhanced osteogenesis by collagen-binding peptide from bone sialoprotein *in vitro* and *in vivo*. J. Biomed. Mater. Res. A 2013;101A:547-54.
[105] Kim HK, Kim JH, Park DS, Park KS, Kang SS, Lee JS, et al. Osteogenesis induced by a bone forming peptide from the prodomain region of BMP-7. Biomaterials 2012;33:7057-63.
[106] Sousa DM, Herzog H, Lamghari M. NPY signalling pathway in bone homeostasis: Y1 receptor as a potential drug target. Curr. Drug Targets 2009;10:9-19.
[107] Teixeira L, Sousa DM, Nunes AF, Sousa MM, Herzog H, Lamghari M. NPY revealed as a critical modulator of osteoblast function *in vitro*: New insights into the role of Y1 and Y2 receptors. J. Cell. Biochem. 2009;107:908-16.
[108] Amin HD, Olsen I, Knowles JC, Donos N. Differential effect of amelogenin peptides on osteogenic differentiation *in vitro*: Identification of possible new drugs for bone repair and regeneration. Tissue Eng. Pt. A 2012;18:1193-202.
[109] Luu HH, Song WX, Luo X, Manning D, Luo J, Deng ZL, et al. Distinct roles of bone morphogenetic proteins in osteogenic differentiation of mesenchymal stem cells. J. Orthop. Res. 2007;25:665-77.
[110] Miyazono K, Kamiya Y, Morikawa M. Bone morphogenetic protein receptors and signal transduction. J. Biochem. 2010;147:35-51.
[111] Little SC, Mullins MC. Bone morphogenetic protein heterodimers assemble heteromeric type I receptor complexes to pattern the dorsoventral axis. Nat. Cell. Biol. 2009;11:637-43.

[112] Foletta VC, Lim MA, Soosairajah J, Kelly AP, Stanley EG, Shannon M, et al. Direct signaling by the BMP type II receptor via the cytoskeletal regulator LIMK1. J. Cell. Biol. 2003;162:1089-98.
[113] Hoodless PA, Haerry T, Abdollah S, Stapleton M, Oconnor MB, Attisano L, et al. MADR1, a MAD-related protein that functions in BMP2 signaling pathways. Cell 1996;85:489-500.
[114] Fujii M, Takeda K, Imamura T, Aoki H, Sampath TK, Enomoto S, et al. Roles of bone morphogenetic protein type I receptors and smad proteins in osteoblast and chondroblast differentiation. Mol. Biol. Cell. 1999;10:3801-13.
[115] Lee K-S, Kim H-J, Li Q-L, Chi X-Z, Ueta C, Komori T, et al. Runx2 is a common target of transforming growth factor β1 and bone morphogenetic protein 2, and cooperation between Runx2 and Smad5 induces osteoblast-specific gene expression in the pluripotent mesenchymal precursor cell line C2C12. Mol. Cell. Biol. 2000;20:8783-92.
[116] Javed A, Bae J-S, Afzal F, Gutierrez S, Pratap J, Zaidi SK, et al. Structural coupling of Smad and Runx2 for execution of the BMP2 osteogenic signal. J. Biol. Chem. 2008;283:8412-22.
[117] Kirsch T, Sebald W, Dreyer MK. Crystal structure of the BMP-2-BRIA ectodomain complex. Nat. Struct. Biol. 2000;7:492-6.
[118] Kirsch T, Nickel J, Sebald W. BMP-2 antagonists emerge from alterations in the low-affinity binding epitope for receptor BMPR-II. Embo J. 2000;19:3314-24.
[119] Knaus P, Sebald W. Cooperativity of binding epitopes and receptor chains in the BMP/TGF beta superfamily. Biol. Chem. 2001;382:1189-95.
[120] Senta H, Park H, Bergeron E, Drevelle O, Fong D, Leblanc E, et al. Cell responses to bone morphogenetic proteins and peptides derived from them: Biomedical applications and limitations. Cytokine Growth F. R. 2009;20:213-22.
[121] Egusa H, Kaneda Y, Akashi Y, Hamada Y, Matsumoto T, Saeki M, et al. Enhanced bone regeneration via multimodal actions of synthetic peptide SVVYGLR on osteoprogenitors and osteoclasts. Biomaterials 2009;30:4676-86.
[122] LI Guang-zan, FENG Lian-fang, GU Xue-ping, XU Zhong-bin, HU Guo-hua, Jin-hua L. Synthesis of PSt-TMI copolymer and studies of the copolymerization kinetics. J. Funct. Pol. 2005:127.33.
[123] Staatz WD, Walsh JJ, Pexton T, Santoro SA. The alpha 2 beta 1 integrin cell surface collagen receptor binds to the alpha 1 (I)-CB3 peptide of collagen. J. Biol. Chem. 1990;265:4778-81.
[124] Takeuchi Y, Suzawa M, Kikuchi T, Nishida E, Fujita T, Matsumoto T. Differentiation and transforming growth factor-β receptor down-regulation by collagen-α2β1 integrin interaction is mediated by focal adhesion kinase and its downstream signals in murine osteoblastic cells. J. Biol. Chem. 1997;272:29309-16.
[125] Reyes CD, García AJ. Engineering integrin-specific surfaces with a triple-helical collagen-mimetic peptide. J. Biomed. Mater. Res. A. 2003;65A:511-23.

[126] Wojtowicz AM, Shekaran A, Oest ME, Dupont KM, Templeman KL, Hutmacher DW, et al. Coating of biomaterial scaffolds with the collagen-mimetic peptide GFOGER for bone defect repair. Biomaterials 2010;31:2574-82.
[127] Qin C, Baba O, Butler WT. Post-translational modifications of SIBLING proteins and their roles in osteogenesis and dentinogenesis. Crit. Rev. Oral Biol. M. 2004;15:126-36.
[128] Chen S, Chen L, Jahangiri A, Chen B, Wu Y, Chuang H-H, et al. Expression and processing of small integrin-binding ligand N-linked glycoproteins in mouse odontoblastic cells. Arch. Oral. Biol. 2008;53:879-89.
[129] Staines KA, MacRae VE, Farquharson C. The importance of the SIBLING family of proteins on skeletal mineralisation and bone remodelling. J. Endocrinol. 2012;214:241-55.
[130] Chen Y, Bal BS, Gorski JP. Calcium and collagen binding properties of osteopontin, bone sialoprotein, and bone acidic glycoprotein-75 from bone. J. Biol. Chem. 1992;267:24871-8.
[131] Fisher LW, Torchia DA, Fohr B, Young MF, Fedarko NS. Flexible structures of SIBLING proteins, bone sialoprotein, and osteopontin. Biochem. Bioph. Res. Co. 2001;280:460-5.
[132] Bianco P, Riminucci M, Bonucci E, Termine JD, Robey PG. Bone sialoprotein (BSP) secretion and osteoblast differentiation: relationship to bromodeoxyuridine incorporation, alkaline phosphatase, and matrix deposition. J. Histochem. Cytochem. 1993;41:183-91.
[133] Rezania A, Healy KE. Biomimetic peptide surfaces that regulate adhesion, spreading, cytoskeletal organization, and mineralization of the matrix deposited by osteoblast-like cells. Biotechnol. Progr. 1999;15:19-32.
[134] Rezania A, Healy KE. The effect of peptide surface density on mineralization of a matrix deposited by osteogenic cells. J. Biomed. Mater. Res. 2000;52:595-600.
[135] Drevelle O, Bergeron E, Senta H, Lauzon M-A, Roux S, Grenier G, et al. Effect of functionalized polycaprolactone on the behaviour of murine preosteoblasts. Biomaterials 2010;31:6468-76.
[136] Drevelle O, Daviau A, Lauzon M-A, Faucheux N. Effect of BMP-2 and/or BMP-9 on preosteoblasts attached to polycaprolactone functionalized by adhesive peptides derived from bone sialoprotein. Biomaterials 2013;34:1051-62.
[137] Hayashibara T, Hiraga T, Yi B, Nomizu M, Kumagai Y, Nishimura R, et al. A synthetic peptide fragment of human MEPE stimulates new bone formation *In Vitro* and *In Vivo*. J. Bone Miner. Res. 2004;19:455-62.
[138] Addison WN, Nakano Y, Loisel T, Crine P, McKee MD. MEPE-ASARM peptides control extracellular matrix mineralization by binding to hydroxyapatite: an inhibition regulated by PHEX cleavage of ASARM. J. Bone Miner. Res. 2008;23:1638-49.
[139] Sprowson AP, McCaskie AW, Birch MA. ASARM-truncated MEPE and AC-100 enhance osteogenesis by promoting osteoprogenitor adhesion. J. Orthop. Res. 2008;26:1256-62.
[140] Merry K, Dodds R, Littlewood A, Gowen M. Expression of osteopontin mRNA by osteoclasts and osteoblasts in modelling adult human bone. J Cell Sci. 1993;104:1013-20.
[141] Denhardt DT, Guo X. Osteopontin: a protein with diverse functions. FASEB J. 1993;7:1475-82.

[142] Suttie JW. Synthesis of vitamin K-dependent proteins. FASEB J. 1993;7:445-52.
[143] Saito T, Arsenault AL, Yamauchi M, Kuboki Y, Crenshaw MA. Mineral induction by immobilized phosphoproteins. Bone 1997;21:305-11.
[144] Shin H, Zygourakis K, Farach-Carson MC, Yaszemski MJ, Mikos AG. Modulation of differentiation and mineralization of marrow stromal cells cultured on biomimetic hydrogels modified with Arg-Gly-Asp containing peptides. J. Biomed. Mater. Res. A. 2004;69:535-43.
[145] Takahata M, Awad H, O'Keefe R, Bukata S, Schwarz E. Endogenous tissue engineering: PTH therapy for skeletal repair. Cell Tissue Res. 2012;347:545-52.
[146] Arrighi I, Mark S, Alvisi M, von Rechenberg B, Hubbell JA, Schense JC. Bone healing induced by local delivery of an engineered parathyroid hormone prodrug. Biomaterials 2009;30:1763-71.
[147] Gafni RI, Brahim JS, Andreopoulou P, Bhattacharyya N, Kelly MH, Brillante BA, et al. Daily parathyroid hormone 1-34 replacement therapy for hypoparathyroidism induces marked changes in bone turnover and structure. J. Bone Miner. Res. 2012;27:1811-20.
[148] Bab I, Gazit D, Chorev M, Muhlrad A, Shteyer A, Greenberg Z, et al. Histone H4-related osteogenic growth peptide (OGP): a novel circulating stimulator of osteoblastic activity. EMBO J. 1992;11:1867-73.
[149] Hui Z, Yu L, Xiaoli Y, Xiang H, Fan Z, Ningbo H, et al. C-terminal pentapeptide of osteogenic growth peptide regulates hematopoiesis in early stage. J. Cell. Biochem. 2007;101:1423-9.
[150] Mattii L, Battolla B, Moscato S, Fazzi R, Galimberti S, Bernardini N, et al. The small peptide OGP(10-14) acts through Src kinases and RhoA pathways in Mo-7e cells: Morphologic and immunologic evaluation. Med. Sci. Monitor. 2008;14:BR103-8.
[151] Fazzi R, Testi R, Trasciatti S, Galimberti S, Rosini S, Piras F, et al. Bone and bone-marrow interactions: haematological activity of osteoblastic growth peptide (OGP)-derived carboxy-terminal pentapeptide. Mobilizing properties on white blood cells and peripheral blood stem cells in mice. Leukemia res. 2002;26:19-27.
[152] Miguel SMS, Namdar-Attar M, Noh T, Frenkel B, Bab I. ERK1/2-activated de novo Mapkapk2 synthesis is essential for osteogenic growth peptide mitogenic signaling in osteoblastic cells. J. Biol. Chem. 2005;280:37495-502.
[153] Gabarin N, Gavish H, Muhlrad A, Chen Y-C, Namdar-Attar M, Nissenson RA, et al. Mitogenic Gi protein-MAP kinase signaling cascade in MC3T3-E1 osteogenic cells: Activation by C-terminal pentapeptide of osteogenic growth peptide [OGP(10–14)] and attenuation of activation by cAMP. J. Cell. Biochem. 2001;81:594-603.
[154] Acharya AP, Dolgova NV, Moore NM, Xia CQ, Clare-Salzler MJ, Becker ML, et al. The modulation of dendritic cell integrin binding and activation by RGD-peptide density gradient substrates. Biomaterials 2010;31:7444-54.
[155] Chen Z-x, Chang M, Peng Y-l, Zhao L, Zhan Y-r, Wang L-j, et al. Osteogenic growth peptide C-terminal pentapeptide [OGP(10–14)] acts on rat bone marrow mesenchymal stem

cells to promote differentiation to osteoblasts and to inhibit differentiation to adipocytes. Reg. Pept. 2007;142:16-23.

[156] Shuqiang M, Kunzheng W, Xiaoqiang D, Wei W, Mingyu Z, Daocheng W. Osteogenic growth peptide incorporated into PLGA scaffolds accelerates healing of segmental long bone defects in rabbits. J. Plast. Reconstr. Aes. 2008;61:1558-60.

[157] Saska S, Scarel-Caminaga RM, Teixeira LN, Franchi LP, Santos RAD, Gaspar AMM, et al. Characterization and *in vitro* evaluation of bacterial cellulose membranes functionalized with osteogenic growth peptide for bone tissue engineering. J. Mater. Sci-Mater. M. 2012;23:2253-66.

[158] Moore NM, Lin NJ, Gallant ND, Becker ML. The use of immobilized osteogenic growth peptide on gradient substrates synthesized via click chemistry to enhance MC3T3-E1 osteoblast proliferation. Biomaterials 2010;31:1604-11.

[159] Pregizer S, Baniwal SK, Yan X, Borok Z, Frenkel B. Progressive recruitment of Runx2 to genomic targets despite decreasing expression during osteoblast differentiation. J. Cell. Biochem. 2008;105:965-70.

[160] Manton KJ, Leong DFM, Cool SM, Nurcombe V. Disruption of heparan and chondroitin sulfate signaling enhances mesenchymal stem cell-derived osteogenic differentiation via bone morphogenetic protein signaling pathways. Stem Cells 2007;25:2845-54.

[161] Dombrowski C, Song SJ, Chuan P, Lim X, Susanto E, Sawyer AA, et al. Heparan sulfate mediates the proliferation and differentiation of rat mesenchymal stem cells. Stem Cells Dev. 2009;18:661-70.

[162] Benoit DSW, Durney AR, Anseth KS. The effect of heparin-functionalized PEG hydrogels on three-dimensional human mesenchymal stem cell osteogenic differentiation. Biomaterials 2007;28:66-77.

[163] Vacharathit V, Silva EA, Mooney DJ. Viability and functionality of cells delivered from peptide conjugated scaffolds. Biomaterials 2011;32:3721-8.

[164] Gilmore L, Rimmer S, McArthur SL, Mittar S, Sun D, MacNeil S. Arginine functionalization of hydrogels for heparin binding—a supramolecular approach to developing a pro-angiogenic biomaterial. Biotechnol. and Bioeng. 2013;110:296-317.

[165] Ganss B, Kim RH, Sodek J. Bone sialoprotein. Crit. Rev. Oral Biol. M. 1999;10:79-98.

[166] Sodek J, Ganss B, McKee MD. Osteopontin. Crit. Rev. Oral Biol. M. 2000;11:279-303.

[167] Sargeant TD, Aparicio C, Goldberger JE, Cui H, Stupp SI. Mineralization of peptide amphiphile nanofibers and its effect on the differentiation of human mesenchymal stem cells. Acta Biomater. 2012;8:2456-65.

[168] Lee JS, Lee JS, Wagoner-Johnson A, Murphy WL. Modular peptide growth factors for substrate-mediated stem cell differentiation. Angew Chem. Int. Edit. 2009;48:6266-9.

[169] Lee JS, Lee JS, Murphy WL. Modular peptides promote human mesenchymal stem cell differentiation on biomaterial surfaces. Acta Biomater. 2010;6:21-8.

[170] Hoang QQ, Sicheri F, Howard AJ, Yang DSC. Bone recognition mechanism of porcine osteocalcin from crystal structure. Nature 2003;425:977-80.

[171] Prieto S, Shkilnyy A, Rumplasch C, Ribeiro A, Arias FJ, Rodríguez-Cabello JC, et al. Biomimetic calcium phosphate mineralization with multifunctional elastin-like recombinamers. Biomacromolecules 2011;12:1480-6.
[172] Benoit DSW, Nuttelman CR, Collins SD, Anseth KS. Synthesis and characterization of a fluvastatin-releasing hydrogel delivery system to modulate hMSC differentiation and function for bone regeneration. Biomaterials 2006;27:6102-10.
[173] Reinoso RF, Sánchez Navarro A, García MJ, Prous JR. Preclinical pharmacokinetics of statins. Method. Find. Exp. Clin. 2002;24:593-613.
[174] Mundy G, Garrett R, Harris S, Chan J, Chen D, Rossini G, et al. Stimulation of bone formation *in vitro* and in rodents by statins. Science 1999;286:1946-9.
[175] Edwards CJ, Spector TD. Statins as modulators of bone formation. Arthritis. Res. 2002;4:151-3.
[176] Whang K, Grageda E, Khan A, McDonald J, Lawton M, Satsangi N. A novel osteotropic biomaterial OG-PLG: *In vitro* efficacy. J. Biomed. Mater. Res. A. 2005;74A:247-53.
[177] Park KW, Waki H, Kim W-K, Davies BSJ, Young SG, Parhami F, et al. The small molecule phenamil induces osteoblast differentiation and mineralization. Mol. Cell. Biol. 2009;29:3905-14.
[178] Wu X, Ding S, Ding Q, Gray NS, Schultz PG. A small molecule with osteogenesis-inducing activity in multipotent mesenchymal progenitor cells. J. Am. Chem. Soc. 2002;124:14520-1.
[179] Alves H, Dechering K, Van Blitterswijk C, De Boer J. High-throughput assay for the identification of compounds regulating osteogenic differentiation of human mesenchymal stromal cells. PLoS ONE 2011;6:e26678.
[180] Brey DM, Motlekar NA, Diamond SL, Mauck RL, Garino JP, Burdick JA. High-throughput screening of a small molecule library for promoters and inhibitors of mesenchymal stem cell osteogenic differentiation. Biotechnol. Bioeng. 2011;108:163-74.
[181] Doorn J, Leusink M, Groen N, Van De Peppel J, Van Leeuwen JPTM, Van Blitterswijk CA, et al. Diverse effects of cyclic AMP variants on osteogenic and adipogenic differentiation of human mesenchymal stromal cells. Tissue Eng. Pt. A. 2012;18:1431-42.
[182] Doorn J, Siddappa R, Van Blitterswijk CA, De Boer J. Forskolin enhances *in vivo* bone formation by human mesenchymal stromal cells. Tissue Eng. Pt. A. 2012;18:558-67.
[183] Zhang J-f, Li G, Chan C-y, Meng C-l, Lin MC-m, Chen Y-c, et al. Flavonoids of Herba Epimedii regulate osteogenesis of human mesenchymal stem cells through BMP and Wnt/β-catenin signaling pathway. Mol. Cell. Endocrinol. 2010;314:70-4.
[184] Tseng P-C, Hou S-M, Chen R-J, Peng H-W, Hsieh C-F, Kuo M-L, et al. Resveratrol promotes osteogenesis of human mesenchymal stem cells by upregulating RUNX2 gene expression via the SIRT1/FOXO3A axis. J. Bone Miner. Res. 2011;26:2552-63.
[185] Shakibaei M, Shayan P, Busch F, Aldinger C, Buhrmann C, Lueders C, et al. Resveratrol mediated modulation of Sirt-1/Runx2 promotes osteogenic differentiation of mesenchymal stem cells: potential role of Runx2 deacetylation. PLoS ONE. 2012;7:e35712.

[186] Tzeng SY, Hung BP, Grayson WL, Green JJ. Cystamine-terminated poly(beta-amino ester)s for siRNA delivery to human mesenchymal stem cells and enhancement of osteogenic differentiation. Biomaterials 2012;33:8142-51.
[187] Pandita D, Santos JL, Rodrigues J, Pêgo AP, Granja PL, Tomás H. Gene delivery into mesenchymal stem cells: a biomimetic approach using RGD nanoclusters based on Poly(amidoamine) dendrimers. Biomacromolecules 2011;12:472-81.
[188] Santos JL, Oramas E, Pêgo AP, Granja PL, Tomás H. Osteogenic differentiation of mesenchymal stem cells using PAMAM dendrimers as gene delivery vectors. J. Control Release. 2009;134:141-8.
[189] Santos JL, Oliveira H, Pandita D, Rodrigues J, Pêgo AP, Granja PL, et al. Functionalization of poly(amidoamine) dendrimers with hydrophobic chains for improved gene delivery in mesenchymal stem cells. J. Control Release. 2010;144:55-64.
[190] Santos JL, Pandita D, Rodrigues J, Pêgo AP, Granja PL, Balian G, et al. Receptor-mediated gene gelivery using PAMAM dendrimers conjugated with peptides recognized by mesenchymal stem cells. Mol. Pharm. 2010;7:763-74.
[191] Santos JL, Pandita D, Rodrigues J, Pêgo AP, Granja PL, Tomás H. Non-viral gene delivery to mesenchymal stem cells: methods, strategies and application in bone tissue engineering and regeneration. Curr. Gene Ther. 2011;11:46-57.
[192] Jacob JJ, Andersson GBJ, Bell JE, Weinstein SL, Dormans JP, Gnatz SM, et al. The burden of musculoskeletal diseases in the united states: prevalence, societal and economic cost. Rosemont, IL: American Academy of Orthopaedic Surgeons 2008.
[193] Peters A, Brey DM, Burdick JA. High-throughput and combinatorial technologies for tissue engineering applications. Tissue Eng. Pt. B- Rev. 2009;15:225-39.
[194] Anderson DG, Levenberg S, Langer R. Nanoliter-scale synthesis of arrayed biomaterials and application to human embryonic stem cells. Nat. Biotechnol. 2004;22:863-6.
[195] Luo W, Yousaf MN. Developing a self-assembled monolayer microarray to study stem cell differentiation. J. Colloid. Interf. Sci. 2011;360:325-30.
[196] Huang NF, Patlolla B, Abilez O, Sharma H, Rajadas J, Beygui RE, et al. A matrix micropatterning platform for cell localization and stem cell fate determination. Acta Biomater. 2010;6:4614-21.
[197] Kurkuri MD, Driever C, Johnson G, McFarland G, Thissen H, Voelcker NH. Multifunctional polymer coatings for cell microarray applications. Biomacromolecules 2009;10:1163-72.
[198] Fernandes TG, Kwon S-J, Bale SS, Lee M-Y, Diogo MM, Clark DS, et al. Three-dimensional cell culture microarray for high-throughput studies of stem cell fate. Biotechnol. Bioeng. 2010;106:106-18.
[199] Unadkat HV, Hulsman M, Cornelissen K, Papenburg BJ, Truckenmüller RK, Carpenter AE, et al. An algorithm-based topographical biomaterials library to instruct cell fate. Proc. Natl. Acad. Sci. 2011;108:16565-70.

CHAPTER III

EFFECT OF CELL DENSITY ON MESENCHYMAL STEM CELLS RE-ORGANIZATION WITHIN HYDROGEL-BASED 3D MATRICES*

F. Raquel Maia, [1,2‡] Ana H. Lourenço,[1,2‡] Pedro L. Granja [1,2,3] Raquel M. Gonçalves,[1] and Cristina C. Barrias*[1]

[1] INEB - Instituto de Engenharia Biomédica, Rua do Campo Alegre, n.º 823, 4150-180 Porto, Portugal

[2] FEUP – Faculty of Engineering, Universidade do Porto, Rua Dr. Roberto Frias s/n, 4200-465 Porto, Portugal

[3] ICBAS - Instituto de Ciências Biomédicas Abel Salazar, Universidade do Porto, Rua de Jorge Viterbo Ferreira n.º 228, 4050-313 Porto, Portugal

‡ Authors contributed equally for this work.

* Submitted in 2013.

ABSTRACT

Cell behaviour within 3D matrices is regulated by a number of matrix-intrinsic and extrinsic factors that must be carefully controlled, as they differentially affect distinct cellular activities. In this study, we have examined the influence of the initial cell entrapping density on the behaviour of human mesenchymal stem cells (hMSCs) cultured within RGD-alginate hydrogels. Initial cell densities in the range of 2×10^6 to 15×10^6 cells/mL were tested. Independently of the cell density, hMSCs in 3D presented steady-state levels of metabolic activity and remained in a nearly non-proliferating state, yet they recovered "normal" activity levels after being retrieved from 3D matrices and re-cultured as monolayers under standard 2D conditions. A high cell density showed to be crucial for promoting the establishment of cell-cell contacts and the formation of multicellular clusters within these matrices, which in turn promoted the deposition of endogenous ECM components, particularly collagen and fibronectin, and stimulated hMSCs differentiation along the osteoblastic lineage. The formation of such ECM-rich multicellular clusters present an interesting potential for tissue engineering applications. Importantly, this study highlights the importance of optimizing the initial cell entrapping density when establishing 3D cultures for specific applications.

Keywords: Cell density; 3D culture; alginate hydrogels; mesenchymal stem cells (MSCs); cell aggregation.

1. INTRODUCTION

Three-dimensional (3D) matrices can be used to create cellular microenvironments that recapitulate many important features of native extracellular matrices (ECM). Therefore, these types of substrates have been widely investigated not only as advanced 3D models for in vitro cell culturing, but also as scaffolds for cell transplantation. Hydrogels have emerged as one of the most widespread types of 3D matrices, as they intrinsically exhibit several ECM-like properties, providing cells with highly-hydrated, permeable and mechanically compliant microenvironments [1, 2]. Due to a number of appealing properties, which include their ability to reversibly form hydrogels under mild conditions, alginates are one of the most common materials used for cell entrapment [3].

More recently, alginates have also become one of the most popular cell vehicles, the so-called bio-inks, to produce artificial tissues or organs of complex 3D structure using bioprinting technologies [4, 5]. Alginate hydrogels are highly versatile, and different strategies can be used to fine-tune their biochemical and viscoelastic properties. Although cells are apparently not able to directly interact with naturally occurring alginate isoforms, “bioactive” alginate derivatives can be easily obtained by chemical grafting with cell-instructive moieties, such as cell adhesive (RGD) or protease-sensitive peptides [6-11].Compared to traditional 2D, 3D cell culturing is much more challenging.

In fact, the evaluation of cell behaviour in 3D microenvironments is a multi-factorial task that should take into account the influence of distinct parameters. These include not only matrix extrinsic factors, such as soluble and direct cell-cell contact signalling, but also several matrix-related factors, such as matrix composition, mechanical properties, mesh size and degradation rate (including protease susceptibility).

Interestingly, while the effect of matrix-related factors in 3D cell cultures has been widely investigated [9, 12, 13], the effect of cell density, which directly influences cell-cell signalling, is frequently overlooked, even if it plays a critical role for some cell types. For example, from standard 2D studies, it is known that high-density cell culture promotes cell-to-cell contact, which might stimulate cell cycle arrest causing cells to stop dividing, a phenomenon commonly known as contact inhibition [14, 15]. On the other hand, cell-to-cell contact can stimulate cellular differentiation [16]. Yet, only a few studies (some summarized in Table 1) have examined the effect of the initial cell seeding density in “true” 3D systems, with cells completely embedded within a hydrogel-like matrix, where cell-cell interactions may be easily hindered if cells are entrapped at too low densities [17].

The “optimal” cell seeding density for a 3D culture is largely dependent on the type of cells and 3D matrix, and might also differently affect distinct cellular activities. For example, Huang *et al.* showed that high-density cultures (in the range of 30×10^6 cells/mL) of bovine chondrocytes in agarose hydrogels produced higher glycosaminoglycans (GAG) and collagen contents when compared to lower density cultures (10×10^6 cells/mL), which was related with the resultant higher tensile moduli of the constructs [18]. Mudera *et al.* evaluated the maturation of muscle-derived cells cultured in 3D collagen gels and showed that higher cell densities (30 and

40×10^6 cells/construct) promoted the expression of contractile genes, but had a negative impact on the culture maturation [19].

In certain cases, optimal effects have been found at intermediate levels within a cell density range. Babalola *et al*., showed that in alginate hydrogels seeded with chondrocytes, increasing the cell density from 10×10^6 to 25×10^6 cells/mL resulted in an increased GAG production (up to 4-fold), but no differences were found when cell density was further raised from 25×10^6 to 50×10^6 cells/mL, indicating that a plateau exists after which increasing cell density has no longer an effect [20].

Many studies reported that increasing the cell density promoted different cellular activities such as cluster formation [21, 22], production of proteins [23, 24] and cell proliferation [25]. However, opposite trends have also been reported. For example, the proliferation of nucleus pulposos cells cultured within alginate beads decreased as the cell density increased from 1.25×10^5 to 1×10^6 cells/mL [26]. Taken together, these examples illustrate well the great differences that can be observed among different matrices and cell types, underscoring the importance of optimizing the cell density in a "true" 3D culture for a specific application.

Here, we have examined the influence of the cell seeding density on the behaviour of bone marrow-derived human mesenchymal stem cells (hMSCs), which are currently recognized as one promising tool for cell-based therapies, upon culture within RGD-alginate 3D matrices.

Table 1. Effect of initial cell density in 3D cell cultures (matrix-entrapped).

Matrices	Cells	Cell densities (10^6 cells/mL)	Observation	Trend with ↑ cell density	Ref
Agarose	Bovine chondrocytes and MSCs	10; 30	GAG and collagen content	↑	[18]
Alginate	Bovine NP cells	0.125; 0.25; 0.5; 1	Cluster formation and cell proliferation	↓	[26]
	Bovine and equine AC, equine MSCs	1; 10; 25; 50	GAGs content (equine ACs and MSCs, intermediate/high concentration)	↑	[20]
	Hepatocytes	1; 2; 5; 10	Aggregate size and albumin production	↑	[21]
Collagen	Human muscle derived cells	4.4; 6.7; 8.9	Myosin gene expression and peak force (intermediate cell density)	↑	[19]
	Human MSCs	0.1; 0.5; 1; 5	GAGs deposition	↑	[27]
Silk- fibroin	Human chondrocytes	20; 50; 100	DNA, GAG and collagen content	↑	[23]
PEG	Pancreatic β-cells	2; 5; 10	Insulin production	↑	[24]
	Embryonic carcinoma cells	0.1; 0.5	Cell proliferation	↑	[25]
	Bovine chondrocytes	5; 20	Cluster formation	↑	[22]

AC – articular chondrocytes; DNA – deoxyribonucleic acid; GAG – glycosaminoglycan; MSCs – mesenchymal stem cells; NP – nucleus pulposus; PEG – poly (ethylene glycol); ↑ – increase; ↓ – decrease.

2. MATERIALS AND METHODS

2.1. Synthesis of RGD-grafted alginate

Ultra-pure sodium alginate with high content of guluronic vs. mannuronic acid units (>60%, NovaMatrix, FMC Biopolymers) with Mw=2×10^5 Da and Mw=3×10^4 Da were used, respectively, as the high (HMW) and low molecular weight (LMW) components of the hydrogel. The HMW alginate was partially oxidized to a theoretical extent of 1% of sugar residues with sodium periodate [6], and grafted with the cell-adhesion peptide (glycine)4 - arginine - glycine - aspartic acid - serine - proline (hereafter abbreviated as RGD), using carbodiimide chemistry, as described in detail in previous studies [10]. Briefly, a 1wt.% alginate solution in 0.1M MES buffer (Sigma) was prepared and stirred overnight (ON). Thereafter, sulfo-NHS (Thermo Scientific) and EDC (Sigma) at a molar ratio of 1:2, and RGD peptides (GenScript, 17 mg/g alginate) were sequentially added. After stirring for 24 h, the reaction was quenched with NH_2OH (Sigma). Non-reacted species were separated by dialysis (MWCO 3500 membrane, Spectrum Lab) against solutions of decreasing concentration of NaCl (Merck) and finally deionized water. The recovered solution was lyophilized and the RGD-alginate was stored at -20ºC until further use. The reaction yield was calculated using the BCA Protein Assay (Pierce), as previously described [9].

2.2. Human mesenchymal stem cells (hMSCs) culture

hMSCs were purchased from Lonza (PT-2501, Lot No. 6F4392). Cells were routinely cultured in a basal medium (hereafter designated as BM) composed of low-glucose Dulbecco's Modified Eagle Medium with glutamax (DMEM, Gibco) supplemented with 10% v/v Fetal Bovine Serum (FBS, MSCs-qualified, Gibco) and 1% v/v Penicillin/Streptomycin (Pen/Strep, Gibco). Cultures were maintained at 37ºC under a humidified atmosphere of 5% v/v CO_2 in air, with culture medium being changed twice a week, and were trypsinized when reaching 70% confluence. In the different studies hMSCs in passage 6 were used.

2.3. 3D culture of hMSCs within RGD-alginate matrices

hMSCs at different densities (D1=2×10^6, D2=5×10^6, D3=7.5×10^6 and D4=15×10^6 cells/mL), were carefully mixed with sterile-filtered (0.22 μm) alginate gel-precursor solution and crosslinking agents, and 3D matrices were prepared by internal gelation as previously described [7, 9, 28]. Briefly, the gel precursor solution was a 50:50 v/v binary mixture of RGD-grafted HMW alginate and unmodified LMW alginate, at a total alginate concentration of 2wt.% in

0.9wt.% NaCl. To trigger hydrogel formation, this solution was mixed with an aqueous suspension of $CaCO_3$ (Fluka), at a $CaCO_3$/COOH molar ratio of 1.6, and a fresh solution of glucone delta-lactone (GDL, Sigma) at a $CaCO_3$/GDL molar ratio of 0.125. The mixture was poured (20 µL per well) into a 24-well suspension culture plate (Greiner) coated with pHEMA [29]. After *in situ* crosslinking (30 min, at 37°C), fresh culture medium was added. hMSCs-laden matrices were cultured in BM or in an osteoinductive medium (OM) composed by low-glucose DMEM with 10%v/v FBS (pre-selected batch from PAA), 1% v/v Pen/Strep, 100 nM dexamethasone (Sigma), 10mM β -glycerophosphate (Sigma) and 0.05 mM 2-phospho-L-ascorbic acid (Fluka). In some studies, hMSCs cultured under standard 2D conditions in tissue culture plates were used as a control. During culture, cell-laden matrices were maintained at 37ºC under a humidified atmosphere of 5% v/v CO_2 in air. For analyses, cells were directly assayed within hydrogels (whole mounts) or were recovered as a suspension after dissolving the hydrogels with 0.25wt.% Trypsin/ 50mM EDTA.

2.4. Cell viability, metabolic activity and proliferation

Cell viability was assessed using the Trypan Blue dye exclusion assay in recovered cells or the Live/Dead Assay (Invitrogen) in whole-mounts. After hydrogel dissolution, the cell suspension was stained with 0.4wt.% Trypan Blue (Sigma) and dead/total cells were counted under the microscope with a Neubauer chamber. Three replicates per condition were analysed.

The Live/Dead assay was performed according to the manufacturer's instructions. Briefly, cell-loaded matrices were washed 3 times with DMEM without phenol red (Gibco), and then incubated with 1 µM calcein AM (live cells) and 2.5 µM ethidium homodimer-1 (EthD-1, dead cells) for 45 min at 37ºC in the dark. Afterwards, the supernatant was replaced by fresh DMEM without phenol red. Samples were imaged by confocal laser scanning microscopy (CSLM, Leica SP2 AOBS).

Cell metabolic activity was assessed using the resazurin assay. Cell-loaded matrices were incubated with 20% v/v of the stock resazurin solution (0.1 mg/mL, Sigma) in medium for 2h at 37ºC. The supernatant was then transferred to a 96-well plate black with clear bottom (Greiner) and fluorescence measurements were carried out using a microplate reader (Biotek Synergy MX) with Ex/Em at 570/590 nm.

For total dsDNA quantification, the 3D matrices were dissolved and hMSCs were recovered by centrifugation (10,000 rpm, 5 min,) washed with PBS, centrifuged again and stored at -20ºC until analysed. Cells were lysed in 1% v/v Triton X-100 for 1h at 250 rpm and 4ºC. Samples were then diluted 1:10 in PBS and used for double-stranded DNA (dsDNA) quantification using the Quant-iT PicoGreen dsDNA kit (Molecular Probes, Invitrogen), according to manufacturer's instructions. Briefly, samples were transferred to a 96-well plate black with clear bottom (Greiner) and diluted in TE buffer (200mM Tris-HCl, 20 mM EDTA, pH7.5). After adding the Quant-iT PicoGreen dsDNA reagent, samples were incubated for 5 min

at RT in the dark, and fluorescence was quantified using a microplate reader with Ex/Em at 480/520 nm. RFUs were converted into ng/mL using a standard curve of DNA in the range of 1-1000 ng/mL. For each condition n=3 replicates were analysed.

2.5. Histological analysis: hematoxylin-eosin and Masson's trichrome stainings

After 14 days of culture, hMSCs-laden alginate matrices were recovered, washed with TBS-Ca (tris-buffered saline, 50 mM Tris in 150 mM NaCl, pH 7.4, with 7.5 mM $CaCl_2$), and fixed with 4% v/v paraformaldehyde (PFA) in TBS-Ca for 20 min. Dehydration was performed using a gradient series of ethanol and samples were then embedded in paraffin blocks. Thereafter, sections (3 µm) were recovered, diafanized in xylene and rehydrated with a series of ethanol solutions of decreasing concentrations and finally water. For the hematoxylin-eosin (H&E) staining, sections were incubated in Gill's Hematoxylin for 5 min, washed in water, and counterstained with Eosyn Y for 1 min. For the Masson's trichrome (MT) staining a modified MT kit (Sigma) was used. Sections were incubated with Celestine Blue for 5 min, washed in water, stained with Gill's Hematoxylin for 5 min and washed again in water for 2 min. Afterwards, sections were incubated for 1h with Bouin solution, washed in water, stained in Biebrich Scarlet-Acid Fuchsin solution for 5 min, and washed again. Sections were then mordant in fresh phosphomolybdic acid/phosphotungstic acid solution for 5 min and stained with aniline blue for 5 min. Finally sections were dehydrated, diafanized in xylene, mounted using histofluid mounting medium (Marienfeld) and imaged under an optical microscope.

2.6. Ki67 immunostaining

Paraffin sections of the different samples were obtained as already described in the previous section, diafanized and rehydrated. Sections were washed three times in TBS-Ca for 5 min, and heat-induced epitope retrieval in 10 mM sodium citrate (Sigma) buffer at pH 6 was conducted for 10 min. After washing 3 times in TBS-Ca, cells were permeabilized with 0.1% v/v Triton X-100, and washed 3 times in TBS-Ca. To quench auto-fluorescence, sections were incubated for 5 min in fresh 0.1wt.% sodium borohydride (Sigma) in Tris/EDTA solution at pH 9, and washed once again in TBS-Ca. Blocking non-specific binding was performed by incubating with 4% v/v FBS and 1% v/v BSA in PBS for 1h at RT. After another washing step, sections were incubated ON at 4°C with rabbit polyclonal anti-Ki67 (Abcam,1:100). Sections were then washed 3 times in TBS-Ca for 5 min each, and incubated for 1h with Alexa Fluor 594 F(ab')2 fragment of goat anti-rabbit (Molecular Probes-Invitrogen, 1:1000) and counterstained with DAPI (0.1 µg/mL), in blocking solution in the dark. Sections were washed 3 times in TBS-Ca, mounted with Vectashield (Vector) and finally imaged with an inverted fluorescence microscope (Axiovert 200M, Zeiss).

2.7. Analysis of whole-mounted samples: alkaline phosphatase, f-actin and fibronectin stainings

After 7 days in culture, hMSCs-laden 3D matrices were recovered and whole-mounted samples and different compounds were stained.

For alkaline phosphatase (ALP) staining, samples were washed 3 times with TBS-Ca and fixed with 4% v/v PFA in TBS-Ca for 20 min at RT. After washing, samples were incubated for 30 min in Naphthol AS-MX phosphate/Fast Violet B salt (Sigma) at 37ºC, protected from light, and washed again. Images were obtained using an inverted fluorescence microscope.

For F-actin staining, samples were washed with TBS-Ca, fixed with 4% v/v PFA for 20 min and permeabilized for 5 min with 0.1% v/v Triton X-100. Afterwards samples were incubated for 30 min in 1wt.% BSA to block unspecific binding. F-actin filaments were stained with Alexa Fluor 488 phalloidin (Molecular Probes-Invitrogen, 1:40) and nuclei were counterstained with EthD-1 (2.5 µM). Samples were analyzed by CLSM.

Fibronectin (FN) expression was assessed after 7 days of culture. Samples were washed 3 times with TBS-Ca, fixed with 0.2% v/v PFA (20 min, RT), permeabilized with 0.2% v/v Triton X-100 (10 min) and blocked with 1wt.% BSA (20 min). Then they were incubated with rabbit anti-FN (f3648, Sigma, 1:400, ON at 4ºC) followed by secondary antibody Alexa Fluor 594 F(ab')2 fragment of goat anti-rabbit (Molecular Probes-Invitrogen, 1:1000, 1h at RT) and Alexa Fluor 488 phalloidin. Finally, matrices were counterstained with DAPI (0.1 µg/mL) for nuclei staining and were imaged by CLSM.

2.8. Gene expression analysis by qRT-PCR

At day 7, total RNA was extracted from hMSCs recovered from 3D matrices (n=3) using the RNeasy Mini Kit (Qiagen), as recommended by the manufacturer. Subsequently, 0.25 μg of the total RNA were used for random hexamers first strand synthesis to generate single-stranded cDNA using the SuperScript First-strand synthesis system for qReal-Time PCR (qRT-PCR) (Invitrogen). RNA quantification was performed by using a NanoDrop 1000 spectrophotometer. After the cDNA synthesis reaction, qRT-PCR was carried out in a total volume of 20 μL of a mixture containing 1 μL of cDNA (5 ng of total RNA), 0.25 μM of each forward and reverse primers, and 1× iQ SYBR Green Supermix (Bio-Rad). qRT-PCR experiments were run using an iQ5 (Bio-Rad) under the following conditions: 95 °C for 3 min, followed by 30 cycles at 94 °C for 30 s, 60 °C for 45 s, and 72 °C for 30 s, and the last step at 55° for 10 s. All reactions were performed in duplicate. After completion of the PCR cycling, melting curves, obtained by increasing the temperature from 60 to 96 °C in increments of 0.5 °C, were examined to ascertain specificity of the PCR products. The housekeeping gene glyceraldehyde 3-phosphate dehydrogenase (GAPDH) was used as the endogenous assay control. Relative quantification of

gene amplification by qRT-PCR was performed using the cycle threshold (*C*t) values and relative expression levels were calculated as follows: $2^{-(Ct\ gene\ of\ interest - Ct\ GAPDHgene)}$. The expression value for each target gene was normalized to the GAPDH value at each time point. The sequence and length of the primer pairs used is indicated in Table 2.

Table 2. Sequence of Primer Pairs Used for qRT-PCR.

Gene name	Ref. sequence	Sequence of primers	Length (bp)
GAPDH	NM_002046	F: 5' -AGCCACATCGCTCAGACAC- 3'	66
		R: 5' -GCCCAATACGACCAAATCC- 3'	
ALP	BC021289	F: 5'-AGAACCCCAAAGGCTTCTTC-3'	74
		R: 5'-CTTGGCTTTTCCTTCATGGT-3'	
RUNX2	NM_001024630.2	F: 5'-GTGCCTAGGCGCATTTCA-3'	78
		R: 5'-GCTCTTCTTACTGAGAGTGGAAGG-3'	
OCN	NM_199173.4	F: 5'-AGAGTCCAGCAAAGGTGCAG-3'	171
		R: 5'-TCAGCCAACTCGTCACAGTC-3'	

ALP – alkaline phosphatase; F – forward primer; GAPDH – glyceraldehyde 3-phosphate dehydrogenase; OCN – osteocalcin; RUNX2 – runt-related transcription factor 2; R – reverse primer.

2.9. Statistical analysis

Statistical analyses were performed using Graphpad program. All values were presented as the means ± stdev. Statistical significance was assessed by using Kruskal-Wallis, in conjunction with Dunn's post-hoc multiple comparison test. Regarding total DNA and RT-PCR analysis, data was analysed using non-parametric Mann-Whitney test. Differences were considered statistically significant for p values < 0.05.

3. RESULTS

3.1. Effect of initial cell density on hMSCs viability, metabolic activity and proliferation in 3D.

The effect of cell density (D1=2×10^6, D2=5×10^6, D3=7.5×10^6 and D4=15×10^6 cells/mL gel) on hMSCs viability along one week of 3D culture was evaluated using the trypan blue exclusion assay.

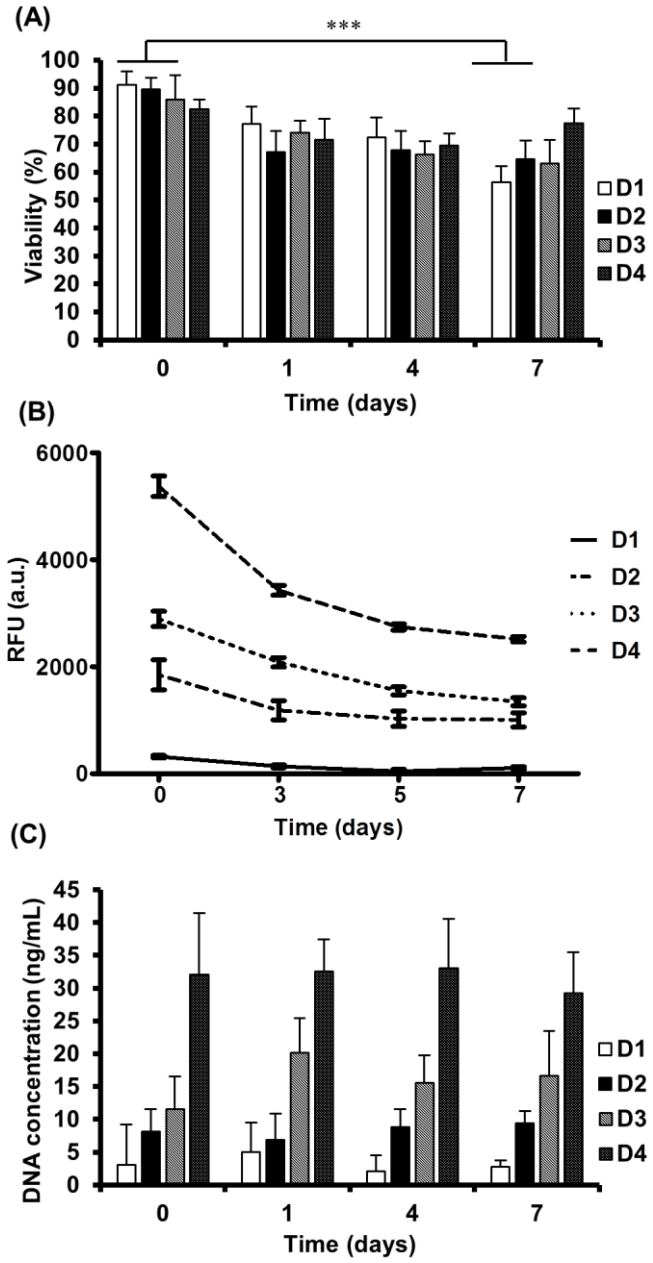

Fig. 1. Effect of cell density on the viability, metabolic activity and proliferation of hMSCs in 3D along 1 week of culture. (**A**) viability (trypan blue assay), (**B**) metabolic activity (resazurin assay) and (**C**) total dsDNA (Picgreen assay) of hMSCs cultured for 1 week in RGD-alginate 3D matrices at different cell densities (D1=2×10^6, D2=5×10^6, D3=7.5×10^6, D4=15×10^6 cells/ml). Data is presented as mean±stdev (n=3), (*) denotes statistical differences ($p<0.05$).

As depicted in Fig. 1A, high cell viabilities were obtained immediately after entrapment (day 0), ranging from 83±3 % (D4) to 91±5 % (D1). The slightly lower cell viability obtained for the highest cell density (D4) may in part be related to the hydrogel dissolution procedure, which required multiple pipetting to convert the hydrogel matrix into a single-cell suspension, which may have lead to some shear-induced damage as reported by others [30]. Along the time, a decrease in cell viability was observed for the entire cell densities tested, which was not statistically significant for the highest cell density (D4). Comparable values were found in the

literature for hMSCs cultured within alginate microspheres at a similar density [8]. The metabolic activity of hMSCs in 3D was monitored along 1 week of culture (Fig. 1B), after validation the resazurin assay in 3D cultures (supplementary data, Fig. S1 [31]). For all the densities tested, the metabolic activity gradually decreased along the period of culture, and for D4 it attained a nearly steady-state profile from day 4.

Cell proliferation was estimated through quantification of the total dsDNA (Fig. 1C). At day 0, the dsDNA content of the different samples was proportional to their respective original cell density, as expected. Yet, in agreement with the previous observations in terms of metabolic activity, no increase on the dsDNA content was observed along the time, further suggesting that the entrapped hMSCs were essentially in a non-proliferating state.

To evaluate the reversibility of the apparent metabolic inhibition, hMSCs cultured at the highest cell density (D4) were recovered from alginate matrices after 1 week of 3D culture, re-plated under standard 2D conditions, and cultured for one additional week. As depicted in Fig. 2A, the metabolic activity of recovered hMSCs gradually increased along the time, increasing up to 5-fold by day 15. Along this time, hMSCs proliferated, as detected by routine optical microscopy observations. Live/Dead assay images (Fig. 2B, C) show that hMSCs were mostly viable both at the beginning and at the end of the assay, exhibiting a round shape in 3D (Fig. 2B) and a well spread shape in 2D, where they formed monolayers (Fig. 2C).

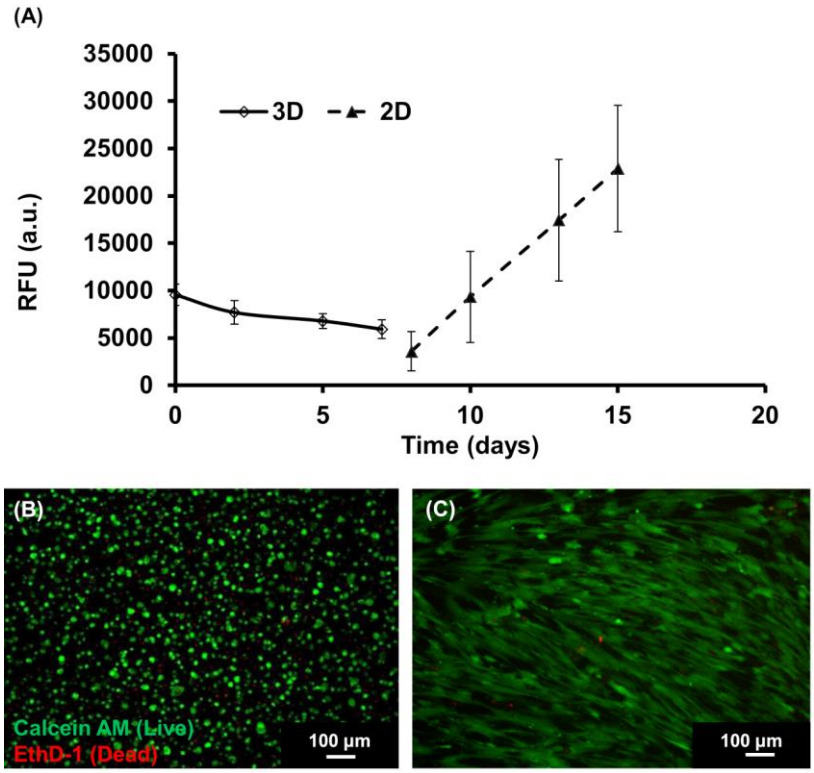

Fig. 2. Alteration of hMSCs metabolic activity upon transference from 3D to 2D culture. (**A**) Metabolic activity of hMSCs along one week in 3D culture followed an additional week in 2D. Data is presented as mean±stdev (n=3). Live/Dead viability assay performed (**B**) at the beginning of the experiment in 3D, and (**C**) at end of the 2D culture. Live cells are stained in green (calcein AM) and dead cells are stained in red (EthD-1).

3.2. hMSCs morphology and endogenous ECM production at different densities

RGD-alginate 3D matrices laden with hMSCs at different densities were cultured under basal and osteoinductive conditions and histological evaluation of H&E-stained samples was performed at day 14. As shown in Fig. 3, hMSCs under basal conditions remained essentially round and homogeneously distributed within the matrix, as single entities, independently of the cell density. A similar behaviour was observed for cells cultured at the lowest density under osteogenic conditions (D1). However, at the higher densities (D3 and D4), hMSCs cultured under osteogenic conditions exhibited a more spread shape. Cell morphology and rearrangement within the matrix were particularly distinct at the highest cell density (D4), where well-spread cells and multicellular aggregates were detected. Under these conditions, the alginate matrices were also more degraded (supplementary data, Fig. S2).

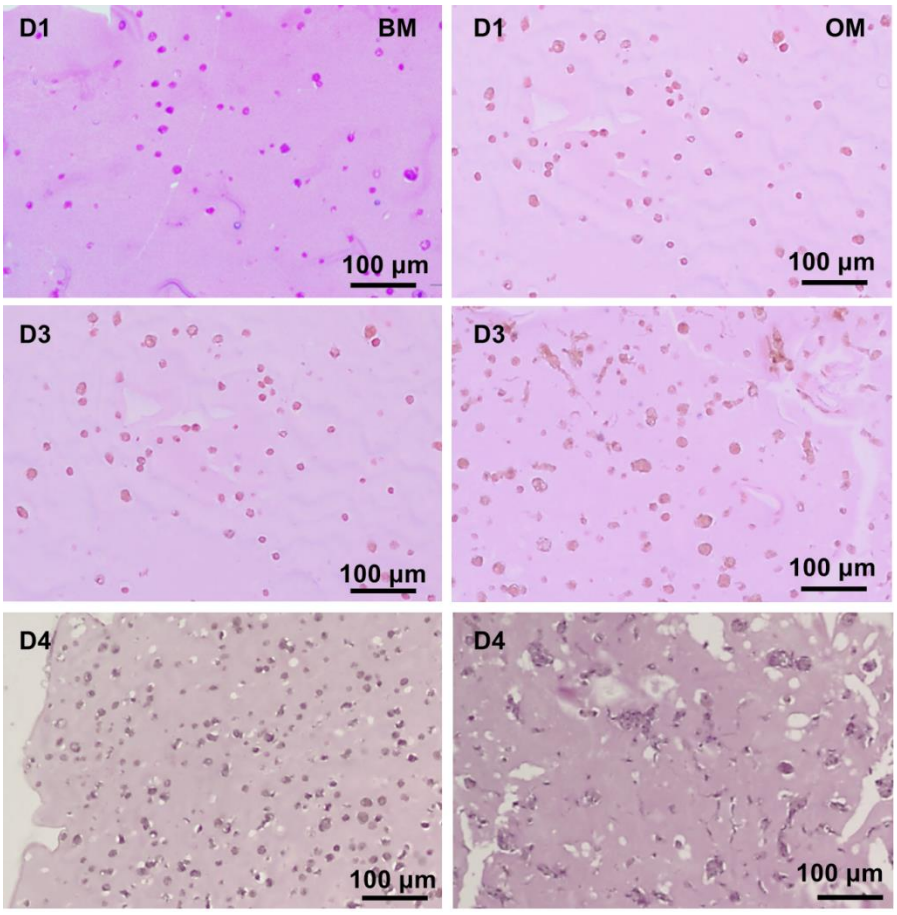

Fig. 3. Effect of cell density and culture conditions on hMSCs spatial distribution within 3D matrices. H&E-stained paraffin sections of hMSCs-laden 3D matrices with different cell densities (D1=2×10^6, D3=7.5×10^6 and D4=15×10^6 cells/ml) cultured under basal (BM) or osteoinductive (OM) conditions for 14 days. H&E stains cells in dark pink/purple. Alginate appears in light pink.

The deposition of ECM (collagen) by entrapped hMSCs was analysed on the same samples in MT-stained sections Fig. 4. The presence of collagen (dark blue staining) was only detected in high-density cultures (D4), mainly within multicellular aggregates.

.

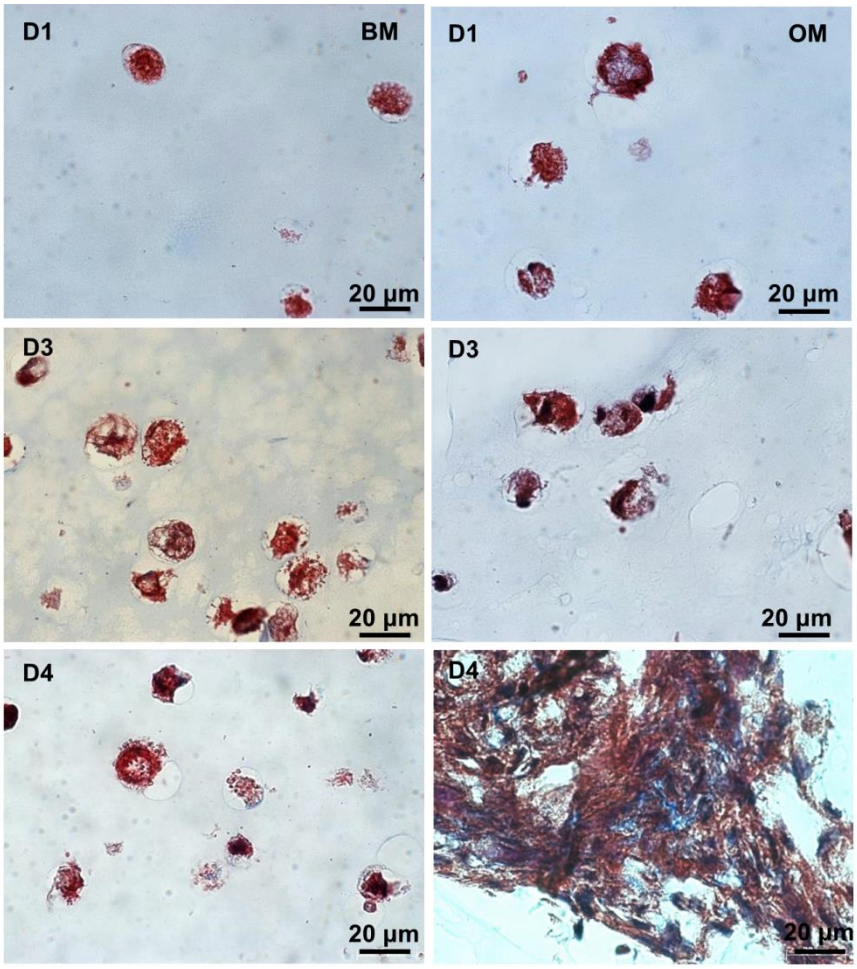

Fig. 4. Effect of cell density on collagen deposition by hMSCs in 3D under basal and osteoinductive conditions. Masson's trichrome (MT)-stained paraffin sections of hMSCs-laden 3D matrices with different cell densities (D1=2×10^6, D3=7.5×10^6 and D4=15×10^6 cells/ml) cultured under basal (BM) or osteoinductive (OM) conditions for 14 days. MT stains collagen in dark blue, nuclei in dark red/purple and cytoplasm in red/pink. Alginate appears in light blue.

3.3. Effect of cell density on hMSCs osteogenic differentiation in 3D

The differentiation of hMSCs when cultured at different densities in basal and osteoinductive media was firstly investigated by analysing the expression of alkaline phosphatase (ALP) activity, an early osteogenic marker, after 1 week of 3D culture. As depicted in Fig. 5A, cultures with higher cell density stained more intensely for ALP activity (in pink), which was particularly evident in regions where cells aggregated. Interestingly, at the highest density, ALP activity was detected even under basal conditions. Therefore, gene expression of

bone phenotypic markers by qRT-PCR was then investigated in these cultures (Fig. 5B), under high-density conditions (D4), RUNX2 and osteocalcin (OCN) slightly increased, as compared with the lower cell density (D1). Yet, ALP gene expression of D4 condition was lower than D1, which might be related with the pattern of ALP activity along osteogenic differentiation, which exhibits an early peak decreasing afterwards. Under osteogenic conditions, no differences were observed between D1 and D4 regarding the gene expression of the same markers (data not shown), probably because of the dominant effect of the exogenously added osteoinductive supplements.

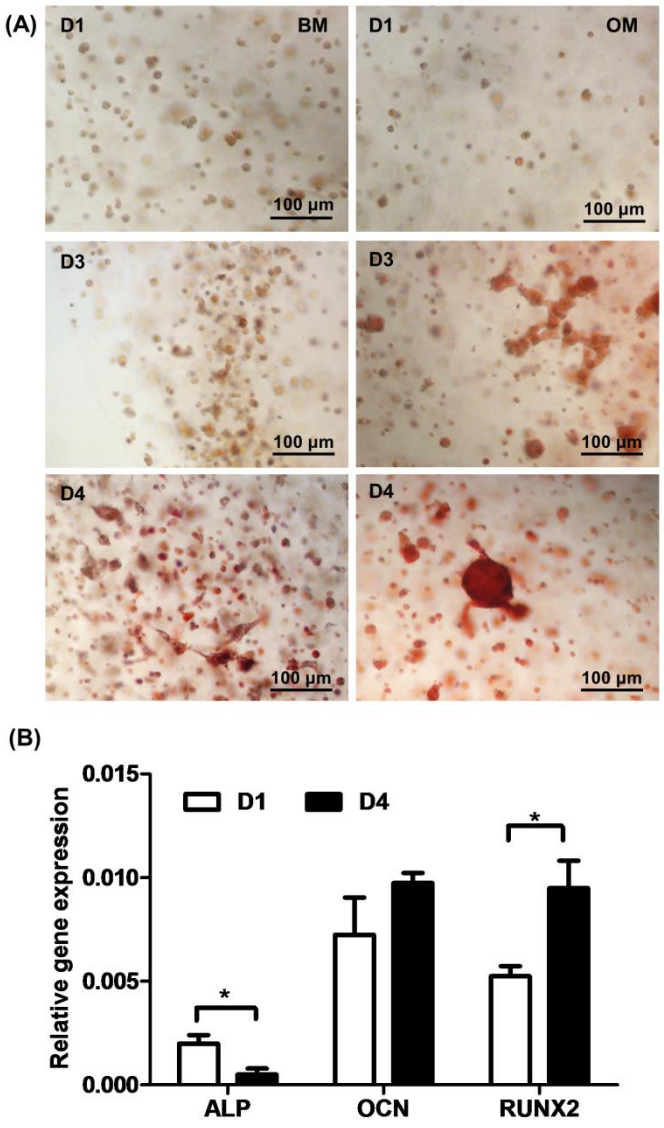

Fig. 5. Effect of cell density on hMSCs osteogenic differentiation in 3D. (**A**) Alkaline phosphatase (ALP)-stained whole mounts of hMSCs-laden 3D matrices with different cell densities (D1=2×10^6, D3=7.5×10^6 and D4=15×10^6 cells/ml) cultured under basal (BM) or osteoinductive (OM) conditions for 7 days. (**B**) qRT-PCR analysis of gene expression of ALP, RUNX2 and OCN for hMSCs-laden 3D matrices cultured under basal conditions for 7 days at D1=2×10^6 cells/ml and D4=15×10^6 cells/ml. Data is presented as mean±stdev (n=3), (*) denotes statistical differences ($p<0.05$).

3.4. hMSCs aggregation in high-density osteoinductive 3D cultures

In view of the prior results, the process of hMSCs aggregation in high-density osteoinductive 3D cultures was further analysed in more detail. F-actin staining of whole-mounted samples (Fig. 6) showed that hMSCs progressively spread and aggregated along two weeks of culture under osteoinductive conditions, while they remained essentially dispersed throughout the matrix under basal conditions.

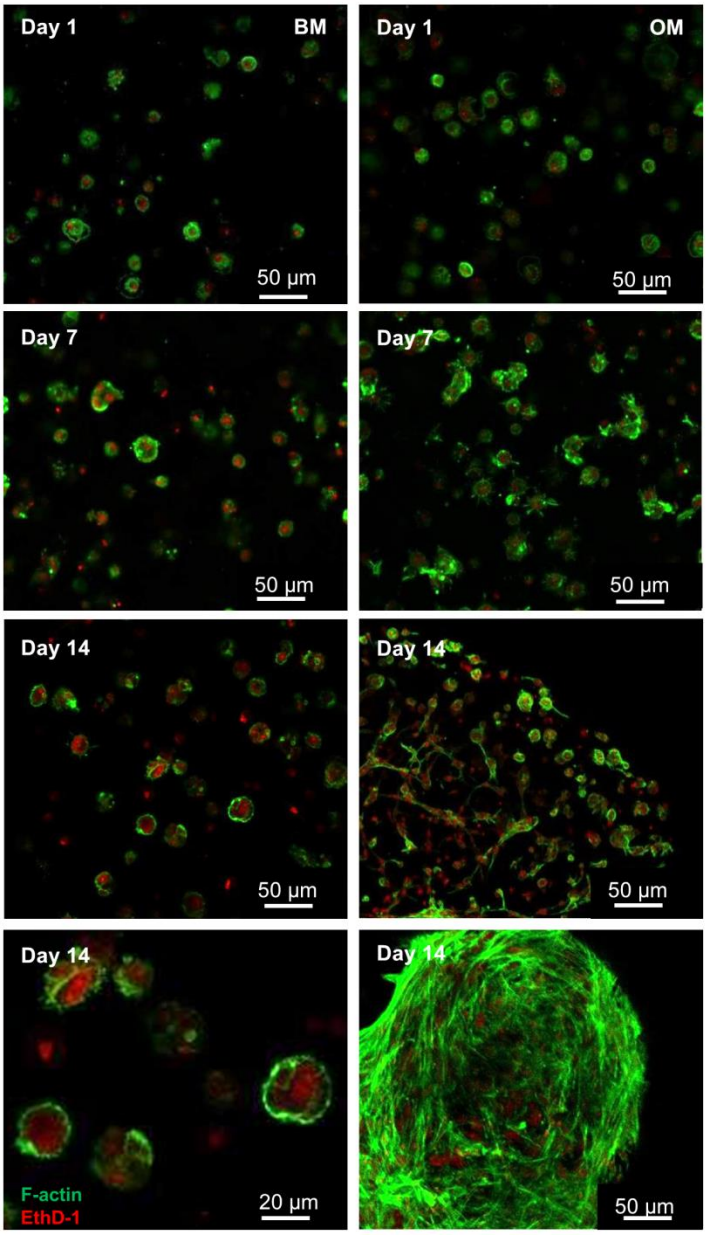

Fig. 6. Formation of hMSCs aggregates in high-density osteoinductive cultures along the time. Morphology and spatial reorganization of hMSCs cultured along 2 weeks in 3D, under basal (BM) or osteoinductive conditions (OM), at a density of D4=15×10^6 cells/mL. Filamentous actin was stained with Alexa Fluor 488 phallodin (green) and images were obtained by CSLM of whole-mounted samples.

Several of these hMSCs clusters were found within each matrix (Fig. 7A), and were stabilized by an extracellular fibronectin mesh (Fig. 7B). Fibronectin expression was also detected in individual cells, but only intracellularly (Fig. 7B, inset). To better investigate the origin of these aggregates, an immunostaining for the cell cycle-related proliferation marker Ki67 was performed. As depicted in Fig. 7C and Fig. 7D only a few Ki67 positive cells were detected, and those were only occasionally present within the hMSCs clusters. Therefore, the hypothesis of cell migration followed by cell–cell adhesion of neighbouring cells with subsequent aggregate formation, as opposed to mitosis, seems more convincing.

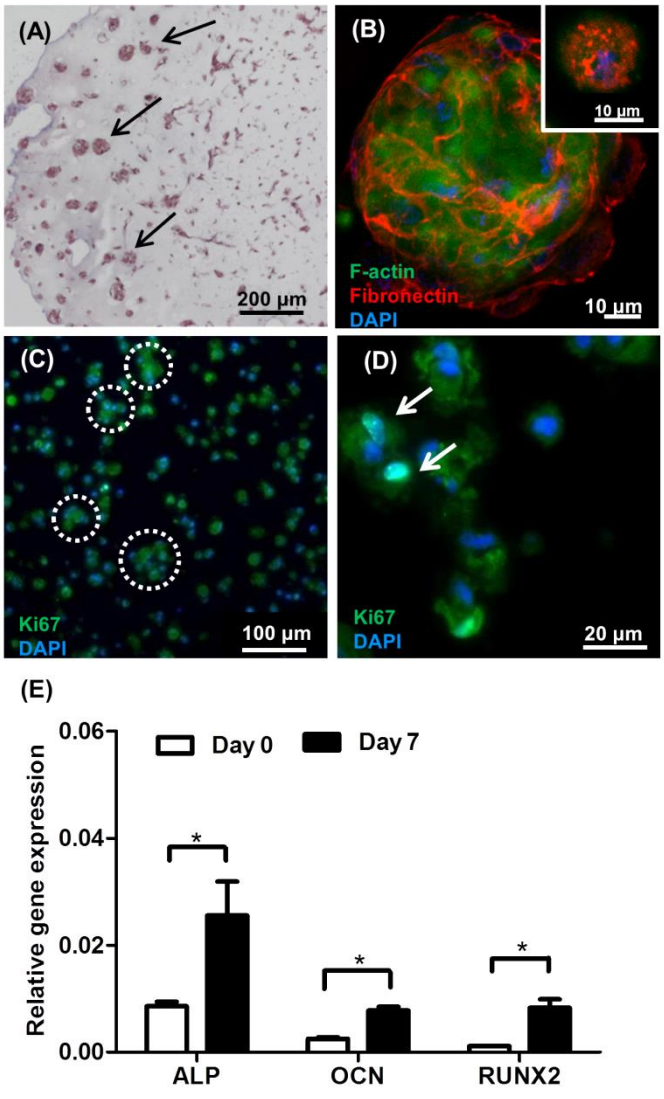

Fig. 7. Formation of hMSCs aggregates in high-density osteoinductive cultures. (**A**) Several hMSCs clusters (black arrows) were detected within RGD-alginate 3D matrices under osteoinductive conditions (OM), after 2 weeks of culture. (**B**) These aggregates were stabilized by a fibronectin mesh (red, inset: FN expression in isolated cells). (**C**) and (**D**) Only a few proliferating hMSCs (Ki67 positive cells, arrows) were detected within the 3D matrices, and only occasionally within clusters (dashed circles). (**E**) qRT-PCR analysis showed that hMSCs retrieved from high-density osteoinductive cultures expressed several osteogenic genes (ALP, RUNX2 and OCN). Data is presented as mean±stdev (n=3), (*) denotes statistical differences ($p<0.05$).

Finally, the expression of osteogenic markers in high-density hMSCs 3D cultures was analysed at the gene level (Fig. 7E). After 7 days in osteoinductive medium, hMSCs expressed higher levels of RUNX2, ALP and OCN, confirming that upon high-density 3D entrapment within alginate hydrogels, hMSCs remained responsive to osteoinductive stimuli and able to differentiate along the osteoblastic lineage

4. DISCUSSION

The effect of cell seeding density on the behaviour of hMSCs cultured under 3D conditions within RGD-alginate hydrogels was evaluated. Densities in the range of 2 to 15 million cells per mL of hydrogel were tested, and cells were cultured in basal and osteoinductive media. Independently of the cell density, low levels of (mitochondrial) metabolic activity were observed when cells were cultured in 3D, which attained a nearly steady state after approximately 3 days of culture. This was consistent with the total dsDNA quantifications that showed that hMSCs in 3D were essentially in a non-proliferative state. Similar results have been previously observed by us [8] and confirmed by other authors, namely with 3D cultures within alginate hydrogels. For example, Markusen and co-workers did not observe MSCs proliferation after cell entrapment at a density of 10×10^6 cell/mL within 1wt% RGD-alginate beads after 2 weeks of culture [30], neither did Duggal *et al.* in similar matrices of 1.8wt% RGD-alginate but at lower cell density (2×10^6 cell/mL) [32]. Studies from Lan and co-workers, using a hepatocytic cell line (HepG2) grown on 2D (collagen-coated plates) and in 3D (1wt% unmodified alginate matrices) at a final density of 2×10^6 cell/mL, have shown that the number of cells cultured on 2D culture increased dramatically after 2 weeks of culture (4.5-fold), while in 3D no significant differences were seen [33]. In addition, Ma and colleagues entrapped MSCs within 1.2wt% alginate beads and observed no proliferation since cells entered the G0/G1 phase but did not progress along the cell cycle to the S phase, remaining in a nearly steady-state [34]. Those studies suggest that cell proliferation in 3D requires strategies to overcome the physical impediment posed by the matrix, which is dependent on the matrix stiffness [35]. Those restrictions may induce growth-arrest, stimulating cell senescence or favouring a quiescent-like steady state. Although future studies need to be carried out to draw a valid conclusion, the results presented here seem to support the last hypothesis. In fact, the cardinal feature of quiescence, which distinguishes it from other non-dividing cell states, such as senescence, apoptosis, and terminal differentiation, is that quiescence is reversible [36].

As shown here, hMSCs not only maintained high viability throughout the 3D culture period, but also seemed to have re-entered the cell cycle when transferred from 3D to 2D, with a concomitant increase in metabolic activity. This is in accordance with the results from Hunt *et al.*, who reported that fibroblasts significantly decrease their metabolic activity upon entrapment within alginate hydrogels, but subsequently recovered a normal mitotic activity upon retrieval from 3D [37].

At the highest cell density tested here (D4=15×10^6 cells/mL), and especially under osteoinductive conditions, 3D-cultured hMSCs were shown to spread along the time, establishing contacts with neighbouring cells and forming multicellular aggregates. These clusters apparently resulted from the self-assembling and intercellular adhesion of previously isolated cells, and not from clonal expansion. This hypothesis is supported by the changes in cell morphology along the time, characteristic of migrating cells, and by the low number of Ki67 positive cells within aggregates.

The fact that cell aggregation is favoured in osteoinductive medium, compared with the basic medium, is probably related to the highest rate of degradation of the hydrogels observed under these conditions. This might be due to the presence of different hydrogel-destabilizing agents in OM, including non gelling-sodium ions and calcium-sequestering agents such as phosphates, which reverse the gelation mechanism [38], and of reducing agents such as ascorbic acid that might contribute to alginate hydrolysis [39]. The alginate hydrogel degradation might in turn be accelerated by the presence of cells, as suggested by others [40]. Clearly, hydrogel swelling and degradation facilitates cell mobility, spreading and aggregation inside the matrix [41]. Other authors have reported a correlation between cell density and the formation of cell aggregates within 3D matrices. For example, Maguire *et al.* [21] described the aggregation of hepatocytes within alginate beads, a process that played a central role in controlling cell differentiation. The aggregation process was dependent on the initial cell seeding density, with larger aggregates being obtained at the highest density tested (5×10^6 cells/ml). Zhang C *et al.* described the spontaneous aggregation of chondrocytes within PEG-based hydrogels [22]. Again, higher cell densities (20×10^6 cells/ml) resulted in an earlier onset of cluster formation and in larger clusters. Notably, cell aggregation resulted in enhanced endogenous ECM production, which is in accordance with our results, as we also demonstrated that the formation of hMSCs aggregates was related with the local deposition of ECM components, namely fibronectin and collagen. Actually, fibronectin polymerization is known to play an important role in the self-assembly of multicellular structures, acting as a “glue” by promoting α5β1-integrin mediated intercellular cohesion [42].

In our study, high-density cultures were also shown to efficiently differentiate along the osteoblastic lineage, as demonstrated by the expression of osteogenic markers at both gene and protein levels. In particular, hMSCs clusters stained intensively for ALP activity after 1 week of culture, even under basal conditions. A correlation between MSCs aggregation and osteogenic differentiation has also been described in some studies, but it has not been fully clarified. In classical 2D studies, for example, the formation of bone nodules has been associated with the expression of a mineralized ECM in MSCs cultures [43], suggesting the importance of cell-cell interactions in osteogenesis. In 3D, a positive effect of cell aggregation in osteogenesis has been mainly reported in studies using MSCs spheroids [44, 45]. As proposed in some of those studies, self-organized cellular structures might be interesting for use in tissue

engineering strategies, since they may function as building blocks for tissue reconstruction [46, 47], and might also enhance the therapeutic efficacy of hMSCs. In fact, the use of hMSCs aggregates in cell-based therapies has been recently proposed as a means to overcome the limitations related with dissociated-cell delivery [48].

The culture of hMSCs as 3D aggregates can self-activate important cellular functions, promoting cell survival and migration, improving resistance to oxidative stress, and enhancing secretion of pro-regeneration mediators [49-51]. Moreover, the presence of an endogenous ECM environment in MSCs aggregates can be regarded as an added benefit, as it might have additional cytoprotective effects promoting cell survival under ischemic and oxidative stress, and even extending hMSCs retention at the injury site [48]. This feature is also important in tissue engineering strategies, as the deposition of new ECM is essential to provide structural support to cells and replace the artificial matrix as it degrades.

5. CONCLUSIONS

The initial cell seeding density at which hMSCs are entrapped within RGD-alginate hydrogels regulates cellular activities within this type of 3D matrices. On high-density cultures, cell viability is better maintained, and cell-cell signalling is promoted as hMSCs are induced to connect to each other and aggregate into multicellular structures, particularly under osteoinductive conditions. Clustered hMSCs produced their own ECM, rich in fibronectin and collagen, and successfully differentiated along the osteoblastic lineage. These hMSCs-ECM microtissues may function as building blocks for tissue reconstruction, and find interesting applications in tissue engineering strategies, especially when combined with advanced bioprinting technologies. Taken together, the results present herein also confirm and highlight the importance of selecting the most appropriate cell entrapping density when establishing 3D cultures for a specific application.

Acknowledgements

This work was financed by FEDER funds through the Programa Operacional Factores de Competitividade (COMPETE) and by Portuguese funds through Fundação para a Ciência e a Tecnologia (FCT): Pest-C/SAU/LA0002/2011, PTDC/SAU-BEB/101235 /2008 and FCOMP-01-0124-FEDER-010915. FRM acknowledges INL-International Iberian Nanotechnology Laboratory for her PhD scholarship. CB has a research position (Ciência 2008) funded by FCT-POPH-FSE, and GMG has an FCT post-doctoral scholarship (SFRH/BPD/85651/2012).

6. REFERENCES

[1] Tibbitt MW, Anseth KS. Hydrogels as extracellular matrix mimics for 3D cell culture. Biotechnol. Bioeng. 2009;103:655-63.

[2] Huang G, Wang L, Wang S, Han Y, Wu J, Zhang Q, et al. Engineering three-dimensional cell mechanical microenvironment with hydrogels. Biofabrication 2012;4:1758-5082.

[3] Vacharathit V, Silva EA, Mooney DJ. Viability and functionality of cells delivered from peptide conjugated scaffolds. Biomaterials 2011;32:3721-8.

[4] Zhang Y, Yu Y, Chen H, Ozbolat IT. Characterization of printable cellular micro-fluidic channels for tissue engineering. Biofabrication 2013;5:025004.

[5] Buyukhatipoglu K, Jo W, Sun W, Clyne AM. The role of printing parameters and scaffold biopolymer properties in the efficacy of a new hybrid nano-bioprinting system. Biofabrication 2009;1:035003.

[6] Evangelista MB, Hsiong SX, Fernandes R, Sampaio P, Kong H-J, Barrias CC, et al. Upregulation of bone cell differentiation through immobilization within a synthetic extracellular matrix. Biomaterials 2007;28:3644-55.

[7] Bidarra SJ, Barrias CC, Fonseca KB, Barbosa MA, Soares RA, Granja PL. Injectable in situ crosslinkable RGD-modified alginate matrix for endothelial cells delivery. Biomaterials 2011;32:7897-904.

[8] Bidarra SlJ, Barrias CC, Barbosa MrA, Soares R, Granja PL. Immobilization of Human Mesenchymal Stem Cells within RGD-Grafted Alginate Microspheres and Assessment of Their Angiogenic Potential. Biomacromolecules 2010;11:1956-64.

[9] Fonseca KB, Bidarra SJ, Oliveira MJ, Granja PL, Barrias CC. Molecularly designed alginate hydrogels susceptible to local proteolysis as three-dimensional cellular microenvironments. Acta Biomater. 2011;7:1674-82.

[10] Rowley JA, Madlambayan G, Mooney DJ. Alginate hydrogels as synthetic extracellular matrix materials. Biomaterials 1999;20:45-53.

[11] Fonseca KB, Maia FR, Cruz FA, Andrade D, Juliano MA, Granja PL, et al. Enzymatic, physicochemical and biological properties of MMP-sensitive alginate hydrogels. Soft Matter 2013;9:3283-92.

[12] Lutolf MP, Gilbert PM, Blau HM. Designing materials to direct stem-cell fate. Nature 2009;462:433-41.

[13] Huebsch N, Arany PR, Mao AS, Shvartsman D, Ali OA, Bencherif SA, et al. Harnessing traction-mediated manipulation of the cell/matrix interface to control stem-cell fate. Nat. Mater. 2010;9:518-26.

[14] Puliafito A, Hufnagel L, Neveu P, Streichan S, Sigal A, Fygenson DK, et al. Collective and single cell behavior in epithelial contact inhibition. Proc. Natl. Acad. Sci. 2012;109:739-44.

[15] Heckman CA. Contact inhibition revisited. J. Cell. Physiol. 2009;220:574-5.

[16] Hohn HP, Grümmer R, Boßerhoff S, Graf-Lingnau S, Reuss B, Bäcker C, et al. The role of matrix contact and of cell-cell interactions in choriocarcinoma cell differentiation. Eur. J. Cell Biol. 1996;69:76-85.

[17] Cukierman E, Pankov R, Stevens DR, Yamada KM. Taking cell-matrix adhesions to the third dimension. Science 2001;294:1708-12.
[18] Huang AH, Yeger-McKeever M, Stein A, Mauck RL. Tensile properties of engineered cartilage formed from chondrocyte- and MSC-laden hydrogels. Osteoarthr. Cartil. 2008;16:1074-82.
[19] Mudera V, Smith AST, Brady MA, Lewis MP. The effect of cell density on the maturation and contractile ability of muscle derived cells in a 3D tissue-engineered skeletal muscle model and determination of the cellular and mechanical stimuli required for the synthesis of a postural phenotype. J. Cell. Physiol. 2010;225:646-53.
[20] Babalola OM, Bonassar LJ. Effects of seeding density on proteoglycan assembly of passaged mesenchymal stem cells. Cell. Mol. Bioeng. 2010;3:197-206.
[21] Maguire T, Davidovich AE, Wallenstein EJ, Novik E, Sharma N, Pedersen H, et al. Control of hepatic differentiation via cellular aggregation in an alginate microenvironment. Biotechnol. Bioeng. 2007;98:631-44.
[22] Zhang C, Sangaj N, Hwang Y, Phadke A, Chang C-W, Varghese S. Oligo(trimethylene carbonate)–poly(ethylene glycol)–oligo(trimethylene carbonate) triblock-based hydrogels for cartilage tissue engineering. Acta Biomater. 2011;7:3362-9.
[23] Talukdar S, Nguyen QT, Chen AC, Sah RL, Kundu SC. Effect of initial cell seeding density on 3D-engineered silk fibroin scaffolds for articular cartilage tissue engineering. Biomaterials 2011;32:8927-37.
[24] Lin C-C, Raza A, Shih H. PEG hydrogels formed by thiol-ene photo-click chemistry and their effect on the formation and recovery of insulin-secreting cell spheroids. Biomaterials 2011;32:9685-95.
[25] Kraehenbuehl TP, Zammaretti P, Van der Vlies AJ, Schoenmakers RG, Lutolf MP, Jaconi ME, et al. Three-dimensional extracellular matrix-directed cardioprogenitor differentiation: Systematic modulation of a synthetic cell-responsive PEG-hydrogel. Biomaterials 2008;29:2757-66.
[26] Stephan S, Eustace Johnson W, Roberts S. The influence of nutrient supply and cell density on the growth and survival of intervertebral disc cells in 3D culture. Eur. Cells Mater. 2011;22:97-108.
[27] Hui TY, Cheung KMC, Cheung WL, Chan D, Chan BP. In vitro chondrogenic differentiation of human mesenchymal stem cells in collagen microspheres: Influence of cell seeding density and collagen concentration. Biomaterials 2008;29:3201-12.
[28] Oliveira SM, Barrias CC, Almeida IF, Costa PC, Ferreira MRP, Bahia MF, et al. Injectability of a bone filler system based on hydroxyapatite microspheres and a vehicle with in situ gel-forming ability. J. Biomed. Mater. Res., Part B 2008;87B:49-58.
[29] Folkman J, Moscona A. Role of cell shape in growth control. Nature 1978;273:345-9.
[30] Markusen JF, Mason C, Hull DA, Town MA, Tabor AB, Clements M, et al. Behavior of adult human mesenchymal stem cells entrapped in alginate-GRGDY beads. Tissue Eng. 2006;12:821-30.

[31] Ng KW, Leong DT, Hutmacher DW. The challenge to measure cell proliferation in two and three dimensions. Tissue Eng. 2005;11:182-91.
[32] Duggal S, Frønsdal KB, Szöke K, Shahdadfar A, Melvik JE, Brinchmann JE. Phenotype and gene expression of human mesenchymal stem cells in alginate scaffolds. Tissue Eng., Part A 2008;15:1763-73.
[33] Lan S-F, Safiejko-Mroczka B, Starly B. Long-term cultivation of HepG2 liver cells encapsulated in alginate hydrogels: A study of cell viability, morphology and drug metabolism. Toxicol. In Vitro 2010;24:1314-23.
[34] Ma H-L, Hung S-C, Lin S-Y, Chen Y-L, Lo W-H. Chondrogenesis of human mesenchymal stem cells encapsulated in alginate beads. J. Biomed. Mater. Res., Part A 2003;64A:273-81.
[35] Bott K, Upton Z, Schrobback K, Ehrbar M, Hubbell JA, Lutolf MP, et al. The effect of matrix characteristics on fibroblast proliferation in 3D gels. Biomaterials 2010;31:8454-64.
[36] Coller HA, Sang L, Roberts JM. A new description of cellular quiescence. PLoS Biol. 2006;4.
[37] Hunt NC, Shelton RM, Grover LM. Reversible mitotic and metabolic inhibition following the encapsulation of fibroblasts in alginate hydrogels. Biomaterials 2009;30:6435-43.
[38] Nicodemus GD, Bryant SJ. Cell encapsulation in biodegradable hydrogels for tissue engineering applications. Tissue Eng. Part B Rev. 2008;14:149-65.
[39] Smidsrod O, Haug A, Larsen B. Degradation of alginate in the presence of reducing compounds. Acta Chem. Scand. 1963;17:2628-37.
[40] Hunt NC, Smith AM, Gbureck U, Shelton RM, Grover LM. Encapsulation of fibroblasts causes accelerated alginate hydrogel degradation. Acta Biomater. 2010;6:3649-56.
[41] Khetan S, Guvendiren M, Legant WR, Cohen DM, Chen CS, Burdick JA. Degradation-mediated cellular traction directs stem cell fate in covalently crosslinked three-dimensional hydrogels. Nat. Mater. 2013;12:458-65.
[42] Robinson EE, Foty RA, Corbett SA. Fibronectin matrix assembly regulates α5β1-mediated cell cohesion. Mol. Biol. Cell 2004;15:973-81.
[43] Maniatopoulos C, Sodek J, Melcher AH. Bone formation in vitro by stromal cells obtained from bone marrow of young adult rats. Cell Tissue Res. 1988;254:317-30.
[44] Wang W, Itaka K, Ohba S, Nishiyama N, Chung U-i, Yamasaki Y, et al. 3D spheroid culture system on micropatterned substrates for improved differentiation efficiency of multipotent mesenchymal stem cells. Biomaterials 2009;30:2705-15.
[45] Hildebrandt C, Büth H, Thielecke H. A scaffold-free in vitro model for osteogenesis of human mesenchymal stem cells. Tissue and Cell 2011;43:91-100.
[46] Lin R-Z, Chang H-Y. Recent advances in three-dimensional multicellular spheroid culture for biomedical research. Biotechnol. J. 2008;3:1172-84.
[47] Guo C-L. Mechanical models for the self-organization of tubular patterns. Biomatter 2013;3:e24926.
[48] Kim J, Ma T. Endogenous extracellular matrices enhance human mesenchymal stem cell aggregate formation and survival. Biotechnol. Prog. 2013;29:441-51.

[49] Bartosh TJ, Ylöstalo JH, Mohammadipoor A, Bazhanov N, Coble K, Claypool K, et al. Aggregation of human mesenchymal stromal cells (MSCs) into 3D spheroids enhances their antiinflammatory properties. Proc. Natl. Acad. Sci. 2010;107:13724-9.
[50] YlÖstalo JH, Bartosh TJ, Coble K, Prockop DJ. Human mesenchymal stem/stromal cells cultured as spheroids are self-activated to produce prostaglandin E2 that directs stimulated macrophages into an anti-inflammatory phenotype. Stem Cells 2012;30:2283-96.
[51] Bhang SH, Lee S, Shin JY, Lee TJ, Kim BS. Transplantation of cord blood mesenchymal stem cells as spheroids enhances vascularization. Tissue Eng., Part A 2012;18:2138-47.
[52] Friedl P, Bröcker EB. The biology of cell locomotion within three-dimensional extracellular matrix. Cell. Mol. Life Sci. 2000;57:41-64.

SUPPLEMENTARY DATA

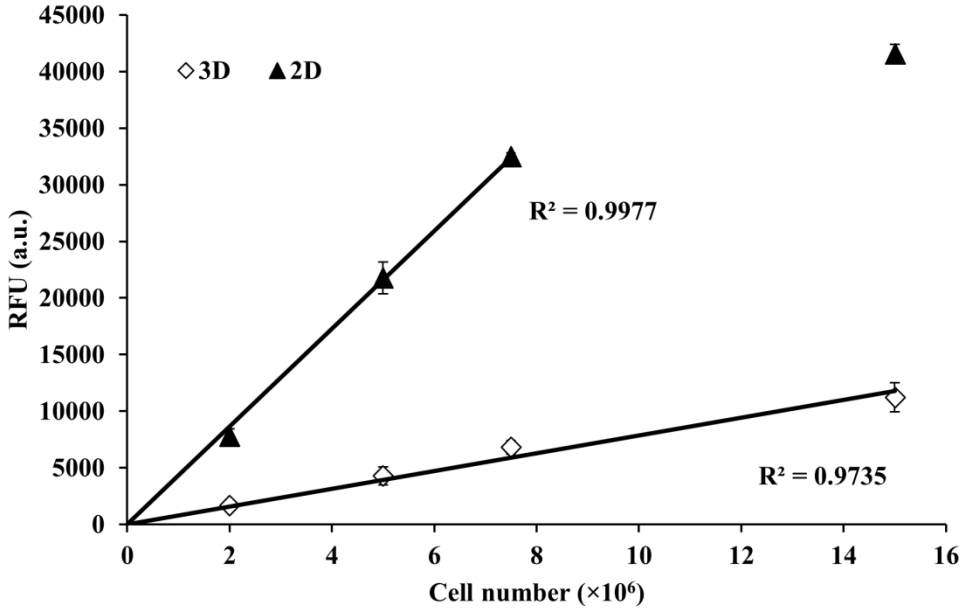

Fig. S1. Resazurin assay performed in 2D and 3D cultured hMSCs for all densities tested. The metabolic activity of hMSCs immediately after entrapment within 3D alginate matrices at low-to-high cell densities was analyzed and compared to that of cells cultured under standard 2D conditions (same total cell number per sample). This test was important to evaluate the effectiveness of using this type of colorimetric metabolic assay, which do not necessarily correlate linearly with increasing cell densities, and might be inadequate to monitor 3D-cultures, as already suggested in the literature [52]. In 2D-cultured hMSCs, a clear rise in metabolic activity was recorded as cell density increased, with a linear response (R^2=0.998) from D1 (40 000 cells per sample) to D3 (150 000 cells per sample), but a loss of linearity at D4. Compared with the 2D-culture, 3D-cultured cells produced a significantly lower fluorescent signal but a linear relationship between fluorescence and cell numbers was still maintained for the entire range of densities (R^2=0.974).

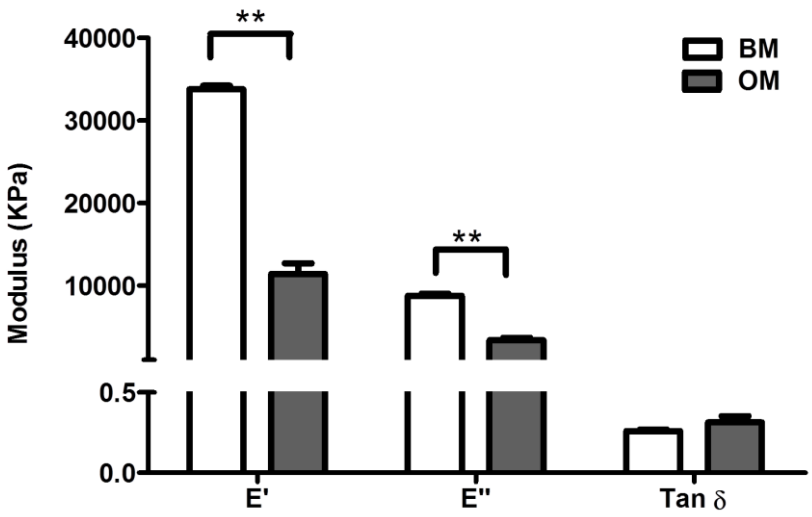

Fig. S2. Dynamic mechanical analysis (DMA) of acellular RGD-alginate matrices after two weeks of culture in BM and OM. The mechanical properties of the hydrogels are more rapidly lost in OM than in BM. Samples (hydrogel cylinders, 5.5 mm diameter and 1.5 mm height) were retrieved from culture and immediately loaded onto the Compression Mode clamp assembly of a TRITEC2000B DMA (Triton Technology). Measurements were performed under RT conditions (humidity ~44%, 20ºC). A user-defined small compression load was applied to guarantee an adequate contact between the swollen samples and the device. A time-scan at a frequency of 1Hz and a strain of 1% (within the linear viscoelastic regimen) was performed during 5 min, and the compressive storage modulus (E', elastic component), loss modulus (E'', viscous component) and damping (E''/E', tan δ) were calculated. At least 6 replicas were tested for each condition. Results are presented as mean±SD. (*) denotes statistical differences ($p<0.05$).

CHAPTER IV

*SELF-ASSEMBLY OF MSC-ECM MICROTISSUES IN SOFT ALGINATE HYDROGEL MATRICES**

F. Raquel Maia, [a,b] Keila B. Fonseca,[a,b] Gabriela Rodrigues, [c] Pedro L. Granja[a,b,d] and Cristina C. Barrias*[a]

[a] INEB - Instituto de Engenharia Biomédica, Rua do Campo Alegre, n.º 823, 4150-180 Porto, Portugal

[b] FEUP – Faculdade de Engenharia, Universidade do Porto, Rua Dr. Roberto Frias s/n, 4200-465 Porto, Portugal

[c] FCUL – Centro de Biologia Ambiental / Departamento de Biologia Animal, Faculdade de Ciências, Universidade de Lisboa, Campo Grande s/n, 1749-016 Lisboa, Portugal

[d] ICBAS - Instituto de Ciências Biomédicas Abel Salazar, Universidade do Porto, Rua de Jorge Viterbo Ferreira n.º 228, 4050-313 Porto, Portugal

* Submitted in 2013.

ABSTRACT

Mesenchymal stem cells (MSCs) can be driven to self-assemble into microtissues in response to specific matrix cues, a process that depends on a balance between cell-matrix and cell-cell interactions. The effect of such cues, and especially their interplay, is still not fully clarified, particularly in 3D-systems. Here, the behaviour of human MSCs (hMSCs) cultured within hydrogel matrices with tailored stiffness and composition was evaluated. hMSCs aggregation only occurred in more compliant matrices (G' ≤ 120 Pa), when compared to stiffer ones, both in the presence and absence of matrix-bound arginine-glycine-aspartic cell-adhesion ligands (RGD; 0, 100 and 200 μM). Fibronectin assembly stabilized cell-cell contacts within aggregates, even in non-adhesive matrices. However, hMSCs were only able to substantially contract the artificial matrix when RGD was present. Moreover, compliant matrices facilitated cell proliferation and provided a permissive environment for hMSCs osteogenic differentiation, even without RGD. Cell interactions with the original matrix became less important as time progressed, while the de novo produced extracellular matrix (ECM) turned into a more critical determinant of cell fate. These data provide further insights into the mechanisms by which hMSCs sense their microenvironment to organize into tissues, and provide new clues to the design of cell-instructive 3D matrices.

Keywords: hydrogels, viscoelastic properties, cell traction, cell-matrix interactions, cell aggregation

1. INTRODUCTION

The important role of the microenvironment in cell behaviour is currently recognized, being well established that cells respond to the intrinsic properties of their matrix, namely to mechanical cues [1]. The work of Engler *et al.* has largely contributed to shed light on the processes of mechanosensing, notably by demonstrating that matrix elasticity directs stem cell lineage specification [2]. It has also long been known that the matrix dimensionality plays a key role in cell signalling events [3, 4] affecting, in particular, the way cells experience mechanical stresses and strains [5]. However, there are still many open questions on the intersection between mechanobiology and 3D, as most studies have been carried out using 2D or "on top" 3D assays that do not recapitulate the normal environment of most cell types.

The effect of matrix cues in "true" 3D systems, where cells are embedded within a hydrogel-like matrix, has been traditionally addressed using ECM-derived hydrogels, such as collagen and fibrin, which do not allow a great level of control over signal presentation. More recently, engineered artificial matrices, with tuneable biochemical and mechanical properties, have also been explored [6, 7]. These 3D models have been vital for systematically deconstructing the role of different signals and their interplay [8, 9]. Surprisingly, only a few studies have focused on the use of very soft hydrogels (storage modulus, G' < 1000 Pa), although the reported results are quite stimulating. In fact, compliant matrices have been shown to facilitate different cellular activities, including spreading [10, 11], proliferation [10, 12], and migration [13], among others, in different cell types.

Apart from the matrix stiffness, the molecular characteristics of the hydrogels, and their resulting viscoelastic behaviour, also have a direct impact on these processes. Cells in 3D must overcome the physical barrier imposed by the polymeric network, and will clearly encounter less resistance in softer and more deformable matrices (G' < 1760 Pa) [14]. For example, Bott *et al.*[10] have shown that the spreading and proliferation of fibroblasts within PEG matrices are increased in softer (G' < 250 Pa) vs. stiffer (G' > 1200 Pa) hydrogels, irrespectively of their degradation profile. Interestingly, the authors also show that fibroblasts are able to contract viscous-like collagen gels [15], but not elastic-like PEG hydrogels with a similar G' (G' ≈ 200 Pa) [10]. Ehrbar *et al.* have shown that preosteoblastic cells entrapped within soft matrices (G' < 94 Pa) can engage in a degradation-independent 3D migration mode, and overcome the matrix resistance by deforming the network and/or using hydrogel defects [13]. Different studies demonstrated that endothelial cells network assembly and tubulogenesis are favoured in low stiffness matrices [16, 17]. Recently, Matyash *et al.* have shown that soft alginate hydrogels (G' < 64 Pa), prepared with sub-stoichiometric concentrations of crosslinking ions, promote extensive neurite growth, even in the absence of cell-adhesion ligands, while protecting neurons against oxidative stress [11]. The communication between cells also seems to be facilitated in compliant matrices. In particular, Reinhart-King *et al.* have shown that pairs of endothelial cells in compliant substrates (G' = 500 Pa) communicate through mechanical signals in a stiffness-dependent manner: when the matrix stiffness is low enough, cells can perceive and react to substrate strains created by the traction stresses of neighbouring cells [18, 19]. Altogether,

these examples emphasize the interest of further exploring cell behaviour in compliant 3D matrices. They also suggest that the molecular characteristics and viscoelastic profile of hydrogels, which are generally poorly discussed, are relevant features with a clear impact on the process of mechanosensing.

Here, the polymer dry-mass content of alginate hydrogels with a bimodal molecular weight distribution was modulated to prepare 3D matrices with very different viscoelastic profiles. While 2 wt.% alginate hydrogels are stiffer and behave predominantly as elastic-like materials, similar to synthetic hydrogels [10], 1 wt.% hydrogels are softer and display a more viscous-like behaviour, typically observed in ECM-derived hydrogels [10]. The hydrogels were also modified with controlled densities of RGD peptides to promote integrin-mediated cell-matrix adhesion. Integrin receptors act as major sensors and integrators of microenvironmental signals, being particularly relevant as mechanotransducers [20]. This versatile system was used to investigate the effect of matrix cues on human mesenchymal stem cells behaviour (hMSCs) in 3D, at different levels, and the interplay between viscoelastic properties and ligand presentation was addressed. A new approach was established to foster the formation of hMSCs aggregates stabilized by endogenous ECM, which better mimic complex tissue structures and provide interesting 3D *in vitro* model systems or building blocks for regenerative therapies [21, 22].

2. MATERIALS AND METHODS

2.1. Synthesis and characterization of RGD-alginate

Sodium alginate (Protanal LF 20/40, a gift from FMC Biopolymers) with a high ratio of guluronate to mannuronate content (>60%) with Mw=1.5×10^5 Da and Mw=2.5×10^4 Da were used, respectively, as the high (HMW) and low molecular weight (LMW) components of the hydrogel matrices [23]. Both were purified through dialysis against deionized water for 3 days (MWCO 3500 membrane, Spectrum Labs), and with activated charcoal (Sigma, 0.5 g per g alginate). The HMW alginate was partially oxidized to a theoretical extent of 1% of sugar residues with sodium periodate [24]. Both components were grafted with the cell-adhesion peptide (glycine)4-arginine-glycine-aspartic acid-serine-proline (hereafter abbreviated as RGD), using aqueous carbodiimide chemistry as previously described [25]. Briefly, alginate solutions (1 wt.%) in MES buffer (0.1M MES, 0.3M NaCl, pH 6.5) were prepared and stirred overnight (ON) at room temperature (RT). N-hydroxy-sulfosuccinimide (Sulfo-NHS, Pierce) and 1-ethyl-(dimethylaminopropyl)-carbodiimide (EDC, Sigma, 27.4 mg/g alginate) were sequentially added at a molar ratio of 1:2, followed by 17 mg of RGD peptide (Genscript) per g of alginate. Control samples were prepared without addition of peptide (hereafter designated as HMW0 or LMW0). After stirring for 20h at RT, the reaction was quenched with hydroxylamine and the solution was

dialysed against deionized water for 3 days (MWCO 3500). After purification with charcoal, RGD-alginate was lyophilized and stored at -20ºC until further use.

The amount of grafted RGD was quantified using the BCA Protein Assay (Pierce). Briefly, samples (1 wt.% RGD-alginate) were incubated in BCA reagent for 60 min at 37ºC in the dark and the absorbance was read at Ex/Em of 540/620 nm in a microplate reader (Power Wave Xs, Biotek). A set of RGD solutions (0 to 1 mg/mL in 1 wt.% HMW0 or LMW0) were used as standards to produce a calibration curve. Typically, the reaction yield was of ca. 90%, determined by the BCA Total Protein assay as described in [6].

2.2. RGD-alginate 3D matrices: compositions and *in situ* hydrogel formation

In-situ forming alginate hydrogel matrices were prepared by internal gelation as described previously [16, 25, 26]. Hydrogel precursor solutions were composed by binary mixtures (50:50 v/v) of HMW and LMW sodium alginate, at different polymer concentrations (1 and 2 wt.%) and RGD densities (0, 100 or 200 µM: along the manuscript these formulations are often referred as 1-0, 1-100, 1-200; and 2-0, 2-100, 2-200; where the first number represents the concentration of alginate and the second number denotes the concentration of RGD). The range of RGD density selected herein is comparable to that of commonly used ECM-derived biological matrices [7]. Sodium alginate solutions were sterile-filtered (0.22 µm) and mixed with an aqueous suspension of $CaCO_3$ (Fluka) at a $CaCO_3$/COOH molar ratio of 1.6 [26]. Then, a fresh sterile solution of glucone delta-lactone (GDL, Sigma) was added to trigger gelation. The $CaCO_3$/GDL molar ratio was set at 0.125, and the gelation time was 1h. For the 3D-culture studies, hydrogel precursor solutions were combined with human mesenchymal stem cells (hMSCs) prior to hydrogel formation, as described in section 2.5.

2.3. Dynamic mechanical analysis of RGD-alginate hydrogels

Samples were assayed in a TRITEC2000B DMA (Triton Technology). Hydrogel cylinders (∅=5.5 mm; h=1.5 mm) were prepared in a QGel^{TM} 3D disc caster. After crosslinking, the discs were pre-equilibrated ON at 37ºC in DMEM with HEPES (Sigma, 25 mM) and 0.01% NaN_3 (Sigma), and then loaded onto the Compression Mode clamp assembly. Measurements were performed under RT conditions (humidity ~44%, 20ºC). A user-defined small compression load was applied to guarantee an adequate contact between the swollen samples and the device. A time-scan (1Hz and 1% strain, within the LVR – linear viscoelastic region) was performed during 5 min, and the compressive storage modulus (E', elastic component), loss modulus (E'', viscous component) and damping (E''/E', tan δ) were calculated. The influence of polymer concentration (1 and 2 wt.%) and RGD density (0, 100 and 200 µM) on the hydrogel mechanical properties

was analysed. At least 5 replicas were tested for each condition, and the experiment was repeated twice. Averages and standard deviations were reported.

2.4. Oscillatory shear rheometry of RGD-alginate hydrogels

Rheological measurements were carried out using a Kinexus Pro rheometer (Malvern). Swollen hydrogel discs were analysed at day 0 (after swelling to equilibrium in culture media for 2h) and after incubation (24h) under standard culture conditions. To guarantee the dimensional homogeneity of the samples, cylindrical discs were casted with 8 mm, and then 4 mm cylinders were punched from the original ones immediately before analysis. All samples were assayed using a plate-and-plate geometry (∅=4 mm, sandblasted surfaces) and were compressed to 20% of their original thickness to avoid slippage. A solvent trap was used to minimize sample drying. All measurements were performed at 37ºC (Peltier system). Stress sweeps (0.1 Hz) were first performed to determine the LVR for all the tested conditions. Frequency sweeps (0.01-2Hz) were then performed within the LVR.

The values of the shear storage modulus (G') presented in Table 1 were obtained at a frequency of 0.1Hz. Samples were analysed in triplicate and the experiment was repeated twice. The initial mesh size (ξ) of alginate hydrogels was calculated as described in [12] using the measured value of the shear modulus to calculate the molecular weight between crosslinks (further details are provided as supplementary information).

2.5. 3D-cultures of hMSCs within RGD-alginate hydrogel matrices

hMSCs were purchased from Lonza (PT-2501, Lot No. 6F4392) and routinely cultured in low-glucose DMEM with glutamax (Gibco), supplemented with Fetal Bovine Serum (FBS, MSCs-qualified, 10% v/v Gibco) and penicillin/streptomycin (1% v/v Pen/Strep, Gibco). RGD-alginate solutions in NaCl (0.9 wt.%) were combined with crosslinking agents and hMSCs (8×10^6cell/mL). The mixture was pipetted (20 µL) onto the wells of a pHEMA-treated [27] 24-well suspension culture plate for crosslinking (1h). Thereafter, fresh medium was added and renewed after 1h. hMSCs-laden hydrogels were finally incubated under standard conditions (37ºC, 5% v/v CO_2). As a control, hMSCs-laden hydrogels inactivated with methanol (20 min) at the onset of culture were used. Samples were imaged at different time points using a stereoscope (SZX10, Olympus) equipped with a digital camera (DP21, Olympus) and an inverted fluorescence microscope (Axiovert 200M, Zeiss). Cell viability was assessed using the Live/Dead assay. Cell-laden matrices were washed 3 times with DMEM without phenol red (Gibco), then incubated (45 min, 37ºC in the dark) with Calcein AM (1 µM, live cells) and Ethidium homodimer-1 (EthD-1, 2.5 µM, dead cells), and finally washed again. Samples were imaged by confocal laser scanning microscopy (CLSM, Leica SP2 AOBS SE).

2.6. Cell morphology and spatial-distribution (f-actin staining and histology)

After 1 and 7 days of culture, cell-laden hydrogels were washed with Tris-buffered saline (TBS, 50 mM Tris in 150 mM NaCl, pH 7.4, Sigma), and fixed with 4 wt.% paraformaldehyde (PFA, Sigma) in TBS-Ca (TBS with 7.5 mM $CaCl_2$) for 20 min.

For cytoskeleton analysis, samples were permeabilized for 5 min with 0.1% v/v Triton X-100/ TBS-Ca and incubated for 30 min in 1 wt.% BSA/TBS-Ca to block unspecific binding. F-actin filaments were stained with Alexa Fluor 488 phalloidin (Invitrogen, 1:40 in 1 wt.% BSA/TBS-Ca, 1h at RT) and nuclei were counterstained with Ethidium homodimer-1 (EthD-1, Invitrogen, 2.5 μM). Samples were analyzed by CLSM.

For histology, samples were dehydrated with a series of ethanol solutions of increasing concentrations and included in paraffin blocks. Thereafter, sections (3 μm) were recovered, diafanized in xylene and rehydrated with a series of ethanol solutions of decreasing concentrations and finally water.

For Hematoxilin and Eosin (H&E) staining, sections were incubated in Gill's Hematoxylin for 5 min and counterstained with Eosyn Y for 1 min. Finally sections were dehydrated, diafanized in xylene and mounted in glass slides using histofluid (Marienfeld) mounting medium. Samples were imaged by optical microscopy.

2.7. Outward cell migration (modified Boyden chamber assay)

Cell migration was analysed using FluoroBlok™ inserts with an 8 μm pore size (Becton Dickenson) placed in a 24-well tissue culture insert carrier plate (Becton Dickenson). hMSCs were pre-labelled with CellTracker Green CMFDA (Molecular Probes) at 15 μM for 30 min, and then entrapped within alginate matrices as previously described. Cell-laden hydrogel matrices were transferred to the FluoroBlok inserts and serum-free medium (upper chamber) or medium with 30% v/v FBS (lower chamber) were added. Every 24h, the serum-free medium in the upper chamber was renewed and fresh FBS was added to the lower chamber to maintain a gradient and promote chemo-attraction. At different time points (0, 24, 48 and 72h), fluorescence intensity from the basal side was measured using a microplate spectrofluorometer (BioTek) in area-scan bottom-reading mode, at wavelengths of 492/517 nm (Ex/Em).

Results are presented as the increase of fluorescence in relation to time 0. Fluorescence images of migrating cells were collected using an inverted fluorescent microscope. Fluorescence-labelled cells within the alginate matrices were imaged by CLSM.

2.8. Assessment of FN fibril formation and α5-integrin subunit expression by immunostaining

Expression of fibronectin (FN) and α5 integrin was assessed by whole-mount immunostaining to better preserve ECM structure and allow for 3D visualization. After 4h and 24h of culture, samples were washed 3 times with TBS-Ca and fixed with 0.2 wt.% PFA in TBS-Ca (20 min at RT). Samples were then permeabilized with 0.2% v/v Triton X-100 during 10 min and blocked with 1 wt.% BSA for 20 min. Matrices were incubated ON at 4ºC with rabbit anti-fibronectin (f3648, Sigma, 1:400) or rabbit anti-integrin α5 antibody (AB1928, Millipore, 1:300), and then with goat anti-rabbit secondary antibody Alexa Fluor 594 F(ab')2 fragment (Molecular Probes-Invitrogen, 1:1000, 1h at RT). Samples were finally incubated with Alexa Fluor 488 phalloidin (Invitrogen, 1:40) for actin staining, and with 4',6-diamidino-2-phenylindole (DAPI, 0.1 µg/mL) for nuclei staining, and were imaged by CLSM.

2.9. DNA synthesis (^{3}H-TdR and BrdU incorporation assays)

For the Tritiated thymidine (^{3}H-TdR) assay, ^{3}H-TdR was added to the 3D culture medium at a final concentration of 1×10^{-3} Ci/mmol at different time points, and samples were analysed 24h later. As a positive control, hMSCs cultured under 2D-conditions in T25 culture flasks were used, and the initial density (6400 cells/cm^2) was adjusted to yield a number of cells per flask equivalent to that in each 3D matrix. At days 1, 3, 5 and 7, hMSCs were recovered from the 3D matrices after treatment with 0.25 wt.% Trypsin/ 50mM EDTA, and incubated for 10 min with 5% v/v trichloroacetic acid to precipitate nucleic acids. The precipitates were then dissolved with 1M NaOH, and the scintillation liquid (LSC cocktail, ULTIMA GOLD, PerkinElmer) added. After 1h in the dark, samples were analysed in a scintillation counter (MicroBeta Trilux, PerkinElmer).

For the Bromodeosyuridine (BrdU) assay, 0.01 mM BrdU (Sigma-Aldrich) was added to the 3D culture medium. After 1 week, cells were recovered from the hydrogels and transferred to glass slides by cytospinning (Shandon Cytospin 4, Thermo). Cells were fixed with 4 wt.% PFA in PBS for 20 min, treated with 2M HCl for 20 min, and incubated for 5 min in PBS containing 0.5% v/v Tween 20 and 0.05 wt.% BSA to block unspecific binding. Samples were then incubated in monoclonal mouse anti-BrdU (DakoCytomation, 1:10, 1h at RT), followed by secondary antibody Alexa Fluor 568 goat anti-mouse IgG (H+L) (Molecular Probes-Invitrogen, 1:1000, 30 min at RT). Nuclei were counterstained with 1 µg/mL DAPI, and slides were observed and imaged using an inverted fluorescence microscope. Total and BrdU+ nucleus were counted using Image J software and the percentage of proliferating cells was calculated.

2.10. Osteogenic differentiation (ALP and OCN expression)

hMSCs-laden alginate matrices were cultured for up to 3 weeks in osteogenic medium consisting of low-glucose DMEM with 10% v/v FBS (pre-selected batch from PAA), 1% v/v Pen/Strep, 100 nM dexamethasone (Sigma), 10mM β-glycerophosphate (Sigma) and 0.05 mM 2-phospho-L-ascorbic acid (Fluka).

For alkaline phosphatase (ALP) staining, samples were washed 3 times with TBS-Ca and fixed with 4% v/v PFA in TBS-Ca (20 min at RT). After washing, samples were incubated for 30 min in Naphthol AS-MX phosphate/Fast Violet B salt (Sigma, 30 min at 37ºC, protected from light) and then washed again. Samples were imaged using a stereoscope.

Expression of osteocalcin (OCN) was probed in paraffin sections obtained as described in section 2.6. Samples were first treated with 10 mM Tris / 1 mM EDTA (pH 9) for 35 min at 95-98°C for antigen recovery. Sections were then incubated with rabbit anti-osteocalcin (ab13420, abcam, 1:400, ON at 4ºC), and then with Alexa Fluor 594 goat anti-rabbit IgG (1:1000, Molecular Probes-Invitrogen, 1h at RT) secondary antibody. Finally, sections were mounted in Fluoroshield™ with DAPI (Sigma) and imaged by CSLM.

2.11. Statistical analyses

Statistical analyses were performed using GraphPad Prism 5.0 software version 5.0a. The non-parametric Mann–Whitney test was used to compare two groups, whereas comparison between more than two groups was performed using the Kruskal–Wallis test followed by Dunn's comparison test. A value of $p < 0.05$ was considered statistically significant.

3. RESULTS

3.1. Physicochemical properties of RGD-alginate hydrogels

Alginate hydrogels with a bimodal molecular weight (MW) distribution (50% LMW and 50% HMW) were prepared with different polymer concentrations (1 and 2wt.%) and densities of tethered RGD peptides (0, 100 and 200 μM). This previously optimized bimodal MW formulation [28] enables the preparation of low stiffness hydrogels (LMW contribution) without impairing the gelling capacity of the precursor solution (HMW contribution).

The hydrogels' microstructures are depicted on Fig. 1A, to illustrate that the network gets less dense as the polymer concentration is decreased from 2wt.% to 1wt.% but, in both cases, it spatially confines the entrapped cells forcing them to adopt a round shape at the onset of the culture (Fig. 1A, insets). Yet, CryoSEM images do not reflect the actual hydrogels mesh sizes,

which were determined using an alternative technique as described below. The influence of polymer concentration and RGD density on the initial mechanical properties of alginate hydrogels was analysed by DMA.

As shown in Fig. 1B, the compressive storage modulus (E', elastic component) was highly dependent of the polymer content. In fact 2wt.% hydrogels presented a storage modulus that was ca. 10-fold higher than that of 1wt.% hydrogels. Additionally, tan ∂ measurements (Fig. 1B) revealed that the 2wt.% hydrogels were predominantly elastic (tan ∂ ≈ 0.2; E'>>E''), while in the 1wt.% hydrogels the viscous component was more prevalent (tan ∂ ≈ 0.4-0.6). The presence of tethered RGD tended to decrease E' while increasing tan ∂, but statistically significantly differences were only observed in terms of E' for the formulation 2-200 as compared to other hydrogels at 2wt.%.

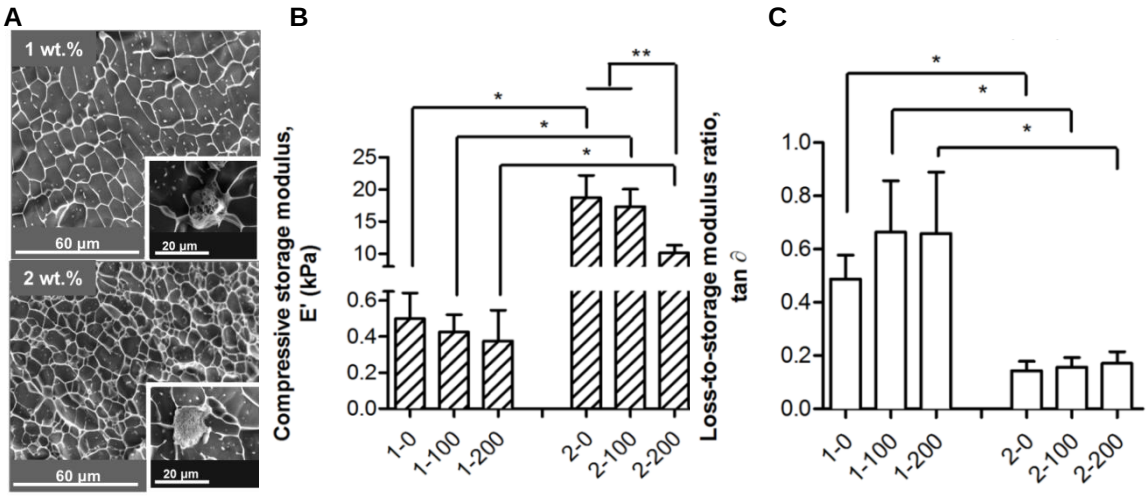

Fig. 1. Microstructure and mechanical properties of alginate hydrogels. (**A**) Microstructural CryoSEM analysis of acellular and hMSCs-laden (inset) alginate hydrogels at 1wt.% and 2wt.%. (**B**) DMA analysis showing average values for the compressive storage modulus (E', elastic component) and tan ∂ (loss-to-storage modulus ratio) of swollen hydrogel discs under unconfined compression. Error bars represent standard deviations for the mean (n=4 or 5).

Table 1 presents additional characterization of acellular and cellularized alginate matrices in terms of their original mesh size and rheological properties along the first 24h of culture. Only matrices with 0 and 200 µM of RGD were analysed, as no great differences were expected when varying the RGD content from 100 to 200 µM.

The mesh size increased as the polymer content decreased, as expected, and was slightly higher in the presence of RGD. Overall the obtained values were within the same range of those reported for alginate hydrogels of similar composition [12], being ca. 2-3 orders of magnitude below the mean cell body size (~10 µm).

In terms of rheological properties, the elastic component of the storage moduli G' was in general lower in RGD-grafted hydrogels compared to unmodified ones. Cellularized hydrogels

tended to be less stiff than acellular gels at similar polymer concentrations, and exhibited weaker concentration-dependence in the absence of RGD. Most importantly, the bulk shear G' decreased along the first 24h of culture in all the formulations, with the exception of the RGD-containing hMSCs-laden 1wt.% matrices, where it effectively increased.

Table 1. Composition, rheological properties and original mesh size of alginate hydrogels.

Name	Polymer dry mass (wt.%)	RGD (μM)	Cells	Incubation time (h)	Storage modulus (G', Pa)	ΔG' after 24h ([a])	Mesh size (ξ, nm)
1-0	1	0	no	0	121 ± 0.1	–	10.9 ± 0.1
			no	24	82 ± 12	↓	–
			yes	0	71 ± 14	–	–
			yes	24	51 ± 12	↓	–
1-200	1	200	no	0	99 ± 3	–	12.1 ± 0.1
			no	24	65 ± 7	↓	–
			yes	0	39 ± 3	–	–
			yes	24	61 ± 21	↑	–
2-0	2	0	no	0	888 ± 38	–	3.8 ± 0.0
			no	24	518 ± 34	↓	–
			yes	0	234 ± 105	–	–
			yes	24	235 ± 21	=	–
2-200	2	200	no	0	461 ± 43	–	5.3 ± 0.1
			no	24	358 ± 17	↓	–
			yes	0	244 ± 42	–	–
			yes	24	165 ± 31	↓	–

([a]) ↑ increase; ↓ decrease; = no alteration; – not assayed.

3.2. Matrix contractility and cell spreading

Upon entrapment, hMSCs remained viable (>80% after 1 week), independently of the hydrogels composition (Fig. 2A). At the onset of the culture, hMSCs exhibited a round shape and were homogeneously distributed through the matrix (Fig. 2B).

As time progressed, hMSCs began to remodel the more pliable 1wt.% matrices. After 24h in 1wt.% RGD-alginate matrices, and independently of the amount of RGD, hMSCs had already contracted the polymeric network, with an average decrease of 47.9±3.5% in diameter, and concomitantly formed a dense multicellular aggregate at the core. In contrast, the 2 wt.% matrices were macroscopically unchanged and cells remained essentially round and dispersed, independently of the density of RGD ligands.

Morphological alterations were not detected in control samples: 1wt.% matrices loaded with inactivated (methanol-treated) cells. In the absence of RGD (Fig. 2C), the contraction of 1wt.% matrices was much less pronounced (12.0±0.8%).

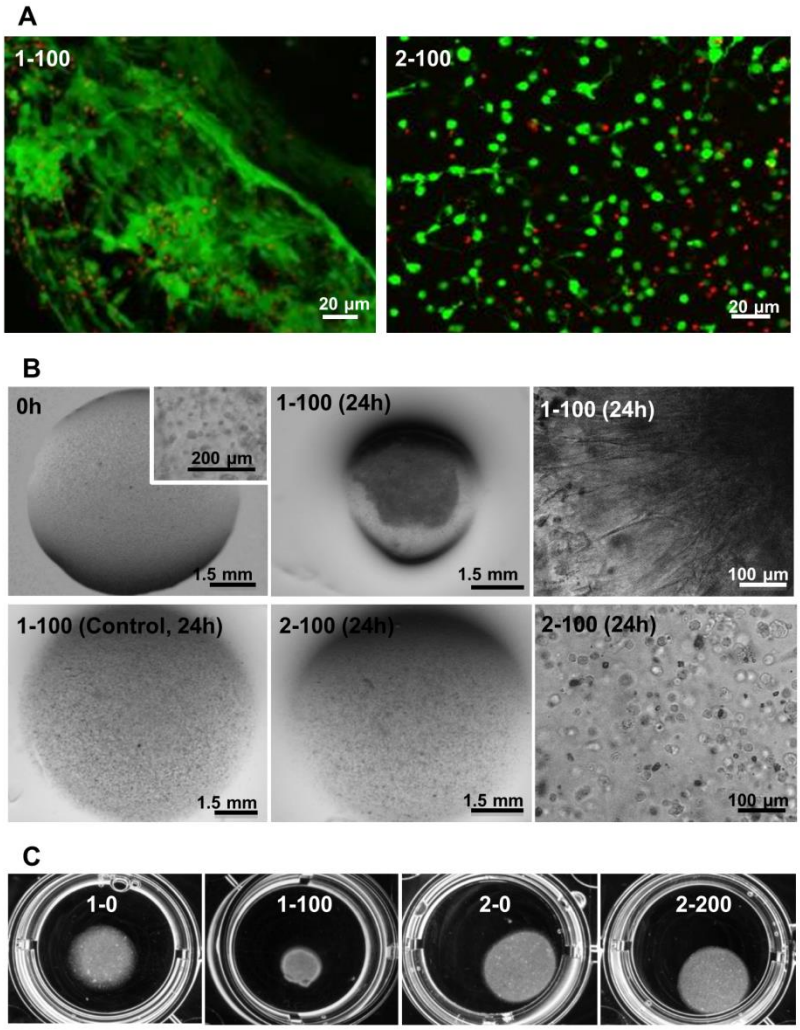

Fig. 2. Cell viability and hMSCs-driven contraction of soft 3D hydrogel matrices. (**A**) hMSCs entrapped within 1 and 2wt.% alginate remained viable after 1 week of culture. (**B**) At the onset of the culture hMSCs were round and dispersed (hMSCs in 1wt.% matrices are depicted as an example, the inset shows entrapped cells at higher magnification), but rapidly (24h) contracted the 1wt.% matrices (independently of the RGD content, 1-100=1-200) forming a multicellular aggregate at the core, which was not observed in non-viable hMSCs (control), nor in hMSCs cultured in stiffer 2wt.% matrices (independently of the RGD content, 2-100=2-200). (**C**) In the absence of RGD, the contraction of 1wt.% matrices after 24h was much less pronounced (original magnification = 10×).

To investigate in more detail the morphology of hMSCs and their spatial re-arrangement within the 3D matrices, F-actin (Fig. 3A) and H&E (Fig. 3B) stainings were performed.

In 1wt.% RGD-alginate matrices (1-100 or 1-200), hMSCs were able to spread and establish cell-cell contacts forming multicellular networks. The H&E staining (Fig. 3B) clearly show that in 1wt.% matrices hMSCs were directed axially towards the core, where they formed a large and dense cell aggregate.

Inside the 2wt.% RGD-alginate matrices, hMSCs remained dispersed throughout the matrix and did not spread significantly. Yet, the presence of short cytoplasmic extensions around the cell (inset in Fig. 3A) suggests that hMSCs were able to interact with matrix-bound RGD motifs.

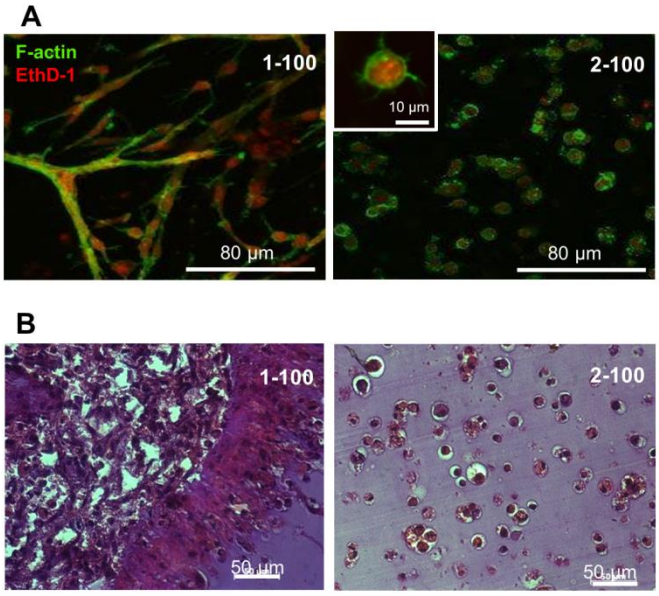

Fig. 3. Morphology and spatial distribution of hMSCs within soft 3D hydrogel matrices. (**A**) F-actin and (**B**) H&E staining of hMSCs-laden matrices, showing that hMSCs entrapped within softer 1wt.% RGD-alginate hydrogels were able to migrate into the core, adopt a more spread shape and establish contacts with neighbouring cells (1-100=1-200). In contrast, hMSCs within stiffer 2wt.% RGD-alginate matrices remained individually dispersed within the matrix and essentially round, albeit showing some cytoplasmic protrusions into the matrix (A, inset).

3.3. Influence of external biochemical stimulation on cell-cell aggregation

It was then investigated if this tendency of hMSCs to migrate into the matrix-core and coalesce in a large cellular aggregate could be inhibited by an applied biochemical stimulus. Outward cell migration was induced by creating an external chemotactic gradient of FBS and was quantified using a modified Boyden chamber assay.

Inserts with fluorescence-blocking membranes were used to monitor the kinetics of outward cell migration. 3D matrices loaded with labelled hMSCs were placed in the upper compartment of the insert (Fig. 4B), and cells leaving the matrix were allowed to migrate through the pores of the membrane into the lower compartment, where the total fluorescence was measured (Fig. 4C). As shown in Fig. 4A, during the first 24h, more hMSCs were able to migrate from the 1wt.% matrices than from the 2wt.% matrices, as anticipated.

After that, hMSCs migration from 1wt.% matrices (where cell aggregates formed, Fig. 4D) stopped or proceeded at very low rates and differences between the various conditions became less significant. hMSCs within 2wt% matrices remained dispersed (Fig. 4E).

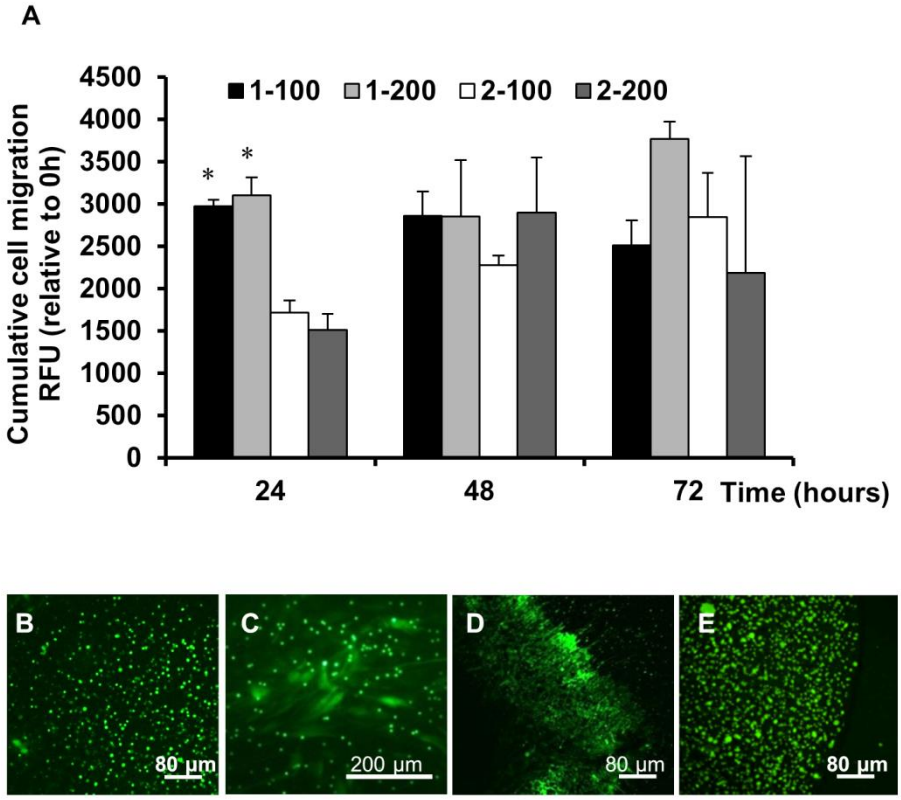

Fig. 4. Outward migration of hMSCs from RGD-alginate 3D matrices in response to an external chemotactic gradient of FBS. (**A**) Entrapped hMSCs (labelled with CellTracker Green) more easily evaded the softer 1wt.% matrices than the stiffer ones. After the first 24h, cell migration decreased and differences became attenuated. (∗) Denotes statistically significant differences (p<0.05) in comparison with 2wt.% matrices. (**B**) Representative picture of a hMSCs-laden disc at the onset of the assay (1=2wt.%). (**C**) Migrating hMSCs attached to the lower side of the insert membrane. (**D**) Aggregated hMSCs within 1wt.% matrices at 24h. (**E**) Dispersed hMSCs within 2wt.% matrices at 24h.

3.4. Expression of fibronectin and its role in the stabilization of cell-cell contacts

Clearly, in the case of the more pliable matrices, and in a time frame of hours, the interactions of entrapped hMSCs with their surrounding matrix, as well as with other cells, globally changed with time. To better characterize this new microenvironment, we determined if matrix properties could affect the ability of the entrapped hMSCs to produce their own ECM. Particular attention was given to the expression of fibronectin (FN), as FN polymerization is known to play an important role in the self-assembly of multicellular structures [29]. After 4h (Fig. 5A-C), intracellular FN expression was detected by immunostaining in all hydrogel

formulations. After 24h (Fig. 5D-F), hMSCs assembled a pericellular FN network only within the 1wt.% matrices (Fig. 5D, E).

In soft RGD-modified matrices, both with 100 µM and 200 µM RGD, this *de novo* formed FN-rich matrix enmeshed the cells, forming an extensive network of elongated, branching fibrils (Fig. 5E). FN fibrils were also generated between aggregated cells even in the non-adhesive 1wt.% matrices (Fig. 5D). In 2wt.% matrices, after 24h (Fig. 5F), FN expression remained mainly restricted to the intracellular space, independently of the presence and density of RGD (0, 100 and 200 µM).

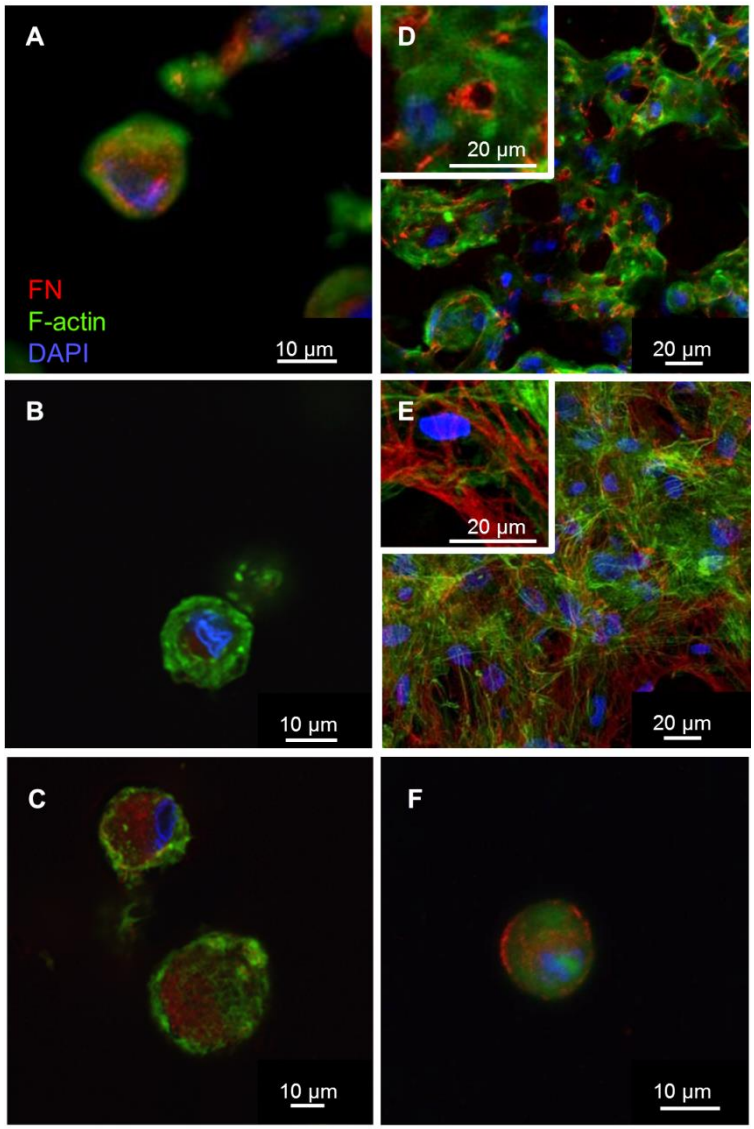

Fig. 5. Fibronectin (FN) matrix assembly assessed by immunofluorescence. hMSCs were cultured within alginate matrices for 4h and 24h, and whole-mounts were fixed for immunostaining with a polyclonal antibody against FN. FN was visualized with Alexa Fluor 594 (red), F-actin was visualized with Alexa Fluor 488 (green) and nuclei were visualized with DAPI (blue) by CLSM. FN expression after 4h in: (**A**) 1-0, (**B**) 1-100 (= 1-200) and (**C**) 2-100 (=2-0 and 2-200). FN expression after 24h in: (**D**) 1-0, (**E**) 1-100 (=1-200) and (**F**) 2-100 (=2-0 and 2-200). Insets: higher magnification images.

Since the α5β1 integrin is the primary receptor for FN, and is known to mediate intercellular cohesion of 3D cellular aggregates [29, 30], the expression of α5 was also analyzed at the same time points. Consistently with the assembly of a FN network, the expression of α5 integrin sub-unit after 24h of culture was also enhanced in the more pliable 1wt.% matrices, particularly at sites of cell aggregation (Figs. 6A and B), independently of the presence and density of RGD.

Interestingly, some α5 integrin expression was also detected in RGD-alginate matrices in cases where FN was mainly detected intracellularly, namely in 2wt.% matrices after 24h (Fig. 6C) and in 1wt.% matrices after 4h (Fig. 6D).

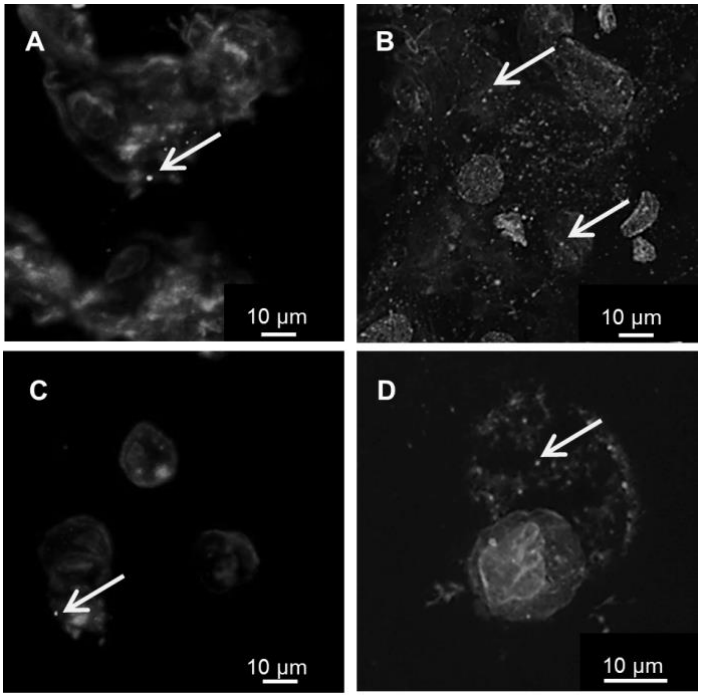

Fig. 6. Expression of α5 integrin sub-unit assessed by immunofluorescence. hMSCs were cultured within alginate hydrogels for 4h and 24h, and whole-mounts were fixed for immunostaining with a polyclonal antibody against α5 integrin. Expression of α5 integrin was visualized with Alexa Fluor 594 (red), F-actin was visualized with Alexa Fluor 488 (green) and nuclei were visualized with DAPI (blue) under CLSM. Black and white images are presented, and the bright white dots (some are indicated with arrows) represent a positive staining. Expression of α5 integrins after 24h in: (**A**) 1-0; (**B**) 1-200 (=1-100), (**C**) 2-100; and after 4h in (**D**) 1-200.

3.5. Effect of matrix stiffness and ligand presentation on hMSCs proliferation

As matrix properties are also likely to affect other cellular activities, namely proliferation, DNA synthesis was followed using the ^{3}H-TdR assay. The proliferative activity of hMSCs within hydrogels was compared between formulations and also with cells cultured under standard 2D conditions.

Cell proliferation in 3D (Fig. 7A) occurred at lower rates than in 2D (Fig. 7B), but considerably varied among matrices of different compositions. Higher proliferation was observed in 1wt.% vs. 2wt.% matrices, and proliferation increased with the amount of RGD.

The BrdU staining showed the presence of a few mitotically-active cells on the populations of hMSCs recovered from the 3D cultures (Fig. 7c, the formulation 1-100 is depicted as an example). Using this assay, a higher number of proliferating cells were detected in the softer matrices (ca. 3% in 1-100 and 9% in 1-200, as compared to ca. 2% both in 2-100 and 2-200 hydrogels), confirming the results obtained with the ^{3}H-TdR assay.

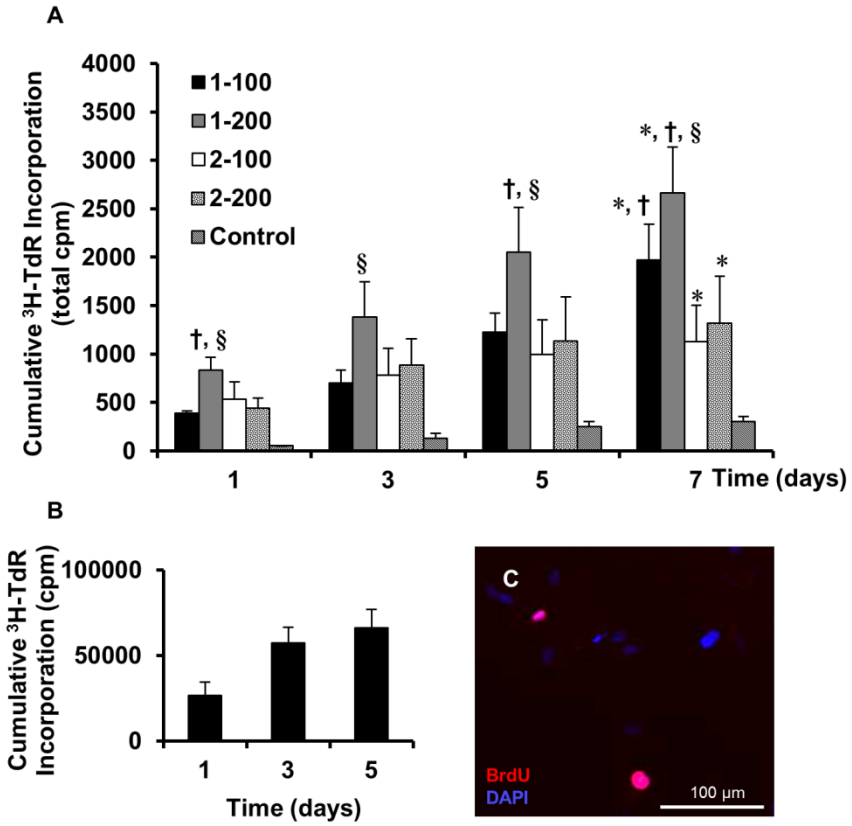

Fig. 7. Effect of hydrogel matrix physico-chemical properties on hMSCs proliferation. The ^{3}H-TdR assay showed that (**A**) hMSCs in 3D proliferated at a much lower rate than (**B**) in 2D. However, in 3D, hMSCs proliferated more in 1wt.% than in 2wt.% matrices. Proliferation also increased in a RGD-dependent manner. Symbols denote statistically significant differences (p<0.05) in comparison to: (∗) day 1, (†) 2wt.% matrices, and (§) 100 µM RGD. (**C**) BrdU immunostaining showing proliferating (red) vs. non-proliferating (blue, DAPI) hMSCs recovered from 1-200 RGD-alginate matrices.

3.6. Effect of matrix stiffness and ligand presentation on hMSCs differentiation

Finally, as the biochemical/mechanical interactions between MSCs and their matrix are known to be key mediators of cell fate, it was further investigated how matrix properties

regulated hMSCs differentiation in 3D. In particular, the expression of the osteogenic markers alkaline phosphatase (ALP) and osteocalcin (OCN) was evaluated, as cell aggregation has been shown to induce osteogenic differentiation [31, 32].

In 1 wt.% matrices, hMSCs expressed high levels of ALP activity (Fig. 8A), even in the absence of RGD and under basal conditions, suggesting a clear relationship between hMSCs aggregation and osteogenic differentiation. In contrasts, in 2wt.% matrices ALP activity was only detected in the presence of RGD. In both cases, the effect of using an osteoinductive medium (OM) added to the effect of the matrix, suggesting that the matrix intrinsic properties and the soluble induction factors acted synergistically in driving hMSCs osteogenic differentiation. In accordance with the ALP results, OCN expression (Fig. 8B) was detected in all the 1wt.% matrices and also in RGD-modified 2wt.% matrices, both under basal and osteoinductive conditions.

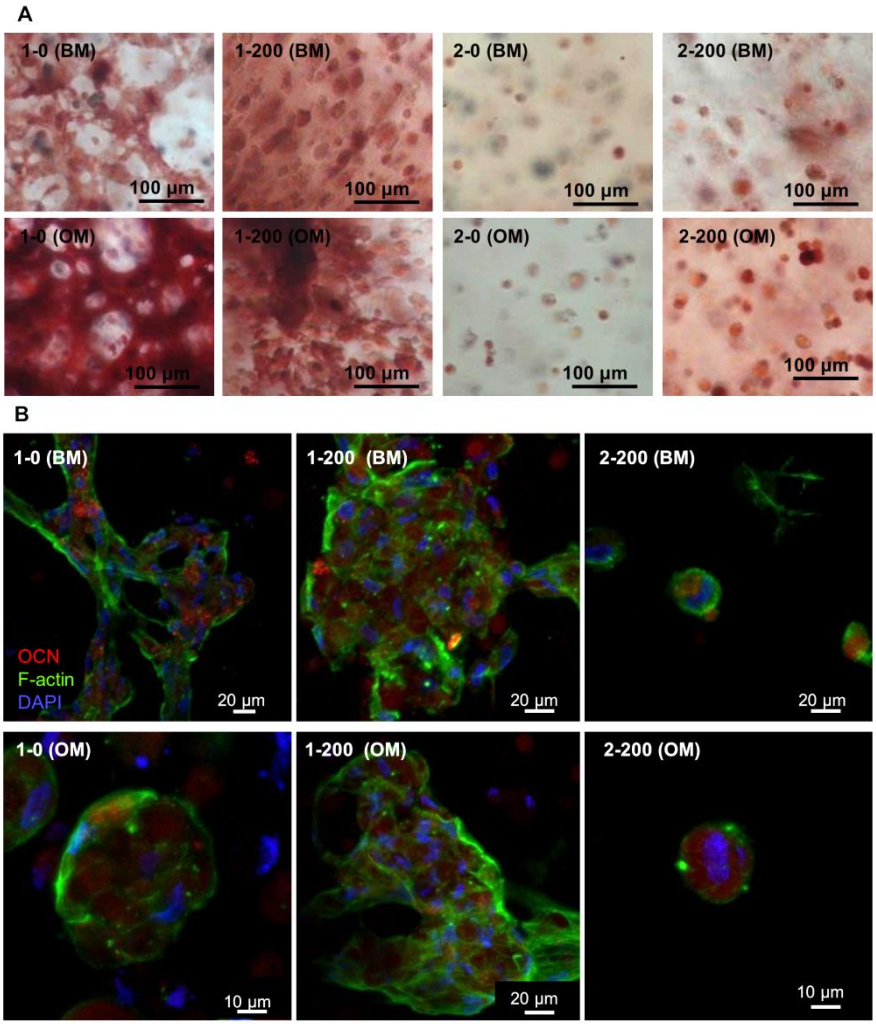

Fig. 8. Effect of hydrogel matrix properties on hMSCs osteogenic differentiation. Expression of (**A**) ALP activity and (**B**) OCN by hMSCs cultured in 3D alginate matrices for 21 days, under basal (BM) and osteoinductive (OM) conditions.

4. DISCUSSION

The present results confirmed that hMSCs are extremely responsive to the viscoelastic properties of their matrix [33], and that these can be modulated to promote specific cell behaviours. Differences on hydrogel rheological and mechanical properties had a clear effect on the tension that hMSCs could exert upon the polymeric network. The entrapped hMSCs were able to significantly contract the softer and more deformable 1wt.% hydrogels, as typically observed with other contractile cell types, such as fibroblasts, when cultured in floating collagen matrices [10, 15]. This suggests that hMSCs were able to pull over the soft gels and connect to each other, driven by a mechanosensing mechanism [18, 19]. As proposed by others, dispersed cells are able to sense their physical microenvironment and balance the mechanical signals conveyed by cell-matrix and cell-cell adhesions [18, 19]. When the matrix stiffness is low enough, cells can perceive and react to substrate strains created by the traction stresses of neighbouring cells. If matrix signals provide a weaker mechanical input than cell-cell interactions, than cells migrate towards one another and coalesce to form multicellular tissue-like structures [19]. Even if it remains to be elucidated whether a similar mechanism of cell communication applies to this particular system, the present results show that matrix mechanical properties can be harnessed to foster tissue formation by promoting cell-cell connection.

By locally remodelling the original alginate matrix, and increasing local matrix density via network contraction and FN assembly, hMSCs dynamically altered their original mechanical environment, and actually reinforced their mechanical shelter [19], which is consistent with previous findings from studies of hMSCs embedded in fibrin gels [33]. Although this is difficult to predict from rheometry data, which describe bulk phase material characteristics but provide limited information on local mechanical features, hMSCs in the softer RGD-alginate matrices effectively stiffened the shear modulus of the hydrogel after 24h of culture.

Here, we additionally show that cell-driven matrix traction was dependent on integrin-mediated cell-matrix adhesion. In fact, while hMSCs also formed FN-stabilized cell-cell aggregates within non-adhesive 1wt.% matrices, they were unable to substantially contract the matrix. On one hand, hMSCs were capable of sensing and responding to matrix stiffness, even in the absence of RGD-activated integrin mechanotransduction. On the other hand, without RGD ligands, even if hMSCs were driven to interact, they were unable to exert significant traction to pull over the matrix, probably due to the lack of matrix-anchor points. The capacity of fibroblasts to organize and contract collagen lattices has also been shown to depend on integrin ligation [34], which further highlights that mechanical regulation is tightly coupled to matrix ligand presentation [5, 35]. Even if a detailed analysis of 3D cell migration was out of the scope of the present study, the results presented here also support the idea that hMSCs entrapped within the softer matrices did not behave as typical path-creating mesenchymal migrating cells, but rather adopted an ameboid-like motility mechanism, behaving more as path-finding cells [36]. In fact, in order to connect to each other, hMSCs had to move within alginate hydrogel matrices without proteolytically degrading them, since alginate is not cleavable by mammalian

enzymes, and even in the absence of RGD ligands. Apart from requiring little or no receptor-facilitated adhesion to the ECM for moving, cells with amoeboid-like motility are able to exert sufficient “pushing” forces to deform the surrounding matrix and deal with the imposed steric hindrance [36]. The viscoelastic properties of the matrix have clearly a direct impact on this process, since a moving cell will encounter less resistance to travel in softer and more deformable matrices [14]. In accordance, Ehrbar *et al.* recently showed that spreading and migration of osteoblasts in PEG hydrogels were impaired in stiffer matrices, even when those were protease-sensitive, but facilitated in hydrogels with lower stiffness, even if cell’s proteolytic activity was inhibited. Apparently, cells could transit from a mesenchymal to an amoeboid mode of migration that was independent of matrix proteolysis but related with matrix deformation, cell shape changes and local matrix defects [13].

In what concerns the microstructure of hydrogels used herein, it is important to emphasize that, while the calculated mesh size was several orders of magnitude below the mean cell body size, this measure only provides a rough estimate of the global microstructure of an “ideal” hydrogel network. As such, it does not give any insight about the existence of network imperfections, which can be caused by different factors such as closed loops of polymer chains, hanging chain ends, slipping chain entanglements, among others [37]. The presence of grafted RGD peptides at crosslinking sites (COOH groups) and, more importantly, the presence of cells during the formation of the hydrogel network, is also anticipated to locally disturb its assembly and result in nano- or micro-sized defects near cells [12]. All these types of network inhomogeneities and defects, which can be a significant source of non-affine deformation [37], have certainly facilitated hMSCs motility by ameboid-like mechanisms in soft alginate hydrogels.

In our system, hMSCs aggregation in softer matrices also correlated with FN fibril assembly and actin stress fiber formation. This is consistent with several reports that highlighted the contribution of FN in promoting intercellular cohesion in 3D microenvironments. In particular, FN fibrillogenesis has been shown to stimulate the self-assembly of fibroblast tissue bodies on collagen gels [38]. In a broader sense, tissue compaction and cohesivity, which are essential both during embryogenesis and wound healing, have also been spatiotemporally correlated with increased FN expression and deposition[29]. In this process, FN acts as “glue” that links adjacent cells by promoting α5β1-integrin mediated strong intercellular cohesion [39]. In the present study, a high expression of α5-integrin subunit was effectively observed, particularly at sites of cell aggregation and FN deposition, as expected. The increased FN deposition might also promote tension generation, accelerating compaction and altering the behaviour of cells responding to mechanical cues [29]. Notably, here it was shown that hMSCs assembled FN patches, even in the absence of matrix-bound RGD, which co-localized with cell aggregates. Some expression of α5 integrin was also detected in cases where FN expression was only intracellular, such as in all RGD-modified matrices after 4h, and also in 2wt% RGD-matrices after 24h. In those cases, α5 integrins were probably activated by engagement with tethered RGD ligands. Although ligation to α5 integrin is conventionally known to additionally require the PHSRN synergy sequence of FN, a recent study by Huebsch *et al.* suggested that this might

not totally apply to “true” 3D set-ups. In fact, the authors demonstrated that in MSCs cultures in RGD-alginate matrices in 3D, α5 integrin expression localized to the cell-matrix interface in a RGD-dependent manner, suggesting the involvement of RGD moieties [7].

While cell proliferation in 3D progressed at much lower rates than in 2D, as also demonstrated by others [40], it was also favoured in softer vs. stiffer matrices. This was anticipated, as several studies have shown that cell proliferation in 3D is facilitated in more pliable substrates, probably because cells can more easily overcome the physical impediment posed by the matrix and create additional space to grow [10, 12]. FN polymerization, which only occurred in the more compliant matrices, is also known to stimulate cell growth by RGD-dependent and independent mechanisms [41].

Perhaps more surprisingly, it was also shown here that low-stiffness matrices provided a permissive environment for hMSCs osteogenic differentiation, even in the absence of RGD ligands. These results show an opposite trend to most studies found in the literature, which demonstrated not only that osteogenesis is favoured in stiffer matrices [7], but also in the presence of RGD [24]. Here, however, concurrent processes of local matrix stiffening, cell shape, cell-cell aggregation and α5β1 integrin-mediated FN binding certainly played a role, as all these factors have been, in and on themselves, correlated with osteogenesis induction. For example, several studies have shown a correlation between cell aggregation and osteoblastic differentiation [31, 32, 42], and activation of the α5β1 integrin is known to have an important role in MSCs osteogenic differentiation [43, 44]. Consequently, upon cellular self-assembly, a new biochemical/mechanical microenvironment is created by cell–cell and cell–ECM interaction that in turn controls MSCs behaviour.

5. CONCLUSIONS

The present results show that when hMSCs were entrapped within very soft alginate hydrogels they rapidly modified their local mechanical and biochemical environment, became embedded and ultimately resided within a self-synthesised ECM. In such a system, cell interactions with the original matrix become less important as time progresses and the *de novo* produced cell-derived matrix turns into a more critical determinant of cell fate. Even so, the intrinsic properties of the original artificial matrix were clearly central guidance variables, showing not only that hMSCs are particularly responsive to microenvironmental cues, but also that the first hours of interaction with the matrix are decisive. Moreover, this work provided new clues to the design of cell-instructive 3D microenvironments, and better elucidated the interplay between substrate compliance and ligand presentation in cell-in-gel responses. In particular, it established a biomaterial-driven strategy to induce the self-aggregation of MSCs and the formation of MSCs-ECM micro-tissues, with higher proliferation and osteogenic differentiation ability, which might be potentially interesting for therapeutic applications.

Acknowledgements

This work was financed by FEDER funds through the Programa Operacional Factores de Competitividade (COMPETE) and by Portuguese funds through Fundação para a Ciência e a Tecnologia (FCT), in the framework of the projects Pest-C/SAU/LA0002/2011 and BIOMATRIX (PTDC/SAU-BEB/101235/2008 and FCOMP-01-0124-FEDER-010915). Fatima Raquel Maia acknowledges INL-International Iberian Nanotechnology Laboratory for her PhD scholarship. Keila Beltrame Fonseca acknowledges her PhD scholarship from FCT-POPH (SFRH/BD/30057/2006). Cristina Barrias has a research position funded by FCT-POPH-FSE (Ciência 2008). The authors are grateful to Sara Neves and David Gomes from INEB, for the help in the rheological and histological analyses, respectively.

6. REFERENCES

[1] Discher DE, Janmey P, Wang Y-l. Tissue cells feel and respond to the stiffness of their substrate. Science 2005;310:1139-43.

[2] Engler AJ, Sen S, Sweeney HL, Discher DE. Matrix elasticity directs stem cell lineage specification. Cell 2006;126:677-89.

[3] Cukierman E, Pankov R, Yamada KM. Cell interactions with three-dimensional matrices. Curr. Opin. Cell Biol. 2002;14:633-40.

[4] Cukierman E, Pankov R, Stevens DR, Yamada KM. Taking cell-matrix adhesions to the third dimension. Science 2001;294:1708-12.

[5] Reilly GC, Engler AJ. Intrinsic extracellular matrix properties regulate stem cell differentiation. J. Biomech. 2010;43:55-62.

[6] Fonseca KB, Bidarra SJ, Oliveira MJ, Granja PL, Barrias CC. Molecularly designed alginate hydrogels susceptible to local proteolysis as three-dimensional cellular microenvironments. Acta Biomater. 2011;7:1674-82.

[7] Huebsch N, Arany PR, Mao AS, Shvartsman D, Ali OA, Bencherif SA, et al. Harnessing traction-mediated manipulation of the cell/matrix interface to control stem-cell fate. Nat. Mater. 2010;9:518-26.

[8] Lutolf MP, Gilbert PM, Blau HM. Designing materials to direct stem-cell fate. Nature 2009;462:433-41.

[9] Tibbitt MW, Anseth KS. Hydrogels as extracellular matrix mimics for 3D cell culture. Biotechnol. Bioeng. 2009;103:655-63.

[10] Bott K, Upton Z, Schrobback K, Ehrbar M, Hubbell JA, Lutolf MP, et al. The effect of matrix characteristics on fibroblast proliferation in 3D gels. Biomaterials 2010;31:8454-64.

[11] Matyash M, Despang F, Mandal R, Fiore D, Gelinsky M, Ikonomidou C. Novel soft alginate hydrogel strongly supports neurite growth and protects neurons against oxidative stress. Tissue Eng., Part A 2012;18:55-66.

[12] Lee B-H, Li B, Guelcher SA. Gel microstructure regulates proliferation and differentiation of MC3T3-E1 cells encapsulated in alginate beads. Acta Biomater. 2012;8:1693-702.
[13] Ehrbar M, Sala A, Lienemann P, Ranga A, Mosiewicz K, Bittermann A, et al. Elucidating the role of matrix stiffness in 3D cell migration and remodeling. Biophys. J. 2011;100:284-93.
[14] Harley BAC, Kim H-D, Zaman MH, Yannas IV, Lauffenburger DA, Gibson LJ. Microarchitecture of three-dimensional scaffolds influences cell migration behavior via junction interactions. Biophys. J. 2008;95:4013-24.
[15] Grinnell F, Petroll WM. Cell motility and mechanics in three-dimensional collagen matrices. Annu. Rev. Cell Dev. Biol. 2010;26:335-61.
[16] Bidarra SJ, Barrias CC, Fonseca KB, Barbosa MA, Soares RA, Granja PL. Injectable in situ crosslinkable RGD-modified alginate matrix for endothelial cells delivery. Biomaterials 2011;32:7897-904.
[17] Kniazeva E, Putnam AJ. Endothelial cell traction and ECM density influence both capillary morphogenesis and maintenance in 3-D. Am. J. Physiol. 2009;297:C179-C87.
[18] Reinhart-King CA, Dembo M, Hammer DA. Cell-cell mechanical communication through compliant substrates. Biophys. J. 2008;95:6044-51.
[19] Reinhart-King C. How matrix properties control the self-assembly and maintenance of tissues. Ann. Biomed. Eng. 2011;39:1849-56.
[20] Geiger B, Bershadsky A, Pankov R, Yamada KM. Transmembrane crosstalk between the extracellular matrix and the cytoskeleton. Nat. Rev. Mol. Cell Biol. 2001;2:793-805.
[21] Bratt-Leal AM, Kepple KL, Carpenedo RL, Cooke MT, McDevitt TC. Magnetic manipulation and spatial patterning of multi-cellular stem cell aggregates. Integr. Biol. 2011;3:1224-32.
[22] Kinney MA, McDevitt TC. Emerging strategies for spatiotemporal control of stem cell fate and morphogenesis. Trends Biotechnol. 2013;31:78-84.
[23] Fonseca KB, Maia FR, Cruz FA, Andrade D, Juliano MA, Granja PL, et al. Enzymatic, physicochemical and biological properties of MMP-sensitive alginate hydrogels. Soft Matter 2013;9:3283-92.
[24] Evangelista MB, Hsiong SX, Fernandes R, Sampaio P, Kong H-J, Barrias CC, et al. Upregulation of bone cell differentiation through immobilization within a synthetic extracellular matrix. Biomaterials 2007;28:3644-55.
[25] Kuo CK, Ma PX. Ionically crosslinked alginate hydrogels as scaffolds for tissue engineering: Part 1. Structure, gelation rate and mechanical properties. Biomaterials 2001;22:511-21.
[26] Oliveira SM, Barrias CC, Almeida IF, Costa PC, Ferreira MRP, Bahia MF, et al. Injectability of a bone filler system based on hydroxyapatite microspheres and a vehicle with in situ gel-forming ability. J. Biomed. Mater. Res., Part B 2008;87B:49-58.
[27] Folkman J, Moscona A. Role of cell shape in growth control. Nature 1978;273:345-9.
[28] Boontheekul T, Kong H-J, Mooney DJ. Controlling alginate gel degradation utilizing partial oxidation and bimodal molecular weight distribution. Biomaterials 2005;26:2455-65.
[29] Robinson EE, Foty RA, Corbett SA. Fibronectin matrix assembly regulates α5β1-mediated cell cohesion. Mol. Biol. Cell 2004;15:973-81.

[30] Robinson EE, Zazzali KM, Corbett SA, Foty RA. α5β1 integrin mediates strong tissue cohesion. J. Cell Sci. 2003;116:377-86.
[31] Tang J, Peng R, Ding J. The regulation of stem cell differentiation by cell-cell contact on micropatterned material surfaces. Biomaterials 2010;31:2470-6.
[32] Facer SR, Zaharias RS, Andracki ME, Lafoon J, Hunter SK, Schneider GB. Rotary culture enhances pre-osteoblast aggregation and mineralization. J. Dent. Res. 2005;84:542-7.
[33] Winer JP, Oake S, Janmey PA. Non-linear elasticity of extracellular matrices enables contractile cells to communicate local position and orientation. PLoS ONE 2009;4:e6382.
[34] Klein CE, Dressel D, Steinmayer T, Mauch C, Eckes B, Krieg T, et al. Integrin alpha 2 beta 1 is upregulated in fibroblasts and highly aggressive melanoma cells in three-dimensional collagen lattices and mediates the reorganization of collagen I fibrils. J. Cell Biol. 1991;115:1427-36.
[35] Engler A, Bacakova L, Newman C, Hategan A, Griffin M, Discher D. Substrate compliance versus ligand density in cell on gel responses. Biophys. J. 2004;86:617-28.
[36] Brabek J, Mierke C, Rosel D, Vesely P, Fabry B. The role of the tissue microenvironment in the regulation of cancer cell motility and invasion. Cell Commun. Signaling 2010;8:22.
[37] Wen Q, Basu A, Janmey PA, Yodh AG. Non-affine deformations in polymer hydrogels. Soft Matter 2012;8:8039-49.
[38] Sevilla CA, Dalecki D, Hocking DC. Extracellular matrix fibronectin stimulates the self-assembly of microtissues on native collagen gels. Tissue Eng., Part A 2010;16:3805-19.
[39] Sechler JL, Corbett SA, Schwarzbauer JE. Modulatory roles for integrin activation and the synergy site of fibronectin during matrix assembly. Mol. Biol. Cell 1997;8:2563-73.
[40] Markusen JF, Mason C, Hull DA, Town MA, Tabor AB, Clements M, et al. Behavior of adult human mesenchymal stem cells entrapped in alginate-GRGDY beads. Tissue Eng. 2006;12:821-30.
[41] Sottile J, Hocking DC, Langenbach KJ. Fibronectin polymerization stimulates cell growth by RGD-dependent and -independent mechanisms. J. Cell Sci. 2000;113:4287-99.
[42] Khetan S, Guvendiren M, Legant WR, Cohen DM, Chen CS, Burdick JA. Degradation-mediated cellular traction directs stem cell fate in covalently crosslinked three-dimensional hydrogels. Nat. Mater. 2013;12:458-65.
[43] Hamidouche Z, Fromigué O, Ringe J, Häupl T, Vaudin P, Pagès J-C, et al. Priming integrin α5 promotes human mesenchymal stromal cell osteoblast differentiation and osteogenesis. Proc. Natl. Acad. Sci. 2009;106:18587-91.
[44] Martino MM, Mochizuki M, Rothenfluh DA, Rempel SA, Hubbell JA, Barker TH. Controlling integrin specificity and stem cell differentiation in 2D and 3D environments through regulation of fibronectin domain stability. Biomaterials 2009;30:1089-97.

SUPPLEMENTARY DATA

The initial mesh size (ξ) of alginate hydrogels, after being pre-swollen in culture medium, was calculated as described in [12], using rheometry data (the measured value of the shear modulus) to calculate the molecular weight between crosslinks (Mc). Immediately after crosslinking, matrices were incubated in medium for 2h, freeze-dried and weighed. The swelling ratio (q_F) and polymer volume fraction (ν_2) were calculated from the following equations:

1) q_F = *(mass of gel after 2h incubation) / (mass of gel after freeze-drying)*

2) $\nu_2 = 1 + (q_F - 1) \times \rho_P/\rho_M$

Where: ρ_P is the density of the alginate (1.601 $g.cm^{-3}$) and ρ_m is the density of the culture medium (0.99 $g.cm^{-3}$).

The crosslink density η was calculated using the Flory–Rehner equation:

3) $\eta = -[\ln(1-\nu_2) + \nu_2 + \chi 1 \nu_2^2] / [V_1(\nu_2^{1/3} - 0.5\ \nu_2)$

Where: χ1 is the Flory–Huggins interaction parameter (≈ 0.5), V_1 is the molar volume of the solvent (NaCl, 0.5 cm^3), and η is the number of active network chain segments per unit volume ($mol.cm^{-3}$).

The molecular weight between crosslinks was calculated from the measured value of the G' using the following equation:

4) $M_c = C_p RT / G'$

Where: C_P is the concentration of alginate in solution (1 or 2wt.%), R is the gas constant (8.314 $m^3.Pa\ mol^{-1}.K^{-1}$) and T is the temperature.

Finally, the mesh size, ξ, was calculated using the following equation:

5) $\xi = \nu_2^{-1/3}\ l * (2M_c/M_r)^{1/2}\ C_n^{1/2}$

M_r is the molecular weight (390.1 $g.mol^{-1}$) of the repeat unit, l is the carbon–carbon bond length of monomer unit (assumed to be 5.15 Å), and C_n is the ratio for alginate calculated as $C_n = 0.021M_n + 17.95 = 21.1$.

CHAPTER V

HYDROGEL DEPOTS FOR LOCAL CO-DELIVERY OF OSTEOINDUCTIVE PEPTIDES AND MESENCHYMAL STEM CELLS*

F. Raquel Maia,[1,2] Mariana Barbosa,[1] David B. Gomes, [1,2] Nuno Vale,[3] Paula Gomes,[3] Pedro L. Granja,[1,2,4] Cristina C. Barrias[1,*]

[1] INEB - Instituto de Engenharia Biomédica, Rua do Campo Alegre, n.º 823, 4150-180 Porto, Portugal

[2] FEUP – Faculdade de Engenharia, Universidade do Porto, Rua Dr. Roberto Frias s/n, 4200-465 Porto, Portugal

[3] CIQ-UP, Departamento de Química e Bioquímica, Faculdade de Ciências, Universidade do Porto, Rua do Campo Alegre 687, 4169-007 Porto, Portugal

[4] ICBAS - Instituto de Ciências Biomédicas Abel Salazar, Universidade do Porto, Rua de Jorge Viterbo Ferreira n.º 228, 4050-313 Porto, Portugal

* Submitted in 2013.

ABSTRACT

The outcome of cell-based therapies can benefit from carefully designed cell carriers. Injectable vehicles able to direct human mesenchymal stem cells (hMSCs) differentiation down the osteoblastic lineage are particularly relevant for minimally-invasive bone healing strategies. Here we report on the use of alginate (Alg) hydrogels as depots for the co-delivery of osteoinductive signals and hMSCs. Two osteogenic growth peptide (OGP) analogues were synthesized and conjugated to Alg via distinct linkers with high and low sensitivity to proteolytic degradation (OGP2 and OGP3, respectively). Both analogues released bioactive OGP-like fragments *in vitro*, with different kinetics, which stimulated hMSCs proliferation and osteogenesis. hMSCs-laden OGP-Alg hydrogels were tested at an ectopic site in a xenograft mouse model. After 4-weeks, OGP-hydrogels were more degraded and colonized by new vascularized tissue than the control (without OGP). hMSCs produced extracellular matrix, migrated outward the hydrogels and proliferated to some extent. OGP groups stimulated hMSCs osteogenic differentiation, as compared with the control, and none of the groups expressed adipogenic genes. Interestingly, OGP3 also stimulated hMSCs chondrogenic differentiation. Overall, the ability of the proposed platform to direct the fate of transplanted hMSCs *in loco* was demonstrated, and OGP-releasing hydrogels emerged as potentially useful system to promote bone regeneration.

Keywords: Injectable alginate hydrogels, osteoinductive peptides, co-delivery systems, mesenchymal stem cells, guided differentiation, bone regeneration.

1. INTRODUCTION

Hydrogels show great potential as cell vehicles for minimally invasive bone regeneration therapies [1]. These materials form hydrophilic 3D microenvironments that recreate some features of native extracellular matrices (ECM), and can be decorated with cell-instructive cues to facilitate adhesion and direct the phenotype of entrapped cells. Therapeutic approaches aiming at driving mesenchymal stem cells (MSCs) fate in a controlled manner, namely by promoting their differentiation into bone-forming cells through the co-delivery of osteoinductive compounds, are promising for bone healing applications [2, 3].

Strategies involving the use of small and simple compounds, such as peptides, can be advantageous as compared to more complex biomolecules, by leading to less expensive, more stable and easily tunable biomaterial formulations [4]. Up to now, different kinds of osteoinductive peptides have been proposed [5, 6]. In this study, we evaluated the potential of OGP, a naturally occurring tetradeca-peptide identical to the C-terminus of histone H4 (residues 89-102, ALKRQGRTLYGFGG), which is present in plasma at micromolar concentrations [7-9]. The physiologically active form of OGP, which corresponds to its C-terminal pentapeptide sequence YGFGG (OGP10–14), is generated from full-length OGP by proteolytic cleavage [10]. This fragment directly interacts with the cell surface [11-13], activating the OGP signaling pathways MAP kinase, Src and RhoA [14]. Upon intravenous administration, synthetic OGP and OGP10-14 were shown to promote increased bone mass and fracture healing *in vivo* [6, 8, 14]. *In vitro*, OGP peptides were shown to increase the proliferation of osteoblastic-like cells and MSCs and accelerate osteogenesis [15]. In pursuit for superior osteoinductive compounds for bone regeneration therapies, OGP has provided a useful basis for engineering additional OGP analogues with enhanced bioactivity, stability and bioavailability. This includes the design of different peptide sequences to be used on soluble form [10], as well as more complex systems with physically or chemically immobilized OGP for local administration [15-18]. In this context, the aim of this study was to develop protease-responsive delivery systems for OGP analogues, which could simultaneously act as injectable hMSCs vehicles, for minimally invasive healing of small bone defects.

Among the numerous proteases that can be selected to trigger enzyme-activated drug release, those belonging to the metalloproteinases (MMPs) family are particularly attractive. MMPs actively participate in ECM remodeling and degradation, having a key role in wound healing and tissue regeneration, and some are constitutively expressed by both naïve and differentiated hMSCs [19, 20]. Here, different OGP analogues were designed, by flanking the YGFGG N-terminus with the MMP-substrate PVGLIG or its scrambled sequence GIVGPL [21]. Both were chemically grafted to alginate, a polymer with the ability to form hydrogels *in situ*, and one of the materials most widely used for cell entrapment [16, 22]. We hypothesized that in presence of specific MMPs, in particular MMP-2 [19, 21], the bioactive YGFGG fragment would be released from the hydrogel upon enzymatic cleavage of the PVGLIG sequence, while it would remain mostly immobilized when using the scrambled linker. Such OGP-delivery systems may thus be used to provide a local OGP depot that remains in close proximity of target cells at

the injury site, for prolonged time periods. Moreover, these hydrogels can simultaneously be used as hMSCs carriers and delivery vehicles, and specifically act on the transplanted cells, by regulating their proliferation and/or guide their differentiation along the osteoblastic lineage. In this study, the designed OGP analogues and OGP-alginate conjugates were firstly characterized at different levels, and then used for the preparation of OGP-alginate hydrogels. The *in vivo* performance of hMSCs-laden hydrogels was evaluated after 4-weeks of implantation at an ectopic site in a xenograft mouse model.

2. MATERIALS AND METHODS

2.1. Peptides

2.1.1. Synthesis and characterization of OGP analogues

Different OGP-based oligopeptide sequences, hereafter designated by OGP1, OGP2 and OGP3 (full sequences and additional information are depicted in Table 1) were synthesized by solid-phase peptide synthesis (SPPS) using the Fmoc/tBu protection scheme [23]. The polymeric support selected, Fmoc-Gly-Wang resin (1 mmol/g, Iris Biotech), was an hydroxymethylated resin pre-loaded with the Fmoc-protected C-terminal amino acid; it was first deprotected by a 20% solution of piperidine (Sigma-Aldrich) N,N-dimethylformamide (DMF, Sigma-Aldrich). After washing with DMF and dichloromethane (DCM, Sigma-Aldrich), the next Fmoc-protected amino acid (Fmoc-AA-OH, Novabiochem or Bachem) was coupled to the Gly-Wang resin by means of DIPCDI (Fluka) coupling reagent. Then, the Fmoc protecting group was removed again with 20% piperidine in DMF and, after resin washing with DMF and DCM, the following Fmoc-AA-OH was coupled to the peptidyl-resin as before. This process was repeated in the C→N direction until the full amino acid sequence was assembles. Peptide cleavage from the resin occurred in acidic conditions using trifluoroacetic acid (TFA, Sigma-Aldrich), triisopropylsilane (TIS, Sigma-Aldrich) and H_2O (95:2.5:2.5) cocktail [23, 24].

Liquid chromatography-mass spectroscopy (LC-MS) was used to check the molecular weight of the synthesized peptides. Samples were prepared in methanol and all data were collected in positive ion mode, in a LCQ-Deca XP LC-MS system from ThermoFinnigan, equipped with both a diode-array detector (DAD) detector and an electrospray ionization-ion trap mass spectrometer (ESI/IT MS). A high pressure LC (HPLC) method was established for the quantification of the peptides purity on a LaChrom Elite system (Hitachi-Merck) equipped with a quaternary pump a thermostatted (Peltier) automated sampler and a DAD. A Purospher Star RP-C18 column (particle size 5 µm, 4.6 mm i.d. × 150 mm length) was used for the separations. The solvents used for the analysis were: solvent A (0.05% TFA in water) and

solvent B (HPLC-grade acetonitrile). The mobile phase consisted of a linear gradient of 0 to 100% of B in A in 30 min. The flow rate was set at 1 mL/min and the analytes were detected at 220 nm. When necessary (if purity < 90%), peptides were purified by preparative reverse phase LC at medium pressure (RP-MPLC). The elution conditions consisted of a linear gradient from 20% to 30% of acetonitrile in water. The effluent was monitored at an absorbance of 220 nm, absorbing peaks were collected, peptides were lyophilized and analyzed by HPLC and LC-MS. Assessment of the peptides' purity by HPLC was based on the calculation of the relative % of the peptide's peak area as compared to the sum of the areas of all detected peaks.

FRET peptides, kindly provided by Drª Maria Aparecido (UNIFESP, Brazil), were used for some assays. These incorporated an ortho-aminobenzoyl (Abz) fluorescent group and an N-(2,4-dinitrophenyl)-ethylenediamine (EDDnp) quenching group at each side, as donor/acceptor pair, and also a Q residue as a requirement for SPPS (Table 1). FRET-peptides were synthesized using the Fmoc-procedure in an automated solid-phase peptide synthesizer (PSSM 8 system from Shimadzu-Tokyo, Japan), as described elsewhere [25]. Peptides were purified by semi-preparative HPLC, and their molecular weight and purity were checked by amino acid analysis and matrix-assisted laser desorption/ionisation-time of flight (MALDI-TOF) MS, using a Microflex−LT mass spectrometer (Bruker−Daltonics, Billerica, MA, USA). The concentration of the FRET substrates was obtained by colorimetric determination of the EDDnp group (ε=17300 M-1cm-1 at 365 nm), using peptide solutions at 1mg/mL in DMF:Water (1:1).

2.1.2. Enzymatic cleavage of free OGP analogues

Peptide solutions were prepared at 828 μM in Dulbecco's phosphate-buffered saline (DPBS) containing calcium and magnesium (Invitrogen, Carlsbad, CA). Recombinant active human MMP-2 (Calbiochem, 25 nM) was added to each peptide solution. In control samples, the same volume of DPBS was added instead of the enzyme. After 24h of incubation at 37ºC, MMP-2 was removed by ultrafiltration (Amicon Centrifugal Filter, MWCO 10 kDa, Millipore) for 2-5 min at 14,000xg, and the filtrates were recovered for analyses. The extent of peptide cleavage was estimated using the fluorescamine assay [26]. Briefly, each solution was placed (50 μL) into the wells of a 96 black-well plate and reacted with 7 μL of 21.6 mM fluorescamine (Sigma). Fluorescence was measured with an excitation wavelength of 400 nm and an emission wavelength of 460 nm in a microplate reader (SynergyTM Mx, Biotek). All measurements were made using at least n = 3 replicates, and are reported in relative fluorescence units (RFU). The molar masses of intact and digested peptides (t = 24h) were determined by LC-MS analysis.

The kinetics of peptide cleavage by MMP-2 was analyzed using FRET peptides. These were incubated in DPBS and fetal bovine serum (FBS; Gibco; 10% v/v in DPBS), with or without MMP-2 (10 nM). Each solution was placed in triplicate (50 μL) into the wells of a 96 black-well plate maintained on ice, and the peptides were added to a final concentration of 5 μM. The plate was then placed in a thermostatized (37ºC) microplate reader and fluorescence was

continuously measured (Ex= 320 nm, Em= 420 nm) along the first hour of incubation, and then again after 48h at 37ºC. All measurements were made using at least n = 3 replicates.

2.1.3. Effect of peptides on hMSCs proliferation and osteogenic differentiation

Human mesenchymal stem cells (hMSCs) were purchased from Lonza (PT-2501, Lot No. 6F4392) and routinely cultured in basal medium (BM) consisting on low-glucose Dulbecco's Modified Eagle Medium (DMEM) with glutamax (Gibco), supplemented with 1% v/v Penicillin/Streptomycin (Gibco) and 10% v/v FBS (MSCs-qualified, Gibco). Cultures were maintained at 37ºC under a humidified atmosphere of 5% v/v CO_2 in air, with the culture medium changed twice a week, and were trypsinized at 70% confluency. For these studies, hMSCs were seeded at 3000 cells/cm^2 in 24-well tissue culture plates.

Cell proliferation was analyzed using the tritiated thymidine (^{3}H-TdR) incorporation assay. Free peptides were added at a final concentration of 10^{-5} M or 10^{-12} M to culture medium without FBS. The control consisted on culture media with 0.5% v/v FBS. ^{3}H-TdR was added to the different media at a final concentration of 1×10^{-3} Ci/mmol, and cells were incubated for 24h prior to analysis. Cells were detached and treated with trichloroacetic acid (5% v/v, 10 min) to precipitate nucleic acids. The precipitates were then dissolved with NaOH (1M) and scintillation liquid (PerkinElmer) was added. After 1h of incubation in the dark, samples were analyzed in a scintillation counter (MicroBeta Trilux, PerkinElmer).

For analysis of osteogenic differentiation, hMSCs were cultured for 7 days under basal and osteoinductive conditions. The osteogenic medium (OM) consisted of low glucose DMEM supplemented FBS (10% v/v, pre-selected batch, PAA), dexamethasone (Sigma, 100 nM), β-glycerophosphate (Sigma, 10mM) and 2-phospho-L-ascorbic acid (Sigma, 0.05 mM). Free peptides were added at a final concentration of 10^{-5} M or 10^{-12} M to both media. Medium was renewed every 4 days and fresh peptides were added each time. At day 7, cell monolayers were stained for alkaline phosphatase (ALP) activity. After fixation with 4% v/v paraformaldehyde (PFA) in PBS for 20 min, cells were incubated for 30 min in Naphthol AS-MX phosphate/Fast Violet B salt at 37ºC in the dark. After washing, stained monolayers were air-dried and observed under an inverted microscope (Axiovert 200 M, Zeiss). In order to quantify ALP activity, cells were lysed and incubated with the chromogenic substrate p-nitrophenol phosphate (2 mM in 0.2 M bicarbonate buffer, pH 10; 0.05% v/v Triton X-100 and 4 mM $MgCl_2$; 1h at 37 °C). Absorbance was read at 405 nm in a microplate reader (Biotek Synergy MX), and converted into product concentrations using a calibration curve built with serially diluted p-nitrophenol standards.

ALP activity was normalized to total protein content, calculated using the bicinchoninic acid assay (BCA Total Protein assay, Pierce), and expressed as nmol/min/mg protein.

2.2. Peptide-alginate hydrogels

2.2.1. Synthesis of peptide-alginate conjugates

PRONOVA ultrapure sodium alginates LVG and VLFG (hereafter designated as high molecular weight, HMW and low molecular weight, LMW; respectively) with a high guluronic acid content (68% and 67%, respectively) were purchased from FMC Biopolymers. The HMW alginate was partially oxidized with sodium periodate [27, 28]. Aqueous carbodiimide chemistry was used to connect peptide N-terminal amino groups to alginate carboxyl groups via a peptide bond [29]. Briefly, LMW and HMW alginate solutions at 1wt.% in MES buffer (0.1 M, 0.3 M NaCl, pH 6.5, Sigma) were prepared and stirred ON at RT. N-hydroxy-sulfosuccinimide (sulfo-NHS, Pierce) and 1-ethyl-(dimethylaminopropyl)-carbodiimide (EDC, Sigma, 27.4 mg/g alginate) at a molar ratio of 1:2 were sequentially added to the solution, followed by peptides. OGP analogues were conjugated to LMW alginate, and cell-adhesion RGD peptides (GenScript, USA) were conjugated to HMW alginate. Alginate samples that were subjected to the same procedure but without the addition of peptides were used as controls (hereafter designated H0 and L0). The modified alginates were purified by dialysis (MWCO 3500 membrane, Spectrumlabs) against distilled water and saline, filtered (0.2 µm), freeze-dried and stored at -20ºC until used. The grafting efficiency was obtained using the BCA assay [21]. Absorbance readings were converted into peptide concentrations using a calibration curve built with serially diluted peptide solutions in 1wt.% of L0 or H0 alginate. Grafted amounts (mg peptide per gram of alginate) for the different peptides are depicted in Table 1. The OGP-Alg conjugates were reconstituted at the same peptide concentration in DPPB or MMP-2 (25 nM) and incubated for up to 48h at 37ºC. The extent of peptide cleavage by MMP-2 was estimated at 0, 24 and 48h using the fluorescamine assay, as described for the free peptide. At least three replicates per condition were analyzed.

Table 1. Different peptide sequences used and their characteristics.

Name	Amino acid sequence	Mw g/mol	Purity %	Grafted amount mg/g Alg
OGP1	GGGYGFGG	671	90	11.4
OGP2	GGPVG↓LIGGYGFGG	1207	92	20.5
FRET-OGP2	(Abz)-GGPVG↓LIGGYGFGG-Q-(EDDnp)	1662	≥ 95	n.a.
OGP3	GGGIVGPLGYGFGG	1207	99	31.0
FRET-OGP3	(Abz)-GGGIVGPLGYGFGG-Q-(EDDnp)	1662	≥ 95	n.a.
RGD	GGGGRGDSP	759	96	15.9

Note: Alg – alginate; Abz – ortho-aminobenzoyl; EDDnp – *N*-(2,4-dinitrophenyl)-ethylenediamine; F-phenylalanine; FRET – fluorescence resonance energy transfer; G-glycine; I-isoleucine; L-leucine; n.a. – not applicable; P-proline; V-valine; Y-tyrosine. In MMP-sensitive sequences the cleavage site is indicated by an arrow (G↓L). In all OGP analogues the bioactive YGFGG fragment is underlined.

2.2.2. Preparation of peptide-alginate hydrogels: films and cell-laden 3D matrices

Hydrogel-precursor solutions with a previously optimized bimodal molecular weight composition [21, 30] were prepared by combining HMW alginate (modified with RGD) and LMW alginate (modified with OGP analogues) at a 1:1 volume ratio and a final polymer concentration of 2wt.%. For adjusting the final amount of each peptide (150 μM RGD, 190 μM OGP analogues) unmodified and peptide-modified alginates were combined at different ratios and dissolved ON in NaCl (Sigma, 0.9wt.%). Alginate hydrogel films (OGP/RGD-Alg and RGD-Alg) were prepared by spincoating, as described in the next section. To obtain cell-laden hydrogels for *in vivo* studies, hMSCs were added to an alginate solution (15×10^6 cells/mL) with $CaCO_3$ (Fluka, Ca^{2+}/COO^-= 0.288) and δ-gluconolactone (GDL, Sigma, Ca^{2+}/GDL= 0.125), and the mixture was loaded (85 μL) into a QGel™ 3D disc caster and allowed to crosslink (20 min, RT) as previously described [31].

2.2.3. hMSCs proliferation on peptide-alginate hydrogels

To prepare alginate films, 100 μL of peptide-alginate solutions (1.5wt%) was deposited onto round plastic coverslips (13 mm), which had been previously treated with positively-charged poly-D-lysine (30 min in 0.1 mg/mL solution, followed washing and drying) to improve surface-adhesion and retention of negatively-charged alginate films. Samples were spinned for 1 min at 9000 rpm (SCS Cookson Electronics Spincoater model G3P-8) to ensure a homogeneous distribution of the polymer. Films were then crosslinked with calcium (0.1 M $CaCl_2$, 0.01wt% NaN_3, 10 min). Coverslips were transferred to pHEMA-treated 24-well cell culture plates, washed twice with sterile distilled water and culture medium, and seeded with hMSCs at 20000 cells/cm^2. At each time point, ^{3}H-TdR was added to the medium (1×10^{-3} Ci/mmol) and cells were incubated for 24h prior to analysis. At 24h, 48h and 72h, cells were recovered and analyzed as described above.

2.3. *In vivo* studies with hMSCs-laden peptide-alginate hydrogels

2.3.1. Subcutaneous implantation in immunodeficient mice

All animal experiments were conducted following protocols approved by the Ethics Committee of the Portuguese Official Authority on Animal Welfare and Experimentation (DGV). Severe combined immunodeficient (SCID) male mice (CB17/Icr-Prkdc scid/Crl, C17SSMA04S, Charles River, Spain) with 6-week of age were used as recipients. Animals were housed at 22°C with a 12h light/dark cycle and had *ad libitum* access to water and food. Analgesics

(Butorfanol) were administrated 30 min prior to surgery. The animals were anesthetized by inhalation of isoflurane, which was continuously delivered over the course of surgery. The dorsal surgical sites were shaved and sterilized. Single incisions were made and subcutaneous pockets were created for the insertion of hMSCs-laden hydrogel discs (8.5 mm diameter, 1.5 mm height). Three groups were tested: OGP2/RGD-Alg, OGP3/RGD-Alg and RGD-Alg (control), and one of each were placed in each mouse (n= 8 mice, 3 discs per mouse). After implantation, incisions were closed with sutures and analgesics were administrated (0.05 mg Buprenorphine HCl per kg). Animals were routinely monitored for general appearance, activity, and healing of the implant sites, and were euthanized after 4 weeks for implants retrieval. No mice were lost during the study.

2.3.2. Histology

After explantation, collected samples that included the entire hydrogel discs and some adjacent tissue were fixed in PFA (4wt.%,ON at 4ºC) and paraffin embedded. Three-micrometer cross-sections were obtained from 2-3 standardized transversal planes using a Thermo Scientific HM550 microtome.

Histochemical staining: For analysis of alginate degradation/host tissue invasion, sections were stained with Safranin-O/Light-Green (Sigma, hematoxylin was used as counterstain), and glass slides (n=4 mice, 2 slides per mouse) were digitalized using a scanner (NanoZoomer 2.0, Hamamatsu). In each, the total area of the implanted disc was first delineated and then images were analyzed and processed using MeVisLab software (Fraunhofer MEVIS, Bremen, Germany, in order to quantify the partial areas of residual alginate (% orange area) vs. invasion tissue (% blue/green area). Results are presented as average % of host tissue area.

Immunolabelling: Expression of collagen type I (COL1) was probed after antigen recovery with 10mM Tris/1mM EDTA (pH 9) for 35 min at 95-98°C. Sections were incubated with rabbit anti-collagen I primary antibody (ab21285 Abcam, 1:200, ON at 4ºC), and then with Alexa Fluor 594-labelled goat anti-rabbit IgG (Invitrogen-Molecular Probes, 1:1000, 1h at RT) secondary antibody. For proliferating human/mice cells detection, masked epitopes were exposed by treatment with sodium citrate (10mM, pH 6, 35 min at 95-98°C). Sections were incubated with mouse anti-human nuclei (MAB4383-3E1.3 Millipore, 1:400, ON at 4ºC) and rabbit anti-Ki67 (ab15580 Abcam, 1:50) primary antibodies. This was followed by incubation with mouse-on-mouse biotinylated anti-mouse IgG (MOM Kit Vector, 1:1000, 10 min at RT), and finally with Alexa Fluor 555-streptavidin (Invitrogen-Molecular Probes, 1:500, 30 min at RT) and Alexa Fluor 488-labelled goat anti-rabbit IgG (Invitrogen-Molecular Probes, 1:1000, 30 min at RT), respectively. All sections were mounted in Fluoroshield™ with DAPI (Sigma). Control sections for each immunolabeling excluded primary antibody staining. From each disc, 4 whole-section images were obtained using Mosaix-reconstruction (inverted microscope, Axiovert 200 M,

Zeiss). In each image, the total amounts of HuNu+ (human) and HuNu- (mouse) and Ki67+ (proliferating) cells per unit area were counted. Results are presented as average percentages of HuNu+ Ki67+ (proliferative, human) and HuNu- Ki67+ (proliferative, mouse) cells.

2.3.3. qRT-PCR analysis of hMSCs gene expression

Total RNA was extracted from hMSCs recovered from 3D matrices (n=3) using the RNeasy Mini Kit (Qiagen), as recommended by the manufacturer. Subsequently, 0.25 μg of the total RNA were used for random hexamers first strand synthesis to generate single-stranded cDNA using the SuperScript First-strand synthesis system for qReal-Time PCR (qRT-PCR) (Invitrogen). RNA quantification was performed by using a NanoDrop 1000 spectrophotometer. After the cDNA synthesis reaction, qRT-PCR was carried out in a total volume of 20 μL of a mixture containing 1 μL of cDNA (5 ng of total RNA), 0.25 μM of each forward and reverse primers, and 1× iQ SYBR Green Supermix (Bio-Rad). qRT-PCR experiments were run using an iQ5 (Bio-Rad) under the following conditions: 95 °C for 3 min, followed by 30 cycles at 94 °C for 30 s, 60 °C for 45 s, and 72 °C for 30 s, and the last step at 55° for 10 s. All reactions were performed in duplicate. After completion of the PCR cycling, melting curves, obtained by increasing the temperature from 60 to 96 °C in increments of 0.5 °C, were examined to ascertain specificity of the PCR products. The housekeeping gene glyceraldehyde 3-phosphate dehydrogenase (GAPDH) was used as the endogenous assay control. Relative quantification of gene amplification by qRT-PCR was performed using the cycle threshold (*C*t) values and relative expression levels were calculated as follows: $2^{-(Ct\ \text{gene of interest} - Ct\ \text{GAPDHgene})}$. The expression value for each target gene was normalized to the GAPDH value at each time point. The sequence and length of the primer pairs used is indicated in Table 2. For all primers used, the tool NCBI/Primer Blast was used to confirm specificity for human genes only and later corroborated by the absence of bands when tested in mouse cells.

2.4. Statistics

Statistical analyses were performed using GraphPad Prism 5.0 software version 5.0a. The non-parametric Mann–Whitney test was used to compare two groups, whereas comparison between more than two groups was performed using the Kruskal–Wallis test followed by Dunn's comparison test. The critical level of statistical significance chosen was $p < 0.05$.

Table 2. Overview of primer pairs used for qRT-PCR.

Gene name	Ref. sequence	Sequence of primers	Length (bp)
GAPDH	NM_002046	F: 5' -AGCCACATCGCTCAGACAC- 3'	66
		R: 5' -GCCCAATACGACCAAATCC- 3'	
ALP	BC021289	F: 5'-AGAACCCCAAAGGCTTCTTC-3'	74
		R: 5'-CTTGGCTTTTCCTTCATGGT-3'	
Runx2	NM_001024630.2	F: 5'-GTGCCTAGGCGCATTTCA-3'	78
		R: 5'-GCTCTTCTTACTGAGAGTGGAAGG-3'	
OCN	NM_199173.4	F: 5'-AGAGTCCAGCAAAGGTGCAG-3'	171
		R: 5'-TCAGCCAACTCGTCACAGTC-3'	
APM1	NM_004797.3	F: 5′-TGTTGCTGGGAGCTGTTCTACTG-3′	235
		R: 5′-ATGTCTCCCTTAGGACCAATAAG-3′	
COMP	NM_000095.2	F: 5'-GCACCGACGTCAACGAGT-3'	63
		R: 5'-TGGTGTTGATACAGCGGACT-3'	
Sox9	NM_000346	F: 5'-TTCCTCCTGCCTTTGCTTGT-3'	93
		R: 5'-GCTGCTGAAACATTCCCAGAAC-3'	
$VEGF_{165}$	AB021221.1	F: 5'-GCTGCACCCATGGCAGAA -3'	204
		R: 5'-CTCCAGGCCCTCGTCATTG-3'	

Note: ALP – alkaline phosphatase; APM1 – adiponectin; COMP – cartilage oligomeric matrix protein; F – forward primer; GAPDH – glyceraldehyde 3-phosphate dehydrogenase; OCN – osteocalcin; Runx2 – runt-related transcription factor 2; Sox9 – transcription factor SRY (sex determining region Y)-box 9; $VEGF_{165}$ – vascular endothelial growth factor 165; R – reverse primer.

3. RESULTS AND DISCUSSION

3.1. Enzymatic cleavage of free and alginate-conjugated OGP analogues

Different OGP analogues were designed and synthesized by Fmoc/tBu SPPS, where the target bioactive fragment YGFGG was either flanked by a poly-G sequence (in OGP1), the MMP-cleavable substrate PVGLIG (in OGP2) [21], or the PVGLIG-scrambled sequence GIVGPL (in OGP3). Their molecular weight and purity were assessed by LC-MS and HPLC, respectively (Table 1). Mass spectra were acquired in the positive mode, and in all cases the base peaks at m/z 1207.67 and 1207.60, respectively, were consistent with the peptide's molecular ion M+. Base peaks were always significantly more intense than remaining peaks, revealing that the target peptides were obtained as the major synthesis product (purity ≥ 90%, Table 1).

OGP2 and OGP3 were incubated with MMP-2, and enzymatic cleavage was analyzed by reacting fluorescamine with the peptide's primary amines to form fluorescent moieties [32]. The emitted fluorescence was measured at the moment of incubation and after 24h, to estimate the accumulation of N-amino termini in excess over that of the intact substrate, which in turn represents the extent of enzymatic cleavage. As predicted, no significant hydrolysis was detected in DPBS, and the OGP2 peptide was more efficiently cleaved by MMP-2 than OGP3,

with a statistically significant 4-fold increase in RFU in relation to time 0 (p=0.0286), and a 2 fold-increase in relation to OGP3 in MMP-2 (p=0.0286).

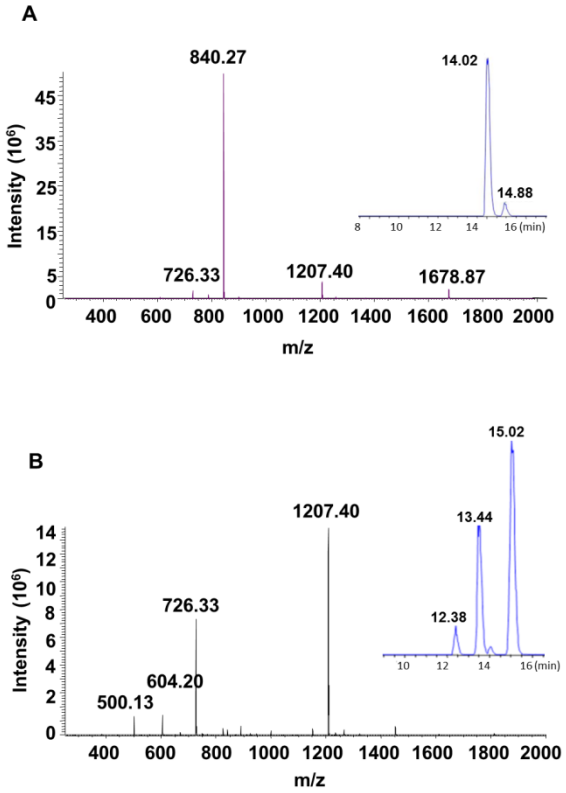

Fig. 1. LC-MS analysis of OGP-based peptides after 24h of incubation with MMP-2. (**A**) OGP2: the base peak at m/z 840.27 is consistent with the molecular ion, M^+, of peptide LIGGYGFGG, an expected fragment of MMP-2-mediated cleavage of the substrate peptide. The peak presents a retention time of 14.02 min (inset). (**B**) OGP3: the base peak corresponds to the peptide's molecular ion M^+ (m/z 1207.40), whereas the peak detected at m/z 604.20 corresponds to the diprotonated peptide $[M+2H]^+$. The peaks detected at m/z 726.33 and at m/z 500.13 correspond to unspecific cleavage. The base peak has a retention time of 15.02 minutes; the fragments detected at m/z 726.33 and at m/z 500.13 have a retention time of 13.44 and 12.38 min, respectively (inset).

Both the intact peptides and their fragments, obtained after enzymatic digestion, were analyzed by LC−MS (Fig. 1). In both cases, only one major peak, corresponding to the original peptides (MW=1207.34), was present at the moment of incubation. Also, when peptides were incubated in DPBS without enzyme, their integrity was fully maintained, suggesting their hydrolytic stability (data not shown). After 24h of incubation with MMP-2, and in the case of OGP2, the original sequence was present in only minute amounts in the recovered sample, whereas the rather intense base peak emerged at m/z 840.27 a.m.u. presenting a retention time of 14.02 min, which is consistent with the molecular ion of the sequence LIGGYGFGG, one of the fragments expected to be released upon MMP-2 cleavage at the predicted scissile bond (G↓L, see Table 1). In what concerns OGP3, the presence of the original peptide sequence in considerable amounts could be confirmed by the fact that the base-peak matched its molecular

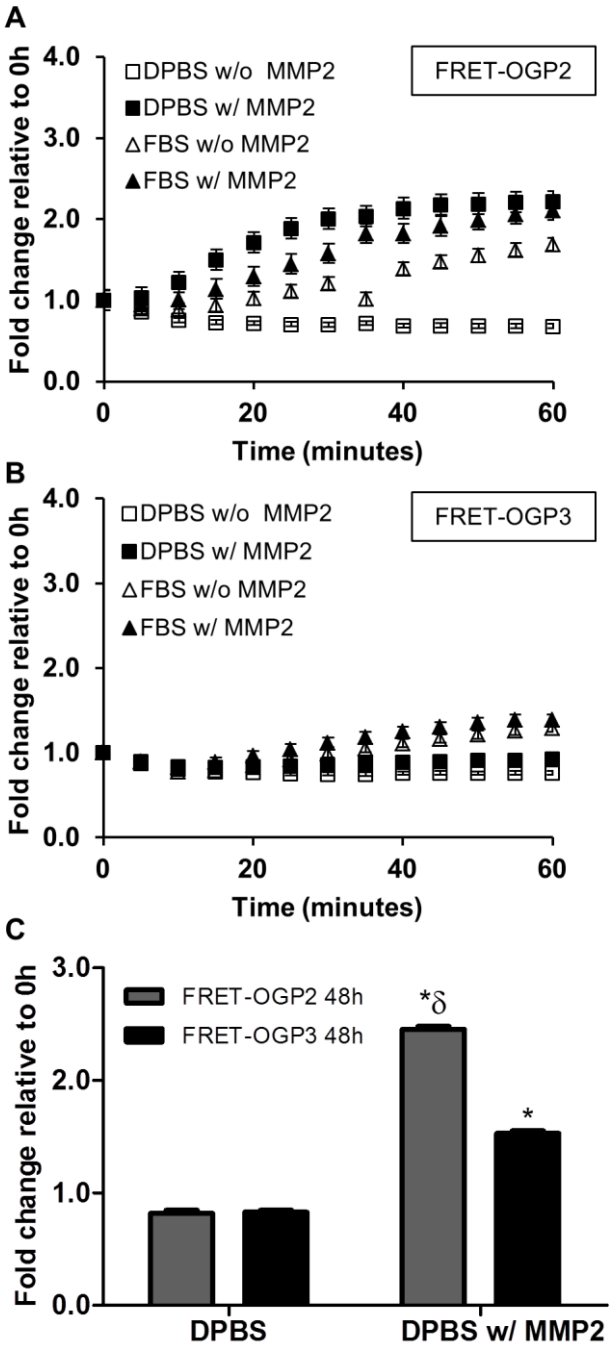

Fig. 2. FRET analysis of OGP analogues cleavage. Kinetics of (**A**) FRET-OGP2 and (**B**) FRET-OGP3 cleavage along 1h of incubation in DPBS or FBS, with or without MMP-2 (10 nM). Samples were maintained in the microplate reader at 37ºC and the emitted fluorescence was monitored in real time. Results are presented as fold change in relation to time 0, as mean ± SD (n=3). The extent of enzymatic cleavage after 48h of incubation (37ºC) in DPBS with and without MMP-2 is depicted for (**C**) FRET-OGP2 and FRET-OGP3. Results are presented as fold change in relation to the control (without MMP-2) as mean ± SD (n=3). Symbols denote statistically significant differences in relation to (∗) DPBS (p=0.05) and (δ) FRET-OGP3 48h (p=0.05).

ion at m/z 1207.40; still, other peaks emerged at m/z 840.27, m/z 726.33 and m/z 500.13 a.m.u, though at lower intensities. The new fragments at m/z 726.33 and m/z 500.13 a.m.u are consistent with unspecific cleavage of OGP3 at between G and Y (see Table 1), yielding GGGIVGPLG (MW=725.8) and YGFGG (MW=499.5). According to Turk *et al.* [33], the scissile bond at GY might in fact exhibit some susceptibility to MMP-2 digestion, although much lower than that of GL in PVGLIG. Interestingly, cleavage of OGP3 at the proposed site will also result in the release of YGFGG.

Peptide cleavage kinetics was further analyzed using FRET-peptides. These exhibit internal fluorescence quenching when intact, but emit fluorescence once cleaved [34], providing a useful tool to monitor peptide digestion in real-time. The increase in emitted fluorescence (RFUs) along the first hour of incubation is presented in Fig. 2A and 2B. In both cases, no hydrolysis occurred in DPBS without MMP-2, and both peptides were cleaved in FBS, even in the absence of added MMP-2. However, while cleavage of OGP2 increased in the presence of MMP-2, this was not observed with OGP3. The fluorescence emitted by the two FRET-OGP analogues when incubated in DPBS with or without MMP-2 was measured again after 48h of incubation (Fig. 2C). In accordance with the previous results obtained using the fluorescamine assay, some cleavage of OGP3 occurred in the presence of MMP-2, but OGP2 was cleaved to a much higher extent.

The two OGP analogues were cleaved in presence of FBS, suggesting that both may be hydrolyzed to some extent by indeterminate serum proteases. Under *in vitro* (cell cultures) and *in vivo* conditions, this feature may account for unspecific OGP release from both peptides. Similar observations have been previously reported by Chau *et al.* [35-37], who designed two dextran–peptide–methotrexate (MTX) conjugates for tumor targeting, where the peptide linkers corresponded to the same sequences used in this study (PVGLIG and GIVGPL) [35-37]. *In vitro,* GIVGPL-dextran conjugates were only minimally hydrolyzed by MMP-2, and PVGLIG-dextran conjugates released the drug in the presence of MMP-2, but remained intact in all the serum-containing conditions [35]. However, *in vivo*, in a more complex proteolytic scenario [36], drug release also took place via cleavage by lysosomal enzymes, which were able to degrade both peptide linkers, leading to nonspecific drug (MTX) release. This probably accounted for the tumor-inhibiting ability of MTX-GIVGPL-dextran conjugate, despite its lack of sensitivity towards MMPs [36].

As shown in Fig. 3, OGP2 retained the susceptibility to MMP-2-cleavage in alginate-conjugated form (OGP2-Alg). Similarly to that observed with the free peptides, OGP3-Alg was also cleaved to some extent, but at a slower rate.

Overall, this part of the study provided proof-of-concept on the correct design of protease sensitive OGP2-Alg conjugates, in the sense that, as expected, these were sensitive to MMP-2 mediated cleavage. Yet, both OGP-Alg may be useful platforms for the delivery of OGP10-14-like fragments.

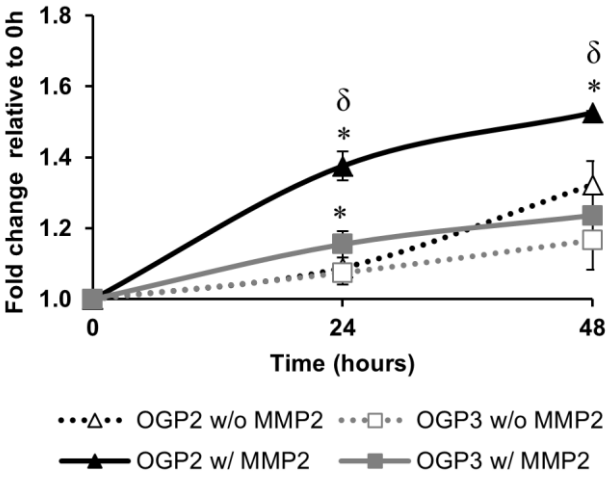

Fig. 3. Enzymatic cleavage Alg-conjugated OGP analogues in the presence of MMP-2. The fluorescamine assay was used to determine the amount of free amine groups present in each sample, which increase as the peptides are cleaved. Results are presented as fold change in relation to t=0 as mean values ± SD (n=3). Symbols denote statistically significant differences in relation to (∗) w/o MMP2 (p=0.05) and (δ) OGP3 (p=0.0383).

3.2. Effect of free and alginate-conjugated OGP analogues in hMSCs: *in vitro* screening studies

To assess the bioactivity of OGP analogues, hMSCs were cultured in the presence of free peptides (added to serum-free culture medium) or OGP-Alg conjugates (used as culture substrates in the form of hydrogel films), and cell proliferation was analyzed by the ^{3}H-TdR assay. Cells were cultured in serum-free conditions to measure the direct action of OGP analogues on hMSCs proliferation without masking effects from serum-OGP. As soluble peptides, the classical forms of OGP and OGP10-14 have been shown to regulate the proliferation of osteoblastic and stromal cells in a biphasic-dependent manner, indicative of an autocrine/paracrine mode of action [38, 39]. As depicted in Fig. 4, we were also able to demonstrate that all the OGP analogues tested in this study enhanced hMSCs proliferation after 24h in relation to the control (culture medium with 0.5% v/v FBS).

The effect of OGP-Alg conjugates was analyzed using OGP2 and OGP1 to evaluate, respectively, the effect of OGP-releasing vs. non-releasing formulations. The tested hydrogels also contained RGD to promote cell adhesion to the films, and RGD-Alg was used as a control. As depicted in Fig. 4, no significant differences were observed between the different groups after 24h. However, after 48h, both OGP analogues enhanced hMSCs proliferation in relation to the control. This effect was even more pronounced after 72h for OGP2-Alg, but it was no longer observed with OGP1-Alg, suggesting that the bioavailability of the active fragment may be important for its bioactivity. This is consistent with previous studies demonstrating the low impact of surface-immobilized OGP10-14 on pre-osteoblastic MC3T3-E1 cells proliferation [11].

To evaluate the effect of OGP analogues on hMSCs differentiation only free peptides were used, as the stability of alginate hydrogels films was lost after 7 days in culture, compromising the ALP assay. After 1 week of culture in BM, ALP activity was increased in the presence of OGP, except when OGP2 was used at 10^{-5} M. In OM, ALP activity increased dramatically in the presence of OGP2, especially when present at 10^{-12} M, which has been defined as being within the optimal effective range in previous studies [40, 41].

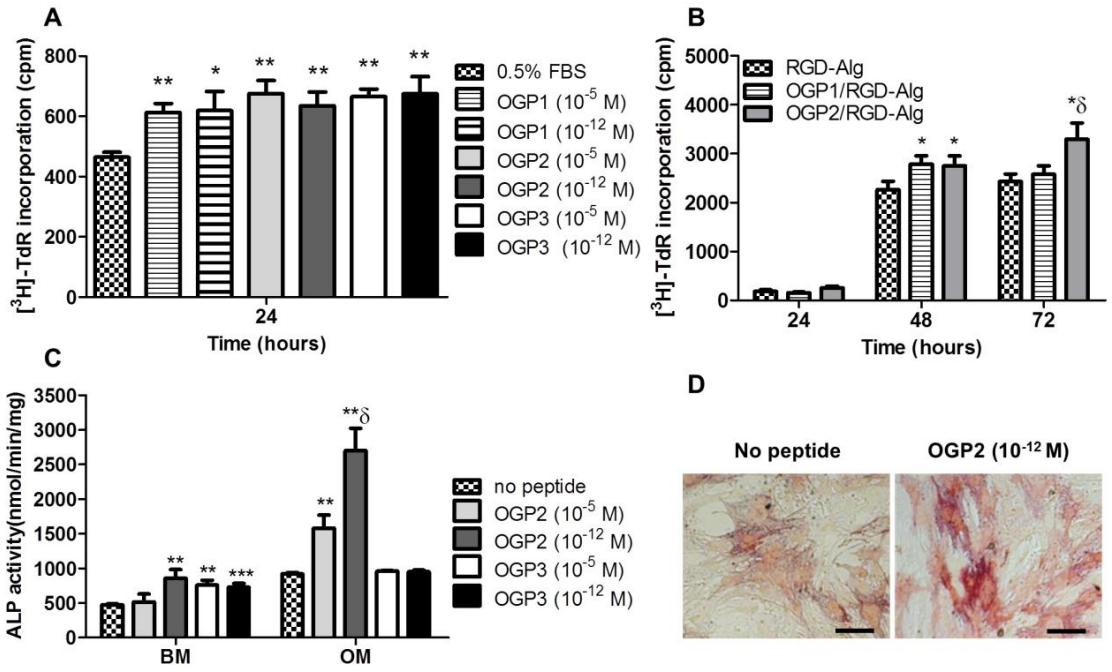

Fig. 4. Effect of free and Alg-conjugated OGP analogues on hMSCs behaviour. (**A, B**) Cell proliferation upon exposure for 24h to (**A**) free or (**B**) Alg-conjugated OGP analogues, assessed by the ^{3}H-TdR assay. (**C**) Expression of ALP activity by hMSCs after 7 days of culture in the presence of free OGP analogues (10^{-5} M or 10^{-12} M) added to BM or OM. Cells cultured in the absence of peptides where used as controls. Symbols denote statistically significant differences in relation to: (*) no peptide within BM or OM groups (** p< 0.02; *** p< 0.005); and (δ) OGP2 (10^{-5} M). (**D**) ALP staining of control and OGP2 (10^{-12} M)-treated cultures in OM (scale bar =100μm).

3.3. *In vivo* studies with hMSCs-laden OGP-alginate hydrogels

After confirming that both OGP2 and OGP3 release bioactive YGFGG-like fragments, the *in vivo* performance of alginate hydrogels as depots for local co-delivery of OGP analogues and hMSCs was evaluated. For this first set of studies, implants were performed at an ectopic site instead of a bone defect, to mitigate the effect of osteoinductive signals intrinsically present at the bone compartment, and to more specifically evaluate the direct impact of OGP analogues on hMSCs. Both OGP-releasing analogues were tested (OGP2/RGD-Alg and OGP3/RGD-Alg

hydrogels) and RGD-Alg hydrogels were used as a control. Given the previous *in vitro* results, both OGP-hydrogels were expected to locally release a bioactive portion of OGP, via proteolytic cleavage of the peptide linkers, albeit at different rate: a faster release from OGP2-Alg, which incorporates the MMP-sensitive PVGLIG linker, was anticipated.

3.3.1. Degradation and host tissue invasion of peptide-alginate hydrogels

The degradation pattern of implanted cell-laden hydrogels was first characterized, as it is a relevant determinant of their *in vivo* performance. Ideally, it should take place within a balanced time frame. It should not prevent cell release, or impede the invasion of host tissue, but should allow the deposition of new ECM before the complete disintegration/dissolution of the hydrogels. As depicted in Fig. 5, alginate fragmentation and host tissue invasion were detected in all samples, but were more significant in OGP groups, although the reasons for this are still unclear. Increased implant degradation in the presence of immobilized OGP peptides has been reported in previous studies, where these were used as covalent crosslinkers for amino acid-based poly(ester urea)s materials [42]. In that case, the higher degradation was explained by the additional free volume in the polymer plugs imparted by the OGP crosslinker and increased swelling due to the presence of peptides [42].

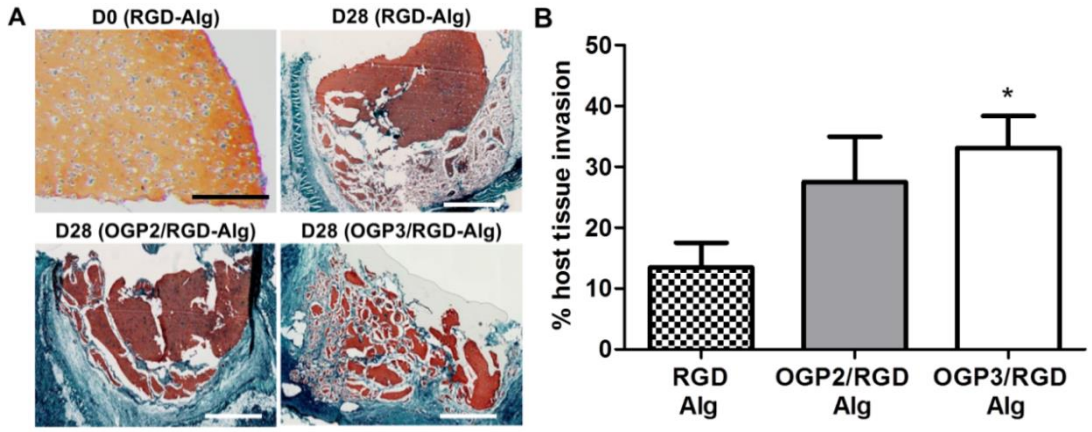

Fig. 5. *In vivo* degradation and host tissue invasion of peptide-Alg hydrogels. (**A**) Images of Safranin-O/Fast green-stained paraffin-sections of hMSCs-laden Alg hydrogels (Alg in orange-red, cells/ECM in blue-green) at day 0 (scale bar: 100 µm), or after 28 days of implantation within the different hydrogels (scale bar: 1mm). (**B**) Quantitative analysis of host tissue invasion (% of blue area per disc) at day 28. Alginate fragmentation/host tissue invasion was more significant in OGP groups. Data is presented as mean ± SD (n=4 mice, 2 sections per mice), * denotes statistical significant differences in relation to control (p=0.0104).

Perfused blood vessels were detected at the implant site in all groups, located mainly within the newly formed tissue but also within the hydrogels (Fig. 6A, where the OGP3 group is depicted as an example). Neo-vascularization was enhanced in OGP3/RGD-Alg, compared to the other groups tested (Fig. 6). It is well accepted that proper vascularization is a prerequisite for the survival of transplanted cells and new tissue formation. Also, it is well established that there is a key interplay between angiogenesis and osteogenesis [43]. So, an osteoinductive compound capable of also stimulating neo-vessels formation would certainly represent a promising therapeutic agent for bone regeneration. Interestingly, an effect of OGP on implant vascularization has been recently reported [42], but the underlying mechanisms remained unclear and, to our knowledge, the authors have not further investigated this phenomenon. In another study, Bocci *et al.* demonstrated the lack of mitogenic and pro-adhesive activity of OGP on microvascular endothelial cell cultures [44]. Here, we investigated whether the level of neo-vascularization correlated with the secretion of proangiogenic factors by transplanted hMSCs [45], and examined the expression of vascular endothelial growth factor 165 ($VEGF_{165}$), which represents one of the most potent endothelial cells mitogens. Unexpectedly, our results revealed higher $VEGF_{165}$ mRNA expression in the OGP2/RGD-Alg, as compared to the other groups. So, it remains to be elucidated whether the higher vascularization observed in the OGP3/RGD-Alg group was promoted by other cell-secreted angiogenic factors, or simply resulted from the higher degradation/invasion of these matrices that, in turn, probably facilitated neo-vascularization.

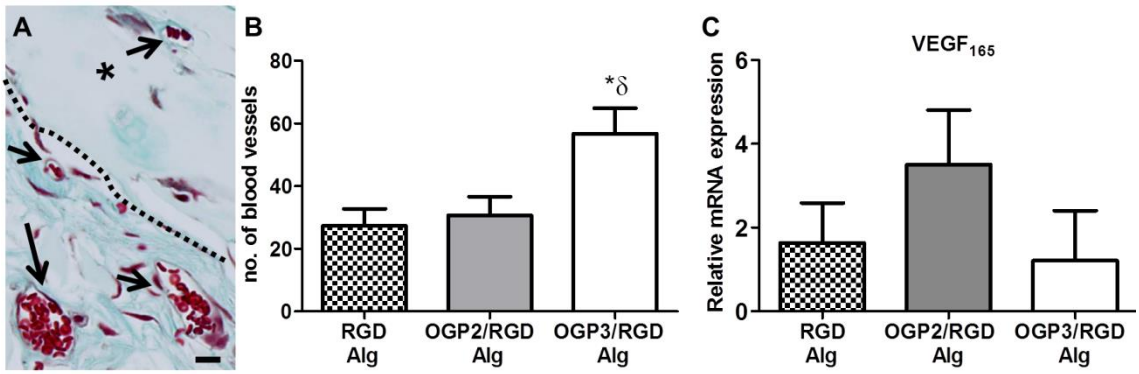

Fig. 6. Implant vascularization and $VEGF_{165}$ expression by transplanted hMSCs. (**A**) Perfused blood vessels (black arrows) at the implant site were identified by MT-staining (erythrocytes in red; ∗ Alg in pale blue; host tissue in green/blue; the dashed line represents host tissue/Alg interface, the OGP3 group is presented as an example; scale bar: 10 μm). (**B**) Quantitative analysis of the average number of vessels at the implant site. Data is presented as mean ± SD (n=4 mice, 6 sections per mice). (**C**) Expression of $VEGF_{165}$ mRNA by transplanted hMSCs analyzed by qRT-PCR (n=3 mice). Results were normalized internally with GAPDH. Symbols denote statistically significant differences in relation to (∗) RGD-Alg (p=0.004) and (δ) OGP2/RGD-Alg (p=0.0359).

ECM deposition (COL1) at the implant site was detected in all the formulations (Fig. 7). OGP groups, especially OGP3/RGD-Alg, stained more intensely for COL1 than the control, and the new collagenous matrix appeared more uniformly distributed throughout the implant area. Within the hydrogels, COL1 was detected intracellularly and in the pericellular space, indicating that transplanted hMSCs were able to produce and secrete their own ECM.

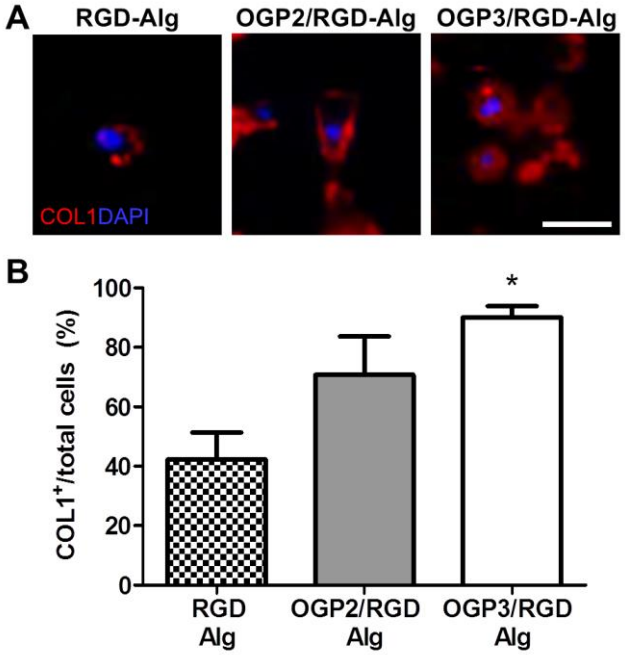

Fig. 7. Expression of collagen type 1 at the implant site. (**A**) Representative images of COL1 (in red) expression on tissue sections from the different groups at day 28 (scale bar: 10 µm). (**B**) Quantification of % of COL1+ cells relative to the total number of cells. Data is presented as mean ± SD (n=4 mice, 4 sections per mice), * denotes statistical differences in relation to the control (p=0.0019).

To evaluate the effect of OGP on cell proliferation, transplanted hMSCs were distinguished from mouse cells by immunolabeling using a human nuclei-specific antibody (HuNu). Although the *in vitro* studies with hMSCs cultures demonstrated a mitogenic effect for all the tested OGP analogues, we have not been able to demonstrate any significant outcome of OGP2 or OGP3 on cell proliferation *in vivo*, at least after 4 weeks of implantation (Fig. 8). A few proliferating cells (Ki67+), both from human (HuNu+ hMSCs) and mouse (HuNu- cells) origin, have been detected within the hydrogel and adjacent host tissue, but there was no statistically significant difference between groups in terms of % of proliferating cells, even if mean values were slightly higher in OGP3 group. This may be in part related with the follow-up time frame. Possibly, OGP analogues may increase cell proliferation in an early stage in the regenerative process but, after 4 weeks of implantation, hMSCs were probably already transiting from a proliferative to a maturation phase, which seems to correlate with our data on hMSCs

expression of lineage-specific genes (see below). A transitory effect of surface-immobilized OGP and OGP10-14 on cell proliferation has been previously shown in osteoblastic MC3T3-E1 cultures, where a positive outcome was observed at day 3, but was no longer seen at day 7 when cells were presumably in a more mature state [11].

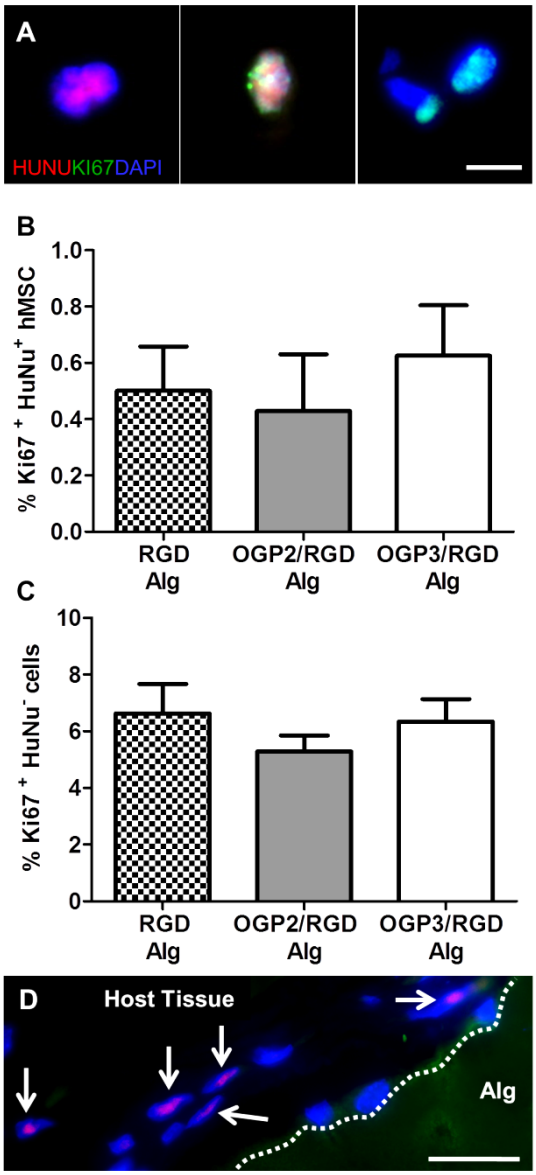

Fig. 8. Proliferative vs. non-proliferative human and mouse cells at the implant site. (**A**) Double immunolabeling with anti-HuNu (red) and Ki67 antibodies (green). Nuclei were counter-stained with DAPI (blue), scale bar represents 5 μm: (left) HuNu+ Ki67- non-proliferative hMSCs; (center) HuNu+ Ki67+ proliferative hMSCs; and (right) HuNu- Ki67+ proliferative mice cells (**B**) Percentage of proliferative hMSCs (HuNu+ Ki67+) in relation to total hMSCs (HuNu+). (**C**) Percentage of proliferative mice cells (HuNu- Ki67+) in relation to total mice cells (HuNu-). Data is presented as mean ± SD (n=4 mice, 4 sections per mice). (**D**) HuNu+ cells (arrows) were also detected outside, integrated in the host tissue. The dashed line represents tissue/alginate interface.

Noteworthy, the human-nuclei specific labeling allowed us to confirm that transplanted hMSCs were located not only inside the alginate matrix, but also outside, integrated in the host tissue (Fig. 8D), demonstrating that the hydrogels effectively acted as cell-delivery systems.

The phenotype of transplanted hMSCs was analyzed by quantifying mRNA expression of osteogenic (Runx2, ALP and OCN), chondrogenic (COMP) and adipogenic (AMP1) markers (Fig. 9). In what concerns the expression of Runx2 and OCN, a key osteoblast transcription factor and its target gene, respectively, we found higher levels of OCN expression in OGP groups, with a concomitant decrease in Runx2 expression, which is consistent with published results on the temporal mRNA expression of these two bone-specific markers during development of the osteoblast phenotype in MC3T3-E1 cultures [12]. The expression of ALP mRNA was also detected in all samples, being higher in OGP2/RGD-Alg than in the other groups. Taken together, these results suggest that hMSCs within OGP-releasing hydrogels were in a more mature stage of osteoblastic differentiation, as compared to the control. An effect of OGP on OCN expression has been previously demonstrated in other *in vivo* experimental settings, namely during healing of femoral fractures in rats [46]. After parental administration of OGP for 1 week, systemic and local mRNA expression of different growth factors were examined after 1, 2, 3 and 4 weeks [46]. Local expression of OCN increased earlier in the OGP-treated group, and its systemic expression remained increased throughout the 4-week period [46]. In what concerns the other investigated lineages, we did not detect expression of the adipogenic gene APM1 in none of the groups, which is consistent with previous i*n vitro* data on the effect of OGP on hMSCs adipogenesis [8], but we detected a higher expression of the chondrogenic genes COMP and Sox9 in the OGP3 group, as compared with the control. Although we have not found any *in vitro* studies investigating the effect of OGP in chondrogenesis, previous *in vivo* studies suggested that OGP stimulates endochondral bone formation in fracture callus of rabbits and rats [46]. Moreover, parentally administered OGP has been shown to regulate the expression of different factors associated with chondrogenesis, both locally and systemically [12], which also suggests that the mode of action of OGP may involve or be mediated by the action of other growth factors. Although this will require further investigation, it seems possible that OGP overlaps the potential to enhance chondrogenesis and osteogenesis, similarly to other growth factors, which have been shown to strongly support the formation of bone as well as of cartilage [47].

One recognized limitation of this study is that all groups have been implanted in the same animal. Thus, circulating peptides released from OGP-hydrogels may have had a systemic effect, affecting also the response observed in the control group. Even so, overall, the most promising results were obtained with the OGP groups, confirming our initial hypothesis on the significance of OGP/hMSCs co-delivery systems. Differences between the two OGP analogues may be related with their different release kinetics and/or the potency of the released bioactive fragment (LIGGYGFGG in OGP2 and YGFGG in OGP3).

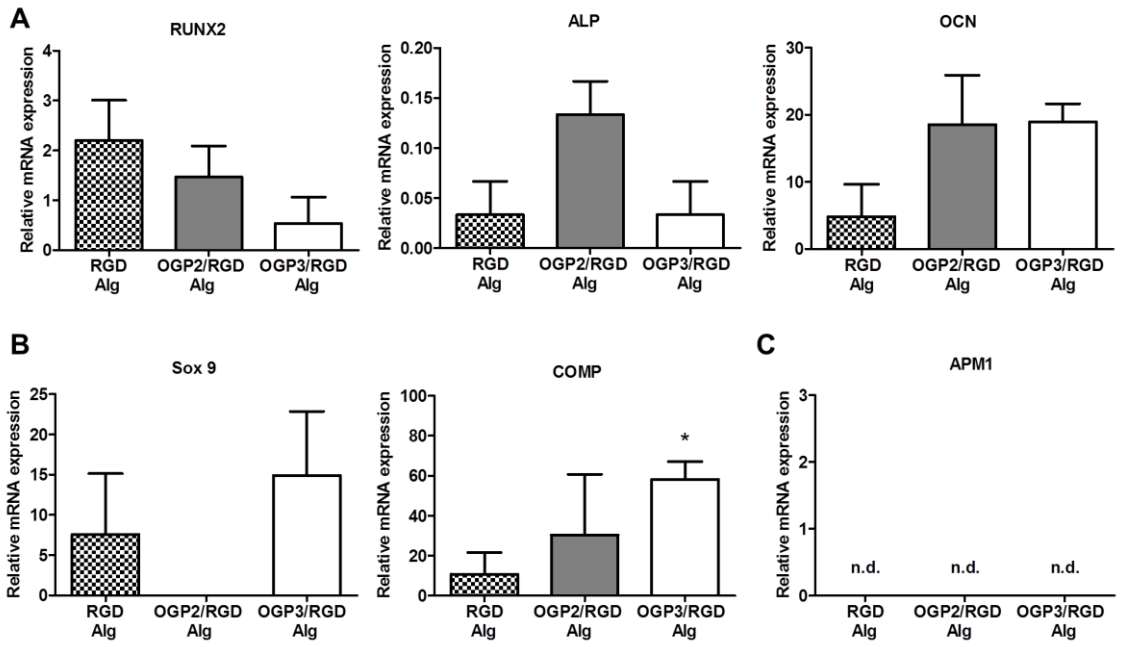

Fig. 9. qRT-PCR analysis of lineage-specific gene expression by hMSCs. (**A**) Osteogenic genes: Runx2, ALP and OCN. (**B**) Chondrogenic genes: Sox9 and COMP. (**C**) Adipogenic gene: APM1. Data is presented as mean ± SD (n=3 mice), (*) denotes statistical significant differences (p=0.0383) relative to RGD-Alg control. Results were normalized internally with GAPDH.

This and other open questions should be addressed in future experiments. In particular, it will be essential to test the proposed system using clinically relevant models, such as critical-sized bone defects or bone fractures, where the effect of locally delivered OGP may be potentiated by the adjuvant action of osteoinductive stimuli, naturally present in the bone compartment.

4. CONCLUSIONS

This study provided proof-of-concept on the correct design of OGP-Alg conjugates with protease-sensitive linkers, and demonstrated their usefulness as a platform for the *in situ* co-delivery of synthetic OGP analogues and hMSCs. Two different peptides were tested and both showed interesting effects. While *in vitro* OGP2 presented better results probably due to increased bioavailability, the more interesting *in vivo* outcome was obtained with OGP3, probably due to its increased resistance to proteolytic degradation and consequent longer persistence at the target site. Importantly, we demonstrated that the local co-delivery of OGP analogues and hMSCs from injectable hydrogels directed the osteogenic and/or chondrogenic differentiation of transplanted hMSCs in an ectopic setting, showing in parallel a positive effect on implant vascularization and ECM production. This novel strategy might provide a useful alternative for minimally invasive healing of small bone defects.

Acknowledgements

This work was financed by FEDER funds through the Programa Operacional Factores de Competitividade (COMPETE) and by Portuguese funds through Fundação para a Ciência e a Tecnologia (FCT), in the framework of the projects Pest-C/SAU/LA0002/2011 and BIOMATRIX (PTDC/SAU-BEB/101235/2008 and FCOMP-01-0124-FEDER-010915). PG and NV thank FCT and FEDER (European Union) for funding through project grants CONC-REEQ/275/QUI and PEst-C/QUI/UI0081/2011. NV also thanks FCT for Post-Doc grant SFRH/BPD/48345/2008. FM acknowledges INL-International Iberian Nanotechnology Laboratory for her PhD scholarship. CB has a research position funded by FCT-POPH-FSE (Ciência 2008). The authors are also grateful to Drª Maria Aparecido (UNIFESP, Brazil) for providing the FRET peptides.

5. REFERENCES

[1] Bhat A, Hoch AI, Decaris ML, Leach JK. Alginate hydrogels containing cell-interactive beads for bone formation. FASEB J. 2013.

[2] Firestone AJ, Chen JK. Controlling destiny through chemistry: small-molecule regulators of cell fate. ACS Chem. Biol. 2009;5:15-34.

[3] Vo TN, Kasper FK, Mikos AG. Strategies for controlled delivery of growth factors and cells for bone regeneration. Adv. Drug Delivery Rev. 2012;64:1292-309.

[4] Benoit DSW, Schwartz MP, Durney AR, Anseth KS. Small functional groups for controlled differentiation of hydrogel-encapsulated human mesenchymal stem cells. Nat. Mater. 2008;7:816-23.

[5] Maia FR, Bidarra SJ, Granja PL, Barrias CC. Functionalization of biomaterials with small osteoinductive moieties. Acta Biomater. 2013;9:8773-89.

[6] Murphy A.R., John P.S., D.L. K. Modification of silk fibroin using diazonium coupling chemistry and the effects on hMSC proliferation and differentiation. Biomaterials 2008;29:2829-38.

[7] Acharya AP, Dolgova NV, Moore NM, Xia CQ, Clare-Salzler MJ, Becker ML, et al. The modulation of dendritic cell integrin binding and activation by RGD-peptide density gradient substrates. Biomaterials 2010;31:7444-54.

[8] Chen Z-x, Chang M, Peng Y-l, Zhao L, Zhan Y-r, Wang L-j, et al. Osteogenic growth peptide C-terminal pentapeptide [OGP(10-14)] acts on rat bone marrow mesenchymal stem cells to promote differentiation to osteoblasts and to inhibit differentiation to adipocytes. Regul. Pept. 2007;142:16-23.

[9] Saska S, Scarel-Caminaga R, Teixeira L, Franchi L, dos Santos R, Gaspar A, et al. Characterization and in vitro evaluation of bacterial cellulose membranes functionalized with osteogenic growth peptide for bone tissue engineering. J. Mater. Sci.: Mater. Med. 2012;23:2253-66.

[10] Bab I, Gazit D, Yu-Chen C, Muhlrad A, Shteyer A, Chorev M. Synthetic peptides and pseudopeptides having osteogenic activity and pharmaceutical compositions containing the same. US 6,479,460 B1, 2002. Yissum Research Development Company of the Hebrew University of Jerusalem.

[11] Moore NM, Lin NJ, Gallant ND, Becker ML. The use of immobilized osteogenic growth peptide on gradient substrates synthesized via click chemistry to enhance MC3T3-E1 osteoblast proliferation. Biomaterials 2010;31:1604-11.

[12] Pregizer S, Baniwal SK, Yan X, Borok Z, Frenkel B. Progressive recruitment of Runx2 to genomic targets despite decreasing expression during osteoblast differentiation. J. Cell. Biochem. 2008;105:965-70.

[13] Manton KJ, Leong DFM, Cool SM, Nurcombe V. Disruption of heparan and chondroitin sulfate signaling enhances mesenchymal stem cell-derived osteogenic differentiation via bone morphogenetic protein signaling pathways. Stem Cells 2007;25:2845-54.

[14] Bab I, Gavish H, Namdar-Attar M, Greenberg Z, Chen Y, Mansur N, et al. Isolation of mitogenically active C-terminal truncated pentapeptide of osteogenic growth peptide from human plasma and culture medium of murine osteoblastic cells. J. Pept. Res. 1999;54:408-14.

[15] Benoit DSW, Durney AR, Anseth KS. The effect of heparin-functionalized PEG hydrogels on three-dimensional human mesenchymal stem cell osteogenic differentiation. Biomaterials 2007;28:66-77.

[16] Vacharathit V, Silva EA, Mooney DJ. Viability and functionality of cells delivered from peptide conjugated scaffolds. Biomaterials 2011;32:3721-8.

[17] Mendes LS, Saska S, Martines MA, Marchetto R. Nanostructured materials based on mesoporous silica and mesoporous silica/apatite as osteogenic growth peptide carriers. Mater. Sci. Eng. C Mater. Biol. Appl. 2013;33:4427-34.

[18] Horii A, Wang X, Gelain F, Zhang S. Biological designer self-assembling peptide nanofiber scaffolds significantly enhance osteoblast proliferation, differentiation and 3-D migration. PLoS ONE 2007;2:e190.

[19] Page-McCaw A, Ewald AJ, Werb Z. Matrix metalloproteinases and the regulation of tissue remodelling. Nat. Rev. Mol. Cell. Biol. 2007;8:221-33.

[20] Fonseca KB, Maia FR, Cruz FA, Andrade D, Juliano MA, Granja PL, et al. Enzymatic, physicochemical and biological properties of MMP-sensitive alginate hydrogels. Soft Matter 2013;9:3283-92.

[21] Fonseca KB, Bidarra SJ, Oliveira MJ, Granja PL, Barrias CC. Molecularly designed alginate hydrogels susceptible to local proteolysis as three-dimensional cellular microenvironments. Acta Biomater. 2011;7:1674-82.

[22] Kolambkar YM, Dupont KM, Boerckel JD, Huebsch N, Mooney DJ, Hutmacher DW, et al. An alginate-based hybrid system for growth factor delivery in the functional repair of large bone defects. Biomaterials 2011;32:65-74.

[23] Fields GB, Noble RL. Solid phase peptide synthesis utilizing 9-fluorenylmethoxycarbonyl amino acids. Int. J. Pept. Protein Res. 1990;35:161-214.

[24] Cortez J, Vorobieva E, Gralheira D, Osório I, Soares L, Vale N, et al. Bionanoconjugates of tyrosinase and peptide-derivatised gold nanoparticles for biosensing of phenolic compounds. J. Nanopart. Res. 2011;13:1101-13.
[25] Almeida PC, Oliveira V, Chagas JR, Meldal M, Juliano MA, Juliano L. Hydrolysis by cathepsin B of fluorescent peptides derived from human prorenin. Hypertension 2000;35:1278-83.
[26] Lorenzen A, Kennedy SW. A fluorescence-based protein assay for use with a microplate reader. Anal Biochem. 1993;214:346-8.
[27] Boontheekul T, Kong H-J, Mooney DJ. Controlling alginate gel degradation utilizing partial oxidation and bimodal molecular weight distribution. Biomaterials 2005;26:2455-65.
[28] Evangelista MB, Hsiong SX, Fernandes R, Sampaio P, Kong H-J, Barrias CC, et al. Upregulation of bone cell differentiation through immobilization within a synthetic extracellular matrix. Biomaterials 2007;28:3644-55.
[29] Rowley JA, Madlambayan G, Mooney DJ. Alginate hydrogels as synthetic extracellular matrix materials. Biomaterials 1999;20:45-53.
[30] Alsberg E, Kong HJ, Hirano Y, Smith MK, Albeiruti A, Mooney DJ. Regulating bone formation via controlled scaffold degradation. J. Dent. Res. 2003;82:903-8.
[31] Oliveira SM, Barrias CC, Almeida IF, Costa PC, Ferreira MRP, Bahia MF, et al. Injectability of a bone filler system based on hydroxyapatite microspheres and a vehicle with in situ gel-forming ability. J. Biomed. Mater. Res., Part B 2008;87B:49-58.
[32] Garesse R, Castell JV, Vallejo CG, Marco R. A fluorescamine-based sensitive method for the assay of proteinases, capable of detecting the initial cleavage steps of a protein. Eur. J. Biochem. 1979;99:253-60.
[33] Turk BE, Huang LL, Piro ET, Cantley LC. Determination of protease cleavage site motifs using mixture-based oriented peptide libraries. Nat. Biotechnol. 2001;19:661-7.
[34] Korkmaz B, Attucci S, Juliano MA, Kalupov T, Jourdan ML, Juliano L, et al. Measuring elastase, proteinase 3 and cathepsin G activities at the surface of human neutrophils with fluorescence resonance energy transfer substrates. Nat. Protoc. 2008;3:991-1000.
[35] Chau Y, Tan FE, Langer R. Synthesis and characterization of dextran−peptide−methotrexate conjugates for tumor targeting via mediation by matrix metalloproteinase II and matrix metalloproteinase IX. Bioconjugate Chem. 2004;15:931-41.
[36] Chau Y, Padera RF, Dang NM, Langer R. Antitumor efficacy of a novel polymer-peptide-drug conjugate in human tumor xenograft models. Int. J. Cancer 2006;118:1519-26.
[37] Chau Y, Dang NM, Tan FE, Langer R. Investigation of targeting mechanism of new dextran-peptide-methotrexate conjugates using biodistribution study in matrix-metalloproteinase-overexpressing tumor xenograft model. J. Pharm. Sci. 2006;95:542-51.
[38] Robinson D, Bab I, Nevo Z. Osteogenic growth peptide regulates proliferation and osteogenic maturation of human and rabbit bone marrow stromal cells. J. Bone Miner. Res. 1995;10:690-6.

[39] Greenberg Z, Chorev M, Muhlrad A, Shteyer A, Namdar M, Mansur N, et al. Mitogenic action of osteogenic growth peptide (OGP): role of amino and carboxy-terminal regions and charge. Biochim. Biophys. Acta 1993;1178:273-80.
[40] Bab I, Chorev M. Osteogenic growth peptide: From concept to drug design. Pept. Sci. 2002;66:33-48.
[41] Spreafico A, Frediani B, Capperucci C, Leonini A, Gambera D, Ferrata P, et al. Osteogenic growth peptide effects on primary human osteoblast cultures: Potential relevance for the treatment of glucocorticoid-induced osteoporosis. J. Cell. Biochem. 2006;98:1007-20.
[42] Stakleff KS, Lin F, Smith Callahan LA, Wade MB, Esterle A, Miller J, et al. Resorbable, amino acid-based poly(ester urea)s crosslinked with osteogenic growth peptide with enhanced mechanical properties and bioactivity. Acta Biomater. 2013;9:5132-42.
[43] Bidarra SJ, Barrias CC, Fonseca KB, Barbosa MA, Soares RA, Granja PL. Injectable in situ crosslinkable RGD-modified alginate matrix for endothelial cells delivery. Biomaterials 2011;32:7897-904.
[44] Bocci G, Danesi R, Fioravanti A, Del Tacca M. The effect of osteogenic growth peptide OGP on proliferation and adhesion of HEMC-1 human endothelial cells. Pharmacol. Res. 2002;45:21-5.
[45] Wu Y, Chen L, Scott PG, Tredget EE. Mesenchymal stem cells enhance wound healing through differentiation and angiogenesis. Stem Cells 2007;25:2648-59.
[46] Brager MA, Patterson MJ, Connolly JF, Nevo Z. Osteogenic growth peptide normally stimulated by blood loss and marrow ablation has local and systemic effects on fracture healing in rats. J. Orthop. Res. 2000;18:133-9.
[47] Mastrogiacomo M, Cancedda R, Quarto R. Effect of different growth factors on the chondrogenic potential of human bone marrow stromal cells. Osteoarthr. Cartil. 2001;9:S36-40.

CHAPTER VI

CONCLUDING REMARKS AND FUTURE PERSPECTIVES

---

1. CONCLUDING REMARKS AND FUTURE PERSPECTIVES

The development of improved cell-based therapeutics based on the use of adult mesenchymal stem cells (MSCs) for tissue regeneration has been attracting great deal of attention. Cell therapies have shown great therapeutic potential in preclinical testing and even in some clinical trials, but have not yet demonstrated consistent positive results, and only a few strategies have reached commercial success. In spite of intensive research in this area, there are still major concerns regarding the selection of the most appropriate MSCs source, their fate after transplantation, as well as the adequacy and standardization of protocols for isolating, expanding and characterizing these cells [1]. Moreover, there is still a limited understanding of their normal biological functions and their role in tissue repair [1].

On the other hand, several technical/scientific issues have to be addressed, namely in what concerns their delivery routes. Compared to systemic infusion, local administration seems more advantageous as it inherently prolongs cell retaining at the target site. Moreover, a new paradigm is that repair of tissues by MSCs is far from being only dependent on the myriad of factors produced by, or provided to, MSCs in culture. Instead, MSCs are highly responsive to the microenvironment generated by injured tissues. Such cross-talk induces them to express factors that seem to be specifically tailored to the immediate needs of the tissue, supporting the suggestion that one of the most useful therapeutic strategies will consist in injecting cells locally for enhancing tissue repair [1, 2].

Compared to direct local administration, advanced delivery strategies using biomaterial carriers, namely 3D hydrogel matrices, are expected to provide additional benefit, as previously discussed. In an attempt to provide an adequate microenvironment to transplanted cells, the tissue engineering field is moving toward the development of increasingly sophisticated matrices that recreate several features of the native ECM. Notably, these “artificial” yet biologically meaningful systems represent complex milieus where cell behaviour is regulated by a number of matrix-intrinsic and -extrinsic cellular and molecular factors that must be carefully controlled, as they differentially affect distinct cellular activities.

In the first experimental section of this thesis (Chapters III and IV), the role of different factors on human MSCs (hMSCs) behaviour upon entrapment in RGD-alginate hydrogels was investigated, particularly in what concerns their effect on the formation of multicellular aggregates. The process by which cells self-assemble to form 3D structures is central to morphogenesis and development of living tissues, and is of growing interest to the field of regenerative medicine. Therefore, the success of engineered living structures will ultimately depend on one hand on our capacity to unraveling the mechanisms of cellular self-assembly and, on the other hand, on our capacity to translate that knowledge into functional therapeutic strategies. In Chapter III, the effect of cell density, a key and frequently overlooked parameter, was shown to have a profound impact on hMSCs behaviour. In high-density cultures, cell

viability was better maintained, and cell-cell signaling was promoted inducing hMSCs to connect to each other and aggregate into multicellular structures, particularly under osteoinductive conditions. Clustered hMSCs produced their own ECM, rich in fibronectin and collagen, and successfully differentiated along the osteoblastic lineage. The importance of selecting the most appropriate cell entrapping density when establishing 3D cultures for a specific application was confirmed.

In Chapter IV, it was possible to shed some light on the mechano-chemical coupling mechanisms involved in the process of hMSCs aggregation within RGD-alginate matrices, and better elucidated the interplay between substrate compliance and ligand presentation in cell-in-gel responses. In particular, it was clearly demonstrated that the intrinsic properties of the artificial matrix are clearly central guidance variables to which hMSCs are particularly responsive. It was demonstrated that artificial matrices can be designed in such a way to provide dynamic cellular microenvironments where cells can rapidly, and by their own, modify the local mechanical and biochemical milieu, becoming embedded and ultimately residing within a self-synthesized ECM. In such a system, cell interactions with the original artificial matrix become less important as time progresses and the *de novo* produced cell-derived ECM turns into a more critical determinant of cell fate. Importantly, this study established a biomaterial-driven strategy to induce the self-aggregation of hMSCs and the formation of hMSCs-ECM micro-tissues, promoting higher hMSCs proliferation and osteogenic differentiation ability, which might be potentially interesting for therapeutic applications.

Overall, these two studies represent a contribution to the growing body of literature on cellular microenvironments and their effect on hMSCs behaviour, and have provided new clues to the design of cell-instructive 3D matrices. Yet, several topics remained to be addressed and new ideas arose during the course of this investigation, which should be the object of future studies. In particular, it would be interesting to further explore the assembly and potential of hMSCs-ECM microtissues. At a more fundamental level, it would be fascinating to follow the dynamics of self-assembly using appropriate bioimaging techniques, namely to be able to clearly measure cell migration and its dependency on matrix viscosity and cell-adhesion anchor points. The present study also fell short on the quantitative measurements of traction stresses, cell-cell and cell-matrix contact points, which would be important to better characterize the interrelated cellular, molecular and mechanical events leading to cell aggregation under the specific conditions tested herein.

As already stated, a vast array of soluble, cellular and matrix signals affect cells response in 3D. Therefore, in order to capture a more global picture of extrinsic control of cell fate to define optimal cellular microenvironments, it would be important to systematically deconstruct the role of each signal and their interplay. Still, while conceptually attractive, such combinatorial studies are also very demanding, requiring high-throughput screening (HTS) tools [3, 4]. To address this challenge, it would be interesting to perform such studies using a cell-in-gel

microarray format, to allow the concomitant analysis of different trial conditions, using less material and cells, on a single microscope slide. With this type of HTS it would be possible to increase even further the complexity of the system, not only in terms of hydrogel composition, using for example protease-sensitive alginate hydrogels [5, 6], but also exploring the co-culture of hMSCs with other relevant cell types [7], which are strategies already under study in our group. The use of high-content bioimaging tools would obviously be the key to perform those studies.

Another important aspect that requires further investigation is whether the reported *in vitro* observations correlate with an *in vivo* response: do ECM-hMSCs aggregates actually have a higher therapeutic potential than individually dispersed entrapped cells? It would be clearly an important achievement to obtain such as proof of concept by testing these systems in a relevant animal model.

In the bone tissue engineering field, it is also becoming clear that pro-regenerative strategies should recapitulate the natural bone regenerative process, involving the coordinated effort of cells, soluble factors and matrix signals, in a time, concentration and site specific fashion [2]. Therefore, the integration of bioactive factors with controlled spatio-temporal kinetics with the appropriate biomaterial carriers will be the key to designing innovative treatments.

In the second experimental part of the present work (Chapter V), a sophisticated approach toward the development of a multifunctional injectable hMSCs carrier was explored, by functionalizing alginate with OGP analogues. The goal was to develop a delivery system incorporating osteoinductive cues, which would induce hMSCs differentiation along the osteoblastic lineage, and remain available at the injury site for prolonged periods of time, in close proximity of target cells. The study provided a proof-of-concept on the correct design of OGP-alginate conjugates with protease-sensitive linkers, and demonstrated their usefulness as a platform for the *in situ* co-delivery of synthetic OGP analogues and hMSCs.

The background composition of the hydrogel matrices selected for implantation (in terms of hMSCs density and alginate concentration) was based on the results from previous chapters: matrices demonstrating absence of hMSCs aggregation and lower osteogenic differentiation were selected, to ensure that the observed effects would be related to the presence of OGP, and not to other factors. Two different peptides were tested and both showed interesting effects. While *in vitro* the OGP analogue with faster release kinetics presented better results probably due to increased bioavailability, the more interesting *in vivo* outcome was obtained with the analogue with lower release kinetics, probably due to its increased resistance to proteolytic degradation and consequent longer persistence at the target site. Importantly, we demonstrated that the local co-delivery of OGP analogues and hMSCs from injectable hydrogels directed the osteogenic and/or chondrogenic differentiation of transplanted hMSCs in an ectopic setting, showing in parallel a positive effect on implant vascularization and ECM production. Thus, the

proposed combined strategy involving the co-delivery of osteoinductive factors and hMSCs via biomaterial carriers appears promising, and may provide a useful alternative for minimally invasive healing of small bone defects.

Nevertheless, further investigation is needed in terms of system optimization, and several topics remained to be addressed. In particular, it will be critical to further characterize the co-delivery system, by moving forward in the *in vivo* studies**.** For the studies presented in this thesis, SCID mice recipients were chosen as the classical model for xenograft studies. Also, implantations were performed at an ectopic site instead of a bone defect, to mitigate the effect of osteoinductive signals intrinsically present at the bone compartment, and to more specifically evaluate the direct impact of OGP analogues on hMSCs.

In future studies it will be essential to test the proposed system using clinically relevant models, such as critical-sized bone defects or bone fractures, where the effect of locally delivered OGP may be even potentiated by the adjuvant action of osteoinductive stimuli, naturally present in the bone compartment. An evaluation at later time points will also be important to clearly detect new bone formation. The capacity of OGP peptides to also induce neo-vessel formation was unexpected but particularly interesting given that bone regeneration is strongly dependent of adequate vascularization, and therefore should be further investigated. A deeper analysis of local and systemic OGP effects on the host is also important. As previously recognized, one limitation of the study was that all groups have been implanted in the same animal. Therefore, it remained unclear whether OGP released from alginate hydrogels entered the circulation, having a systemic effect at distal sites. Moreover, the study was mainly focused on the local effect of the OGP-delivery system on transplanted MSCs, and not on host cells. This will be particularly relevant when implanting OGP-hydrogels at the bone compartment. The use of labeled peptides could be useful to trace their biodistribution in relevant tissues/organs.

Finally, although these materials are able to form hydrogels *in situ*, they have been implanted as pre-formed discs due to technical constraints, and their injectability profile upon *in vivo* administration was not adequately evaluated. However, preliminary studies, both *ex vivo* and *in vivo* showed that alginate hydrogels could be easily injected, using a standard syringe, into critical-sized femoral defects created in the rat, and then crosslink *in situ* after approximately 5 min post injection. In this context, it should be highlighted that this type of injectable biomaterials would only be appropriate for the clinical management of small-sized defects. Nevertheless, these hydrogels can be combined with other biomaterials to obtain mechanically compatible scaffolds for the repair of large bone defects. One possibility relies in preparing injectable hybrid systems, currently under investigation in our group, where hydrogels are reinforced with ceramic components [8-10].

2. REFERENCES

[1] Prockop DJ. Repair of tissues by adult stem/progenitor cells (MSCs): controversies, myths, and changing paradigms. Mol. Ther. 2009;17:939-46.

[2] Vo TN, Kasper FK, Mikos AG. Strategies for controlled delivery of growth factors and cells for bone regeneration. Adv. Drug Delivery Rev. 2012;64:1292-309.

[3] Fernandes TG, Kwon SJ, Bale SS, Lee MY, Diogo MM, Clark DS, et al. Three-dimensional cell culture microarray for high-throughput studies of stem cell fate. Biotechnol. Bioeng. 2010;106:106-18.

[4] Ranga A, Lutolf MP. High-throughput approaches for the analysis of extrinsic regulators of stem cell fate. Curr. Opin. Cell Biol. 2012;24:236-44.

[5] Fonseca KB, Maia FR, Cruz FA, Andrade D, Juliano MA, Granja PL, et al. Enzymatic, physicochemical and biological properties of MMP-sensitive alginate hydrogels. Soft Matter 2013;9:3283-92.

[6] Fonseca KB, Bidarra SJ, Oliveira MJ, Granja PL, Barrias CC. Molecularly designed alginate hydrogels susceptible to local proteolysis as three-dimensional cellular microenvironments. Acta Biomater. 2011;7:1674-82.

[7] Bidarra SJ, Barrias CC, Barbosa MA, Soares R, Amedee J, Granja PL. Phenotypic and proliferative modulation of human mesenchymal stem cells via crosstalk with endothelial cells. Stem Cell Res. 2011;7:186-97.

[8] Oliveira SM, Barrias CC, Almeida IF, Costa PC, Ferreira MRP, Bahia MF, et al. Injectability of a bone filler system based on hydroxyapatite microspheres and a vehicle with in situ gel-forming ability. J. Biomed. Mater. Res., Part B 2008;87B:49-58.

[9] Ribeiro CC, Barrias CC, Barbosa MA. Preparation and characterisation of calcium-phosphate porous microspheres with a uniform size for biomedical applications. J. Mater. Sci.: Mater. Med. 2006;17:455-63.

[10] Barrias CC, Ribeiro CC, Lamghari M, Miranda CS, Barbosa MA. Proliferation, activity, and osteogenic differentiation of bone marrow stromal cells cultured on calcium titanium phosphate microspheres. J. Biomed. Mater. Res. A 2005;72:57-66.